FRANK LABORATORY OF NEUTRON PHYSICS

JOINT INSTITUTE FOR NUCLEAR RESEARCH

ANNUAL REPORT 2007

DUBNA

FRANK LABORATORY OF NEUTRON PHYSICS OF THE JOINT INSTITUTE FOR NUCLEAR RESEARCH

The Joint Institute for Nuclear Research (JINR) is an international centre for experimental and theoretical investigations in the fields of elementary particle physics, nuclear and neutron physics, condensed matter research and related topics.

The JINR structure is determined by the fact that it is governed internationally and has many research specializations. Current scientific and financial affairs of the Institute's Laboratories, common services as well as the work of specialized departments are guided by the Institute Directorate.

The Frank Laboratory of Neutron Physics is one of the eight JINR Laboratories. It was established in 1956, soon after the foundation of JINR.

In 1960 a principally new source of neutrons - the IBR fast pulsed reactor of periodic operation - was created at FLNP under the leadership of Prof. D.I.Blokhintsev (11.01.1908 - 24.01.1979). The birth of this reactor gave rise to a new direction in the development of research neutron sources.

An extended scientific program with this reactor was initiated under the leadership of Nobel Prize Winner and Laboratory Director Prof. I.M.Frank (23.10.1908 - 22.06.1990) and Deputy Director Prof. F.L.Shapiro (06.04.1915 - 30.01.1973). Since 1960, a whole family of unique pulsed neutron sources for nuclear physics and condensed matter physics has been developed and constructed. The latest in the family, the IBR-2 high flux pulsed reactor, was commissioned in February 1984. The Laboratory was named after Prof. I.M.Frank in 1992. In the same year, in JINR the I.M.Frank Prize for Neutron Physics was established.

At present, the scientific activity of the Laboratory focuses on two fields of physics, namely nuclear physics and condensed matter physics. The first involves investigations of the neutron as an elementary particle and studies of compound states in neutron induced reactions. The second investigates pressing problems in the physics and chemistry of solid states, surfaces and liquids, and in molecular biology. Applied investigations are also carried out using nuclear physics methods.

PREFACE

We would like to offer the readers the report on the scientific activity of the Frank Laboratory of Neutron Physics for 2007. The first part presents a brief review of the experimental and theoretical results achieved in the main scientific directions – condensed matter physics, neutron nuclear physics and applied research. The second part includes the reports on the operation of the IBR-2 pulsed reactor and realization of the IREN project. The third part is concerned with the development and creation of elements of neutron spectrometers for condensed matter investigations. The fourth part presents the experimental reports that cover the main scientific directions in greater detail. The list of publications for 2007 completes the report.

Starting in December 2006 after the reactor shutdown the works on the modernization of ***IBR-2*** were mainly focused on:

- defueling of the IBR-2 reactor core and the removal of sodium from the extracted fuel assemblies (FA);
- manufacturing of a standard ASCS, reactor control panel (SNIIP-SYSTEMATOM) and CM system (INEUM);
- manufacturing of a new reactor vessel;
- manufacturing of rolling shielding, stationary reflectors and regulation blocks for the stationary reflector;
- detail design of CM and manufacturing of cryogenic pipelines.

The IREN Project. The main tasks of the Frank Laboratory of Neutron Physics and the Laboratory of Particle Physics in 2007 were the development of engineering infrastructure and the installation of the available equipment of the 1st stage of the LUE-200 accelerator.
In 2007 in accordance with the approved plan-schedule the works on the construction and installation of power supply systems, water-cooling and thermostabilisation systems, control and alarm systems of the 1st stage of the IREN facility were performed. The installation of the accelerator systems was carried out in accordance with the corrected plan-schedule after the accident with the klystron SLAC 5045.

In spite of the IBR-2 reactor shutdown the activities of the Department of Condensed Matter Research and the Department of Spectrometers Complex were focused both on modernization of the spectrometers and scientific research in allied centers in Russia and abroad.

In 2007 on IBR-2 the reconstruction of the neutron guide system of the SCAT, EPSILON and NERA spectrometers was started. The work is conducted within the framework of the BMBF project in cooperation with the personnel of the Spectrometers Complex Department. On channel 10 of IBR-2 the multifunctional reflectometer GRAINS will soon be constructed in place of the available spectrometer KDSOG. In 2007 a detail scheme of the reflectometer was developed and model calculations were made. A special feature of the reflectometer, a vertical scattering plane, will make it possible to study reflection from liquid media. The reflectometer will operate in the time-of-flight mode, which will allow the experiments to be conducted at fixed orientations of the incident beam and the sample. Additional modes of the GRAINS reflectometer will comprise off-specular reflection and small-angle polarized neutron scattering.

In the framework of the Protocol on Cooperation with RRC KI the designing of neutron diffractometer with complementary possibilities as to the available stress-diffractometer FSD on IBR-2, for studying internal stresses in bulk samples on the IR-8 reactor has been started.

For further development of the experimental base on IBR-2 and within the framework of cooperation with the NECSA Corporation (Republic of South Africa) a contract for the purchase of an automated materials testing machine has been concluded. The machine allows on-line experiments to be performed with a wide set of loading (stationary or cyclic) modes on any type of neutron diffractometers with bulk samples of metals and alloys.

Structural changes, spin-state transitions of Co^{3+} ions and insulator-metal transitions in lanthanum cobaltite $LaCoO_3$ have been studied in a wide range of temperatures (10-900 K) and pressures (0-20 GPa). It has been found that pressure induces sharp suppression of magnetic intermediate-spin state (S = 1) and stabilization of nonmagnetic low-spin state (S = 0) of Co^{3+} ions. The insulator-metal transition temperature significantly increases under pressure.

The possibility of using short chain length mono-carboxylic acids ($C_{12}H_{24}O_2$ and $C_{14}H_{28}O_2$) for stabilization of magnetite nanoparticles in magnetic fluids on the basis of non-polar organic solvents has been studied. It has been demonstrated that they can be used to obtain highly stable magnetic fluids.

At the REMUR spectrometer the ferromagnetic-superconducting layered structure V(39nm)/Fe(3.2nm)/10×[V(3.2nm)/Fe(3.2nm)] consisting of a superconducting layer of vanadium V(39nm) and periodic structure 10×[V(3.2nm)/Fe(3.2nm)] has been studied by neutron reflectometry using standing waves of polarized neutrons. For the first time, the

phenomena of formation of a domain structure in the vicinity of vanadium-iron interface and antiferromagnetic ordering in a periodic structure have been observed. Thus, it has been demonstrated that the magnetic state of nanostructures can be controlled using the superconducting transition. This opens up possibilities of designing principally new logic elements for nanoelectronics, in which the state can be encoded both by the magnetic moment value and the resistance.

The magnetic and magnetotransport properties of composite nanogranulated cobalt-based films have been investigated. In nanocomposite alloys $(Co)_x(SiO2)_{1-x}$ near the percolation threshold a magnetic phase transition with the formation of fractal structures has been detected. The obtained experimental data testify that in nanocomposite granulated systems in the range of the structural percolation threshold the magnetic fractal structures are formed, which, in fact, determine the magnetic properties of composites including magnetoresistance.

Neutron diffraction is an exceptionally powerful method for studying structures of biological and model lipid membranes. In particular, by varying the relative content of light and heavy water, it is possible to reliably determine phases of structural factors. One more favourable point is the possibility to carry out *in-situ* experiments in real time. On the DN-2 diffractometer one can follow changes in the membrane structure in the course of hydration with time resolution at a level of 1 min. In 2007 experimental evidences for the phenomenon of reinforcement of the lipid matrix of the outermost layer of mammalian skin, the stratum corneum (SC) by ceramide 6 molecules were obtained. In a series of neutron diffraction experiments it has been found that the extremely strong intermenbrane attraction created by ceramide 6 molecules cannot be destroyed either by long-chain ceramides or long-chain fat acids. The small-angle neutron scattering experiments have shown that the interaction created by ceramide 6 molecules is short-range. The stability of the developed SC membrane to variation of biochemical composition of lipids and water solutions has made it possible to begin experiments to study the substances that can increase the permeability of human skin for drug delivery.

Antibiotic amphotericin B (AmB) widely used in medicine has been studied by small-angle neutron scattering, X-ray diffraction and Fourier spectroscopy. The results of the experiments have shown that AmB is located predominantly in the headgroup region of the membrane at concentrations below 1 mol%. At concentrations above 1 mol% the process of AmB aggregation takes place. The effect of association arises and AmB incorporates into the hydrophobic membrane core.

For the first time the existence of open inner cavities in the effective dendrimer volume accessible to a solvent has been demonstrated and their volume fraction has been estimated. It has been shown that the end groups of a dendrimer are located in its surface layer. The small-angle scattering data have made it possible to determine sizes and to restore the external shape of dendrimers of various generations for three and four functional dendrimers. From a new model of dendrimer structure it follows that its inner sphere is permeable to the solvent, and its density decreases by a factor of at least 2.

Complex investigations into the physical properties of synthetic quartz single crystals and quartz powders in the temperature range of the α-β transition with the use of neutron diffraction and mechanical spectroscopy have been carried out. New data on the behaviour of parameters of a unit cell of quartz powders of two fractions with different average sizes of grains at room temperature and in the temperature range of 540-620°C, as well as atomic coordinates in a unit cell have been obtained. It has been found that the lattice parameters of the powders that vary in the size of grains by an order of magnitude, differ significantly. The α-β phase transition temperature of a fine-grained powder is higher than that of a coarse-grained one by ≈15 ºC (lies in the range of 580-585 ºC).

In 2007 a number of experiments were carried out and some interesting results were obtained in the field of nuclear physics.

The treatment of the results of the experiment on the measurement of the gravitational force $F_g = m_g a$, experienced by a neutron in the Earth's gravitational field (m_g is the gravitational mass of the neutron, and a is its free fall acceleration) has been completed.

A new experiment to study the effect of a refracting medium in neutron optics has been carried out. The effect consists in a change in the frequency of the wave upon passing through a refracting sample moving with acceleration. For the first time it was detected in 2005. In the experiment in 2007 new convincing data were obtained, thus allowing us to speak with full confidence that the existence of the effect is proved.

In 2007 the main result achieved within the framework of activities on the preparation and carrying out of the experiment on the direct measurement of the neutron-neutron scattering cross section at the YAGUAR reactor (RFNC-VNIITF, Snezhinsk) was the construction of a neutron detector meeting all requirements of the experiment. The detector was installed on the experimental setup and successfully underwent tests in calibration measurements on gases in a pulsed operating mode of the YAGUAR reactor. Thus, at the present time the facility for measuring the nn-scattering is ready for operation.

In 2005 it was experimentally demonstrated that diamond nanoparticles could be used as an effective reflector of very cold neutrons. In 2007 the precision measurements of the albedo of very cold neutrons from a diamond nanoparticle layer were carried out by storing them in a trap with the walls made of nanodiamonds.

Within the framework of the experiments to search for neutral currents in nucleon-nucleon interactions and to determine weak π-meson coupling constant the measurements (in collaboration with PNPI, ILL and TU of Munich) of P-odd asymmetry of γ-quanta from the reaction $^{10}B(n,\alpha_1)^{7}Li^{*} \rightarrow {}^{7}Li+\gamma$ were conducted on the polarized cold neutron beam PF1B (ILL, Grenoble). The asymmetry coefficient averaged over three cycles (preliminary value) is $A_\gamma = (4.5 \pm 2.7)\cdot 10^{-8}$.

The first results of the experiment to study the reaction $^{235}U(n_{th},f)$ conducted in 2006 at the IBR-2 reactor using the two-arm time-of-flight heavy ion spectrometer mini-FOBOS were obtained. In the «mass-mass» distribution of fission fragments various peculiarities were revealed, which can be interpreted as the existence of a new channel of many-body decay similar to that observed earlier in $^{252}Cf(sf)$. In the distribution «total kinetic energy – fragment mass» fine structures similar to those found earlier for other fissioning systems were revealed as well.

The complex analysis of experimental data on cascade γ-decay of neutron resonances was continued. The approximation of experimental data on partial widths of primary dipole γ-transitions in the same energy interval substantiated this conclusion: the properties of the nucleus are determined by the coexistence and interaction of excitations of fermion and boson types in the nucleus.

In conclusion, it might be well to point out that great interest is being expressed by the JINR Member States in the work in the field of neutron investigations. It is also significant that in the last few years a lot of young people have come to the Laboratory. All these facts confirm that the Laboratory continues to develop successfully and dynamically, carrying out investigations in the interests of the JINR Member States.

A.V.Belushkin

Director

1. SCIENTIFIC RESEARCH

1.1. CONDENSED MATTER PHYSICS

In view of the IBR-2 reactor shutdown for the next stage of reconstruction, the tasks of the department personnel and work plans under the theme in 2007 differed noticeably from the traditional program of activities. Namely, the scientific work was transferred to the allied centers in Russia and abroad, and the work on the IBR-2 was focused on the realization of the program of modernization of the spectrometers. Out of fundamental and applied research activities developed by the employees of the NICM department, in 2007 several major scientific directions were chosen and preserved. Work in these directions was carried out in other research centers (first of all in neutron and synchrotron centers) under the existing cooperation agreements. In 2007 the first stage of modernization of the spectrometers at the IBR-2 reactor started.

I. Scientific results

The results of the long-term investigations of equilibrium structural-magnetic inhomogeneous states in complex magnetic manganese oxides have been summarized. The quantitative characteristics of the effect of the polaronic narrowing of the bandwidth and the crystal lattice microstrains on the volume fraction of the mesoscopic ferromagnetic and antiferromagnetic clusters have been obtained. In $(La_{1-y}Pr_y)_{0.7}Ca_{0.3}MnO_3$ compound a well-defined dip (**Fig. 1**) in the temperature of transition to the ordered magnetic state and the suppression of all the types of long-range magnetic ordering near the metal-insulator transition point at y=0.9 indicate a key role of the chemical disorder in the structure for the formation of the phase-separated state at the mesoscopic scale. It has been found that the value of internal microstrains is one more important factor influencing phase separation effects [**1**].

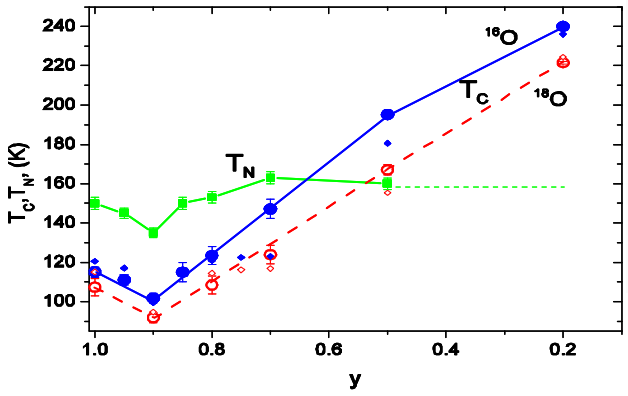

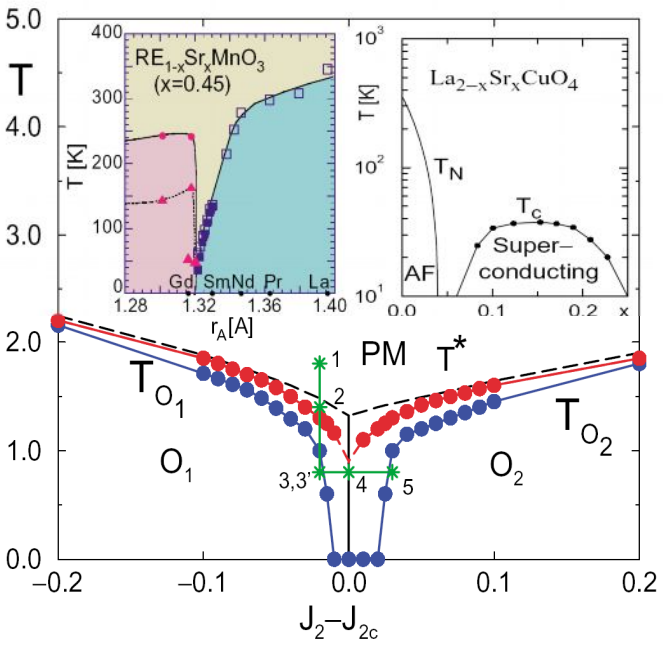

Fig. 1. The Curie (T_C) and Néel (T_N) temperatures as a function of the Pr content in $(La_{1-y}Pr_y)_{0.7}Ca_{0.3}MnO_3$ (left). The Néel temperature is independent of the ^{16}O or ^{18}O content in the sample, whereas for the Curie temperature the dependence is clearly visible. A dip in the transition temperatures at y = 0.9 is in agreement with the predictions of the model of quenched chemical disorder (J. Burgy et al., Phys. Rev. Lett. 2004) resulting in transfer integral fluctuations and mesoscopic phase separation into antiferromagnetic insulating (AFM) and ferromagnetic (FM) phases. The phase diagram obtained on the basis of model calculations is given at the right.

A series of neutron diffraction experiments to determine crystal and magnetic phase states of perovskite-like manganites $Re_{0.5}Sr_{0.5}MnO_3$ (Re = ^{152}Sm, $Nd_{0.772}Tb_{0.228}$ and $Nd_{0.544}Tb_{0.456}$) has been carried out [**2**]. The experiments have been performed to reveal the microscopic origins of the giant oxygen isotope effect discovered recently in $Sm_{1-x}Sr_xMnO_3$ for $x \approx 0.5$. It has been shown that at low temperatures in all the studied compositions there occurs a separation into two crystalline phases *P1* and *P2,* which have identical space symmetry, but different types of Jahn-Teller distortions of MnO_6 octahedra and magnetic ordering of Mn atoms. Unusually great differences in the parameters of unit cells of the coexisting phases have contributed to the success of the structural analysis. The phase *P1* is ferromagnetic and the MnO_6 octahedra are only slightly distorted. The phase *P2* is antiferromagnetic (A-type of ordering) and the MnO_6 octahedra are strongly compressed along the apical direction. The volume fractions occupied by phases *P1* and *P2* in a crystal depend on the average radius of A-cation and upon substitution of ^{18}O for ^{16}O the balance between the phases is shifted towards the phase *P2*. The obtained data unambiguously point to a percolation nature of metal-insulator transition in compositions with Sm upon oxygen isotope substitution due to a sharp (from 65 to 13%) decrease in the volume of the ferromagnetic phase *P1*. The value of the ordered magnetic moment of Mn in phases *P1* and *P2* varies from 1.7 to 3.5 μ_B in all studied compounds. The data on the evolution of microstructural characteristics at a phase transition into a separated state testify that both the initial spread in A-cation radii and internal microstrains have a critical impact on the formation of mesoscopic phase separation.

A detailed neutron diffraction study of atomic and magnetic structure of 314-cobaltite $Sr_3YCo_4O_{10.5+\delta}$ (or $Sr_{0.75}R_{0.25}CoO_{2.625+\delta/4}$), wherein A-positions are perfectly ordered, has been carried out. Two compounds with different oxygen content: close to optimal ("as prepared", $\delta \approx 0$) and with increased δ ("oxidized", $\delta \approx 0.2$) have been investigated. In addition, the data for the compound, in which Co atoms are partially replaced by Fe, namely, $Sr_3YFe_2Co_2O_{10.5+\delta}$, have been obtained [**3**]. All three compositions have been found to have AFM structure of G-type (**Fig. 2**) and Co atoms occupying different positions in a unit cell have different magnetic moments.

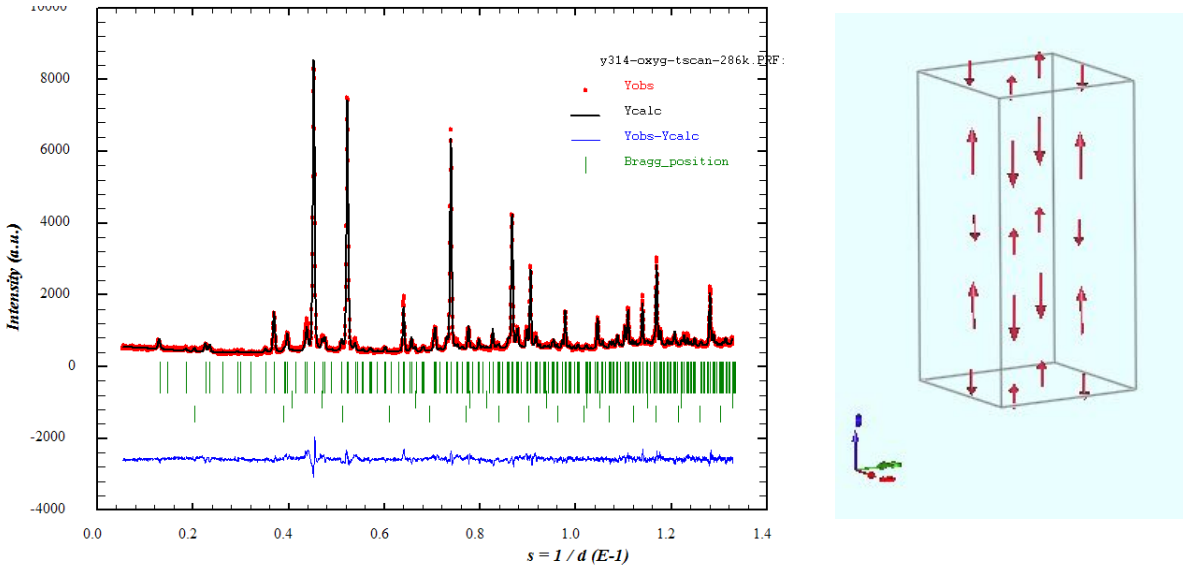

Fig. 2. Magnetic structure of $Sr_3YCo_4O_{10.5+\delta}$ at $\delta \approx 0$ and 0.2. The structure is antiferromagnetic of G-type, i.e. the moments of neighboring Co atoms are oppositely directed. Its specific feature is that Co atoms occupying different positions in a unit cell have different values of magnetic moment.

Structural changes, spin-state transitions of Co^{3+} ions and insulator-metal transitions in lanthanum cobaltite $LaCoO_3$ have been studied [**4**] in a wide range of temperatures (10-900 K) and pressures (0-20 GPa) (**Fig. 3**). It has been found that pressure induces sharp suppression of magnetic intermediate-spin state (S = 1) and stabilization of nonmagnetic low-spin state (S = 0) of Co^{3+} ions. The insulator-metal transition temperature significantly increases under pressure.

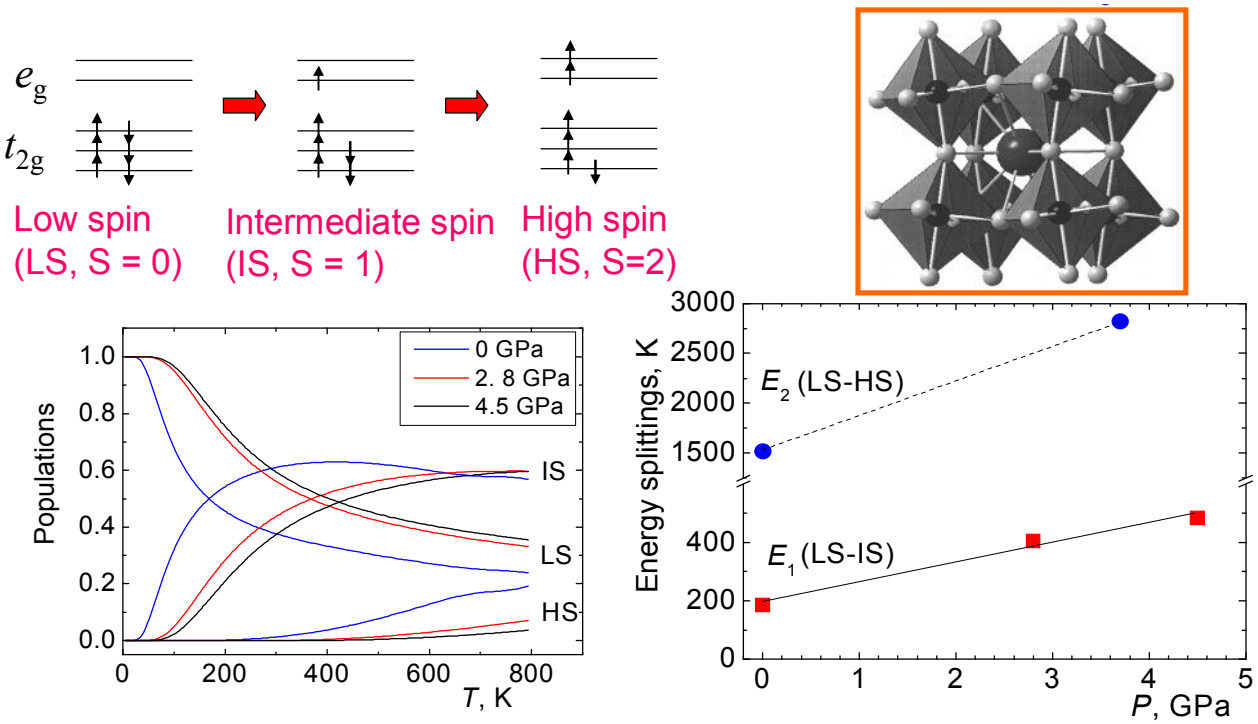

Temperature dependencies of LS, IS and HS states populations in $LaCoO_3$ at different pressures

LS-IS and LS-HS energy splittings as functions of pressure

Fig. 3. Illustrations to the studies of structural changes, spin-state transitions of Co^{3+} ions and insulator-metal transitions in lanthanum cobaltite $LaCoO_3$ in a wide range of temperatures (10-900 K) and pressures (0-20 GPa). Possible spin configurations for Co^{3+} ion including low spin (S=0), intermediate spin (S=1) and high spin (S=2) states are shown at the top left.

Preliminary studies of high pressure effects on the crystal and magnetic structure of some compositions of manganites and cobaltites have been conducted. Under high pressures in $Pr_{0.7}Ba_{0.3}MnO_3$ the suppression of the initial FM state and the appearance of A-type AFM state are observed. At normal pressure in $Pr_{0.7}Ba_{0.3}MnO_{2.6}$ an intermediate G-type AFM state and ground spin-glass state have been revealed. Under pressure the magnetic phase transitions have not been observed. For the cobaltite $PrCoO_3$ at high pressures up to 8.7 GPa at room temperature it has been found that this compound retains orthorhombic structure over the whole studied pressure range. A weak anisotropy of compression of CoO_6 oxygen octahedra has been revealed.

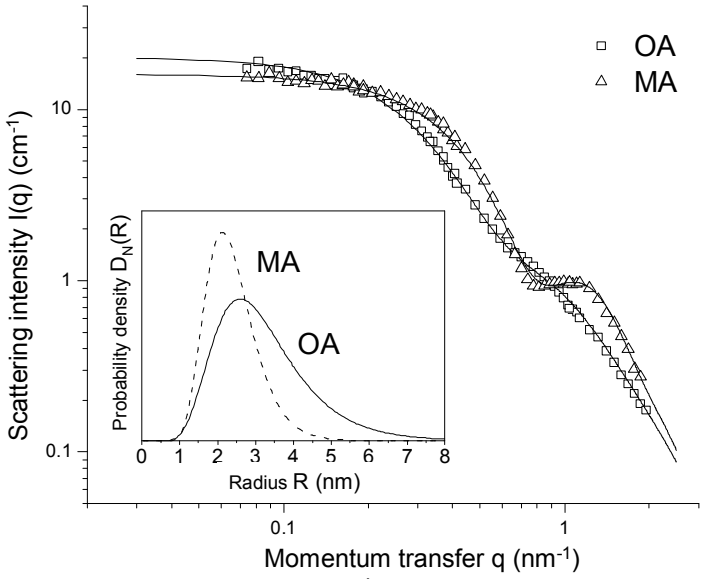

Fig. 4. Nuclear scattering curves $\langle F_N^2(q)\rangle_R$ averaged over the size distribution function of magenetite nanoparticles for magnetic fluids stabilized with oleic (OA) and myristic (MA) acids. The curves are obtained from the treatment of 2D scattering data for polarized neutrons (GKSS). Solid lines show the best fits of the model of non-interacting core-shell particles using the size distribution function of log-normal type. The obtained polydispersity functions are given in the inset.

The analysis of the structural data obtained using small-angle scattering of non-polarized and polarized neutrons for magnetic fluids in organic non-polar media has been performed. The possibility to use short chain length mono-carboxylic acids (lauric, $C_{12}H_{24}O_2$, and myristic, $C_{14}H_{28}O_2$, saturated acids) for stabilizing magnetite nanoparticles has been studied [**5**]. It has been demonstrated that these acids can be used for the synthesis of highly stable magnetic fluids. The structure of new fluids have been compared with that of magnetic fluids stabilized by unsaturated oleic acid $C_{18}H_{34}O_2$ with a C=C double bond kink in the middle of its tail. Great differences have been revealed in the size distribution function of stabilized magnetite, particularly a decrease in the mean particle radius and polydispersity index when short chain length acids are used instead of oleic acid (**Fig. 4**). Thus, if oleic acid stabilizes magnetite over a wide radius interval of 1-10 nm, shorter acids stabilize only a fraction of smaller particles from this interval. It follows from the comparison of the effective thickness of acid shells (obtained by fitting) about the magnetite (~1.4 nm in both cases) that the origin of the observed size regulation effect is connected with different acid organization on the magnetite surface, which determines elastic properties of the stabilizing shell. The study has been carried out in cooperation with the GKSS Research Centre (Geesthacht, Germany), the Budapest Neutron Center (Hungary) and the Center of Fundamental and Advanced Technical Research of the Romanian Academy of Sciences (Timisoara Branch, Romania).

On the basis of small-angle neutron scattering experiments on magnetic fluids the verification of the new basic functions approach in the contrast variation technique for polydisperse multicomponent and superparamagnetic systems [**6**] has been continued. In cooperation with the GKSS Research Centre (Geesthacht, Germany) and the Center of Fundamental and Advanced Technical Research of the Romanian Academy of Sciences (Timisoara Branch, Romania) the comparative experiments on the magnetite/oleic acid/benzene and magnetite/myristic acid/benzene ferrofluids have been carried out. The analysis of the behaviour of squared radius of gyration versus the inverse contrast from the contrast variation data (**Fig. 5, a, b**) makes it possible to specify parameters of the particle size distribution function for stabilized magnetite as well as estimate the thickness of the surfactant shell. The contrast variation data have been compared with the results of the direct modeling in the polarized neutron scattering experiments [**5, 7**]. In cooperation with the University of Pierre and Marie Curie (France) and the GKSS Research Centre the analogous analysis has been made [**8**] for the data of contrast variation on water-based ferrofluids with ionic stabilization (**Fig. 5, c**). Due to the small effect of the scattering from the stabilizing shell (citrate molecules) it is possible in a more explicit way to separate the nuclear and magnetic sizes of particles in the fluid by means of contrast variation.

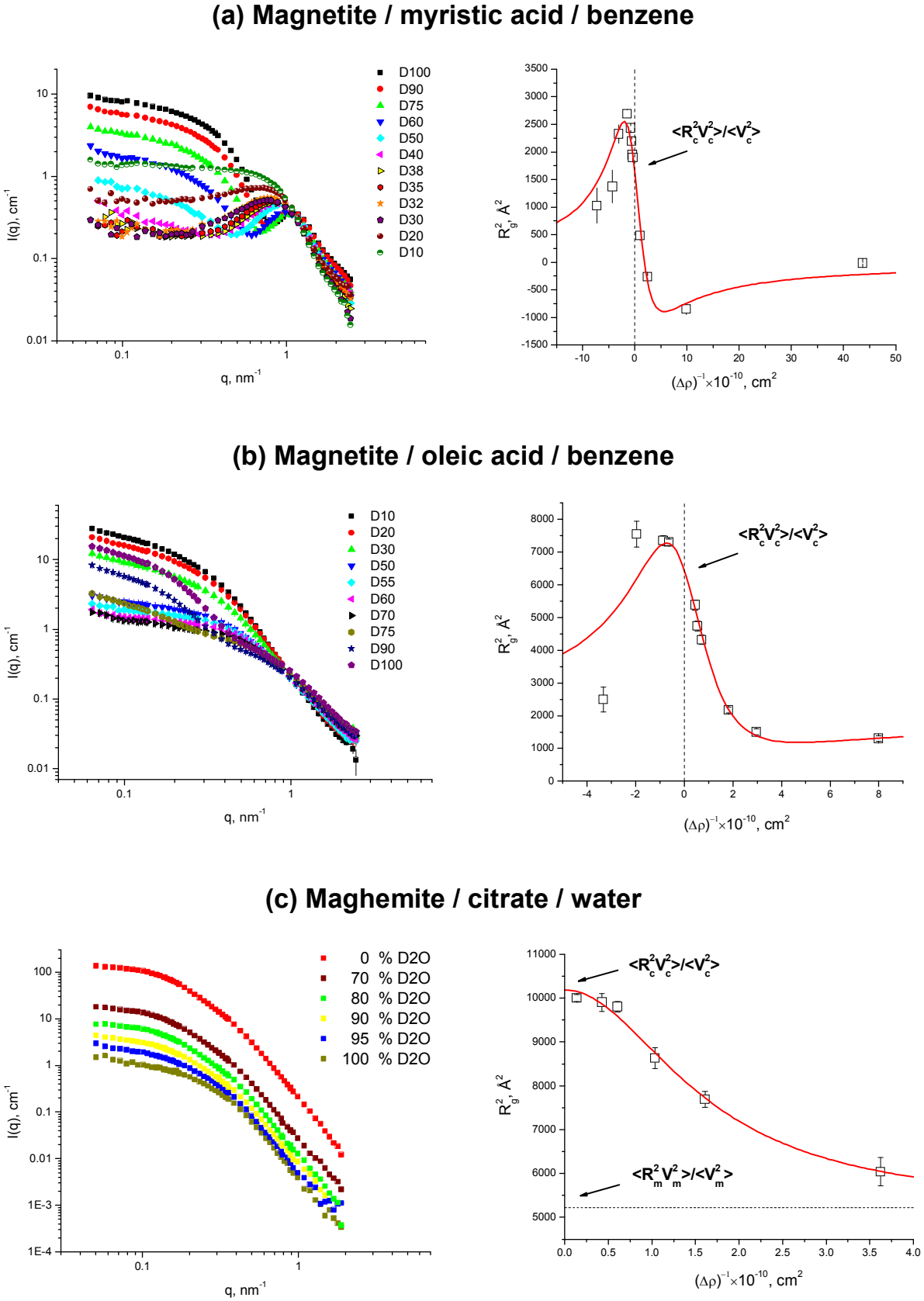

Fig. 5. Contrast variation for different types of ferrofluids. Experimental curves for different content of deuterated solvent in the liquid carrier (indicated in the sample labels) are given at the left. The behavior of the visible squared radius of gyration versus the inverse contrast in the system is shown at the right. Lines correspond to theoretical curves.

The study of surfactant solutions used in stabilization of ferrofluids has continued. In cooperation with the Budapest Neutron Center the experiments on small-angle neutron scattering from solutions of surfactants (oleic, myristic, stearic acids) in a non-polar liquid (D-benzene) have been performed. Using the dependence of the scattering on the concentration of the solute the character of interaction between acid molecules has been analyzed. A significant influence of the van der Waals attraction on the behavior of the acid molecules in solutions has been revealed, which explains a shift towards small acid concentrations in the transformation from isotropic liquid to liquid-crystal state, especially in the case of stearic acid solutions [**9**]. In cooperation with LRB JINR the simulations of molecular dynamics of the solvent at the interface with the dissolved acid molecule have been performed [**10**]. It has been shown that the organization of the solvent on the molecular surface differs only slightly for three acids. This points out to the fact that the solvent-solute interaction cannot explain the difference in the behavior of these acids in solutions. Thus, the main component in the interaction, which determines such differences, is the van der Waals interaction.

In cooperation with the Institute Laue Langevin (France) the studies of stable nanocomposite lamellar films on the basis of symmetric diblock copolymers with Fe_3O_4 nanoparticles have continued. The reflectometry and GISANS experiments have been carried out. It has been determined that the nanoparticles form periodic layers within a polymer matrix. Depending on the volume concentration and size of nanoparticles, new structural mesophases predicted earlier theoretically have been revealed for the first time. A new structural transition has been observed and it has been demonstrated that in complex nanocomposite systems not only the matrix structure determines the ordering of the ensemble of nanoparticles, but also the nanoparticles influence the morphology of nanocomposite films. By increasing the concentration of nanoparticles, the conditions have been found under which the lamellar structure becomes unfavourable because of the arrangement of nanoparticles only within polystyrene. This leads to morphological changes resulting in the formation of cylindrical structure. The investigations have been conducted with three sets of films of different thicknesses and volume fraction of nanoparticles from 0% to 50%. The nanocomposite films based on asymmetric diblock copolymers and nanoparticles with the volume fraction from 0% to 15% have been studied as well.

Within the framework of the studies of fullerene dispersions in low-polarity nitrogen-containing solvents and their mixtures the experiments on time-of-flight mass-spectroscopy have been carried out. The results of the investigations of cluster organization in the systems C_{60}/N-methil-2-pyrrolidone (C_{60}/NMP) and C_{60}/N-methil-2-pyrrolidone/water have substantiated the conclusions about the sizes and density of the clusters in the system made earlier on the basis of small-angle neutron scattering experiments. It has been shown that the cluster decomposition in the system C_{60}/NMP on addition of water is due to the detachment of monomers, but at the same time the detachment of clusters with a number of fullerene molecules from 2 to 14 is not observed. The modeling of experimental UV-Vis data has been performed to estimate the contribution of the Mie scattering to optical curves. According to the results of modeling, the reason for the solvatochromic effect in the system C_{60}/NMP is the transition of fullerene molecules into a new electron state connected with the formation of donor-acceptor C_{60}–NMP complexes in the solution. The formation of C_{60}–NMP complexes in the system has also been confirmed by the mass-spectroscopy measurements [**11-13**].

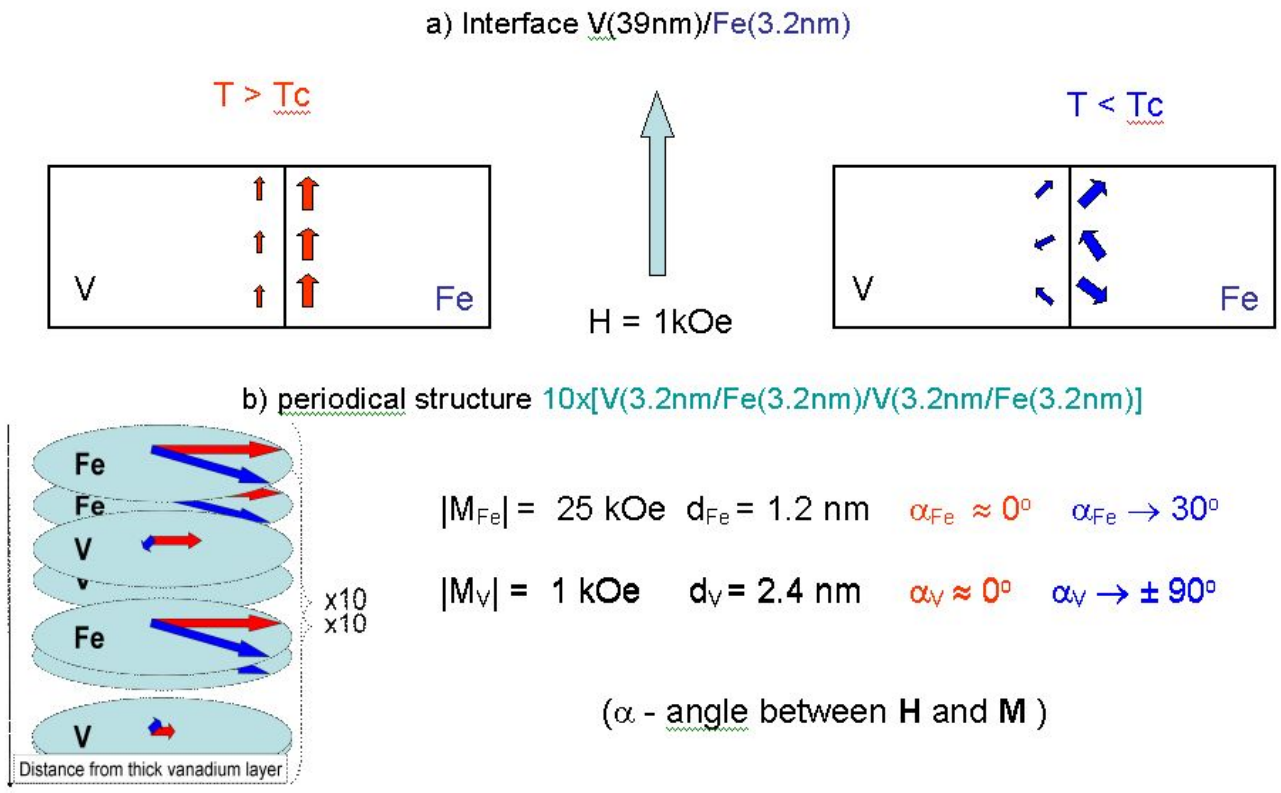

Fig. 6. a) Distribution of magnetization near the interface in the bilayer V(39nm)/Fe(3.2nm). At T = 7 K > T_C in a magnetic field of 1 kOe the area in the vicinity of the interface is magnetized. At the transition to the superconducting state (T_C = 3.7 K) at T= 3 K the state appears to be demagnetized. The demagnetized state is energetically more favourable, since the magnetic field acting on the superconducting pair proves to be less than in the case of the magnetized state.

b) Distribution of magnetization in the periodic structure. At the transition to the superconducting state the magnetic ordering of both the magnetization of iron layers and the induced magnetization of vanadium layers undergoes a change. The vanadium layers are ordered antiferromagnetically, which, in principle, supports the theoretical conclusions.

At the REMUR spectrometer the ferromagnetic-superconducting layered structure V(39nm)/Fe(3.2nm)/10×[V(3.2nm)/Fe(3.2nm)] (**Fig. 6**) consisting of a superconducting layer of vanadium V(39nm) and periodic structure 10×[V(3.2nm)/Fe(3.2nm)] has been studied by neutron reflectometry using standing waves of polarized neutrons [**14**]. For the first time, at the transition of a vanadium layer to the superconducting state, the phenomena of formation of a domain structure in the vicinity of vanadium-iron interface and antiferromagnetic ordering in a periodic structure have been observed. Thus, it has been demonstrated that the magnetic state of nanostructures can be controlled using the superconducting transition. This opens up possibilities of designing principally new logic elements for nanoelectronics, in which the state can be encoded both by the magnetic moment value and the resistance.

The magnetic and magnetotransport properties of composite nanogranulated cobalt-based films have been investigated. In nanocomposite alloys $(Co)_x(SiO2)_{1-x}$ near the percolation threshold a magnetic phase transition with the formation of fractal structures has been detected. The obtained experimental data [**15**] testify that in nanocomposite granulated systems in the range of the structural percolation threshold the magnetic fractal structures are formed, which, in fact, determine the magnetic properties of composites including magnetoresistance.

At the YuMO spectrometer the influence of dimethyl sulfoxide (DMSO), a well-known organic solvent, which is widely used in cell biology, cryobiology, pharmacology, medicine and

agriculture, on the structure of lipid membranes of phospholipids (DMPC) has been investigated over a wide range of DMSO molar concentrations $0.0 \leq X_{DMSO} \leq 1.0$ in an excess of a solvent at temperatures T = 12.5 and 55°C. The dependences of the repeat distance d of multilamellar membranes and the thickness d_b of single vesicles on the molar concentration X_{DMSO} in the $L_{\beta'}$ gel and L_{α} liquid-crystalline phases in an excess of a water-DMSO solvent have been determined. The intermembrane distance d_s has been determined from the repeat distance d and the membrane thickness d_b. It has been shown [**16**] that an increase in the molar concentration X_{DMSO} leads to a considerable decrease in the intermembrane distance and that at X_{DMSO} = 0.4 the neighboring membranes are virtually in steric contact with each other, which results in the fusion of single membranes into multilamellar structures. The use of the contrast variation method makes it possible for the first time to determine the number of DMSO molecules strongly bound to the membrane. The number of these molecules for one polar head of the lipid molecule is 6.9 and their total volume is 820 $Å^3$, which is comparable to the volume of the polar head of the lipid molecule and accounts for the previously observed phase transition of the lipid membrane to the phase characterized by interdigitation of chains.

The ultrastructure of rat liver and heart mitochondria has been investigated by small-angle neutron scattering [**17**] at the YuMO spectrometer. The influence of low tonicity of incubation medium on the change in the inner mitochondrial membrane packing has been studied. The analysis of interference peaks has revealed that under the effect of low tonicity the ordered lamellar packing of the membranes undergoes a transition to an ordered nonlamellar (presumably hexagonal) packing. The electron microscopy data also give evidence in favour of hexagonal packing. Experiments to study the structure of mitochondrial mitoplasts by atomic-force microscopy have been started. The purpose of the experiments is to prove the existence of multi-enzyme lipid-protein complexes participating in oxidative phosphorylation.

Antibiotic amphotericin B (AmB) widely used in medicine has been studied by small-angle neutron scattering, X-ray diffraction and Fourier spectroscopy. The results of the experiments [**18**] have shown that AmB is located predominantly in the headgroup region of the membrane at concentrations below 1 mol%. At concentrations above 1 mol% the process of AmB aggregation takes place. The effect of association arises and AmB incorporates into the hydrophobic membrane core.

Work to search for new experimental techniques complementary to neutron scattering for studying the magnetic fluid properties has been carried out. For the first time the μSR-method has been applied to investigate the magnetic fluid properties [**19**]. The ferrofluid on the basis of D_2O with Fe_3O_4 nanoparticles has been studied in the temperature range from 114 to 300 K in zero and transverse magnetic field conditions. A distinct μSR-signal has been observed in both cases. In zero field measurements a drop in the relaxation rate and muon spin polarization to zero level at T = 230 K followed by fast increasing of the latter in the temperature interval of 240 - 255 K have been observed. The investigation has been performed in cooperation with the Dzhelepov Laboratory of Nuclear Problems.

For the first time the existence of open inner cavities in the effective dendrimer volume accessible to a solvent has been demonstrated and their volume fraction has been estimated. It has been shown [**20**] that the end groups of dendrimers are located in its surface layer. The application of novel mathematical treatment techniques has made possible not only size determination but also *ab initio* shape reconstruction for dendrimers of various generations for three and four functional dendrimers (**Fig. 7**). A new model for interpreting the results of small-angle neutron scattering from dendrimer solutions has been proposed. Within its frameworks the inner dendrimer sphere has been demonstrated to be permeable to a solvent, whose density is lower than the density of the solvent beyond the dendrimer by a factor of at least 2.

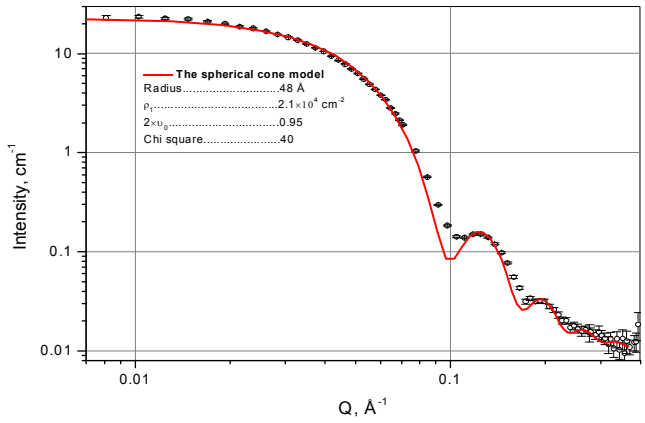

SANS data approximated by analytical curve for the model of spherical sectors.

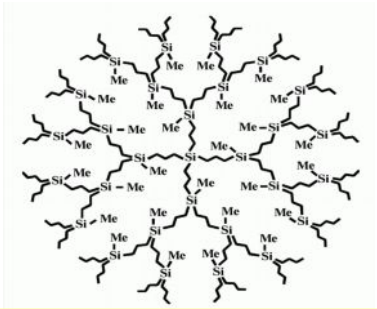

Chemical structure of dendrimer molecule and its 3D model.

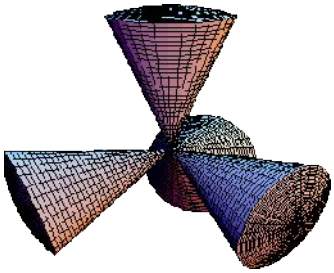

Fig. 7. Small-angle neutron scattering data, structural chemical formula and 3D structural model of four functional dendrimers.

Neutron diffraction is an exceptionally powerful method for studying structures of biological and model lipid membranes. In particular, by varying the relative content of light and heavy water, it is possible to reliably determine phases of structural factors. One more favourable point is the possibility to carry out *in-situ* experiments in real time. On the DN-2 diffractometer one can follow changes in the membrane structure in the course of hydration with time resolution at a level of 1 min (**Fig. 8**). In 2007 the experimental evidences for the phenomenon of reinforcement of the lipid matrix of the outermost layer of mammalian skin, the stratum corneum (SC) by ceramide 6 molecules were obtained. In a series of neutron diffraction experiments it has been found [**21**] that the extremely strong intermembrane attraction created by ceramide 6 molecules cannot be destroyed either by long-chain ceramides or long-chain fat acids. The small-angle neutron scattering experiments have shown that the interaction created by ceramide 6 molecules is short-range (**Fig. 9**). The stability of the developed SC membrane to variation of biochemical composition of lipids and water solutions has made it possible to begin experiments to study the substances that can increase the permeability of human skin for drug delivery.

Complex investigations [**22**] into the physical properties of synthetic quartz single crystals and quartz powders in the temperature range of the α-β transition with the use of neutron diffraction and mechanical spectroscopy have been carried out. New data on the behaviour of parameters of a unit cell of quartz powders of two fractions with different average sizes of grains at room temperature and in the temperature range of 540-620°C, as well as atomic coordinates in a unit cell have been obtained. It has been found that the lattice parameters of the powders that vary in the size of grains by an order of magnitude, differ significantly. The α-β phase transition temperature of a fine-grained powder is higher than that of a coarse-grained one by ≈15 ºC (lies in the range of 580-585 ºC).

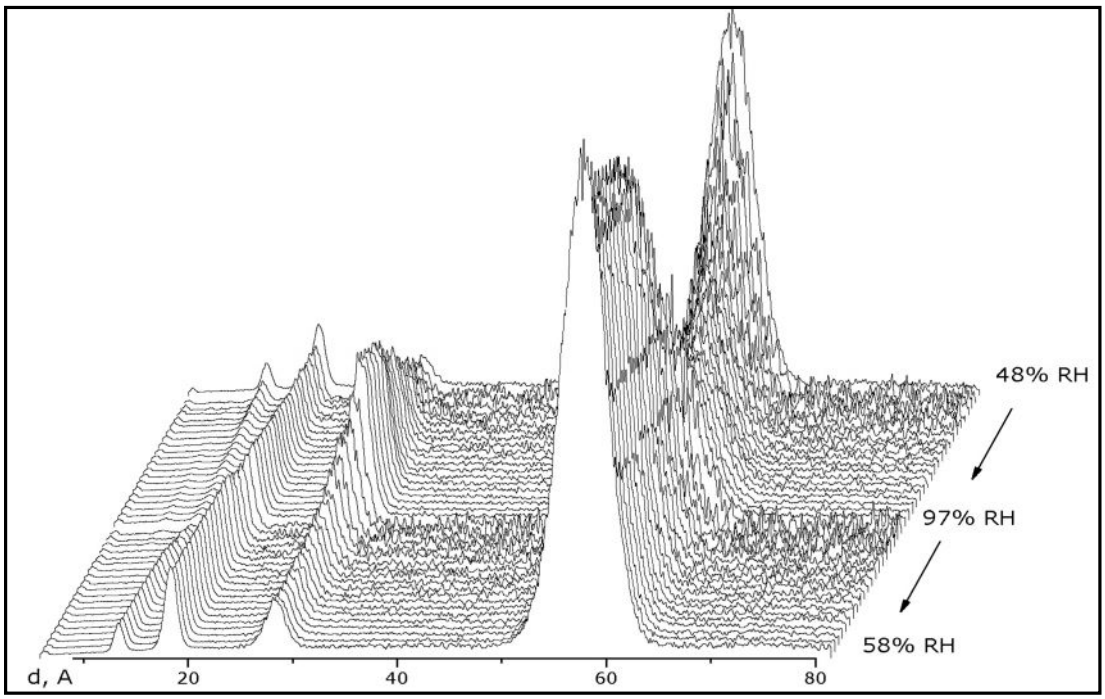

Fig. 8. Real-time diffraction makes it possible to efficiently investigate structure and phase transitions in lipid membranes. On the DN-2 diffractometer one can follow changes in the membrane structure in the course of hydration with time resolution at a level of 1 min.

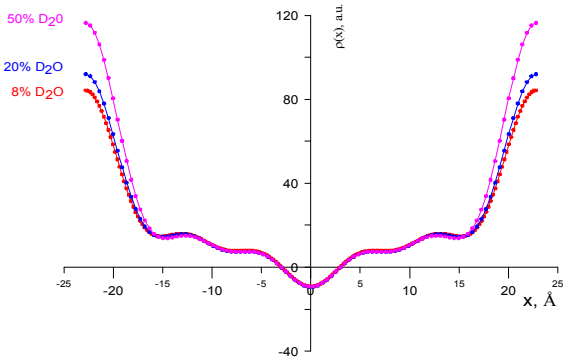

Calculated neutron scattering density profile for basic membrane at T=32°C and 60% humidity.

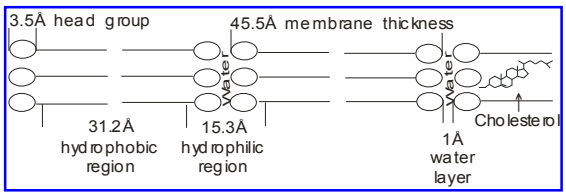

Structural results for fully hydrated quaternary Ceramide 6/Cholesterol/Palmitic Acid/Cholesterol sulfate membrane

Fig. 9. Fourier neutron scattering density profile reconstructed from neutron diffraction data (left) in the direction perpendicular to the membrane plane. Its peculiarity is a small gap (about 1 Å) between neighbouring bilayers (right).

At the DIN-2PI spectrometer the diffusion processes in liquid lithium (T = 500K and 830K) and lithium-hydrogen melt (T = 830 K, content of hydrogen impurity ~ 1 % at.) have been investigated by the quasi-elastic slow neutron scattering technique [**23**]. The found characteristics of diffusion processes for pure lithium and, in particular, self-diffusion coefficient are in good agreement with the calculations and the results obtained by the capillary method. It has been found

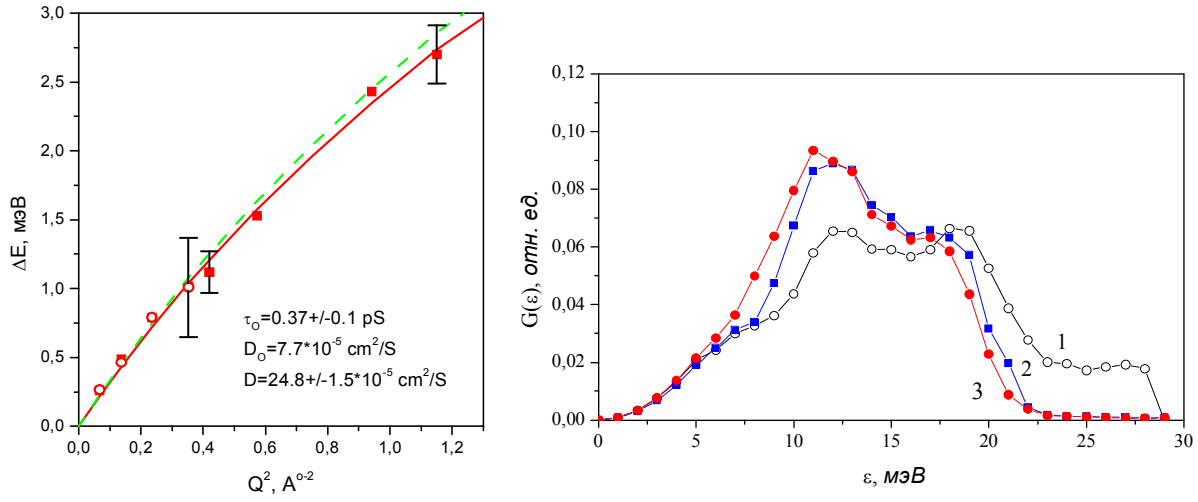

The width of quasielastic scattering for Li-H mixture (full symbols) and H in Li (open symbols) at T=830 K as a function of Q^2.

Density of phonon states for Ta at 293 K (1), 1584 K (2) and 2300 K (3).

(*a*) (*b*)

Fig. 10. Examples of the experimental results obtained with the DIN spectrometer. The dependencies of quasielastic scattering peak width on momentum transfer for Li-H mixtures (left) and of density of phonon states in tantalum for various temperatures (right). For the first time we succeeded in performing neutron inelastic scattering measurements at a temperature of 2300 K.

that the character of hydrogen diffusion processes in lithium-hydrogen melt is practically indistinguishable from the diffusion of lithium atoms (**Fig. 10a**). This testifies that in the above-mentioned conditions hydrogen is present in the melt as lithium hydride LiH.

For the first time, neutron inelastic scattering spectra have been obtained for Group V transition metal Tantalum (Ta) in the temperature range from room temperature to 2300 K (**Fig. 10b**). To obtain the required temperature of the sample, a recently constructed high-temperature thermostat TS3000 was used. The accuracy of the obtained spectra appeared to be sufficient to reconstruct the phonon state density G(ε) of tantalum for all temperatures of the measurement. The reconstruction of frequency spectra was performed by the successive iteration technique with due regard for the multiphonon neutron scattering effect. No satisfactory explanation of the temperature evolution of the frequency spectra has been provided yet and the problem calls for further investigation, in particular, for the evaluation of influence of electron-phonon interaction.

II. Instrument developments

In 2007 on IBR-2 the reconstruction of the neutron guide system of the SCAT, EPSILON and NERA spectrometers was started. The work is conducted within the framework of the BMBF project in cooperation with the personnel of the SC Department. According to the approved requirements specification a sketch design of the mechanical and optical units of the neutron guide system has been made and the tie-in of the available constructions of the neutron guide channels located in the ring corridor and the experimental hall has been carried out with reference to real building constructions.

In cooperation with the Research Centre Jülich the neutron spin-echo technique based on the rotation of magnetic field has been studied. The magnetic field was created by the system of two perpendicular to each other coils with a foil sandwiched between them, whose magnetic properties had been studied. The analysis of the dependence of internal magnetization of the foil on an insignificant external magnetic field has been performed. The mathematical model of the behavior of the spin as a neutron beam passes through a magnetic field created by the system of two coils with a magnetic foil in between has been developed. It adequately describes the experimental data [**24**].

On channel 10 of IBR-2 the multifunctional reflectometer GRAINS will soon be constructed in place of the available spectrometer KDSOG. A special feature of the reflectometer, a vertical scattering plane, will make it possible to study reflection from liquid media (including polarized neutrons for investigations of interfaces with magnetic nanoparticles). The reflectometer will operate in the time-of-flight mode, which will allow the experiments to be conducted at fixed orientations of the incident beam and the sample. Additional modes of the GRAINS reflectometer will comprise: (1) possibilities to study off-specular reflection and GISANS scattering; (2) angular encoding in a horizontal plane with Larmor precession of neutron spin; (3) 3D polarimetry on the basis of Larmor precession of neutron spin. In April of 2007 the concept of the reflectometer within the framework of the respective project was supported by JINR PAC for Condensed Matter. The design of the reflectometer and techniques to be realized on the facility have been reported and discussed at a number of scientific Workshops and Conferences. Draft design (**Fig. 11**) and technical project have been completed.

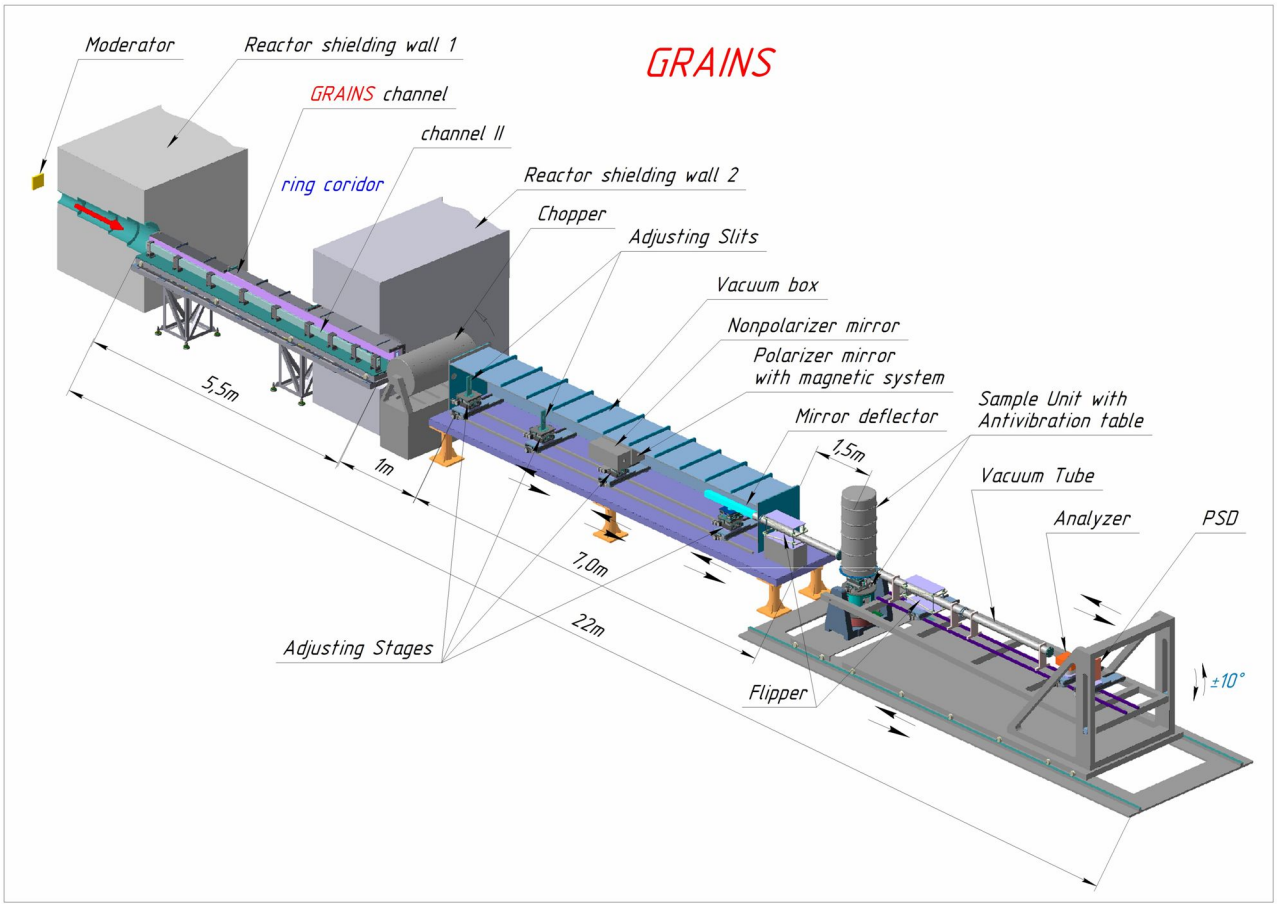

Fig. 11. General layout of the new neutron reflectometer GRAINS at the IBR-2M reactor. The neutron source is at the right; the total flight path is about 30 m.

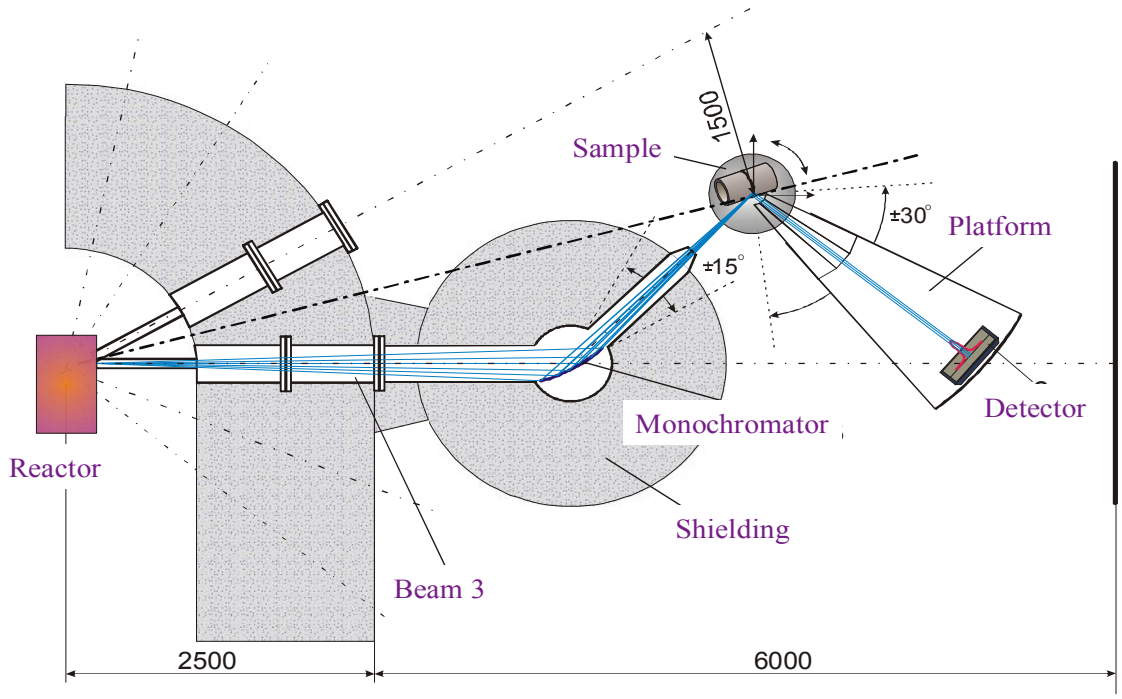

Fig. 12. Principal schematic of a new neutron diffractometer at the IR-8 reactor in RRC KI intended to study internal stresses in bulk samples. The diffractometer is designed according to a classical two-axis scheme, but with the application of state-of-the-art technologies in primary neutron beam monochromatization and scattered neutron detection.

In the framework of the Protocol on Cooperation with RRC KI the designing of neutron diffractometer for studying internal stresses in bulk samples on the IR-8 reactor (**Fig. 12**) has been started. The concept of the diffractometer supposes the use of modern technologies of forming neutron beams and of detecting scattered neutrons. This diffractometer will provide complementary possibilities as to the available stress-diffractometer FSD at IBR-2.

For further development of the experimental base on IBR-2 and within the framework of cooperation with the NECSA Corporation (Republic of South Africa) a contract for the purchase of an automated materials testing machine (**Fig. 13**) has been concluded. The machine allows on-line experiments to be performed with a wide set of loading (stationary or cyclic) modes on any type of neutron diffractometers with bulk samples of metals and alloys.

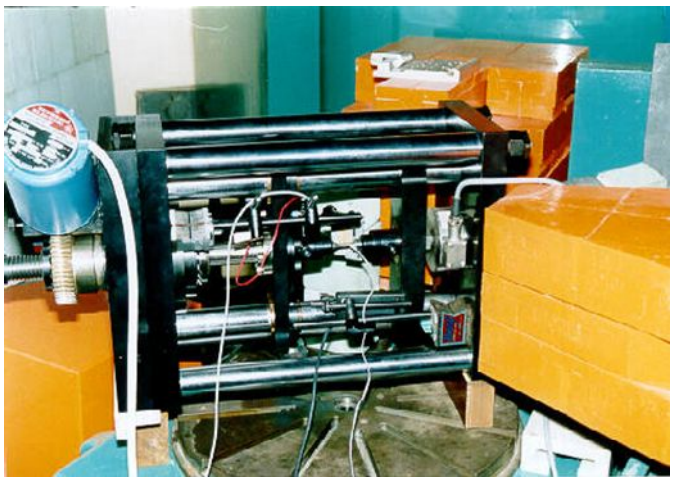

Fig. 13. External view of the materials testing machine for on-line experiments with metals and alloys. Machine operates in several static and dynamic (cyclic) regimes.

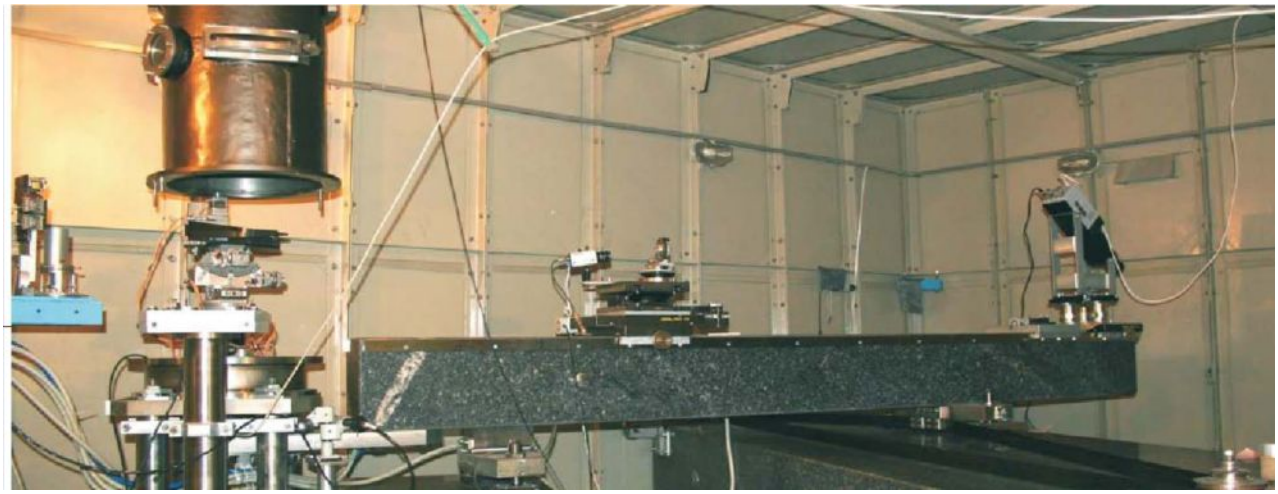

Fig. 14. General view of the energy-dispersive EXAFS-spectroscopy station manufactured by JINR at the SIBIR-2 synchrotron radiation source in RRC KI.

In the spring of 2007 the physical startup of the energy-dispersive EXAFS-spectroscopy station (**Fig. 14**) at SIBIR-2 was performed and the first results were obtained. Its distinctive feature is the possibility to obtain absorption spectra in a very short time — less than 10^{-3} s as compared to classical EXAFS-stations where it takes ~ $10^3 \div 10^4$ s. This opens up a possibility to study dynamic processes proceeding under the action of external factors. The experimental procedure was trialed in the measurements of X-ray absorption spectra (EXAFS-and XANES-regions) at the Co *K*-edge in $La_{1-x}Sr_xCoO_3$ (x = 0 and 0.5) carried out in the Hamburg Synchrotron Radiation Center in the framework of the Agreement between the Laboratory HASYLAB (DESY) and Kurchatov Center of Synchrotron Radiation.

The test experiments have been carried out at the MEDIANA station of the SIBIR-2 synchrotron source in RRC KI. In particular, at the MEDIANA station the possibilities to conduct high-pressure experiments with sapphire anvil cells and *in situ* experiments to study hydrogenation processes of electrolytic deposits in electrochemical cells have been explored. It has been demonstrated that both types of experiments can produce valuable results.

The calculations to estimate the efficiency of use of the mirror neutron guide for various geometries of the beam of the DIN-2PI spectrometer have been carried out, a draft design of the neutron guide and main units for its assembling and positioning at the neutron beam has been developed, the components for mirror segments of the neutron guide have been purchased. The dismantling of radiation shielding of the spectrometer has been completed in order to install the mirror neutron guide.

On the basis of the analysis of the results of these calculations a conclusion has been drawn on the optimal variants of geometry and reflective coating of the planned mirror neutron guide, namely:

- the coating with the double critical angle is optimal from the view point of the “gain/price” ratio;
- the mirror neutron guide 12.5 m long, with the input window 200×22 mm^2 and the output window 70×120 mm^2 is optimal from the geometrical view point in the case of the DIN-2PI spectrometer;
- the proposed size of the output window makes it possible to work with samples of the investigated material of the characteristic dimension 50x100 mm^2 under the condition that such sample is in the neutron flux of constant intensity both in the vertical and in the horizontal planes.

Thus, the projected mirror neutron guide will make it possible to solve two chief tasks: to increase the intensity of cold neutrons (E < 5 MeV) on sample by a factor of 4-6 and, simultaneously, to decrease the sizes of the investigated samples by a factor of 2-3. The solution of both these tasks will allow significant improvement of quality of the DIN-2PI spectrometer and enhancement of its characteristics to put it on par with the best foreign analogues.

References

1. V.Yu.Pomjakushin, D.V.Sheptyakov, K.Conder, E.V.Pomjakushina, A.M.Balagurov. Phys. Rev. B, 2007, v. 75, p. 054410.
2. A.M.Balagurov, I.A.Bobrikov, V.Yu.Pomjakushin, D.V.Sheptyakov, N.A.Babushkina, O.Yu.Gorbenko, M.S.Kartavzeva, A.R.Kaul. JETP (accepted).
3. D.V.Sheptyakov, O.A.Drozhzhin, V.Yu.Pomjakushin, S.Ya.Istomin, I.A.Bobrikov, E.V.Antipov, A.M.Balagurov. "Crystal and magnetic structures of $Sr_3YCo_4O_{10.5+\delta}$: Y-314 phases with different oxygen content" (in press).
4. D.P.Kozlenko, N.O.Golosova, Z.Jirak, L.S.Dubrovinsky, M.Tucker, Y.LeGodec, B.N.Savenko. Phys. Rev. B, 2007, v. 75, p. 064422.
5. M.V.Avdeev, D.Bica, L.Vékás, O.Marinica, M.Balasoiu, V.L.Aksenov, L.Rosta, V.M.Garamus, A.Schreyer. J. Mag. Mag. Mater., 2007, v. 311, p. 6.
6. M.V.Avdeev. "Contrast variation in small-angle scattering experiments on polydisperse and superparamagnetic systems: basic functions approach". J. Appl. Cryst. 40 (2007) 56-70.
7. A.V.Feoktystov, M.V.Avdeev, V.L.Aksenov, L.A.Bulavin, D.Bica, L.Vekas, V.M.Garamus, R.Willumeit. Contrast variation in small-angle neutron scattering from magnetic fluid magnetite/myristic acid/benzene, Surface Investigations. Accepted.
8. M.V.Avdeev, E.Dubois, G.Mériguet, E.Wandersman, V.Garamus, A.V.Feoktystov, R.Perzynski. SANS analysis of a water-based magnetic fluid with charged stabilization: contrast variation and scattering of polarized neutrons, submitted to J. Appl. Cryst.
9. V.I.Petrenko, M.V.Avdeev, L.A.Bulavin, V.L.Aksenov, L.Almásy, L.Rosta, V.Garamus. Interaction of mono-carboxylic acids in benzene by small-angle neutron scattering, submitted to Chem. Phys. Lett.
10. I.A.Bodnarchuk, Kh.T.Kholmurodov, V.I.Petrenko, M.V.Avdeev. Partial Volume of Fatty Acids in Benzene by Molecular Dynamic Simulations, submitted to Rus. J. Chem. Phys.
11. V.L. Aksenov, M.V. Avdeev, O.A. Kyzyma, L. Rosta, M.V. Korobov. Age effect of solution C_{60}/N-methilpyrrolidone on the cluster structure in the system C_{60}/N-methilpyrrolidone/water // Crystallography Report, 2007, v. 52, pp. 523-527.
12. O.A.Kyzyma, L.A.Bulavin, V.L.Aksenov, M.V.Avdeev, T.V.Tropin, M.V.Korobov, S.V.Snegir, L.Rosta. Aggregation in C_{60}/NMP, C_{60}/NMP/water and C_{60}/NMP/Toluene mixtures. Fullerenes, Nanotubes and Carbon Nonstructures. Accepted.
13. E.A.Kyzyma, M.V.Avdeev, V.L.Aksenov, L.A.Bulavin, S.V.Snegir, Reorganization of fullerene clusters in C_{60}/N-methyl-2-pyrrolidone/water, Surface Investigations. Accepted.
14. V.L.Aksenov, Yu.V.Nikitenko, A.V.Petrenko, V.M.Uzdin, Yu.N.Khaidukov, H.Zabel. Crystallography Reports, 2007, v. 52, p. 403.
15. M.E.Dokukin, N.S.Perov, Ye.B.Dokukin, A.Kh.Islamov, A.I.Kuklin, Yu.E.Kalinin, A.V.Sitnikov. Bulletin of the Russian Academy of Sciences. Physics, 2007, v. 71, p. 1643.
16. Yu.Ye.Gorshkova, V.I.Gordeliy. Investigation of the interaction of dimethyl sulfoxide with lipid membranes by small-angle neutron scattering. Crystallography Reports, 2007, v. 52, pp.584–588.
17. T.N.Murugova, V.I.Gordeliy, A.I.Kuklin, I.M.Solodovnikova, L.S.Yaguzhinsky. Study of three-dimensionally ordered structures of intact mitochondria by small-angle neutron scattering. Crystallography Reports, 2007, v. 52, pp.545-548.
18. M.Here, A.Islamov, A.Kuklin, M.Gago, W.I.Gruszecki. Effect of antibiotic amphotericin B on structural and dynamic properties of lipid membranes formed with egg yolk phosphatidylcholine. Chemistry and Physics of Lipids 147 (2007) 78–86.

19. M.Balasoiu, D.Bica, L.Vekas, V.N.Duginov, K.I.Gritsaj, V.A.Zhukov, T.N.Mamedov, V.G.Olshevskiy, K.Petrescu. JINR communications, P14-2007-21, Dubna, 2007.
20. A.V.Rogachev, A.Yu.Cherny, A.N.Ozerin, V.I.Gordeliy, A.I.Kuklin. Spherical sector model for describing the experimental small-angle neutron scattering data for dendrimers. Crystallography Reports, 2007, v.52, pp. 546-550.
21. M.A.Kiselev. Crystallography Reports, 2007, v.52, p. 549.
22. A.N.Nikitin, G.V.Markova, A.M.Balagurov, R.N.Vasin, O.V.Alekseeva. Crystallography Reports, 2007, v.52, p. 450.
23. N.M.Blagoveshchenski, V.A.Morozov, A.G.Novikov, D.V.Savostin, V.V.Savostin, A.L.Shimkevich. Study of the microdynamics of liquid lithium and lithium-hydrogen melt by inelastic neutron scattering. Crystallography Reports, 2007, v.52, p.406.
24. A.Ioffe, V.Bodnarchuk, K.Bussmann. R.Müller. Larmor labeling by time gradient magnetic fields. Physica B, 397 (2007) 108-111.
25. M. Jernenkov, S. Klimko, V. Lauter-Pasyuk, B.P. Toperverg, H.J. Lauter, V.L.Aksenov, Larmor precession reflectometry for multilayer studies. Nucl. Instr. Methods A (2007) in press.

1. НАУЧНЫЕ ИССЛЕДОВАНИЯ

1.1. ФИЗИКА КОНДЕНСИРОВАННЫХ СРЕД

В связи с остановкой реактора ИБР-2 на проведение очередного этапа реконструкции, задачи коллектива отдела и планы работ по теме на 2007 г. заметно отличались от традиционных. А именно, научная работа была перенесена в родственные центры в России и за рубежом. Из фундаментальных и прикладных направлений, разрабатываемых сотрудниками отдела НИКС ЛНФ, в 2007 г. были оставлены несколько основных, работа по которым в других научных центрах, прежде всего нейтронных и синхротронных, была обеспечена существующими соглашениями о сотрудничестве. В 2007 г. начат первый этап программы модернизации спектрометров на реакторе ИБР-2.

I. Научные результаты

Подведены итоги многолетних исследований равновесных структурно-магнитных неоднородных состояний в сложных магнитных оксидах марганца. Получены количественные характеристики влияния на поляронное сужение зоны проводимости микронапряжений в решетке и объемной доли мезоскопических ферро- и антиферромагнитных кластеров. В соединении $(La_{1-y}Pr_y)_{0.7}Ca_{0.3}MnO_3$ обнаружен хорошо выраженный провал (**рис. 1**) в температуре перехода в упорядоченное магнитное состояние и подавление всех типов дальнего магнитного порядка вблизи точки перехода металл – изолятор $y \approx 0.9$, что указывает на ключевую роль химического беспорядка в структуре на формирование фазово-расслоенного состояния на мезоскопическом масштабе размеров. Установлено, что уровень внутренних микронапряжений является еще одним важным фактором, влияющим на эффекты фазового расслоения [**1**].

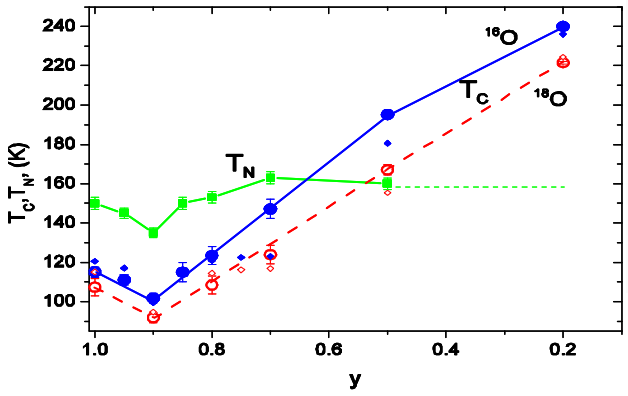

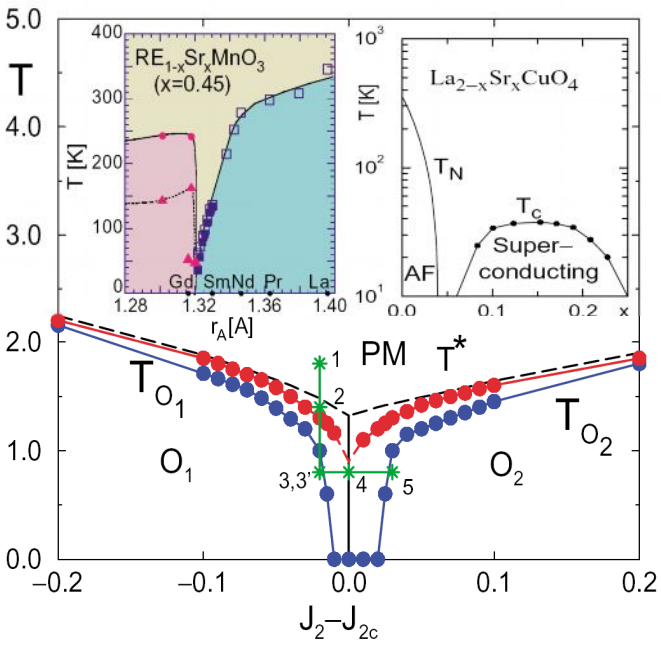

Рис. 1. Зависимости (слева) температур Кюри (T_C) и Неля (T_N) от содержания Pr в составе $(La_{1-y}Pr_y)_{0.7}Ca_{0.3}MnO_3$. Температура Неля не зависит от содержания изотопа кислорода ^{16}O или ^{18}O в образце, тогда как для температуры Кюри зависимость хорошо видна. Провал в значениях температур перехода при $y = 0.9$ соответствует предсказаниям модели замороженного химического беспорядка (J. Burgy et al., Phys. Rev. Lett. 2004), приводящего к флуктуациям интеграла перескока и мезоскопическому фазовому расслоению на АФМ-диэлектрическую и ФМ-металлическую фазы. Справа показана фазовая диаграмма, полученная на основе модельных расчетов.

Выполнена серия структурных нейтронных экспериментов по определению кристаллических и магнитных фазовых состояний перовскитоподобных манганитов $Re_{0.5}Sr_{0.5}MnO_3$ (Re = ^{152}Sm, $Nd_{0.772}Tb_{0.228}$ и $Nd_{0.544}Tb_{0.456}$) [**2**]. Эксперименты выполнены для выявления микроскопических причин гигантского кислородного изотопического эффекта, открытого недавно в $Sm_{1-x}Sr_xMnO_3$ для x ≈ 0.5. Показано, что при низких температурах во всех изученных составах происходит расслоение на две кристаллические фазы *P*1 и *P*2, которые имеют одинаковую пространственную симметрию, но различающиеся типы ян-теллеровских искажений октаэдров MnO_6 и магнитного упорядочения атомов Mn. Успеху структурного анализа способствовали необычно большие различия в параметрах элементарных ячеек сосуществующих фаз. Фаза *P*1 ферромагнитна и MnO_6 октаэдры лишь слегка искажены. Фаза *P*2 антиферромагнитна (A-тип упорядочения), в ней MnO_6 октаэдры сильно сжаты в апикальном направлении. Относительные объемы, занимаемые фазами *P*1 и *P*2 в кристалле, зависят от среднего радиуса A-катиона и при замещении ^{16}O на ^{18}O перераспределяются в пользу фазы *P*2. Полученные данные однозначно свидетельствуют о перколяционной природе перехода метал-изолятор в соединении с Sm при кислородном изотопическом замещении, вследствие резкого (с 65% до 13%) уменьшения доли ферромагнитной фазы *P*1. Величина упорядоченного магнитного момента Mn в фазах *P*1 и *P*2 изменяются от 1.7 до 3.5 μ_B во всех изученных составах. Данные об эволюции микроструктурных характеристик при фазовом переходе в расслоенное состояние свидетельствуют о том, что как исходный разброс в радиусах A-катионов, так и внутренние микронапряжения оказывают критическое влияние на формирование мезоскопического фазового расслоения.

Проведено детальное нейтронное дифракционное исследование атомной и магнитной структуры 314-кобальтита $Sr_3YCo_4O_{10.5+\delta}$ (или $Sr_{0.75}R_{0.25}CoO_{2.625+\delta/4}$), в котором A-позиции являются идеально упорядоченными. Изучены два состава с разным содержанием кислорода: близкого к оптимальному (“as prepared”, δ ≈ 0) и с увеличенным δ (“oxidized”, δ ≈ 0.2). Кроме того, получены данные для состава, в котором атомы Co частично заменены на Fe, а именно, $Sr_3YFe_2Co_2O_{10.5+\delta}$ [**3**]. Для всех трех составов установлен G-тип AFM структуры (**рис. 2**), причем атомы Co, находящиеся в различных позициях элементарной ячейки, имеют различную величину магнитного момента.

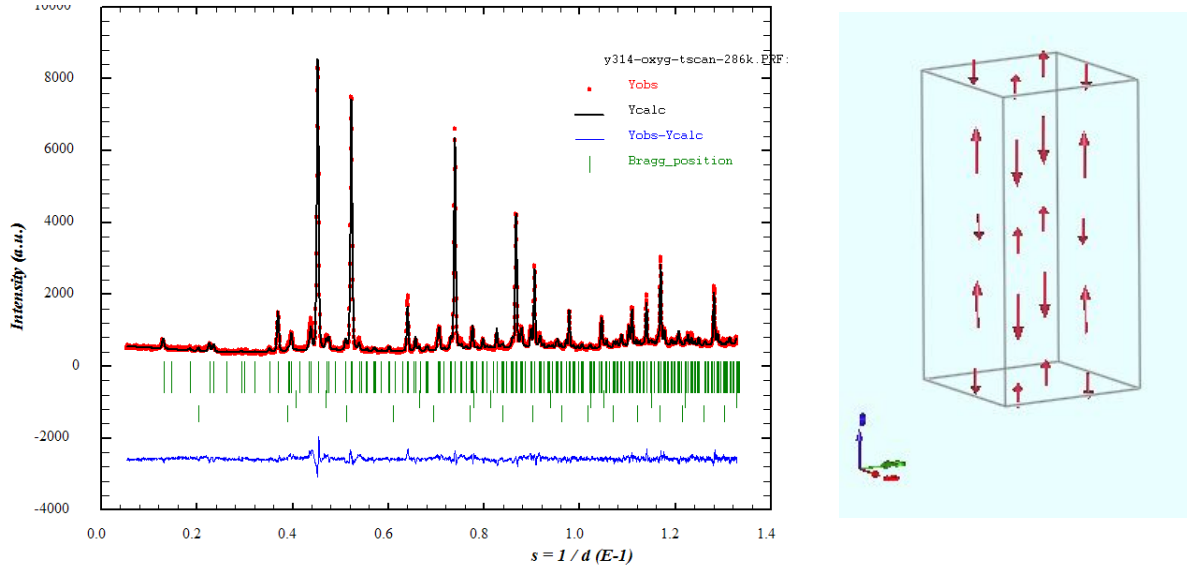

Рис. 2. Магнитная структура соединения $Sr_3YCo_4O_{10.5+\delta}$ при δ ≈ 0 и 0.2. Структура антиферромагнитная, G-типа, т.е. моменты соседних атомов Co направлены противоположно. Ее особенностью является то, что атомы Co, находящиеся в различных позициях элементарной ячейки, имеют различную величину магнитного момента.

Проведено исследование [**4**] структурных изменений, переходов между различными спиновыми состояниями ионов Co^{3+} и перехода диэлектрик-металл в кобальтите лантана $LaCoO_3$ в широком диапазоне температур 10-900К и давлений 0-20 ГПа (**рис. 3**). Установлено, что под давлением происходит резкое подавление магнитного промежуточно-спинового состояния (S = 1) и стабилизация немагнитного низкоспинового состояния (S = 0) ионов Co^{3+}. Температура перехода диэлектрик-металл существенно возрастает под давлением.

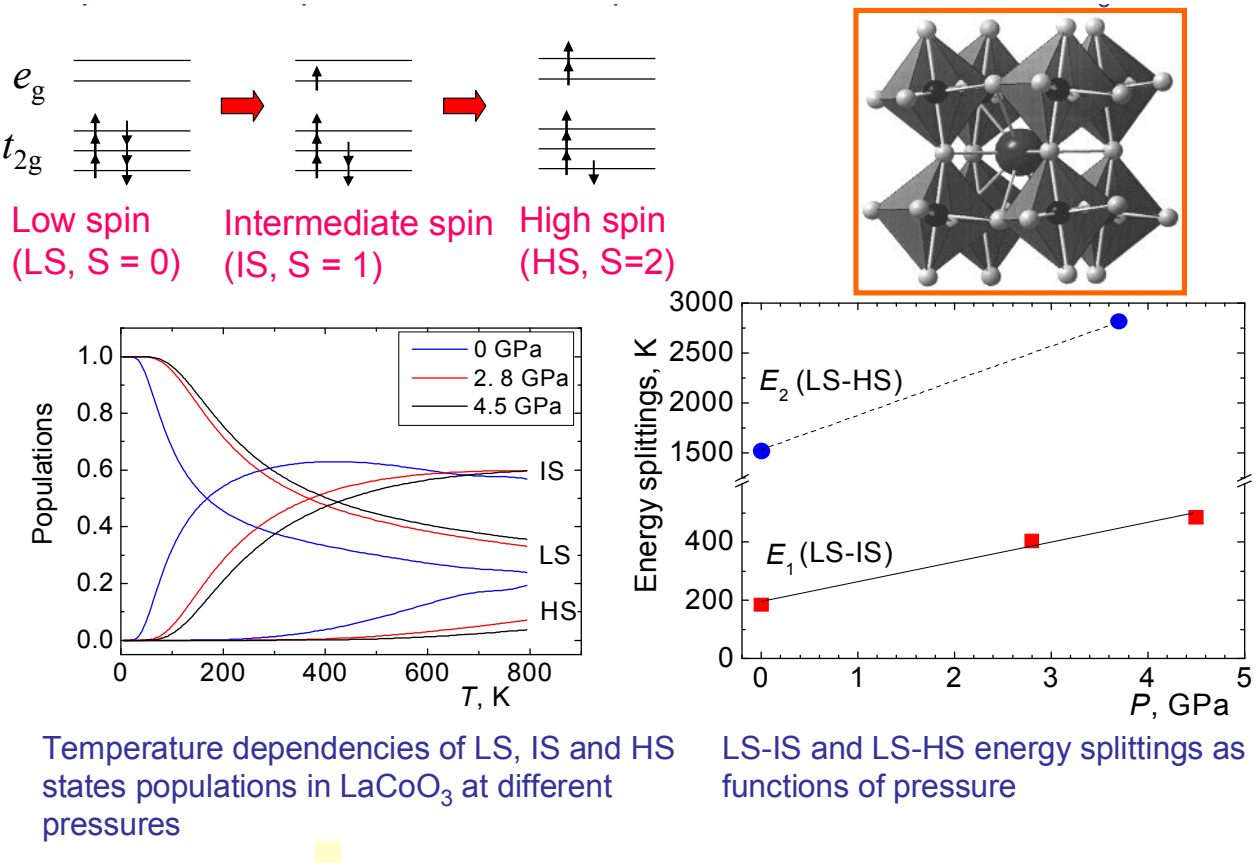

Рис. 3. К исследованиям переходов между различными спиновыми состояниями ионов Co^{3+} и перехода диэлектрик-металл в кобальтите лантана $LaCoO_3$ в широком диапазоне температур 10-900 К и давлений 0-20 ГПа. Вверху слева показаны возможные спиновые конфигурации для иона Co^{3+}, включающие низко- (S=0), промежуточно- (S=1) и высокоспиновые (S=2) состояния.

Проведены предварительные исследования влияния высокого давления на кристаллическую и магнитную структуру некоторых составов манганитов и кобальтитов. В $Pr_{0.7}Ba_{0.3}MnO_3$ при высоких давлениях наблюдается подавление исходного ферромагнитного (ФМ) состояния и появление антиферромагнитного (АФМ) состояния А-типа. В $Pr_{0.7}Ba_{0.3}MnO_{2.6}$ при нормальном давлении наблюдалось промежуточное АФМ состояние G-типа и основное состояние спинового стекла. Под давлением магнитных фазовых переходов не наблюдалось. Для кобальтита $PrCoO_3$ при высоком давлении до 8.7 ГПа при комнатной температуре установлено, что это соединение сохраняет орторомбическую структуру во всем исследуемом диапазоне давлений. Обнаружена слабая анизотропия сжатия кислородных октаэдров CoO_6.

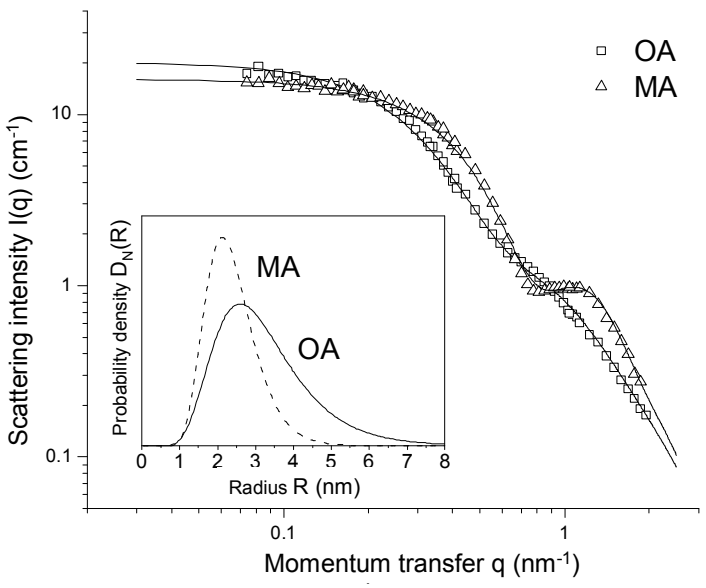

Рис.4. Одномерные кривые ядерного рассеяния $\langle F_N^2(q)\rangle_R$, усредненного по функции полидисперсности частиц наномагнетита, как результат обработки двумерных картин рассеяния поляризованных нейтронов (данные ГКСС), в магнитных жидкостях, стабилизированных с использованием олеиновой (ОА) и миристиновой (МА) кислот. Сплошные линии – лучшая подгонка модели невзаимодействующих частиц типа «ядро-оболочка» с использованием логнормальной функции распределения по размерам ядра. Полученные функции полидисперсности показаны во вставке.

Проведен анализ структурных данных, полученных методом малоуглового рассеяния неполяризованных и поляризованных нейтронов для магнитных жидкостей в органических неполярных основах. Исследована возможность использования коротких монокарбоксильных кислот (насыщенные лауриновая $C_{12}H_{24}O_2$ и миристиновая $C_{14}H_{28}O_2$ кислоты) для стабилизации наночастиц магнетита [**5**]. Показано, что данные кислоты могут быть использованы для получения высокостабильных образцов. Проведено сравнение структуры новых образцов с классическими магнитными жидкостями, стабилизированными ненасыщенной олеиновой кислотой $C_{18}H_{34}O_2$ с изгибом в центре из-за двойной связи C=C. Обнаружены существенные различия в функции распределения по размерам стабилизированного магнетита: имеет место уменьшение среднего радиуса частиц и индекса полидисперсности при переходе от олеиновой кислоты к коротким насыщенным кислотам (**рис. 4**). Таким образом, если олеиновая кислота стабилизирует магнетит в широком диапазоне размеров 1-10 нм, то более короткие кислоты стабилизируют только фракцию малых частиц из этого интервала. Из сравнения полученной из подгонки эффективной толщины оболочек кислот вокруг магнетита (~1.4 нм в обоих случаях) следует, что причина наблюдаемого эффекта регулирования размера связана с различной организацией кислот на поверхности магнетита, определяющей упругие свойства стабилизирующей оболочки. Работа выполнена совместно с Исследовательским центром Гиестхахта ГКСС (Германия), Будапештским нейтронным центром (Венгрия) и Исследовательским центром фундаментальных и прикладных исследований Румынской Академии наук (Отделение Тимишоары, Румыния).

На основе экспериментов по малоугловому рассеянию нейтронов на магнитных жидкостях продолжена проверка нового подхода базисных функций для вариации контраста на полидисперсных многокомпонентных и суперпарамагнитных системах [**6**]. Совместно с Исследовательским центром Гиестхахта ГКСС (Германия) и Исследовательским центром фундаментальных и прикладных исследований Румынской Академии наук (Отделение Тимишоары, Румыния) были проведены сравнительные эксперименты на системах магнетит/олеиновая кислота/бензол и магнетит/миристиновая кислота/бензол. Анализ поведения квадратичного радиуса инерции от обратного контраста из данных по вариации контраста (**рис. 5а,б**) позволяет уточнять параметры функции распределения стабилизированного магнетита по размерами и оценивать толщину оболочки ПАВ. Данные вариации контраста сравнивались с результатами прямого моделирования и экспериментов

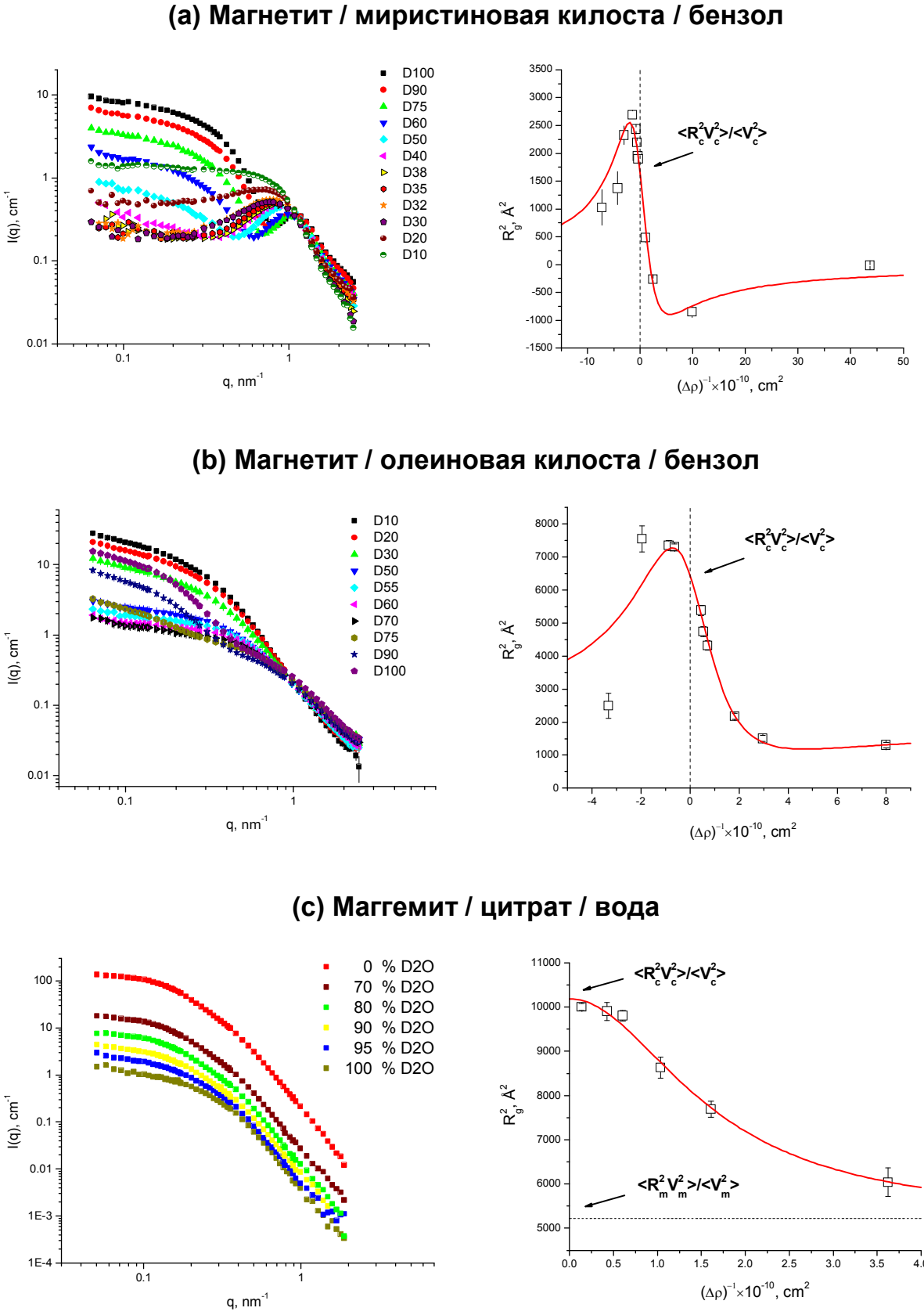

Рис. 5. Вариация контраста для различных видов магнитных жидкостей. В левом столбце – экспериментальные кривые рассеяния при различной доли дейтерированного растворителя в жидкой основе (указана в названиях образцов). В правом столбце – поведение видимого квадратичного радиуса инерции от обратного контраста в системе. Линии показывают теоретические кривые.

по рассеянию поляризованных нейтронов [**5,7**]. Совместно с Университетом Пьера и Марии Кюри (Франция) и Исследовательским центром Геестхахта ГКСС (Германия) аналогичный анализ проведен [**8**] для данных вариации контраста на водных магнитных жидкостях с ионной стабилизацией (**рис. 5в**). Из-за малого влияния на рассеяния стабилизирующей оболочки (молекулы цитрата), наиболее наглядным образом становится возможным разделение ядерного и магнитного размера частиц в жидкости посредством вариации контраста.

Продолжены исследования растворов ПАВ, используемых при стабилизации магнитных жидкостей. Совместно с Будапештским нейтронным центром проведены эксперименты по малоугловому рассеянию нейтронов на растворах ПАВ (олеиновая, миристиновая и стеариновая кислоты) в неполярной жидкости (D-бензоле). По зависимости рассеяния от концентрации растворенного вещества проанализирован характер взаимодействия между молекулами кислот. Обнаружено существенное влияние притяжения Ван-дер-Ваальса на поведение молекул кислот в растворе, которое объясняет сдвиг перехода из изотропной жидкости в жидкокристаллическое состояние в сторону малых концентраций кислот, особенно в случае растворов стеариновой кислоты [**9**]. Совместно с ЛРБ ОИЯИ проведено [**10**] моделирование молекулярной динамики растворителя в окрестностях растворенной молекулы кислоты. Показано, что организация растворителя на поверхности молекул слабо различается для трех кислот. Это указывает на то, что взаимодействие «растворитель-растворенное вещество» не отвечает за различия в поведении данных кислот в растворе. Таким образом, главной компонентой взаимодействия, определяющей такие различия, является взаимодействие Ван-дер-Ваальса.

Совместно с Институтом Лауэ-Ланжевена (Франция) продолжена работа по исследованию стабильных нанокомозитных ламелларных пленок на основе симметричных диблок-сополимеров с Fe_3O_4 наночастицами. Проведены эксперименты по рефлектометрии и GISANS. Получено, что наночастицы формируют в пределах полимерной матрицы периодически слои. В зависимости от объемной концентрации и размера наночастиц впервые обнаружены новые структурные мезофазы, предсказанные ранее теоретически. Наблюден новый структурный переход и показано, что в сложных нанокомозитных системах не только структура матрицы определяет упорядочение ансамбля наночастиц, но также наночастицы влияют на морфологию нанокомозитных пленок. Увеличивая концентрацию наночастиц, были отслежены условия, при которых ламелларная структура становится невыгодной из-за расположения наночастиц только в пределах полистирена. Как результат имеют место морфологические изменения, приводящие к образованию цилиндрической структуры. Исследования были проведены на трех сериях пленок с различной толщиной и объемной долей наночастиц от 0% до 50%. Также исследованы нанокомозитные пленки на основе асимметричных диблок-сополимеров и наночастиц с объемной долей от 0% до 15%.

В рамках изучения дисперсий фуллерена в слабополярных азотосодержащих растворителях и их смесях проведены эксперименты по времяпролетной масс-спектроскопии. Результаты исследований кластерной организации в системах C_{60}/N-метил-2-пирролидон (C_{60}/NMP) и C_{60}/N-метил-2-пирролидон/вода методом масс-спектроскопии подтвердили выводы о размерах и плотности кластеров в системе сделанные ранее на основе экспериментов по малоугловому рассеянию нейтронов. Показано, что разрушение кластеров в системе C_{60}/NMP после добавления воды происходит в результате отщепления мономеров, при этом отщепление кластеров, с количеством молекул фуллерена от 2 до 14, не наблюдается. Проведено моделирование экспериментальных УФ-Вид данных с целью оценить вклад рассеяния Ми в оптические кривые. Причиной сольватохромного эффекта в системе C_{60}/NMP, по результатам моделирования, является переход фуллерена в новое электронное состояние, связанное с образованием донорно-акцепторных комплексов C_{60}–NMP в растворе. Образование комплексов C_{60}–NMP в системе подтвердили и масс-спектроскопические измерения [**11-13**].

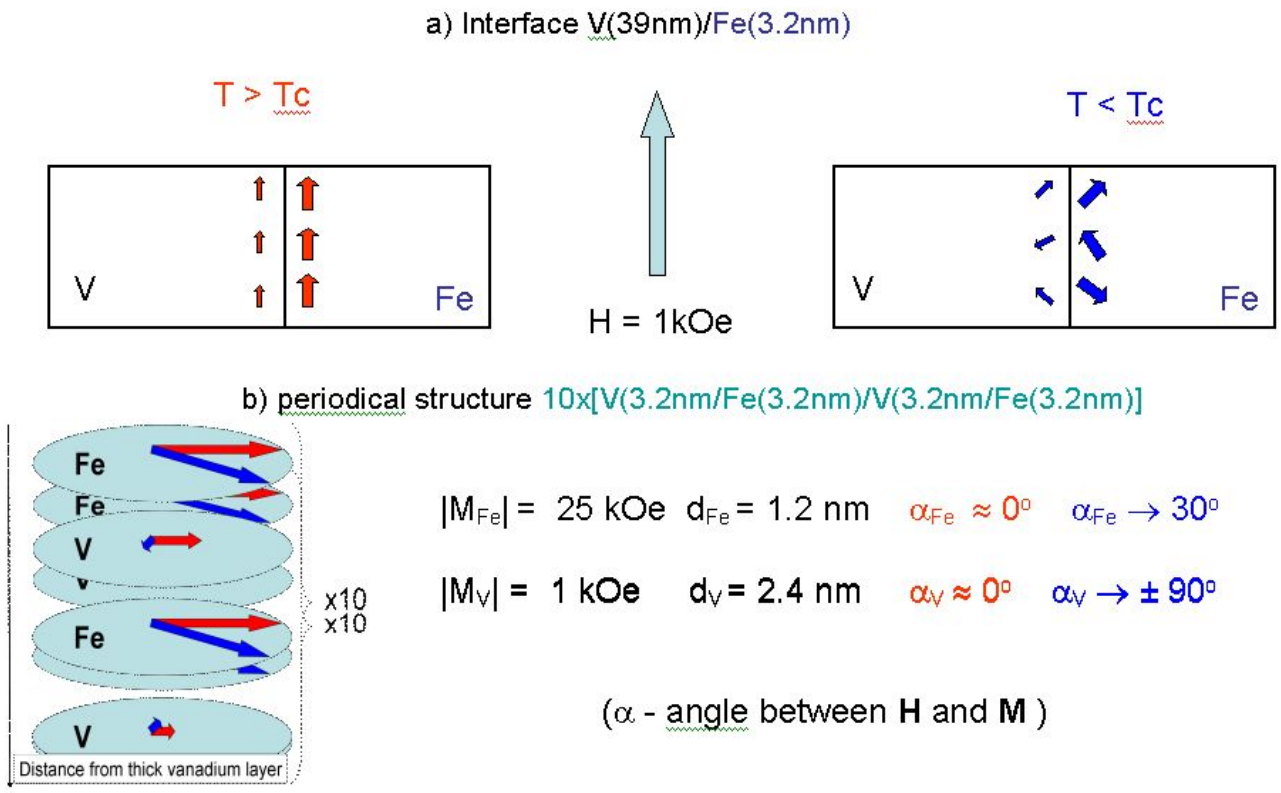

Рис. 6. Распределение (*a*) намагниченности вблизи границы раздела в бислое V(39нм)/ Fe(3.2 нм). При T = 7 K > T_C в магнитном поле 1 кЭ область в окрестности границы раздела намагничена. При переходе в сверхпроводящее состояние (T_C = 3.7 K) при T= 3 K состояние оказывается размагниченным. Размагниченное состояние энергетически более выгодно, так как действующее магнитное поле на сверхпроводящую пару оказывается меньше, чем у намагниченного состояния. Внизу (*b*) показано распределение намагниченности в периодической структуре. При переходе в сверхпроводящее состояние изменяется магнитное упорядочение как намагниченности слоёв железа, так и наведённой намагниченности слоёв ванадия. Слои ванадия упорядочиваются антиферромагнитно, что, в принципе, подтверждает выводы теории.

На спектрометре РЕМУР методом рефлектометрии нейтронов с использованием стоячих волн поляризованных нейтронов выполнены исследования ферромагнитно-сверхпроводящей составной структуры V(39нм)/Fe(3.2нм)/10×[V(3.2нм)/Fe(3.2нм)] (**рис. 6**), состоящей из сверхпроводящего слоя ванадия V(39нм) и периодической структуры 10×[V(3.2нм)/Fe(3.2нм)] [**14**]. Впервые, при переходе слоя ванадия в сверхпроводящее состояние, были наблюдены явления образования доменной структуры в окрестности границы раздела ванадий-железо и антиферромагнитное упорядочение в периодической структуре. Таким образом, показано, что магнитным состоянием наноструктуры можно управлять с помощью сверхпроводящего перехода. Это открывает возможности разработки принципиально новых логических элементов для наноэлектроники, в которых состояние кодируется и по величине магнитного момента, и по сопротивлению.

Исследованы магнитные и магнитотранспортные свойства композитных наногранулированных пленок на основе кобальта. В нанокомпозитных сплавах $(Co)_x(SiO2)_{1-x}$ в области перколяции обнаружен магнитный фазовый переход с образованием фрактальных структур. Полученные экспериментальные данные [**15**] свидетельствуют о том, что в нанокомпозитных гранулированных системах в области перколяционного перехода образуются магнитные фрактальные структуры, которые и определяют магнитные свойства композитов, в том числе и магнитосопротивление.

На спектрометре ЮМО исследовалось влияние DMSO, хорошо известного органического растворителя, который находит широкое применение в клеточной биологии,

криобиологии, фармакологии, медицине и в сельском хозяйстве, на структуру липидных мембран фосфолипидов (DMPC) в широком диапазоне молярных концентраций DMSO $0.0 \leq X_{DMSO} \leq 1.0$ в избытке растворителя при T = 12.5 $^{\circ}C$ и T = 55 $^{\circ}C$. Определена зависимость периода повторяемости d мультислойных мембран и толщины одиночных везикул d_b в гель- и жидкокристаллической фазах от X_{DMSO} в избытке растворителя DMSO/вода. Комплементарное использование величин d и d_b позволило определить межмембранное расстояние d_s. Показано [**16**], что с ростом концентрации DMSO межмембранное расстояние значительно уменьшается, и при концентрации растворителя $X_{DMSO} = 0.4$ соседние мембраны находятся практически в стерическом контакте друг с другом, что приводит к слиянию одиночных мембран в мультислойные ламеллярные структуры. С использованием метода вариации контраста впервые определено количество молекул DMSO, сильно связанных с мембраной. Число таких молекул, приходящихся на одну полярную голову липидной молекулы равно 6.9, а их общий объем составляет 820 $Å^3$, что сравнимо с объемом полярной головы липидной молекулы и объясняет ранее наблюдавшийся фазовый переход липидной мембраны в фазу с взаимным проникновением цепей.

Методом МУРН на спектрометре ЮМО проводились исследования ультраструктуры митохондрий сердца и печени крысы [**17**]. Исследовано влияние низкой тоничности среды инкубации на изменение упаковки внутренней митохондриальной мембраны. Анализ интерференционных пиков показал, что под влиянием низкой тоничности среды упаковка мембраны переходит от упорядоченной ламеллярной к упорядоченной неламеллярной (предположительно гексагональной). Данные электронной микроскопии также свидетельствуют в пользу гексагональной упаковки. Начаты эксперименты по исследованию структуры митопластов митохондрий с помощью атомно-силовой микроскопии. Цель экспериментов – доказательство существования мультиферментных липидно-белковых комплексов, участвующих в окислительном фосфорилировании.

Широко используемый в медицине антибиотик (амфотерицинин В) (АмВ) изучался с помощью малоуглового рассеяния нейтронов, рентгеновской дифракции и Фурье спектроскопии (FTIR). Результаты экспериментов показали [**18**], что при концентрациях ниже одного мольного процента АмВ преимущественно локализуется вблизи головных групп мембраны. При концентрации выше этого уровня происходит процесс агрегации. Появляется эффект ассоциации, и поэтому происходит встраивание антибиотика в гидрофобную мембранную часть.

Проводилась работа по поиску новых, дополняющих рассеяние нейтронов, экспериментальных методов исследования свойств магнитных жидкостей. Впервые для изучения их свойств был применен метод мюонной спектроскопии [**19**]. Исследована феррожидкость на основе D_2O с Fe_3O_4 наночастицами, в диапазоне температур 114-300 К в нулевом и поперечном спину мюона магнитном поле. Практически во всех случаях наблюдалась значительная релаксация спина. В отсутствие внешнего магнитного поля наблюдается падение скорости релаксации и поляризации спина мюона до нулевого значения при температуре 230 К, а затем резкий рост поляризации в диапазоне 240-255 К. Работа выполнена совместно с Лаборатории ядерных проблем им. В.П. Джелепова.

Впервые показано, что существуют открытые внутренние полости в эффективном объеме дендримера, доступные растворителю, рассчитана их объемная доля. Показано [**20**], что концевые группы дендримеров локализованы в его поверхностном слое. Применение современных математических методов обработки позволило получить не только размеры, но и восстановить *ab initio* формы дендримеров различных генераций для трех и четырех функциональных дендримеров (**рис. 7**). Предложена новая модель для интерпретации результатов малоуглового рассеяния нейтронов растворами дендримеров. В ее рамках показано, что внутренняя сфера дендримера является проницаемой для растворителя, плотность которого ниже плотности растворителя вне дендримера как минимум в 2 раза.

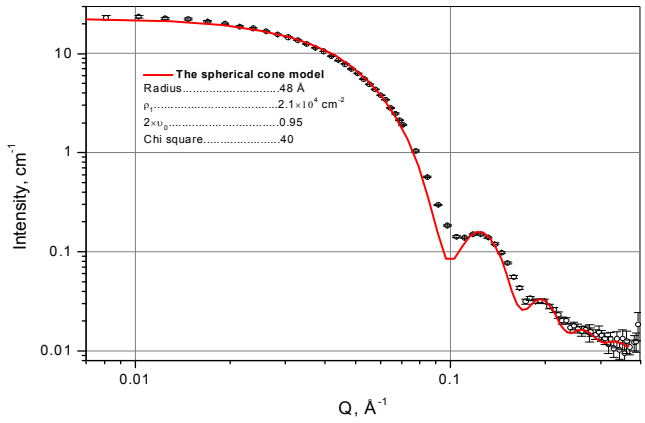

SANS data approximated by analytical curve for the model of spherical sectors.

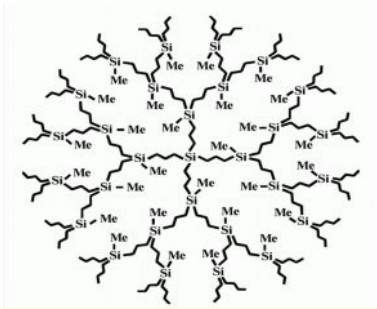

Chemical structure of dendrimer molecule and its 3D model.

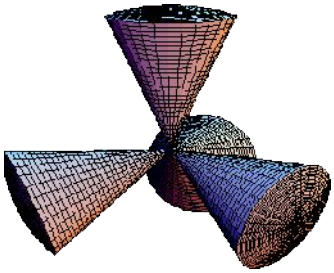

Рис. 7. Данные малоуглового рассеяния нейтронов, структурная химическая формула и 3D модель структуры четырех функциональных дендримеров.

Дифракция нейтронов является исключительно эффективным методом изучения структуры биологических и модельных липидных мембран. В частности, с помощью вариации содержания легкой и тяжелой воды удается надежно определять фазы структурных факторов. Еще одним благоприятным обстоятельством является возможность проводить эксперименты в режиме *in situ* в реальном времени. Так на дифрактометре ДН-2 удается проследить за изменениями структуры мембраны в ходе гидратации с разрешением по времени на уровне 1 минуты (**рис. 8**). В 2007 г. получены экспериментальные доказательства явления укрепления липидной матрицы верхнего слоя кожи человека stratum corneum (SC) молекулами церамида 6. В серии экспериментов, выполненных методом дифракции нейтронов, было установлено [**21**], что сверхсильное межмембранное взаимодействие создаваемое молекулами церамида 6 не может быть разрушено ни длинноцепочечными церамидами, ни длинноцепочечными жирными кислотами. Эксперименты, выполненные методом малоуглового рассеяния нейтронов, показали, что взаимодействие, создаваемое молекулами церамида 6, является короткодействующим (**рис. 9**). Устойчивость разработанной мембраны SC к вариации биохимического состава липидов и водных растворов, позволила начать эксперименты по исследованию веществ, увеличивающих проницаемость кожи человека для транспортировки лекарств.

Проведено комплексное изучение [**22**] физических свойств синтетического монокристаллического кварца и кварцевого порошка в температурной области α-β перехода методами нейтронной дифракции и механической спектроскопии. Получены новые данные по поведению параметров элементарной ячейки кварцевых порошков двух фракций с разной средней величиной зерен при комнатной температуре и в температурном интервале 540-620 ºС, а также координаты атомов в элементарной ячейке. Установлено, что параметры решетки у порошков, отличающихся размером зерен на порядок, заметно различаются. Температура α-β фазового перехода у мелкозернистого порошка больше, чем у крупнозернистого на ≈15 ºС (лежит в интервале 580-585 ºС).

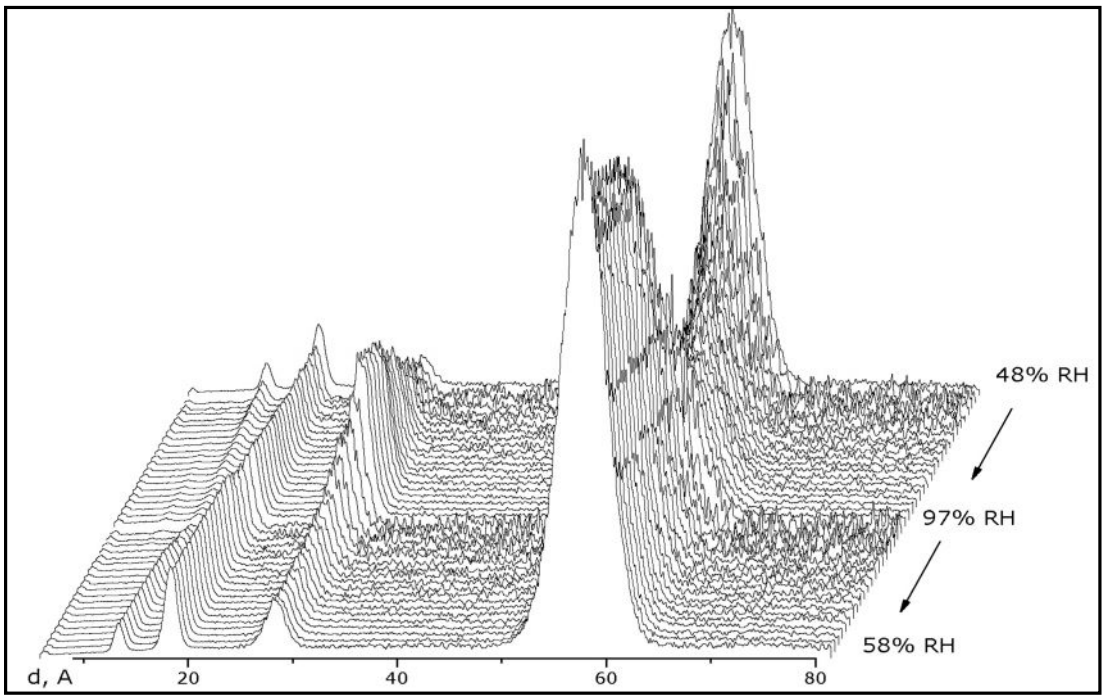

Рис. 8. Дифракция в реальном времени позволяет эффективно исследовать структуру и фазовые переходы в липидных мембранах. На дифрактометре ДН-2 удается проследить за изменениями структуры мембраны в ходе гидратации с разрешением по времени на уровне 1 минуты.

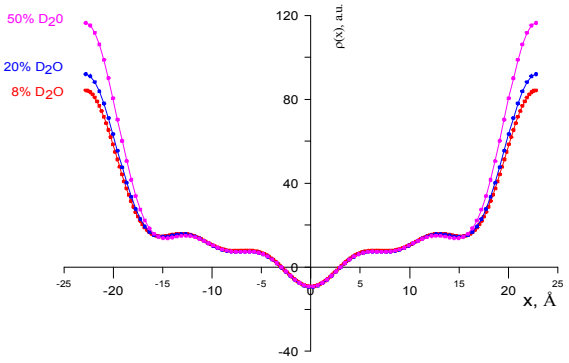

Calculated neutron scattering density profile for basic membrane at T=32°C and 60% humidity.

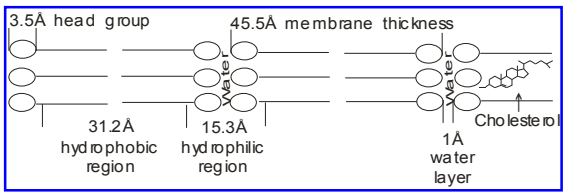

Structural results for fully hydrated quaternary Ceramide 6/Cholesterol/Palmitic Acid/Cholesterol sulfate membrane

Рис. 9. Восстановленный (слева) из нейтронных дифракционных данных фурье-профиль рассеивающей плотности в направлении, перпендикулярном плоскости мембраны. Его особенностью является малый (около 1 Å) зазор между соседними бислоями (справа). Это означает, что вода практически не входит в промежуток между молекулами церамида, что связано со сверхсильным межмембранным взаимодействием

На спектрометре ДИН-2ПИ методом квазиупругого рассеяния медленных нейтронов исследованы диффузионные процессы в жидком литии (Т = 500К и 830К) и расплаве литий-водород (Т = 830 К, концентрация примеси водорода ~ 1 % ат.) [**23**]. Найденные характеристики диффузионных процессов для чистого лития и, в частности, коэффициент самодиффузии находятся в хорошем согласии с расчетом и результатами, полученными

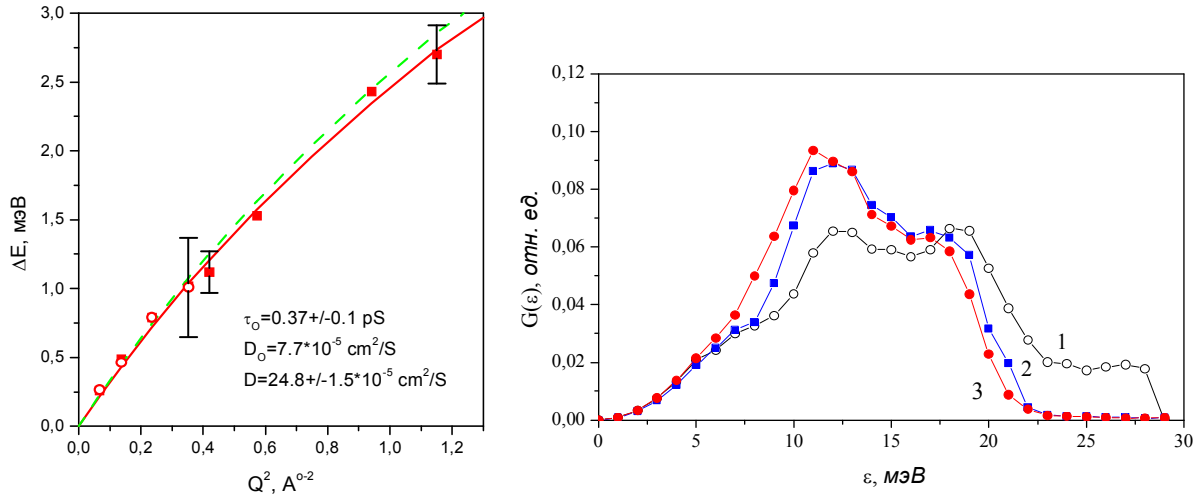

The width of quasielastic scattering for Li-H mixture (full symbols) and H in Li (open symbols) at T=830 K as a function of Q^2.

Density of phonon states for Ta at 293 K (1), 1584 K (2) and 2300 K (3).

(*a*) (*b*)

Рис. 10. Примеры результатов экспериментов, проведенных на спектрометре ДИН. Показаны зависимости ширины пика квазиупругого рассеяния от переданного импульса для смесей лития и водорода (слева) и плотность фононных состояний в тантале для различных температур (справа). Впервые удалось провести измерения неупругого рассеяния нейтронов при температуре 2300 К.

капиллярным методом. Было установлено, что характер диффузионных процессов водорода в расплаве литий-водород практически неотличим от диффузии атомов лития (**рис. 10a**). Это свидетельствует о том, что в указанных выше условиях водород присутствует в расплаве в форме гидрида лития LiH.

Впервые измерены спектры неупругого рассеяния нейтронов для переходного металла V-ой группы тантала (Ta) в интервале температур от комнатной до 2300 К (**рис.10b**). Для получения необходимой температуры образца использовался созданный недавно высокотемпературный термостат TS3000. Точность полученных спектров оказалась достаточной для восстановления плотности фононных состояний G(ε) тантала для всех температур измерения. Восстановление спектров частот проводилось методом последовательных итераций с учетом эффекта многофононного рассеяния нейтронов. Температурная эволюция спектров частот пока не нашла удовлетворительного объяснения и требует дальнейшего изучения, в частности, оценки влияния электрон-фононного взаимодействия.

II. Методические результаты

В 2007 г. на ИБР-2 началась реконструкция нейтроноводной системы спектрометров SCAT, EPSILON и NERA. Работа ведется в рамках проекта с BMBF совместно сотрудниками отделов НИКС и КС. По согласованному техническому заданию выполнено эскизное проектирование механических и оптических узлов нейтроноводной системы и проведена привязка существующих конструкций нейтроноводных каналов расположенных в кольцевом коридоре и экспериментальном зале к реальным строительным конструкциям.

Совместно с Исследовательским центром Юлиха проведено исследование метода нейтронного спин-эхо, основанного на вращении магнитного поля. Магнитное поле

создавалось системой двух перпендикулярных друг другу обмоток, между которыми находилась фольга, магнитные свойства которой были изучены. Проведен анализ зависимости внутренней намагниченности фольги от незначительного внешнего магнитного поля. Была разработана математическая модель поведения спина при прохождении нейтронного пучка через магнитное поле, создаваемое системой двух обмоток с магнитной фольгой, которая удовлетворительно описывает экспериментальные данные [**24**].

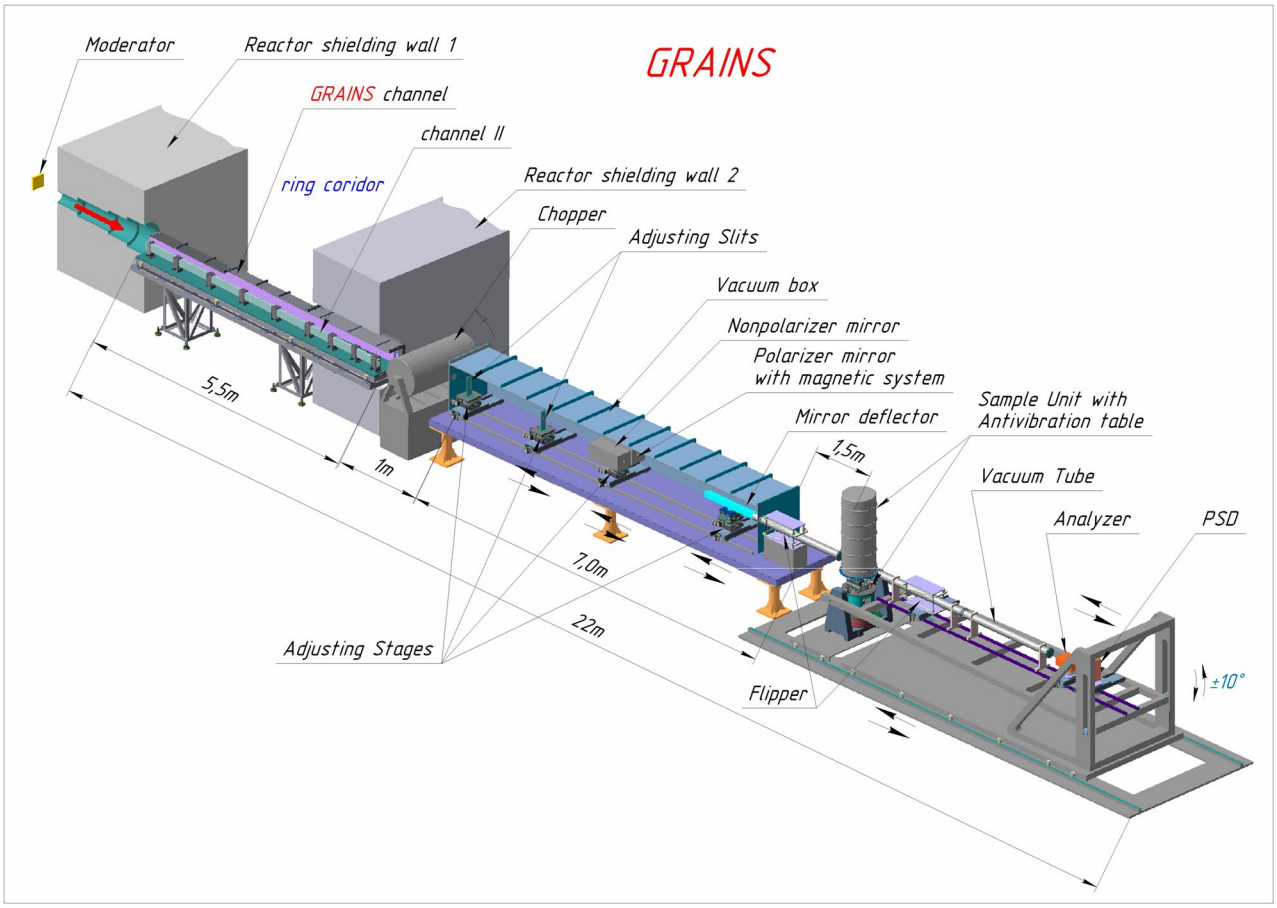

Рис. 13. Принципиальная схема нового нейтронного рефлектометра GRAINS на реакторе ИБР-2М. Нейтронный источник расположен слева, полная пролетная база до детектора составляет около 30 м.

На канале 10 ИБР-2 вместо существующего спектрометра KDSOG вскоре будет начато сооружение многофункционального рефлектометра GRAINS. Принципиальной особенностью рефлектометра является использование вертикальной плоскости рассеяния, что позволяет изучать отражение от жидких сред (включая поляризованные нейтроны для исследования границ раздела с магнитными наночастицами). На рефлектометре будет использован TOF метод, что позволит проводить эксперименты при фиксированных ориентациях первичного пучка и образца. Дополнительные режимы на установке GRAINS включают в себя: (1) возможности изучения незеркального отражения и рассеяния GISANS; (2) угловое кодирование в горизонтальной плоскости на основе Ларморовской прецессии спина нейтронов [**25**]; (3) 3D поляриметрия на основе Ларморовской прецессии спина нейтронов. Концепция рефлектометра в рамках соответствующего проекта была поддержана ПКК по конденсированным средам ОИЯИ в апреле 2007. Схема рефлектометра и методы, которые будут реализованы на установке, доложены и обсуждены на ряде научных совещаний и конференциях. Завершены эскизный (**рис. 13**) и технический проекты.

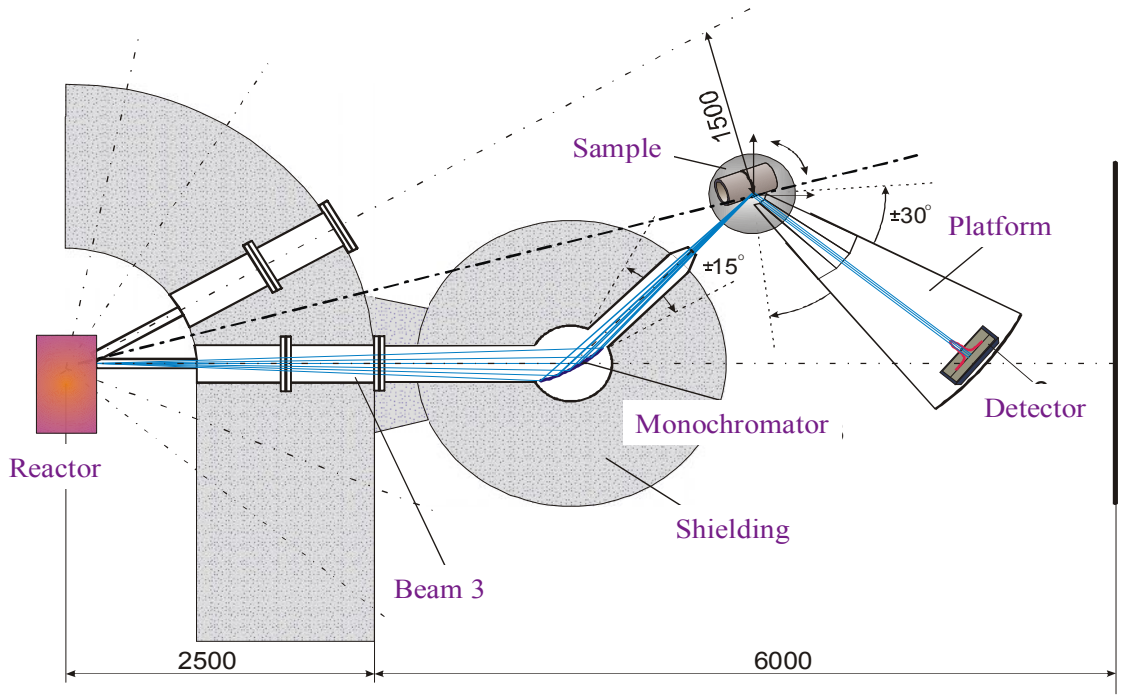

Рис. 14. Принципиальная схема нового нейтронного дифрактометра на реакторе ИР-8 в РНЦ КИ, предназначенного для изучения внутренних напряжений в объемных материалах и деталях. Дифрактометр выполнен по классической двуосной схеме, но с использованием современных технологий в монохроматизации первичного пучка и регистрации рассеянных нейтронов.

В рамках протокола о сотрудничестве с РНЦ КИ начато проектирование нейтронного дифрактометра для изучения внутренних напряжений в объемных изделиях на реакторе ИР-8 (**рис. 14**). Концепция дифрактометра предполагает использование современных технологий формирования нейтронного пучка и детектирования рассеянных нейтронов. Этот дифрактометр обеспечит комплементарные возможности по отношению к существующему на ИБР-2 стресс-дифрактометру FSD.

Для дальнейшего развития экспериментальной базы на ИБР-2 и в рамках сотрудничества с корпорацией NECSA (ЮАР) реализован контракт на приобретение автоматизированной нагрузочной машины (**рис. 15**). Машина позволяет проводить on-line эксперименты с широким набором режимов нагрузки (стационарной или циклической) на любом типе нейтронных дифрактометров с объемными образцами металлов и сплавов.

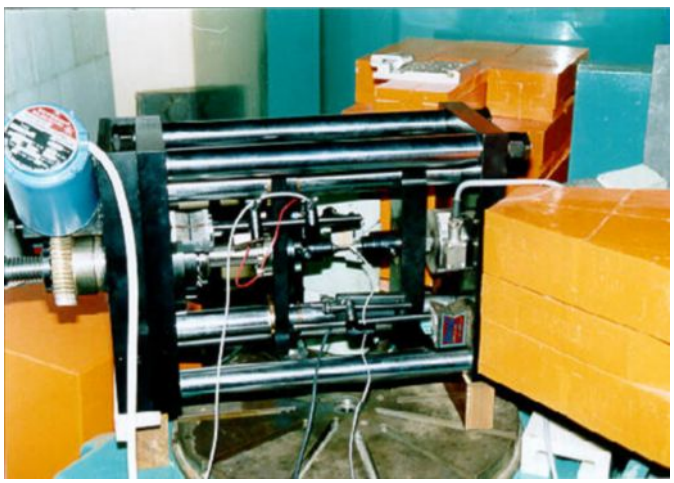

Рис. 15. Внешний вид нагрузочной машины для on-line экспериментов с металлами и сплавами. Машина позволяет реализацию различных статических и динамических (циклических) режимов работы.

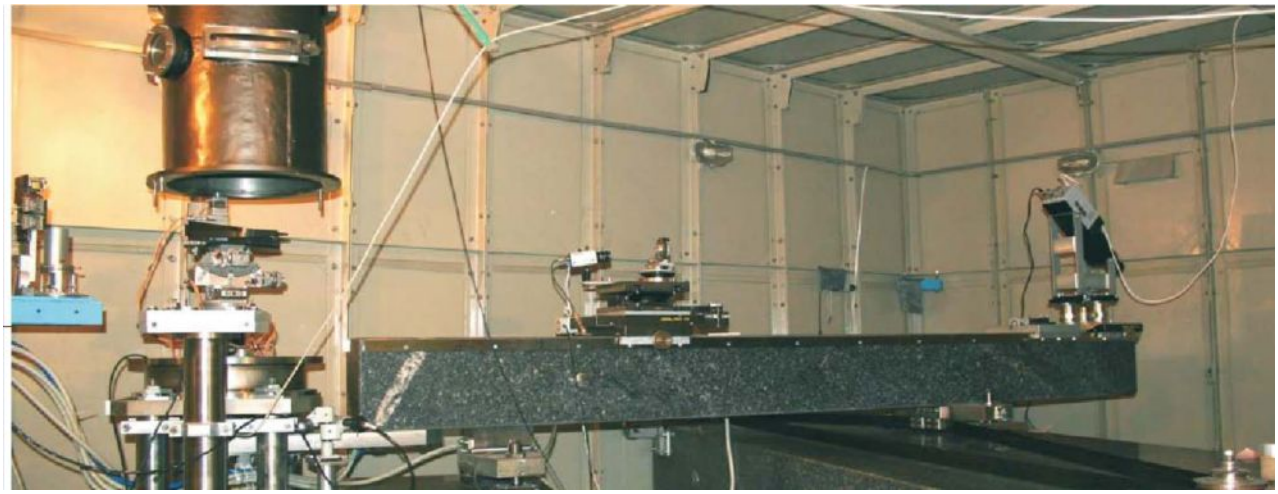

Рис. 16. Общий вид станции энергодисперсионной EXAFS-спектроскопии на источнике синхротронного излучения СИБИРЬ-2 в РНЦ КИ, изготовленной силами ОИЯИ.

Весной 2007 г. был осуществлен физический пуск станции энергодисперсионной EXAFS-спектроскопии (**рис. 16**) на СИБИРЬ-2 и получены первые результаты. Ее отличительной особенностью является возможность измерения спектров поглощения за очень короткое время — меньше 10^{-3} с, в отличие от классических EXAFS-станций, на которых требуется время ~ $10^3 \div 10^4$ с. Благодаря этому открывается возможность исследовать динамические процессы, происходящие при внешнем воздействии. Методика экспериментов по измерению рентгеновских спектров поглощения (EXAFS- и XANES-области) на *K*-крае Co в соединении $La_{1-x}Sr_xCoO_3$ с x = 0,0 и 0.5, проведенных в Гамбургском центре синхротронных исследований в рамках соглашения между лабораторией HASYLAB (DESY) и Курчатовским центром синхротронного излучения и нанотехнологий.

Пробные эксперименты проведены на станции МЕДИАНА на синхротронном источнике СИБИРЬ-2 в РНЦ КИ. В частности, изучались возможности проведения экспериментов при высоких давлениях в камерах с сапфировыми наковальнями и *in situ* экспериментов процессов гидрирования электролитических осадков в электрохимических ячейках. Показано, что в обоих типах экспериментов можно получать значимые результаты.

Проведены расчетные работы по оценке эффективности использования зеркального нейтроновода для различной геометрии пучка спектрометра ДИН-2ПИ, создан эскизный проекта нейтроновода и основных узлов для его сборки и юстирования на нейтронном пучке, проведена закупка комплектующих для зеркальных сегментов нейтроновода. Завершены работы по разборке физической защиты спектрометра для установки зеркального нейтроновода.

На основе анализа результатов этих расчетов сделаны выводы об оптимальных вариантах геометрии и отражающего покрытия планируемого зеркального нейтроновода, а именно:

- оптимальным с точки зрения отношения «фактор выигрыша/цена» является покрытие с двойным критическим углом отражения;
- оптимальным с геометрической точки зрения в условиях спектрометра ДИН-2ПИ является зеркальный нейтроновод длинной 12,5 м, входным окном 200х22 мм^2 и выходным окном 70х120 мм^2;
- предлагаемый размер выходного окна дает возможность работать с образцами исследуемого вещества характерных размеров 50х100 мм^2 при условии, что такой образец оказывается в нейтронном потоке постоянной интенсивности как в вертикальной, так и в горизонтальной плоскостях.

Таким образом, создаваемый зеркальный нейтроновод позволит решить две главные задачи: повысить интенсивность холодных нейтронов (E < 5 мэВ) на образце в (4-6) раз и при этом уменьшить размеры исследуемых образцов в (2-3) раза. Решение обеих этих задач будет означать существенное улучшение качества спектрометра ДИН-2ПИ и приближение его характеристик к лучшим зарубежным аналогам.

Литература

1. V.Yu.Pomjakushin, D.V.Sheptyakov, K.Conder, E.V.Pomjakushina, A.M.Balagurov Phys. Rev. B, 2007, v. 75, p. 054410.
2. А.М. Балагуров, И.А. Бобриков, В.Ю. Помякушин, Д.В. Шептяков, Н.А. Бабушкина, О.Ю. Горбенко, М.С. Картавцева, А.Р. Кауль, ЖЭТФ, принята в печать.
3. D.V. Sheptyakov, O.A. Drozhzhin, V.Yu. Pomjakushin, S.Ya. Istomin, I.A. Bobrikov, E.V. Antipov, A.M. Balagurov "Crystal and magnetic structures of $Sr_3YCo_4O_{10.5+\delta}$: Y-314 phases with different oxygen content". Готовится в печать.
4. D.P.Kozlenko, N.O.Golosova, Z.Jirak, L.S.Dubrovinsky, M.Tucker, Y. Le Godec, B.N.Savenko, Phys. Rev. B, 2007, v. 75, p. 064422.
5. M.V.Avdeev, D.Bica, L.Vékás, O.Marinica, M.Balasoiu, V.L.Aksenov, L.Rosta, V.M.Garamus, A.Schreyer, J. Mag. Mag. Mater., 2007, v. 311, p. 6.
6. M.V.Avdeev "Contrast variation in small-angle scattering experiments on polydisperse and superparamagnetic systems: basic functions approach" J. Appl. Cryst. 40 (2007) 56-70.
7. А.В.Феоктистов, М.В.Авдеев, В.Л.Аксенов, Л.А.Булавин, Д.Бика, Л.Векаш, В.М.Гарамус, Р.Виллумайт, Вариация контраста в малоугловом рассеянии нейтронов на магнитной жидкости магнетит/миристиновая кислота/бензол, Поверхность, принято к печати.
8. M.V.Avdeev, E.Dubois, G.Mériguet, E.Wandersman, V.Garamus, A.V.Feoktystov, R.Perzynski, SANS analysis of a water-based magnetic fluid with charged stabilization: contrast variation and scattering of polarized neutrons, submitted to J. Appl. Cryst.
9. V.I.Petrenko, M.V.Avdeev, L.A.Bulavin, V.L.Aksenov, L.Almásy, L.Rosta, V.Garamus, Interaction of mono-carboxylic acids in benzene by small-angle neutron scattering, submitted to Chem. Phys. Lett.
10. И.А.Боднарчук, Х.Т.Холмуродов, В.И.Петренко, М.В.Авдеев, Определение предельного парциального молярного объема растворов монокарбоксильных кислот в бензоле методом молекулярно-динамического моделирования, направлено в Ж. хим. физ.
11. V.L. Aksenov, M.V. Avdeev, O.A. Kyzyma, L. Rosta, M.V. Korobov. Age effect of solution C_{60}/N-methilpyrrolidone on the cluster structure in the system C_{60}/N-methilpyrrolidone/water // Crystallography Report 2007, v. 52, pp. 523-527.
12. O.A. Kyzyma, L.A. Bulavin, V.L. Aksenov, M.V. Avdeev, T.V. Tropin, M.V. Korobov, S.V. Snegir, L. Rosta. Aggregation in C_{60}/NMP, C_{60}/NMP/water and C_{60}/NMP/Toluene mixtures // Fullerenes, Nanotubes and Carbon Nonstructures. Accepted.
13. Е. А. Кизима, М. В. Авдеев, В. Л. Аксенов, Л. А. Булавин, С. В. Снегир. Реорганизация кластеров фуллеренов в системе C_{60}/N-метил-2-пирролидон/вода // Поверхность, принята к печати.
14. В.Л.Аксенов, Ю.В.Никитенко, А.В.Петренко, В.М.Уздин, Ю.Н.Хайдуков, Х.Цабель, Кристаллография, 2007, т. 52, с. 403.
15. М.Е.Докукин, Н.С.Перов, Е.Б.Докукин, А.Х.Исламов, А.И.Куклин, Ю.Е.Калинин, А.В.Ситников, Известия РАН. Серия Физическая, 2007, т. 71, с. 1643.
16. Ю. Е. Горшкова, В. И. Горделий, Исследование взаимодействия диметилсульфоксида с липидными мембранами с помощью малоуглового рассеяния нейтронов, Кристаллография, 2007, т. 52, с. 584–588.

17. Т.Н.Муругова, В.И.Горделий, А.И.Куклин, И.М.Солодовникова и Л.С.Ягужинский. Регистрация трехмерно упорядоченных структур в интактных митохондриях с помощью метода малоуглового рассеяния нейтронов. Кристаллография, 2007, т. 52, с.545-548.
18. M.Here, A.Islamov, A.Kuklin, M.Gago, W.I.Gruszecki. Effect of antibiotic amphotericin B on structural and dynamic properties of lipid membranes formed with egg yolk phosphatidylcholine. Chemistry and Physics of Lipids 147 (2007) 78–86.
19. М.Балашою, Д.Бика, Л.Векаш, К.И.Грицай, В.Н.Дугинов, В.А.Жуков, Т.Н.Мамедов, В.Г.Ольшевский, К.Петреску, Сообщение ОИЯИ, Р14-2007-21, Дубна, 2007.
20. А.В. Рогачев, А.Ю. Черный, А.Н. Озерин, В.И. Горделий, А.И. Куклин. Модель шаровых секторов для описания экспериментальных данных малоуглового рассеяния нейтронов на дендримерах. Кристаллография, 2007, т. 52, с. 546-550.
21. М.А.Киселев, Кристаллография, 2007, т. 52, с. 549.
22. А.Н.Никитин, Г.В.Маркова, А.М.Балагуров, Р.Н.Васин, О.В.Алексеева, Кристаллография, 2007, т. 52, с. 450.
23. Н.М.Благовещенский, В.А.Морозов, А.Г.Новиков, В.В.Савостин, Д.В.Савостин, А.Л.Шимкевич. Изучение микродинамики жидкого лития и расплава литий–водород методом неупругого рассеяния нейтронов. Кристаллография, 2007, т. 52, № 3, с. 498 – 504 (англ. вариант: Crystallography Reports. 52 (2007) 406).
24. A.Ioffe, V.Bodnarchuk, K.Bussmann. R.Müller, Larmor labeling by time gradient magnetic fields, Physica B, 397 (2007) 108-111.
25. M. Jernenkov, S. Klimko, V. Lauter-Pasyuk, B.P. Toperverg, H.J. Lauter, V.L.Aksenov, Larmor precession reflectometry for multilayer studies, Nucl. Instr. Methods A (2007) in press.

1.2. NEUTRON NUCLEAR PHYSICS

Introduction

In the course of 2007 in view of the IBR-2 reactor shutdown for the modernization the main studies in the field of neutron nuclear physics at the Frank Laboratory of Neutron Physics were carried out on neutron beams of other nuclear centers of Russia, Bulgaria, Poland, Czech Republic, Germany, Republic of Korea, China, France, USA, Japan as well as at the EG-5 accelerator in FLNP. The studies were in traditional directions: the investigation of time and spatial parity violation processes in the interaction of neutrons with nuclei; studying of quantum-mechanical characteristics, energy and dynamics of the fission process; experimental and theoretical investigation of the electromagnetic properties and beta-decay of the neutron; gamma-spectroscopy of neutron-nuclear interactions, structure of atomic nucleus, obtaining of the new data for reactor applications and nuclear astrophysics; experiments with ultracold neutrons; applied investigations.

1. Experimental investigations

1.1 Fundamental properties of the neutron

1.1.1 Works within the framework of preparation and carrying out of experiment on the direct measurement of the cross section of neutron-neutron scattering at the YAGUAR reactor (RFNC-VNIITF, Snezhinsk)

In 2007 the main result achieved within the framework of this activity was the construction of a neutron detector meeting all requirements of the experiment. It should be pointed out that these requirements are rather stringent. Never had there existed neutron detectors that could combine high

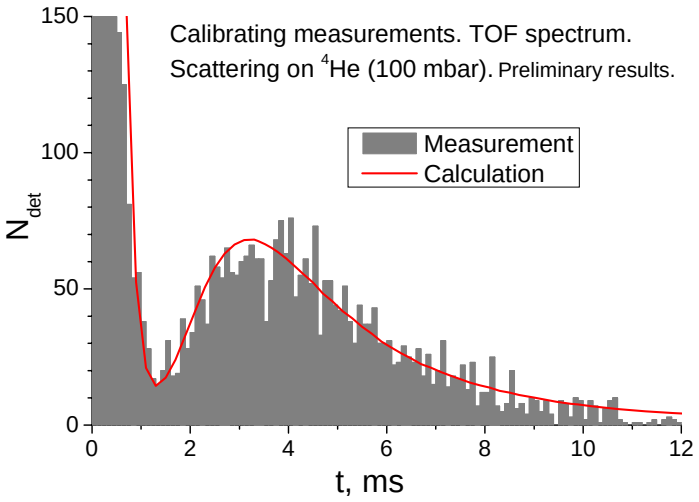

Fig. 1. Time-of-flight spectrum of detected neutrons

counting rate (~10^6 s^{-1}), neutron detection efficiency ~100 %, high energy resolution (no worse than 10%) and low γ-quantum sensitivity ~10^{-9}. The detector was installed on the experimental setup and successfully underwent tests in calibration measurements on gases in a pulsed operating mode of the YAGUAR reactor. The results of preliminary data processing obtained in gas measurements are given in **Fig. 1**. The time-of-flight spectrum of detected neutrons is presented in this figure. Thus, at the present time the facility for measuring the nn-scattering is ready for operation.

In 2008 it is planned to complete calibrations on inert gases, to achieve the necessary background conditions and to start measurements of the nn-scattering cross section.

1.1.2 Investigation of the n-e scattering

The preparatory works for the experiment to extract the n,e-scattering length from the energy dependence of angular distributions of the thermal neutron scattering by noble gases on the vertical neutron channel of the TRONS facility were carried out.

Simulation experiment taking into account the thermal motion of gas was carried out by the Monte-Carlo method. In order to compare three variants of account of thermal motion (Placzek,

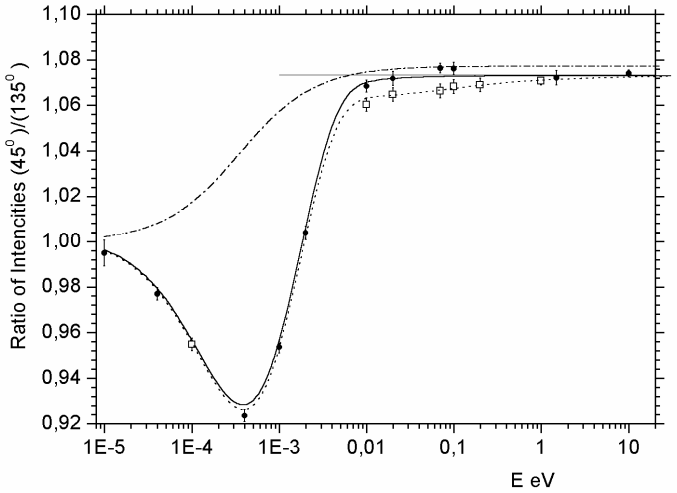

Fig. 2. Anisotropy of neutron scattering by argon forward-backward calculated for different variants of account of thermal motion of gas atoms. Dot-dash curve - the Placzek approximation, dotted and solid line correspond to the Turchin approach taking into account the n,e scattering and without it, respectively. Straight line – calculation without taking into account thermal motion of atoms.

Turchin and Monte-Carlo), for each of them the forward-backward anisotropy for the distribution angles $\theta_1 = 45^o \pm 5^o$ and $\theta_2 = 135^o \pm 5^o$. were calculated. The results of calculations are presented in Fig.2.

Also, calculations of the angular anisotropy $45^0/135^0$ were carried out in the geometry close to the classical Kron-Ringo experiment under the assumption of application of the circular ^{3}He-counter with the pressure of 10 atm. The anisotropy was calculated by way of analytical integration within the limits of distribution angles $\pm 2.5^0$ and $\pm 5^0$, and also using the Monte-Carlo method. The results of these calculations for xenon are given in Fig. 3. Here the effect of n,e-scattering manifests itself as a dip in the region of energies of thermal neutrons, the depth of which just depends on the value of n,e-interaction length. Comparison of analytical calculations of anisotropy with the calculations by the Monte-Carlo method shows that in the studied range of neutron distribution angles at the analysis of primary experimental data and extraction of the n,e-interaction length from them, it will be possible to be restricted to the application of the Turchin formalism that will essentially simplify the analysis of experiment.

Owing to the originality of the conducted experiment almost all the approaches for account of numerous corrections with the accuracy on the order of 10^{-4} of the share from the nuclear scattering prove to be new as needed. In particular, the model-free account of thermal motion of atoms of target has revealed details in the angular anisotropy, which are not usually conveyed by the used Placzek model (it is too coarse for our purposes). Kinematic description of motion of neutron and atom just as the accurate correction for the energy release by neutron scattered for different angles will allow one to obtain the precision value of the n,e-scattering length from the measured scattering anisotropy.

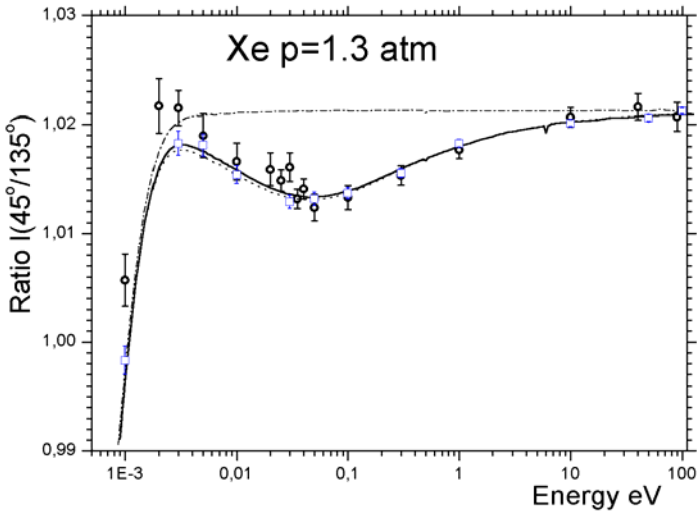

Fig. 3. The calculated anisotropy of neutrons scattered on xenon: solid and dotted curves – calculation within the Turchin approach taking into account the n,e-scattering for the distribution angles $\pm 2.5^0$ and $\pm 5^0$, dashed curves – with no account for the n,e-scattering. Results of the calculation by the Monte-Carlo method (taking into account the n,e-scattering): light squares – scattering in the small space, light points – in the real geometry.

Neutron optics

1.2.1 Verification of weak equivalence principle for the neutron

In 2007 the data processing from the experiment to verify the equivalence principle for the neutron conducted in 2006 completed. Results of the study were published.

The idea of the experiment is to compare changes of the neutron energy **mgh** at its fall from the height h with the value of energy $\Delta E = \hbar\Omega$ transferred to the neutron at the interaction with non-stationary device. It is illustrated by **Fig. 4**.

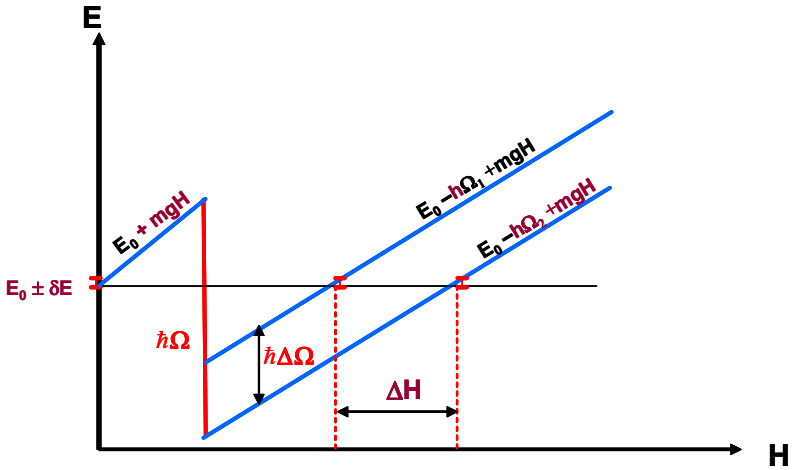

Fig. 4. Idea of the experiment.

The narrow energy spectrum of neutrons **f(E)** is formed by a monochromator placed at the height **H=0**. In order to enter the detector and be detected neutrons must past through the analyzer, which is placed below the monochromator for the **H** value and has the same spectrometric properties. The neutrons are accelerated in the Earth's gravitational field on the way from the monochromator to the analyzer. Since the width of spectral function **f(E)** is small, the system

becomes nontransparent already at a relatively small distance **H**. However, if on this way the neutron energy additionally decreases for the value $\Delta E = \hbar\Omega$, than one may find a position of the analyzer, at which it transmits neutrons. Here the dependence of the system transmission on the analyzer position is described by the symmetrical function

$$\Phi(h) = \int f(E) f(E + m_g g_n H - \hbar\Omega) dE, \qquad (1)$$

The maximum of this function or scanning curve is determined by the condition

$$m_g g_n H = \hbar\Omega. \qquad (2)$$

Having determined it in experiment and knowing the value of Ω frequency, one may measure the gravitational force acting on the neutron.

Neutron interference filters (NIF) were used as a monochromator and analyzer, and the controllable decrease of the neutron energy was achieved by way of diffraction on the moving grating.

Measurements of scanning curves (1) are conducted for collection of frequencies Ω_j. For each of the curves one may find a position of maximum H_j, which may be counted from certain arbitrary value h_0, under the assumption that $H_j = h_0 + \Delta H_j$. The system of equations found from these measurements

$$\Delta H_j = \frac{\hbar\Omega_j}{m_g g_n} + \eta, \qquad (3)$$

makes it possible to determine the gravitational force $m_g g_n$ acting on the neutron. The constant η

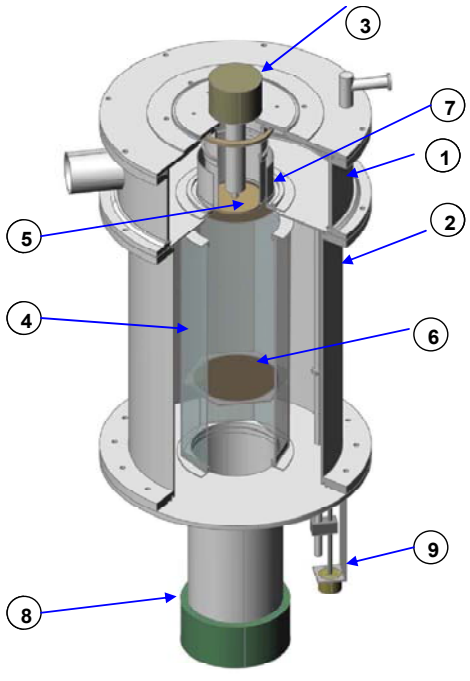

Fig. 5. Gravitational UCN spectrometer. 1- chamber of the spectrum refining, 2- vacuum chamber of the spectrometer, 3- motor-rotary drive of the diffraction grating, 4- mirror neutron guide, 5- diffraction grating on the silicon disk, 6- filter-analyzer in the mobile carriage, 7- filter-monochromator, 8-detector, 9- step motor to shift the analyzer.

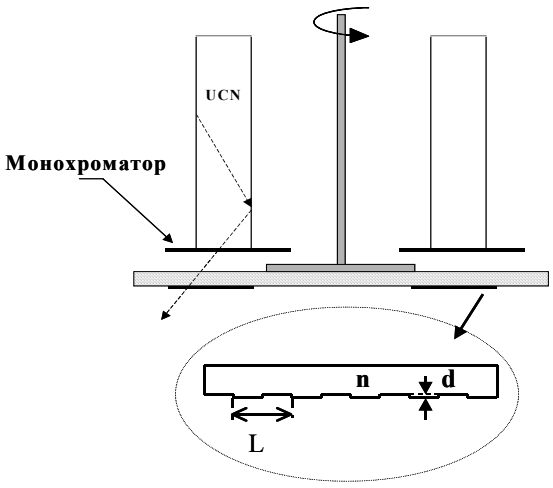

Fig. 6. Upper part of the spectrometer. Circular corridor, monochromator and grating.

takes into account both the above-mentioned diffraction shift and the unknown point of reference h_0**.** It should be emphasized that formula (3) does not contain parameters of spectrometric elements.

The experiment was carried out with the gravitational UCN spectrometer on the ultracold

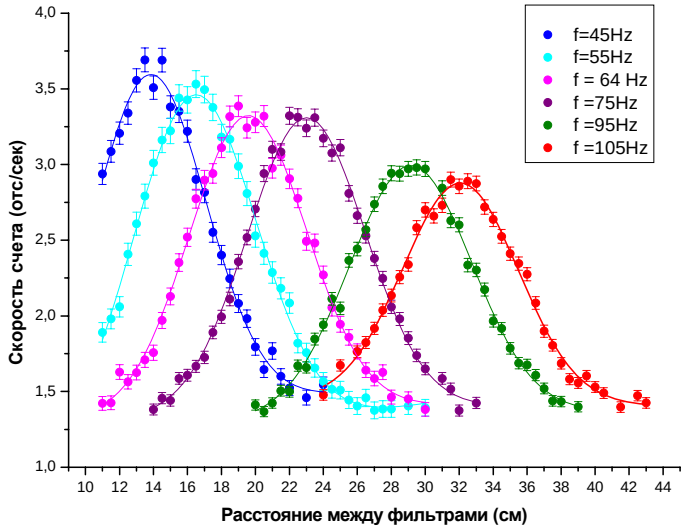

Fig. 7. Scanning curves measured at various rotating frequencies of the grating and fitting Gaussian functions**.**

neutron source of the Institute Laue Langevin (Grenoble, France). The diagram of the experiment is given in Figs. 5, 6.

In the experiment a rotatory grating prepared on the surface of silicon disk **150 mm** in diameter and **0.6** of thickness was used. On the peripheral ring-shaped region of disk, radial grooves were pitted, the width of which was proportional to the radius. This provided for the constant angular distance between grooves, which was equal to the half of the precisely known angular period. It was the value $\alpha = 2\pi/N$ **,** where **N=75398**. The depth of the groove was **0.14 μm** and was chosen in such a way so as to provide the difference of phases $\Delta\varphi = \pi$ of the neutron waves passed through different elements of grating.

The UCN spectrometry was carried out with the help of two identical five-layer interference filters. Each of them had one resonance in transmission at the energy of about **107 neV**. One of them serving as a monochromator was ring-shaped and was placed at the outlet of the supply circular corridor (see Fig. 6). Right under it the diffraction grating was placed. Having passed through the grating, the neutrons proceeded to the vertical mirror neutron guide, inside of which the second interference filter, the analyzer, was placed. The latter could be shifted throughout the height. The neutrons passed through the analyzer were recorded by the detector.

At the fixed rotating frequency of the grating the measurement of scanning curve was carried out, i.e. of the dependence of counting rate on the position of carriage with the filter-analyzer. The rotating frequency of the grating constantly changed. The measurements were carried out in order to collect frequencies from 45 to 107 revolutions per second, that corresponded to the modulation frequency of neutron wave $\Omega = (2.1 \div 5.1)\times 10^7$ radian/s. Two series of such measurements, which differed in the reference point of distances h_0, were carried out**.**

Each of the obtained scanning curves corresponding to diffraction peak of order minus one was fitted by Gaussian function with linear background (see Fig.7.)

$$n = a + bH + A\exp\left(-\frac{(H - H_m)^2}{2\sigma^2}\right). \qquad (4)$$

Out of five parameters determined in such way the parameter $\mathbf{H_m}$ corresponding to the center of the Gaussian curve is essential. The subsequent processing was aimed at the determination of the coefficient B of the linear relation $\mathbf{H_m = c + Bf}$ between the rotating frequency of grating **f** and the value $\mathbf{H_m}$. (See Fig. 8.). The linear MNK-fit of data of two series led to the final value $\mathbf{B_{exp} = 0.30366 \pm 0.000654}$.

Theoretical value of B equals to

$$\mathbf{B_{th}} = \frac{2\pi\hbar \mathbf{N}}{\mathbf{mg}}. \qquad (5)$$

where **N** – the exactly known total number of grating periods. Substituting the table values of neutron masses **m** into (5), the local value of acceleration of gravity **g=980.507(2**), measured at the site of experiment we obtain $\mathbf{B_{th} = 0.304203}$ for theoretical value of coefficient**.**

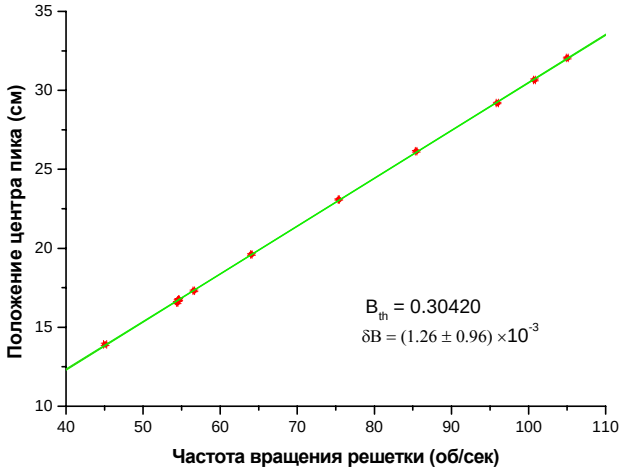

Fig. 8. Dependence of the position of maximum of scanning curve on the rotating frequency of the grating.

Thus, the given result is quite in agreement with the calculation, in which the table value of neutron mass and the value of local gravitational acceleration of macroscopic bodies have been used. It is easy to express the degree of this agreement by the relation $\gamma = \mathbf{B_{exp}} / \mathbf{B_{th}} = \mathbf{mg} / \mathbf{m_g g_n}$. It was obtained: $\mathbf{1\text{-}\gamma = (1.8 \pm 2.1)\times 10^{-3}}$ for the value of the equivalence factor determined in such a way**.**

1.2 Investigation of spatial and time parity violation in the interaction of neutrons with nuclei

1.2.1 Measurement of P-odd asymmetry of the γ-quanta emission in the reaction $^{10}B(n,\alpha_1)^7Li^* \rightarrow ^7Li+\gamma$

Within the framework of the experiments to search for neutral currents in nucleon-nucleon interactions and to determine weak π-meson coupling constant the measurements (in collaboration with PNPI, ILL and TU of Munich) of P-odd asymmetry of γ-quanta from the reaction $^{10}B(n,\alpha_1)^7Li^* \rightarrow ^7Li+\gamma$ were conducted on the polarized cold neutron beam PF1B (ILL, Grenoble).

Weak interactions in nucleon-nucleon systems at low energies are described in the approximation of one-meson exchange (exchanges of π, ρ, ω mesons with transfer of different isospin values 0, 1, 2), where the parity is violated in one of the vertices of NN-diagram. Weak NN-potential is parameterized by a set of 6, in some models of 7, weak meson-nucleon constants. The constants are determined on the basis of the standard model and quark structure of nucleons, however, due to the uncertainties at the account of interference of strong interaction, different approaches give essentially different values of constants. The π-meson coupling constant f_π is

especially sensitive to the model. On the other hand, f_π is entirely determined by the exchange of Z^0-boson between quarks, i.e. by the neutral current. Experiments on scattering of polarized protons on proton target unambiguously registered charged currents in NN-interactions. The values of coupling constants h_ρ^0 and h_ω^0 extracted from these data within the limits of experimental error coincide with the theoretical Diplank-Donahugh-Nolsten «best values» (DDH «best values»). At the same time, the experiment where there were attempts to determine weak π-meson constant give non-coinciding values in the wide range (from 0 to ~$9\cdot10^{-7}$). The theoretical «best value» $f_\pi = 4.6\cdot10^{-7}$. The strictest restrictions were obtained from experiments with ^{18}F ($f_\pi \le 1.2\cdot10^{-7}$) and from our recently completed experiment with ^6Li ($f_\pi \le 1.1\cdot10^{-7}$). Thus, so far there is no unambiguous confirmation of neutral currents in weak NN-interactions.

Before that 2 series of measurements of P-odd asymmetry of γ-quanta from the $^{10}B(n,\alpha_1)^7Li^* \rightarrow ^7Li+\gamma$ reaction were carried out on the cold polarized neutron beam PF1B (ILL, Grenoble). The value $\alpha_\gamma = (5.1 \pm 3.8)\cdot10^{-8}$ was obtained. According to calculations of the Chuvilsky group, the γ-quanta asymmetry $\alpha_\gamma = 1.1\cdot10^{-8}$, if other weak meson-nucleon constants (for the most part h_ρ^0, since it gives the largest contribution to the value of asymmetry) equal to the theoretical Diplank-Donahugh-Nolsten «best values».

This year in measurements a new system of recording of current signals was applied. The method allows one to make a procedure similar to the integration of signal for considerably shorter periods of time than analog integrators. This made it possible to quit the low-frequency region where the contribution of fluctuations of reactor power and noises is maximal and to decrease the error of determining the effect more than by a factor of 1.5: $\alpha_\gamma = (3.9 \pm 3.9)\cdot10^{-8}$. The asymmetry value summed over three cycles (preliminary): $\alpha_\gamma = (4.5 \pm 2.7)\cdot10^{-8}$. The estimation of weak π-meson constant from the obtained data $f_\pi \le 4.7\cdot10^{-7}$. Thus, so far the experimental accuracy is not enough to observe the asymmetry effect in the reaction $^{10}B(n,\alpha_1)^7Li^* \rightarrow ^7Li+\gamma$, but the obtained value points to the f_π value smaller than the «best value».

1.2.2 Search for and investigation of the structure of subthreshold neutron p-resonances in lead isotopes by the combined correlation gamma spectroscopy method

Analysis of the experimental data obtained in control experiments of 2005-2006 on channel 1 of the IBR-2 reactor to search for negative neutron p-resonance in lead isotopes ^{204}Pb and ^{207}Pb completed.

These experiments were carried out on the modernized gamma-spectrometer COCOS with the improved effectiveness and operation speed aimed at verification of the earlier obtained data on the existence of the negative neutron p-resonance in ^{207}Pb isotope instead of ^{204}Pb as was expected on the basis of the work to observe spin rotation of thermal neutrons at the interaction with lead.

Results of the performed analysis did not confirm the presence of considerable deviation of the cross section of radiative capture from the 1/v law in the neutron energy (1 – 5) eV for ^{207}Pb isotope observed in experiments of 2002-2003 and testified to the existence of negative p-resonance in this isotope. If such deviation exists, than it is insignificant and for this isotope the contribution of p-wave does not exceed (5-6)% of s-wave.

For ^{204}Pb isotope the unknown deviation within the limits of error of experimental data was not detected either. This may not unambiguously testify to the absence of negative p-resonance, since in the conducted measurements gamma-transition is recorded, which is mixed around the thermal region of neutron energy from s- and p-resonances, simultaneously, the partial width of such transition for p-wave is unknown. If it is considerably smaller than in s-wave, than it may lead to the impossibility of observation of negative p-resonance by the used method within the limits of experimental accuracy (3-4)%.

1.2.3 Measurement of parameters of low-voltage neutron resonances of Xe

In experiments on optical polarization of Xe isotopes carried out in KEK (2004), it was revealed that table data for resonances 9.5 eV (^{129}Xe) and 14.4 eV (^{131}Xe) do not describe the

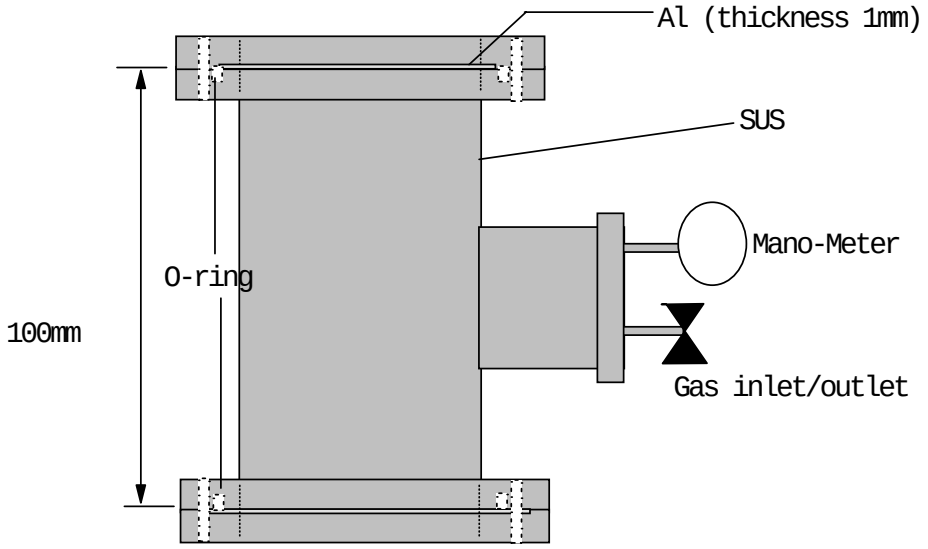

Fig. 9. Vessel-target to measure total neutron cross section of Xe.

measured transmission data. Moreover, in the course of comparison of data from different libraries

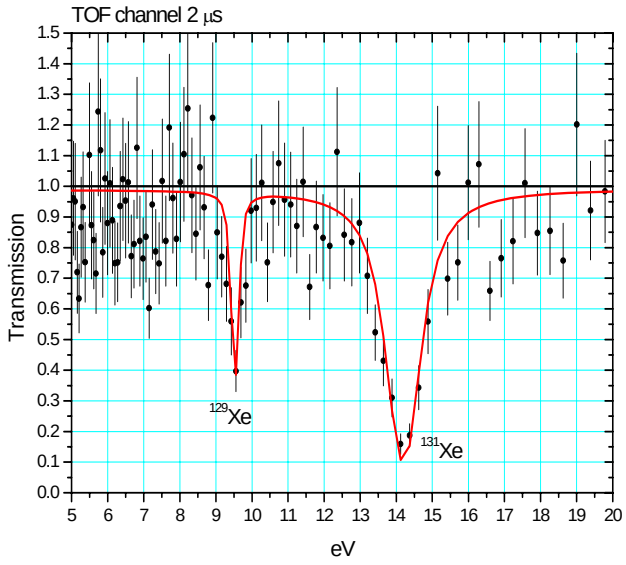

Fig. 10. Neutron transmission of natural Xe. Curve – result of fitting.

(ENDF VII, JENDL 3.3, JEF 2.2) considerable discrepancies were also noted. In this connection, on the Pohang Neutron Source (Republic of Korea) special measurements of the total neutron cross section were carried out. For this a vessel-target was manufactured, its diagram is shown in Fig. 9.

The vessel was filled with natural mixture of Xe isotopes at the pressure of 1 atm. In Fig. 10 the measured transmission and results of fitting are presented. In **Tables 1 and 2** the obtained values of parameters are given. Results of the given study are submitted for publication in the journal «Nuclear Instruments and Methods».

Table 1. Parameters of resonance 9.5 eV ^{129}Xe

Value	Initial[1]	Present study
E (eV)	9.5	9.531±0.016
Γ_n (meV)	6.0	12.68±0.18
Γ_γ (meV)	110	114.2±1.7

Table 2. Parameters of resonance 14.4 eV ^{131}Xe

Value	Initial [1]	Present study
E (eV)	14.4	14.19±0.04
Γ_n (meV)	216	242.7±0.5
Γ_γ (meV)	94	419.7±0.5

1.3 Investigations of the properties of atomic nuclei

1.3.1 Search for exotic modes of fission on the IBR-2 reactor using the «Mini-Fobos» facility

In the previous experiments, in which the spontaneous fission of ^{252}Cf was studied, numerous indications were detected on the existence of the unusual, at least threefold, decay channel, which was called threefold collinear cluster decay [2]. For the investigation of the observed effect the study of various nuclear fissionable systems at various excitation energies up to the survival threshold of nuclear shells was planned. One of the reactions chosen for the study was the reaction ^{235}U (n_{th}, f).

The experiment was carried out on the thermal neutron beam of the IBR-2 reactor at the Frank Laboratory of Neutron Physics using the two-arm time-of-flight heavy ion spectrometer miniFOBOS [3]. Detectors of the spectrometer allow one to find both the primary fragment masses and the final ones (i.e. before and after neutron release), vector of velocity (of pulse), and also fragment path in gas of the ionization chamber in each arm of the spectrometer.

In the experiments a specific two-dimensional bump in the mass-mass distribution of fission fragments was observed [4] (see **Fig. 11a**). The effect was revealed only in one arm of the spectrometer, namely on the part of the target substrate. The yield of events forming the bump is about $5*10^{-3}$ per one double fission. This estimation was obtained after the subtraction of «tail» 2 from «tail» 1. The corresponding subtractive spectrum (the bump as such) is shown in Fig. 11b. The yield maximum in the bump lies in the vicinity of masses 68–70 associated with magic Ni isotopes.

One more manifestation of clusterization was obtained as a result of special treatment of the mass-mass fragments. The selection of fission fragments was carried out in accordance with their velocity and pulse. The events having approximately the same velocities and lying simultaneously outside «tails» of the scattered events in fragment distribution over pulses were selected. (**Figs. 12a,b**)

[1] Low Energy Neutron Physics, Subvolume B, Tables of Neutron Resonance Parameters, Edited by H. Schopper ISBN 3-540-63277-8, Springer-Verlag Berlin Heidelberg, 1998.
[2] Yu.V. Pyatkov et al., Phys. Atom. Nucl. V.66, 1631 (2003).
[3] D. V. Kamanin et al., International Symposium on Exotic Nuclei, Peterhof, Russia, 5-12 July 2004. Conference proceedings. Published by World Scientific Publishing Co. Pte. Ltd., 2005, p. 588-591.
[4] Yu. V. Pyatkov et al., Preprint JINR E15-2005-99, Dubna, 2005

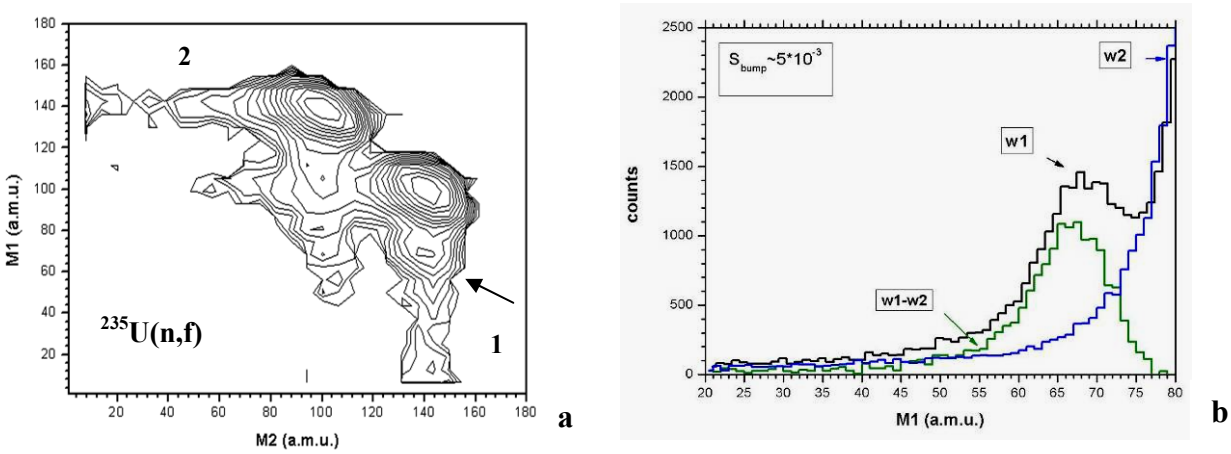

Fig. 11. Mass-mass distribution of fragments (logarithmic scale) obtained in the reaction ^{235}U(n,f) (a). The peculiarity of spectrum 1 in question is denoted by an arrow. The projection of distribution on axis M1 (b): «tail» 1 gives spectrum w1, «tail» 2 – spectrum w2, and the result of their subtraction is denoted as w1-w2.

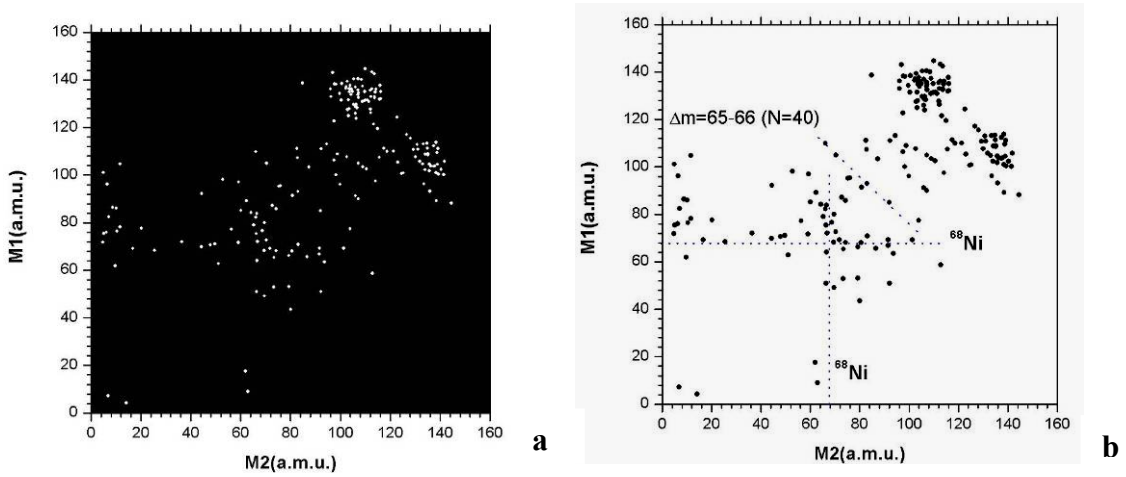

Fig. 12. Mass-mass distribution for fission events with approximately equal velocities taken outside the «tails» of scattered fragments in the pulsed distribution (a). Specific structure in the shape of a straight angle is clearly seen in the distribution center. Vertex of the angle is located at the point (68, 68) presumably related to the magic isotope ^{68}Ni (b).

A specific structure in the distribution center is noteworthy. It looks like a straight angle with the vertex lying in the vicinity of the point (68, 68) a.m.u., which presumably corresponds to the magic nucleus ^{68}Ni $_{40}$. Using the same selection, a similar structure (rectangle) was earlier revealed in the mass-mass distribution of fragments of spontaneous fission of nucleus ^{252}Cf [^{5}]. Certain points on the distribution lie approximately on the line M1+M2=const (slanting dotted line in Fig. 12b). The corresponding «missing fragment» is also related to the known neutron subshell N=40.

The basic meaning of the presented results is that they mainly confirm the results obtained earlier for various fissionable systems.

1.3.2 Investigation of escape of delayed neutrons at the «ISOMER-M» facility

As the continuation of investigations of characteristics of delayed fission neutrons of major and minor reactor isotopes in 2006-2007, measurements of the delayed neutron yield at the fission

[5] Yu. V. Pyatkov et al., Preprint JINR E15-2004-65, Dubna, 2004

of isotope ^{245}Cm by thermal neutrons at the «Isomer-M» facility of channel 11b of IBR-2 completed. In spite of the high enrichment of the studied sample by isotope ^{245}Cm (95.46%) and large fission cross section of it by thermal neutrons (~2145 b), accompanying isotopes ^{244}Cm and ^{246}Cm create constant background of prompt neutrons of the spontaneous fission and determine the smallness of the effect-background relation in measurements of the delayed neutron yield. This circumstance required to carry out the modernization of the measurement module to provide the maximal stability of operation, to optimize the operation mode of the facility and to take accurately into account all the components of background in the course of measurements.

On the completion of processing of all the experimental data, the value of total delayed neutron yield at the fission of isotope ^{245}Cm by thermal neutrons ν_d = (0.64±0.02)% was obtained. This value is the second known experimental result and stands out from the first one by the twice better accuracy. The comparison of this result with the global systematics of the delayed neutron yields showed that it coincided with the value obtained within the framework of the simplified variant of this systematics.

1.3.3 Gamma-spectroscopy of neutron-nuclear interactions

Complex analysis of the experimental data on the process of cascade gamma-decay of the neutron resonance makes it possible to obtain fundamentally new information on the properties of nuclear matter lower than the excitation energy approximately 5-10 MeV. Its most important result is the fundamentally new information on the dynamics of interaction and transition into each other of superfluid and common state of nuclear matter. The approximation of a large set of experimental values of density of excited levels of nuclei from the mass region $39<A<201$ showed that excitations of the phonon type determine the structure of excited levels for 90% and more at least lower than the half of neutron binding energy. Analysis of the published experimental data on the intensities of primary gamma transitions of the neutron capture with the energy about 2 keV carried out at FLNP by the original method made it possible to improve these results and estimate their maximal systematic error. In addition, the fact of absence of abrupt change of parameters of the cascade gamma decay from the possible change of structure of neutron resonance in this interval of their energies was established. The approximation of experimental data on the partial widths of primary dipole gamma transitions in the region of neutron binding energy confirmed strong influence of the superfluid state of nucleus on this parameter of the cascade gamma decay of neutron resonance as well. Thus, the possibility and necessity of the direct experimental and theoretical study of superfluidity of the heated nucleus up to its temperature of no lower than 0.5 MeV was demonstrated.

1.3.4 Investigation of (n,p) and (n,α) reactions

The experiments to determine coefficients of the forward-backward correlation in the reaction ^{14}N(n,p)^{14}C continued at the EG-5 accelerator, FLNP JINR, in the region of proximate low-lying resonances. Due to the technical reasons in 2007 beam time at the accelerator was restricted. Measurements in 5 energy points were carried out both to check the results obtained earlier and at different energies. Nevertheless, the data are insufficient for carrying theoretical analysis.

At the neutron time-of-flight source of the Moscow Meson Factory, INP RAS, in Troitsk test measurements at the flare duration of 5 μs for the experiments to determine P-even correlations in the reaction ^{35}Cl(n,p)^{35}S were carried out. On the basis of the obtained data the estimation of possibilities to study P-even correlations in the reaction ^{35}Cl(n,p)^{35}S was performed. At the same beam parameters as in the test measurement (flare duration 5 μs, frequency 50 Hz, average current of protons on the target 1.5-1.7 μA) it is possible to reach the accuracy of $5\cdot10^{-2}$ in the energy intervals under study for 3 days of measurements.

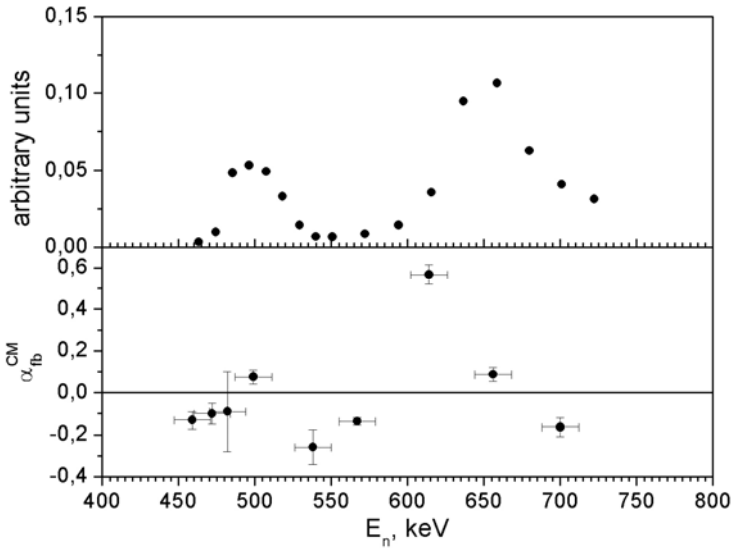

Fig. 13. Upper diagram – relative proton yield from the reaction $^{14}N(n,p)^{14}C$; lower diagram – values of the forward-backward correlation in the system of mass center.

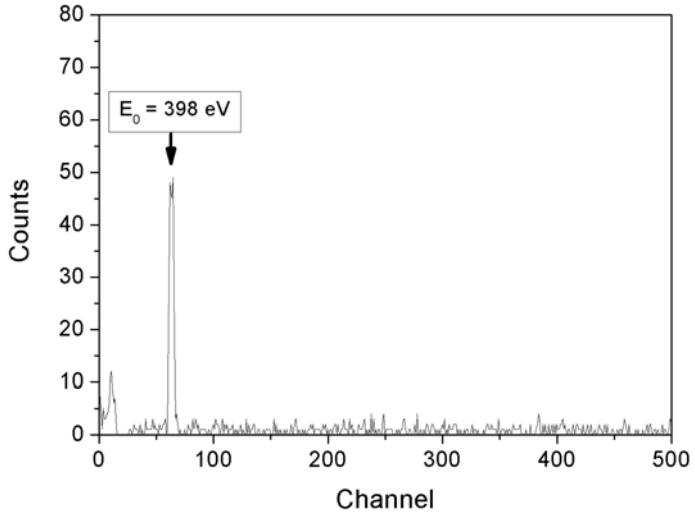

Fig. 14. Time-of-flight spectrum of the reaction $^{35}Cl(n,p)^{35}S$ at the flare duration of 5 μs and frequency 50 Hz. Value of channel 1 μs.

2. Theoretical investigations

It was shown by the extrapolation of the optical potential of neutron interaction with matter on the region of large densities, which take place in the neutron star, that in the neutron star the forces of neutron striction occur, which compress the star in addition to the gravitation forces. It was shown by way of numerical calculations that the effect of optical forces on the mass, star radius and distribution of density in it surpasses the influence of effects of the general relativity theory. Also, it was shown that in the presence of resonance in neutron-neutron scattering in the star pulsations may occur and the star may explode with a great energy production.

Based on the assumption that the neutron wave function appears to be a wavepackage, the question is posed: does the package width change with the energy growth or not? To answer this question the experiment to determine temperature dependence of the scattering cross section of slow neutrons in He^4 gas was carried out. As follows from the results of experiment, the wavepackage width decreases with the energy growth in inverse proportion to the neutron velocity.

On the basis of algebraic approach to the description of process of neutron transportation in homogenous and fine medium new formulae for the neutron albedo from layers of substances of the

given thickness were obtained. The new formulae have the advantage as compared to the known ones obtained earlier on the basis of the diffusion theory, since they may be applied in a wider range of parameter change. They may be used to calculate reactors and radiation protection.

The method of long-wave neutron holography was developed without a reference beam, which allows one to record holographic image of magnetic and non-magnetic macroscopic structure of non-transparent objects and to reproduce image in visible light. The method is based on obtaining the neutron beam in coherent superposition of states with two various energies. The difference of energies and wave vectors of these states creates in space a neutron precession wave, the length of which is greater than the de Broglie wavelength in several orders.

Full solution of the problem on the neutron interaction with substances having helicoid magnetic structure was obtained. The matrix amplitudes of reflection and transmission of helicoid magnetic mirrors were calculated and the effect of resonance reflection with spin flip was detected.

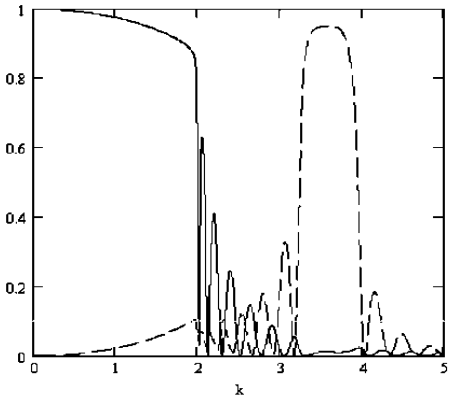

The Figure illustrates reflection coefficients with spin flip (dotted curve) and without spin flip (solid curve) at helicoid mirror of the final thickness at the polarization of incident neutron antiparallel to the helicoid vector. The Y-axis represents the reflection coefficient, and the X-axis – the wave neutron vector in dimensionless units. One can see that the reflection with spin flip is of resonance character, and the resonance takes place at the wave neutron vector, which is equal to the helicoid one.

3. Applied and methodical research

3.1 Investigation of element composition and structure of near-surface layers of solids at the EG-5 accelerator

On charged particle beams of the EG-5 accelerator analytical investigations using nondestructive nuclear-physical techniques: RBS (Rutherford backscattering method) and ERD (elastic recoil detection method) were conducted. Depth profiles of various elements starting from hydrogen and deuterium up to gadolinium and tungsten were measured.

In cooperation with Institute of Electrical Engineering of SAS (Bratislava, Slovak Republic) nano-layers of metals and metallic oxides applied on silicon substrates were analyzed. Using the nondestructive RBS method, elemental analysis of the layer containing 1.9×10^{16} at/cm^2 of gadolinium, 2.7×10^{15} at/cm^2 of scandium and 4.5×10^{16} at/cm^2 of oxygen was performed. Fig. 15 shows the spectrum of helium ions with the energy 2.035 MeV scattered for the 170º angle on the sample, the thickness of which is 17 nanometers. The thickness of superficial layer and its elemental content were determined as a result of computer processing of the experimental spectrum.

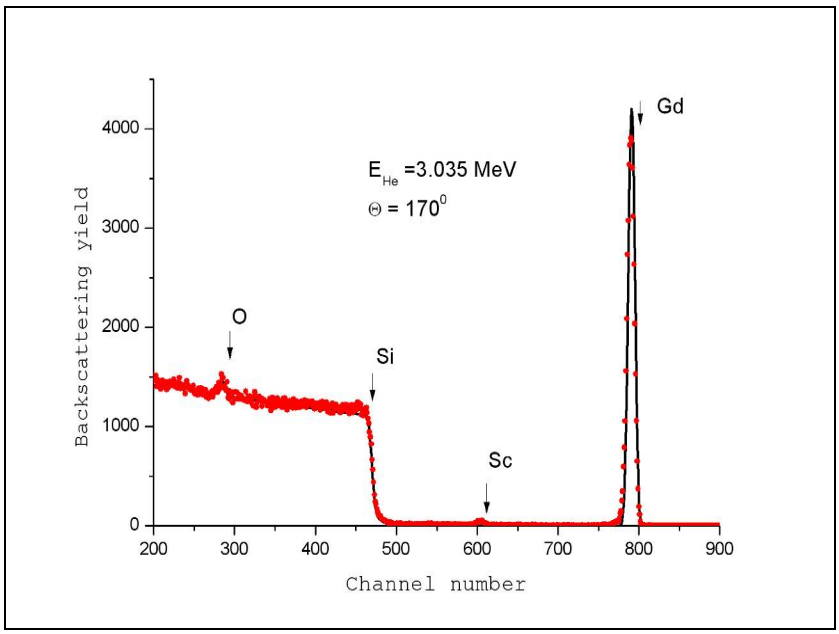

Fig. 15. Experimental spectrum (dots) and calculated (line) one for the optimized model of sample.

Similar investigations were carried out in cooperation with Voronezh State University. The analysis of samples of lamellar structures with the thickness of layers ranging from nanometers to 1-2 micron was carried out. For elemental analysis of lamellar structures of micron thickness the proton beam obtained from the EG-5 accelerator, FLNP, was also used. Using the ERD method, the analysis of silicon samples saturated with hydrogen and deuterium was carried out.

In cooperation with Institute of Physics of the Marie Curie-Sklodowska University and Lublin University of Technology (Lublin, Poland) and also with Sumy Institute for Surface Modification (Sumy, Ukraine) samples of modifies constructional materials were analyzed. In particular, detailed investigations of a change of superficial properties of stainless steel implanted by various doses of nitrogen were performed. Also, investigations of the process of extraction of positive charged ions from plasma aimed at optimization of ion sources for implanters were carried out.

3.2 Analytical investigations using neutron activation analysis at the IBR-2 reactor

Ecology

Biomonitoring

In March, 2007 in Dubna at the XX anniversary Meeting of the UN Commission on Transboundary Air Pollution in Europe the works of the NAA sector carried out in the framework of the international program "Atmospheric heavy metal deposition in Europe—estimation based on moss analysis" were summed up. The scope of these works covers several regions of Central Russia, Southern Urals, Belarus, Bulgaria, Slovakia, Poland, Romania, Serbia, Macedonia, Croatia and Greece, as well as Mongolia and Vietnam, where more than 2500 samples of moss-biomonitors were collected and analyzed.

The results of the analysis for European countries on 13 elements: Al, As, Cd, Cr, Cu, Fe, Hg, Ni, Pb, Sb, Ti, V and Zn have been submitted to the European Atlas of heavy metal atmospheric deposition and the complete data on 40-43 elements, including lanthanides (rare earth elements) and actinides (uranium and thorium) have been published in the papers relating to the regions concerned. To evaluate levels of environmental pollution in the industrial ecologically stressed regions of Russia, the results of the analysis of moss-biomonitors from Prioksko-Terrasny

and Voronezh biosphere reserves obtained in collaboration with the Institute of Global Climate and Ecology (Moscow) were used as background values.

In 2007, possible ways of collaboration with the University of Stellenbosh (SAR) in the field of biomonitoring (study of distribution of atmospheric methyl-mercury depositions using moss-biomonitors and NAA) were outlined.

Ecosystem assessment

In 2007, in the frameworks of the RFBR-Romanian Academy project "Geochronology and study of retrospective pollution of unconsolidated bottom sediments from oxygen-containing and oxygenless water areas of the Western part of the Black Sea" the treatment of the NAA results of the bottom sediments collected at the Black Sea shelf of the Romanian coast was completed and the retrospective pollution assessment for this region was made. In 2007, in cooperation with the Romanian team three publications and a report to RFBR were prepared on the project.

The work to study aerosol filters from Slovakia was completed and the results of multielement NAA of the collection of aerosol filters of different years received from Bratislava, which made it possible to characterize the dynamics of atmospheric pollution of the Slovak capital by heavy metals for the last 15 years, were submitted for publication.

In cooperation with the University in Opole (Poland) the complex investigation to assess the environmental condition on the "anomalous territory" in western Poland with the increased radiation background owing to the Chernobyl accident and technogenic industrial impact has been carried out. First results are presented in the joint paper accepted for publication by Polish journal "Ecological Chemistry and Engineering" in 2007.

In collaboration with Dubna University the study of the distribution of a number of heavy metals in the vicinity of road interchanges in Dubna and in Moscow (Schelkovskoe and Minskoe highways) has been completed. The results have been reported at two International Conferences and submitted for publication.

The results of NAA (JINR) and AAS (University in Skopje) of 200 soil samples from the area of the lead-zinc industrial complex in Macedonia have served as a basis for the Atlas of heavy metal distribution maps to be published in Macedonia.

Food and human health

In 2007, at the reactor of MEPhI (Moscow) work to analyze foodstuffs continued in the frameworks of the joint project of the NAA sector with the Nuclear Energy Corporation of South Africa (NECSA): "Comparative study of the impact of consumption of foodstuffs grown in several industrial regions of Russia and Southern Africa on children's health using nuclear-physical analytical methods".

The determination of a number of short-lived isotopes in foodstuffs was conducted at the reactor of Budapest Neutron Center in October, 2007. The treatment of the results is underway.

Within the framework of the IAEA Coordination Program "Exposure of women of reproductive age to toxic and potentially toxic elements in developing countries" in cooperation with the Russian State Medical University (Moscow), the Analytical Center of the Geological Institute of RAS and I.M.Sechenov Moscow Medical Academy the work to interpret the results of multielement analysis of blood samples of specially selected patients from one of the industrial regions of Moscow has been continued. These investigations have supported the hypothesis about the correlation of such toxic elements as lead, zinc and stibium with the body mass index of the examined patients.

Biotechnologies

In the NAA sector in collaboration with the Andronikashvili Institute of Physics (Tbilisi, Georgia) studies on new biotechnologies using various microorganisms to clean up contaminated environment from toxic metals (mercury, chromium, etc.) have been continued. New results of the studies into the possibility of application of natural strains of *Arthrobacter oxidans* bacteria, isolated from basalts to reduce toxic Cr(VI) to stable nontoxic Cr(III) were presented at the International Conference on Modern Trends in Activation Analysis (September 17 – 21, Tokyo, Japan). A series of seven papers in the field of application of nuclear-physical methods in biotechnologies is submitted for the JINR 2007 scientific research competition.

Materials science

Synthesis of fine-grained diamonds

In 2007 the joint paper (in cooperation with the Institute of Solid State and Semiconductor Physics of Belarusian Academy of Sciences) on the study of effect of neutron irradiation on the properties of synthetic diamonds using Ni-Mn-C-Al_2O_3 system as an example was submitted to "Crystallography Reports", and the summarized data on the behavior of defects in fine-grained diamonds under exposure to neutron irradiation in the presence of catalysts are to be included as a separate chapter in the book "Diamond and Related Materials" (Nova Science Publishers, Inc., USA, 2007, in press).

Archeology

Within the framework of cooperation with the State Hermitage (Saint-Petersburg) the statistical analysis of the earlier obtained NAA results of ceramic samples from ancient burial mounds (Syrtea Smolensk region and North Caucasus) has been performed. The results were discussed at the Workshop in the Hermitage (November 23, 2007), where directions of further investigations were outlined.

Radioecology

In cooperation with Comenius University in Bratislava in the low-background laboratory of the Department of Physics for the first time radiometric measurements have been carried out with 50 samples of moss-biomonitors collected in Minsk and Gomelsk areas of Belarus 20 years after the Chernobyl accident. The results of the measurements have demonstrated that the level of ^{137}Cs activity in Gomelsk area is three times higher than that of in Minsk area. High content of ^{210}Pb has been observed in this area, which is most probably due to the post-disaster cleanup operations in 1986. Publication in a peer reviewed journal is in preparation.

1.2. НЕЙТРОННАЯ ЯДЕРНАЯ ФИЗИКА

Введение

В течение 2007 в связи с остановкой реактора ИБР-2 на модернизацию основные работы в области нейтронной ядерной физики в ЛНФ им. И. М. Франка проводились нейтронных пучках других ядерных центров России, Болгарии, Польши, Чехии, Германии, Республики Корея, Китая, Франции, США, Японии, а также на ускорителе ЭГ-5 в ЛНФ. Исследования проводились в традиционных направлениях: изучение процессов нарушения пространственной и временной четности при взаимодействии нейтронов с ядрами; изучение квантово-механических характеристик, энергетики и динамики процесса деления; экспериментальное и теоретическое исследование электромагнитных свойств нейтрона и его бета-распада; гамма-спектроскопия нейтронно-ядерных взаимодействий; структура атомного ядра; получение новых данных для реакторных приложений и для ядерной астрофизики; эксперименты с ультрахолодными нейтронами; прикладные исследования.

1. Экспериментальные исследования

1.1 Фундаментальные свойства нейтрона

1.1.1 Работы в рамках подготовки и проведения эксперимента по прямому измерению сечения рассеяния нейтрона на нейтроне на реакторе ЯГУАР (РФЯЦ-ВНИИТФ, г.Снежинск)

Основным результатом за 2007, достигнутом в рамках этой деятельности, является то, что удалось создать нейтронный детектор, удовлетворяющий всем требованиям эксперимента. Необходимо отметить, что эти требования весьма жесткие и противоречивые.

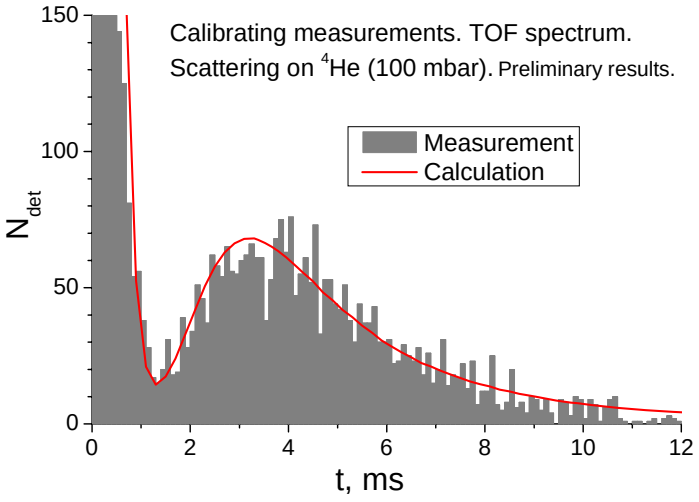

Рис. 1 Времяпролётный спектр зарегистрированных нейтронов

Никогда ранее не создавались нейтронные детекторы, совмещающие в себе такие свойства, как высокую скорость счета (~10^6 c^{-1}), эффективность регистрации нейтронов ~100%, высокое энергетическое разрешение (не хуже 10%), и низкую чувствительность к γ-квантам ~10^{-9}. Детектор был смонтирован на экспериментальной установке и прошел успешное испытание в калибровочных измерениях на газах в импульсном режиме работы реактора

ЯГУАР. Результаты предварительной обработки результатов, полученных в газовых измерениях, представлены на Рис. 1. На этом рисунке представлен времяпролётный спектр зарегистрированных нейтронов. Таким образом, в настоящее время установка для измерения nn-рассеяния полностью готова.

В 2008 году планируется закончить калибровки на инертных газах, добиться необходимых фоновых условий и начать измерения сечения nn-рассеяния.

1.1.2 Исследование n-e рассеяния

Проведены подготовительные работы к эксперименту по извлечению длины n,e-рассеяния из энергетической зависимости угловых распределений рассеяния тепловых нейтронов благородными газами на вертикальном нейтронном канале установки ТРОНС.

Подготовленный к эксперименту вертикальный нейтронный канал представляет собой откачиваемую трубу из нержавеющей стали с внутренним диаметром 100 мм и длиной около 10м. Коллимационное отверстие на входе канала – 80 мм, на выходе – 20 мм. Это обеспечивает то, что диаметр расходящегося нейтронного пучка внутри камеры рассеяния длиной 1 м не будет превышать 25 мм.

При анализе угловых распределений медленных нейтронов, рассеянных газами в экспериментах по определению структурных факторов и длины n,e-рассеяния, возникает необходимость учета теплового движения атомов газа. Корректный учет этой поправки необходим при извлечении n,e-эффекта, поскольку анизотропия рассеяния из-за теплового движения атомов газа существенно больше анизотропии, вызванной n,e-взаимодействием.

В отличие от других работ, где вообще не учитывается влияние теплового движения на описание эффекта дифракции, в предложенном нами описании углового распределения рассеянных нейтронов (с включенным в него вкладом n,e-рассеяния) эта поправка учитывается и в дифракционном члене.

Был проведен модельный эксперимент с учетом теплового движения газа методом Монте-Карло. Для сравнения трех вариантов учета теплового движения (Плачека, Турчина и Монте-Карло) для каждого из них рассчитывалась анизотропия вперед-назад для

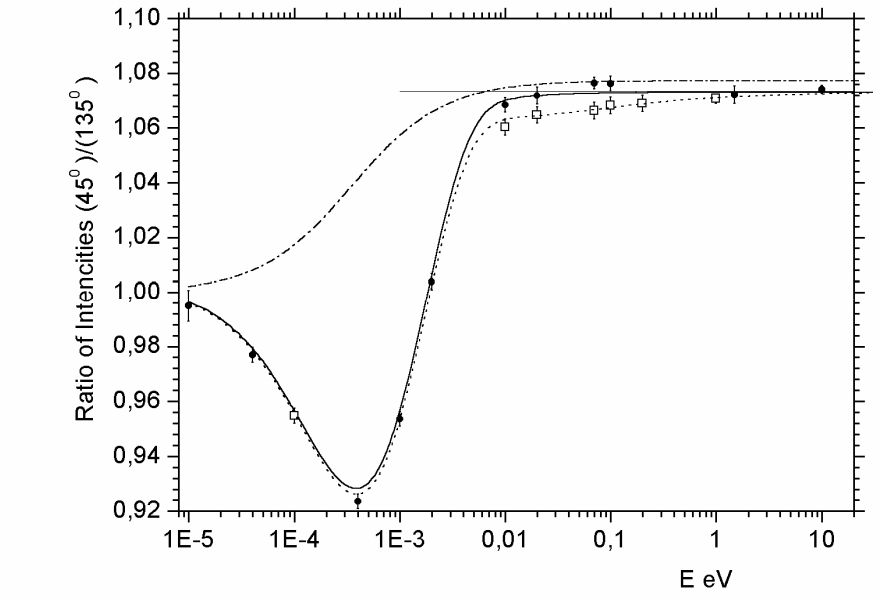

Рис. 2 Анизотропия рассеяния нейтронов аргоном вперед-назад, рассчитанная для разных вариантов учета теплового движения атомов газа. Штрих- пунктирная кривая – приближение Плачека, точечная и сплошная линии соответствуют подходу Турчина с учетом n,e-взаимодействия и без него, соответственно. Прямая линия – расчет без учета теплового движения атомов.

углов рассеяния $\theta_1 = 45^o \pm 5^o$ и $\theta_2 = 135^o \pm 5^o$ (для двух первых вариантов проводилось интегрирование в указанных пределах углов, а в расчетах по Монте-Карло отбирались события, приводящие к попаданию рассеянных нейтронов в указанные интервалы). Результаты вычислений представлены на Рис. 2. Значение отношения вперед-назад меньшие единицы появляются, когда начальная скорость нейтрона уменьшается настолько, что становится сравнимой со скоростью атома. Тогда для атомов, движущихся по направлениям, близким к скорости нейтронов, поток нейтронов, пропорциональный относительной скорости нейтрон-атом, становится значительно меньше, чем для атомов, движущихся навстречу нейтронам. Поэтому вероятность рассеяния назад превышает вероятность рассеяния вперед. Если скорость нейтрона много меньше скорости атома, то почти неподвижный нейтрон симметрично бомбардируется атомами спереди и сзади, и распределение рассеянных нейтронов приближается к симметричной форме.

Были проведены также расчеты угловой анизотропии $45^0/135^0$ в геометрии, приближающейся к классическому опыту Крона- Ринго в предположении применения кольцевого ^{3}He-счетчика с давлением 10 атм. Анизотропия вычислялась аналитически интегрированием в пределах углов рассеяния $\pm 2{,}5^0$ и $\pm 5^0$, а также с использованием метода Монте-Карло. Результаты этих расчетов для ксенона представлены на Рис. 3.

Формализм Турчина и метод Монте-Карло описывают анизотропию во всем диапазоне начальных энергий нейтронов одинаково, и можно утверждать, что формализм Турчина дает правильный учет теплового движения атомов в задачах рассеяния нейтронов на благородных газах. Приближение Плачека совершенно неправильно описывает анизотропию при энергиях нейтрона ниже 10 мэВ и, кроме того, не дает также правильной асимптотики при переходе к большим энергиям, при которых коэффициент анизотропии не зависит уже от теплового движения атомов. На Рис. 3 эффект n,e-рассеяния проявляется ямкой в области энергий тепловых нейтронов, глубина которой как раз зависит от величины длины n,e-взаимодействия. Сравнение аналитических расчетов анизотропии с расчетами методом Монте-Карло показывают, что в исследованном диапазоне углов рассеяния нейтронов при

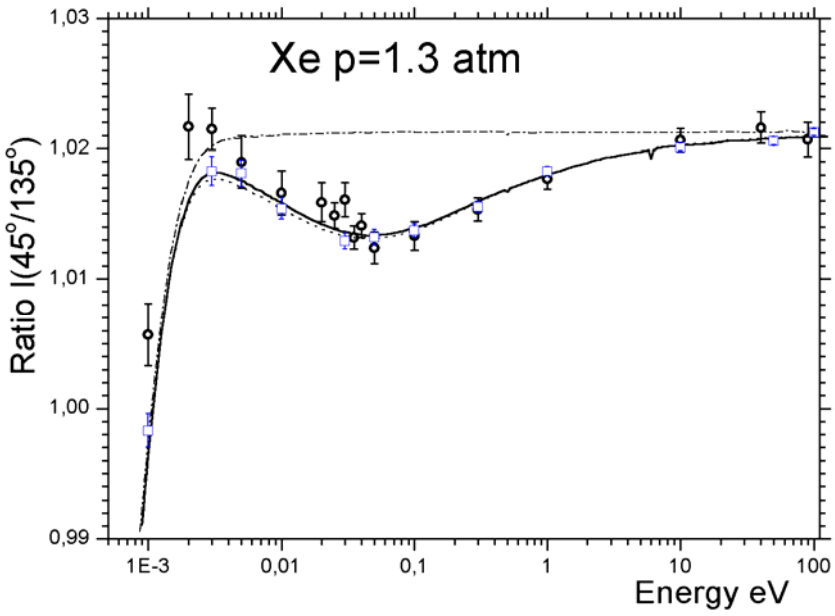

Рис. 3 Расчетная анизотропия рассеянных нейтронов на ксеноне: сплошная и точечная кривые – расчет в подходе Турчина с учетом n,e-взаимодействия для углов рассеяния $\pm 2{,}5^0$ и $\pm 5^0$, пунктирная кривая – без учета n,e-рассеяния. Результаты расчетов методом Монте-Карло (с учетом n,e-взаимодействия): светлые квадраты – рассеяние в малом пространстве, светлые точки – в реальной геометрии.

анализе первичных экспериментальных данных и извлечении из них длины n,e-взаимодействия можно будет ограничиться применением формализма Турчина, что существенно упростит анализ эксперимента.

Также были проведены расчеты телесных углов и эффективностей детекторов в реальной геометрии для рассеивающих газов Ar, Kr, Xe и энергий нейтронов от 12 мэВ до 400 мэВ. Отношение вероятностей регистрации нейтронов, рассеянных на углы 135 и 45 градусов, дает величину поправочного множителя к экспериментальному отношению отсчетов детекторов $45^0/135^0$.

В силу оригинальности осуществляемого эксперимента почти все подходы для учета многочисленных поправок с точностью порядка 10^{-4} доли от ядерного рассеяния по необходимости оказываются новыми. В частности, безмодельный учет теплового движения атомов мишени выявил тонкости в угловой анизотропии, которые не передает обычно используемая модель Плачека (она слишком груба для наших целей). Кинематическое описание движения нейтрона и атома, как и точная поправка на сброс энергии нейтроном, рассеиваемым на разные углы, позволят получить прецизионную величину длины n,e-рассеяния из измеренной анизотропии рассеяния.

В 2008 году планируется проведение в Троицке эксперимента с рассеянием тепловых нейтронов на аргоне при низких давлениях (порядка атмосферного) с использованием метода времени пролета. В эксперименте будет реализована возможность получения значения b_{ne} для разных энергетических участков спектра нейтронов (и разных значений электронного форм-фактора атома $f(E,\vartheta)$) взамен усредненного по спектру значения b_{ne}.

1.1.3 Изучение возможности поиска многомерной гравитации

Теоретически рассмотрены возможности экспериментальной проверки с помощью рассеяния нейтронов различных энергий ньютоновского закона тяготения ($F \sim 1/r^2$) на малых (менее 5мм) расстояниях. Отклонение от закона можно ожидать в случае справедливости идеи о существовании многомерной гравитации. В рамках теоретической модели, связанной с длиной электрослабого взаимодействия, в борновском приближении получены выражения для амплитуд гравитационного рассеяния нейтронов. Сила тяготения при этом записывается в виде: $F_n = -G\frac{m_1 m_2}{r^{n+2}}R_c^n$, где R_c - некоторое характеристическое расстояние, n=0,1,2,…. характеризует многомерность гравитации и при n =0 формула переходит в обычную ньютоновскую формулу, записанную выше. Формула должна быть справедлива при $r \le R_c$. При $r > R_c$ должен выполняться ньютоновский закон гравитации. Можно также получить:

n	1	2	3	4
R_c, см	1.2×10^{17}	2.8	8×10^{-6}	1.4×10^{-8}

Значение n =1 в приведенной таблице следует отбросить, так как величина R_c превосходит размеры солнечной системы и орбиты планет были бы нестабильны. Размеры R_c менее 1 см трудно проверить с помощью макроскопических экспериментов, однако опыты с нейтронами могут быть в принципе возможны.

Амплитуду гравитационного рассеяния можно найти в борновском приближении. Так например для n =2 она имеет вид:

$$f(\varphi)= \frac{2}{3} m_n^2 m_T G_f^2 c^7 \hbar \int_0^{R_c} \frac{\sin qr}{qr^2} dr$$

где $q=2k\sin\varphi/2$, k – волновое число, φ - угол рассеяния, m_n и m_T - взаимодействующие массы, G_f - константа Ферми.

Вычислено влияние гравитационного рассеяния на асимметрию (вперед-назад) рассеяния нейтронов, взаимодействующих с ядрами при энергиях нейтронов от ультрахолодных (10^{-10} эВ) до нескольких ГэВ. Анализ результатов показывает, что эксперименты подобного рода при существующей точности вряд ли могут служить проверкой идеи существования многомерной гравитации.

Однако, несмотря на отрицательные результаты оценок поиски возможных проявлений многомерной гравитации с помощью нейтронов следует продолжать, вследствие важности поставленной задачи.

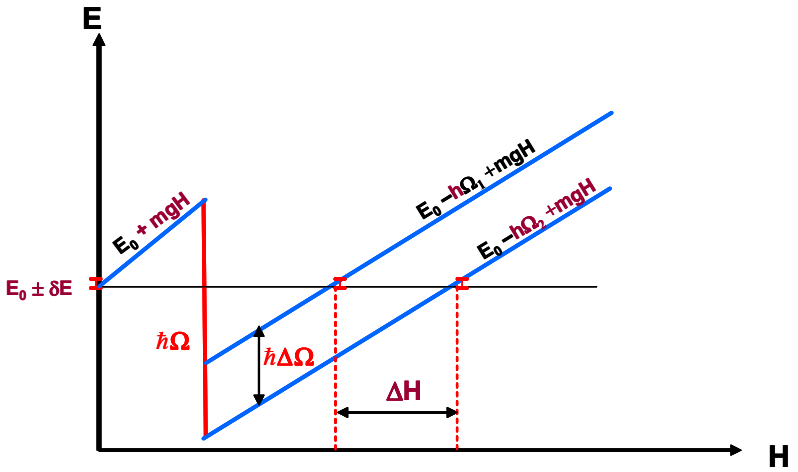

Рис. 4 Идея эксперимента.

Нейтронная оптика

1.2.1 Проверка слабого принципа эквивалентности для нейтрона

В 2006 году была закончена обработка данных эксперимента по проверке принципа эквивалентности для нейтрона, выполненного в 2006 году. Результаты работы опубликованы.

Идея эксперимента состоит в сравнении изменения энергии нейтрона **mgh** при его падении с высоты h с величиной энергии $\mathbf{\Delta E = \hbar\Omega}$, переданной нейтрону, при взаимодействии с нестационарным устройством. Она поясняется рисунком. 4.

Узкий энергетический спектр нейтронов **f(E)** формируется монохроматором, расположенным на высоте **H=0**. Для того чтобы попасть в детектор и быть зарегистрированными нейтроны должны пройти через анализатор, расположенный ниже монохроматора на величину **H** и обладающий такими же спектрометрическими свойствами. На пути между монохроматором и анализатором нейтроны ускоряются в гравитационном поле Земли. Поскольку ширина спектральной функции **f(E)** мала, то уже при относительно малом расстоянии **H** система становится непрозрачной. Однако, если на этом пути энергия нейтронов дополнительно уменьшается на величину $\mathbf{\Delta E = \hbar\Omega}$, то можно найти положение анализатора, при котором он пропускает нейтроны. При этом зависимость пропускания системы от положения анализатора описывается симметричной функцией

$$\mathbf{\Phi(h) = \int f(E) f(E + m_g g_n H - \hbar\Omega) dE}, \qquad (1)$$

Максимум этой функции или кривой сканирования определяется условием

$$\mathbf{m_g g_n H = \hbar\Omega}. \qquad (2)$$

Определив его в эксперименте и зная величину частоты **Ω**, можно измерить гравитационную силу, действующую на нейтрон.

В качестве монохроматора и анализатора использовались нейтронные интерференционные фильтры (НИФ), а контролируемое уменьшение энергии нейтрона достигалось путем дифракции на движущейся решетке.

Измерения кривых сканирования (1) проводятся для набора частот $\boldsymbol{\Omega_j}$. Для каждой из кривых можно найти положение максимума $\mathbf{H_j}$, которое можно отсчитывать от некоторого произвольного значения h_0, положив $\mathbf{H_j = h_0 + \Delta H_j}$. Найденная из этих измерений система уравнений

$$\Delta \mathbf{H_j} = \frac{\hbar \boldsymbol{\Omega_j}}{\mathbf{m_g g_n}} + \boldsymbol{\eta}, \qquad (3)$$

позволяет определить гравитационную силу $\mathbf{m_g g_n}$, действующую на нейтрон. Константа $\boldsymbol{\eta}$ учитывает как упомянутое выше постоянное дифракционное смещение, так и неизвестное начало отсчета h_0. Подчеркнем, что формула (3) не содержит параметров спектрометрических элементов.

Эксперимент был поставлен с гравитационным спектрометром УХН на источнике ультрахолодных нейтронов Института Лауэ – Ланжевена (Гренобль, Франция). Схема эксперимента иллюстрируется рисунками 5, 6.

В эксперименте использовалась вращающаяся решетка, приготовленная на поверхности кремниевого диска диаметром **150 мм** и толщиной **0.6мм**. На периферической области диска, имевшей форму кольца, были вытравлены радиальные канавки, ширина которых была пропорциональна радиусу. Это обеспечивало постоянное угловое расстояние между канавками, равное половине точно известного углового периода. Он составлял величину

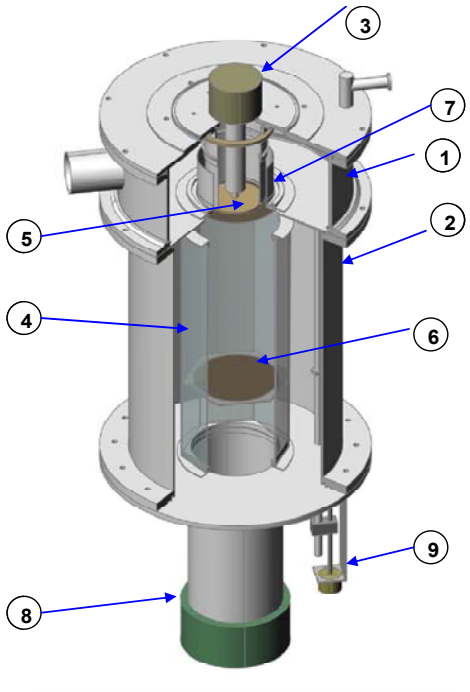

Рис. 5 Гравитационный спектрометр УХН. 1- камера очистки спектра, 2- вакуумная камера спектрометра, 3- мотор-привод вращения дифракционной решетки, 4- зеркальный нейтроновод, 5- дифракционная решетка на кремниевом диске, 6- фильтр-анализатор в подвижной каретке, 7- фильтр - монохроматор, 8-детектор, 9- шаговый двигатель для перемещения анализатора.

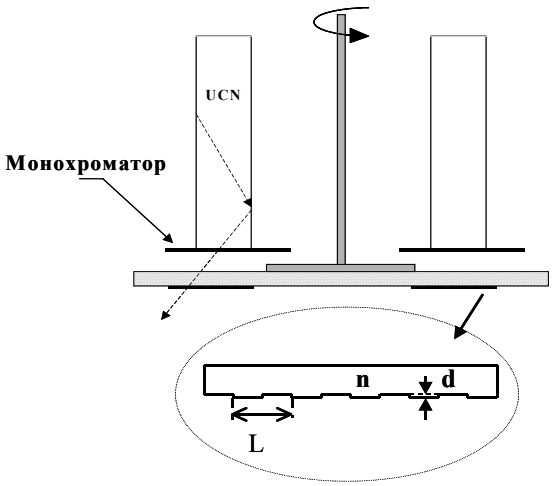

Рис. 6 Верхняя часть спектрометра. Кольцевой коридор, монохроматор и решетка

$\alpha = 2\pi/N$, где **N=75398**. Глубина канавки составляла величину **0.14мкм** и была выбрана таким образом, чтобы обеспечить разность фаз $\Delta\varphi = \pi$ нейтронных волн, прошедших через разные элементы решетки.

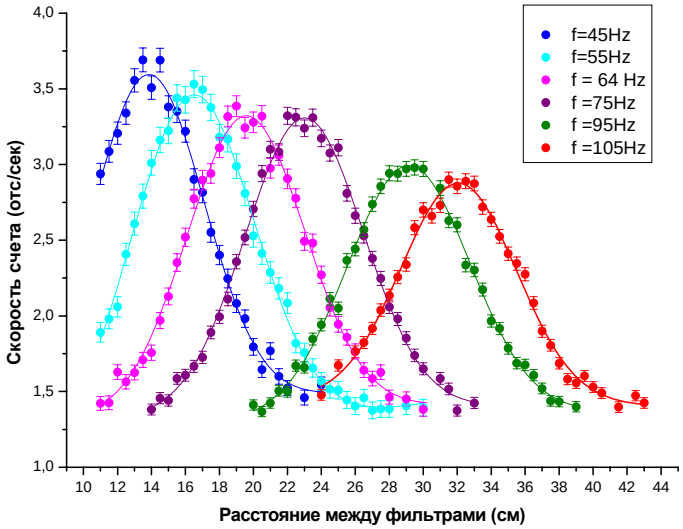

Рис. 7 Кривые сканирования, измеренные при различных частотах вращения решетки, и фитирующие их гауссовые функции

Спектрометрия УХН осуществлялась с помощью двух идентичных пятислойных интерференционных фильтров. Каждый из них имел один резонанс в пропускании при энергии около **107 нэВ**. Один из них, служивший монохроматором, имел форму кольца и был расположен на выходе подводящего кольцевого коридора (см. Рис. 6). Непосредственно под ним располагалась дифракционная решетка. Пройдя решетку, нейтроны поступали в вертикальный зеркальный нейтроновод, внутри которого размещался второй интерференционный фильтр – анализатор. Последний можно было перемещать по высоте. Нейтроны, прошедшие через анализатор регистрировались детектором.

При фиксированной частоте вращения решетки проводилось измерение кривой сканирования, то есть зависимости скорости счета от положения каретки с фильтром-анализатором. Частота вращения решетки непрерывно измерялась. Измерения проводились для набора частот от 45 до 107 оборотов в секунду, что соответствовало частоте модуляции нейтронной волны $\Omega = (2.1 \div 5.1)\times 10^7$ радиан/сек. Были проведены две серии таких измерений, отличавшихся точкой отсчета расстояний h_0.

Каждая из полученных кривых сканирования, соответствующая пику минус первого дифракционного порядка, фитировалась гауссовской функцией с линейным фоном (см. Рис. 7)

$$n = a + bH + A\exp\left(-\frac{(H - H_m)^2}{2\sigma^2}\right). \qquad (4)$$

Из пяти определенных таким образом параметров существенным является параметр $\mathbf{H_m}$ – соответствующий центру гауссовской кривой. Целью дальнейшей обработки было определение коэффициента B линейной связи $\mathbf{H_m = c + Bf}$ между частотой вращения решетки **f** и величиной $\mathbf{H_m}$. (См Рис. 8). Линейный МНК-фит данных двух серий привел к итоговому значению $\mathbf{B_{exp} = 0.30366 \pm 0.000654}$.

Теоретическое значение величины B равно

$$\mathbf{B_{th}} = \frac{2\pi\hbar\mathbf{N}}{\mathbf{mg}}. \qquad (5)$$

где **N** – точно известное полное число периодов решетки.

Подставляя в (5) табличное значения массы нейтрона **m**, локальное значение ускорения свободного падения **g=980.507(2**), измеренное в месте проведения эксперимента, получаем для теоретического значения коэффициента $\mathbf{B_{th} = 0.304203.}$

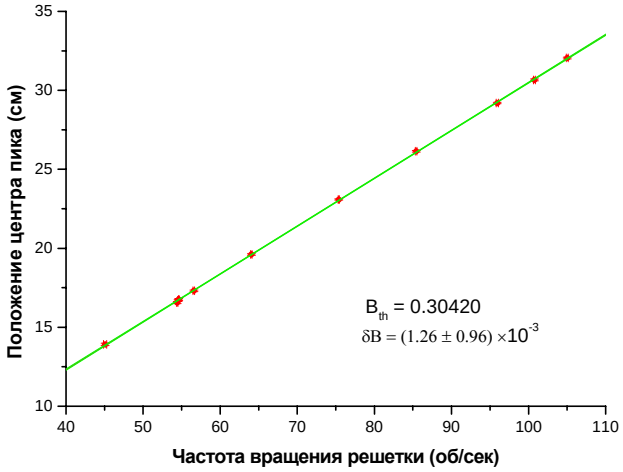

Рис. 8 Зависимость положения максимума кривой сканирования от частоты вращения решетки

Таким образом, данный результат вполне согласуется с расчетом, в котором использовалось табличное значение массы нейтрона и величина локального ускорения свободного падения макроскопических тел. Степень этого согласия удобно выразить через отношение $\boldsymbol{\gamma = B_{exp}/B_{th} = mg/m_g g_n}$. Для величины определенного таким образом фактора эквивалентности было получено: $\mathbf{1-\gamma = (1.8 \pm 2.1)\times 10^{-3}.}$

1.2.2 Взаимодействие нейтрона с ускоряющимся веществом

Хорошо известно, что для любых волн значение волнового числа **k** в среде отличается от его вакуумного значения $\mathbf{k_0}$. Отношение этих величин называется показателем преломления среды. При этом общепризнанное мнение состоит в том, что если волна, пройдя через преломляющую среду, снова выходит в вакуум, то абсолютное значение ее волнового числа в точности такое же, что и у исходной волны, хотя направление ее распространения и может, разумеется, измениться (см. Рис. 4). Это утверждение справедливо для всех видов волн, но только для случая, когда среда покоится или движется с постоянной скоростью **v**. В этом последнем случае движение образца может изменить лишь фазу прошедшей волны, что связано с изменением эффективной длины образца $\mathbf{\Delta L = v\tau}$, где $\boldsymbol{\tau = L/nc}$ - время прохождения через образец длиной **L,** а **c** – скорость волны в вакууме.

Однако, в конце прошлого столетия было найдено теоретически, что если образец преломляющего вещества движется с линейным ускорением, то волновое число и, соответственно, частота, прошедшей через него волны изменяются. Впервые это было

показано Tanaka[1] для случая классической оптики, а позже аналогичный результат был получен и для нейтронных волн[2,3]. Эффект Танака столь мал, что несмотря на фантастическую чувствительность современных оптических методов он так и не наблюдался на опыте.

Однако нейтронно-оптический эксперимент по наблюдению эффекта ускоряющийся среды оказался осуществимым и был недавно поставлен с ультрахолодными нейтронами[4]. Величина переданной энергии при прохождении нейтрона сквозь преломляющий образец, движущийся с ускорением **a**, описывается простым выражением $\Delta E = \left(\frac{1-n}{n}\right) maL$. Использование УХН ограничивает толщину образца L. Однако этот недостаток полностью компенсируется двумя обстоятельствами. Во-первых, в случае УХН фактор $(1-n)/n$ довольно значителен и может быть порядка 0.5, в то время как, для холодных нейтронов с длиной волны, например, 2нм, его величина порядка 10^{-3}. А во-вторых, методы спектрометрии УХН, основанные в частности на применении нейтронных интерферометров Фабри-Перо, обладают совершенно уникальным разрешением

Именно такой спектрометр и был использован для детектирования эффекта ускоряющейся среды в нейтронной оптике. В качестве образцов использовались кремниевые пластины с толщиной 0.6 или 2мм, которые приводились в гармоническое движение с частотой несколько десятков Гц. При этом ускорение образца также менялось по гармоническому закону и достигало в максимуме величины порядка 8g (g - ускорение свободного падения). Передача энергии, которую надо было зарегистрировать, была порядка 0.2÷0.6neV. Эксперимент был поставлен таким образом, что обусловленное эффектом ускоряющейся среды периодическое изменение энергии нейтронов должно было приводить к осцилляции скорости счета. В силу ряда причин искомый эффект являлся не единственным, влияющим на величину потока нейтронов. Однако, измеряя фазу осцилляции скорости счета можно было однозначно установить соотношение эффекта ускоренной среды и иных систематических эффектов. В 2006г. Было сообщено, что результаты первого эксперимента, осуществленного в 2005г, с несомненностью свидетельствуют о существовании впервые наблюдаемого эффекта изменения энергии нейтронов при

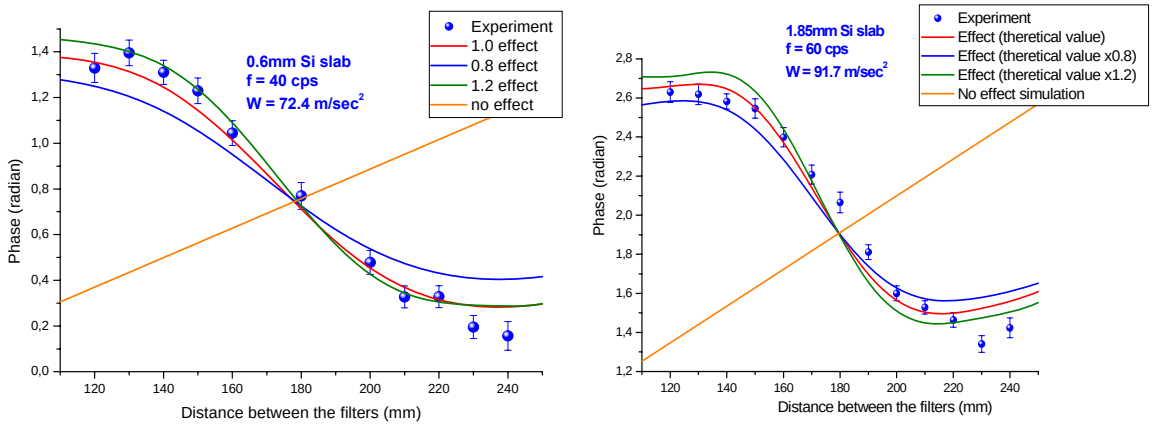

Рис. 9 Фаза осцилляции скорости счета детектора в зависимости от расстояния между фильтрами.

прохождении через ускоряющийся образец.

В 2007г. эксперимент был повторен с несколько улучшенными условиями. Измерения были проведены для двух образцов. Для каждого образца было произведено два измерения: с частотой 40Гц и максимальным значением ускорения 72.4 м/сек^2, и с частотой 60Гц и

[1] K.Tanaka. Phys.Rev.A 25 (1982) 385.
[2] F.V. Kowalski. Phys. Lett.A 182, (1993), 335.
[3] V.G.Nosov, A.I.Frank. Phys. of Atomic Nuclei, 61, (1998) 613.
[4] A.I. Frank, P.Geltenbort, G.V.Kulin, D.V. Kustov, V.G. Nosov and A. N. Strepetov. JETP Letters, 84 (2006), 363.

максимальным значением ускорения 81.7 м/сек^2 . Во всех четырех сериях измерений эффект был надежно установлен.

На Рис. 9 представлены результаты двух таких измерений. Экспериментальные результаты (синие точки) весьма удовлетворительно согласуются с теоретическими предсказаниями (красная кривая) и категорически противоречат расчету, выполненному в предположении о неизменности энергии УХН, прошедших через ускоряющийся образец (оранжевая прямая).

Таким образом, использование УХН позволило впервые наблюдать новый оптический эффект, который носит совершенно общий характер. Дело в том, что понятие показателя преломления может быть введено для волн любой природы и единственным требованием здесь является наличие в среде рассеивающих центров. Поэтому частицы любой природы должны менять свою энергию при прохождении через ограниченный в пространстве объем среды, движущийся с ускорением.

1.3 Исследование свойств ультрахолодных нейтронов

1.3.1 Изучение взаимодействия нейтронов с наночастицами

Ультрахолодные нейтроны (УХН) и очень холодные нейтроны (ОХН) интенсивно взаимодействуют с наночастицами благодаря тому, что длина волны этих нейтронов и размер этих частиц одного порядка величины — несколько нанометров, а значит сечение упругого когерентного рассеяния нейтронов на частицах велико. Полное сечение взаимодействия ОХН с наночастицами было детально изучено как экспериментально, так и теоретически, используя макроскопические толстые образцы наночастиц. Полученные результаты позволяют заключить, что наблюдаемые чрезвычайно короткая длина диффузии ОХН в среде с наноструктурой и достаточно малые потери ОХН при их диффузионном движении внутри такой среды (при условии, что среда состоит из материалов с малым сечением захвата), позволят получить коэффициент отражения от такой наноструктурированной поверхности близкий к единице в широком диапазоне скоростей нейтронов: от нуля до ~100 м/с. Поэтому планируется исследовать возможность хранения ОХН в ловушке со стенками из нанопорошка толщиной несколько сантиметров.

Были проведены первые измерения хранения очень холодных нейтронов (40-160 м/с) в

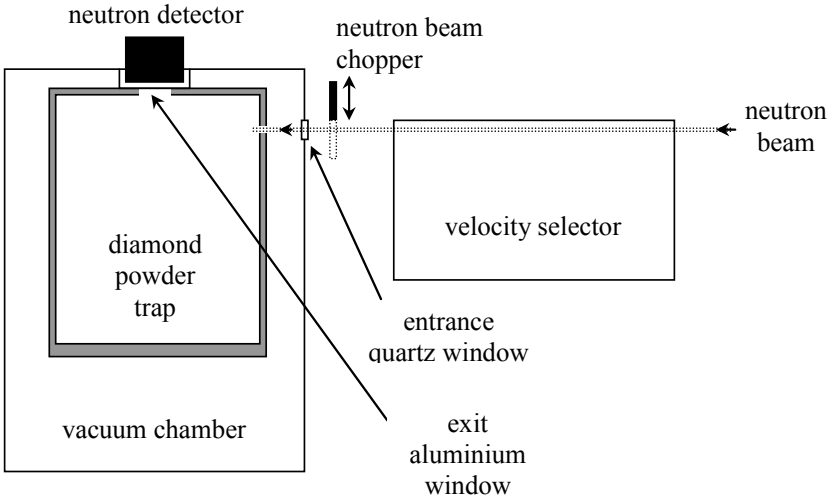

Рис. 10 Схема эксперимента

ловушке (объёмом ~70 литров), стенки которой состоят из порошка нанодисперсных алмазов (толщина стенок ~2 см, характерный диаметр наноалмазов 5-10 нм). Схема экспериментальной установки показана на Рис. 10.

Рис. 11 Вид внутренней поверхности ловушки.

Пучок очень холодных нейтронов (со скоростями 40-160 м/с) диаметром 13 мм, проходит через селектор скоростей (с разрешением от 20% до 5%) и заполняет ловушку, через входное отверстие 2×2 см^2. Вид ловушки внутри представлен на Рис. 11. Нейтроны, попавшие в ловушку, с некоторой вероятностью могут быть зарегистрированы детектором через окно диаметром 6 см, площадь которого мала по сравнению с площадью стенок ловушки и не влияет на время хранения нейтронов в ловушке. Вероятность регистрации нейтронов зависит от среднего числа их отражений от стенок ловушки.

Входящий пучок нейтронов перекрывается прерывателем с частотой ~1 Гц. По экспоненте спада скорости счета нейтронов после перекрытия пучка, определяется

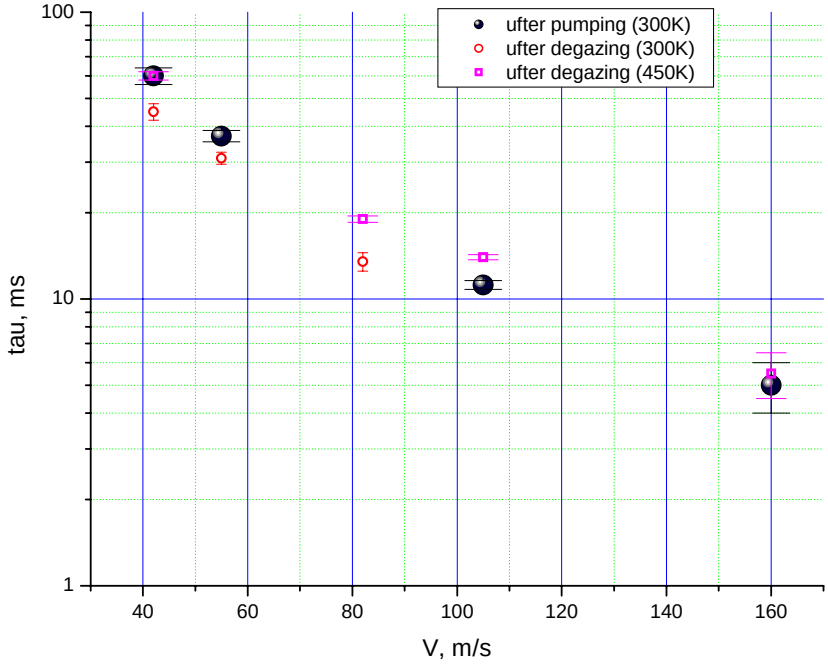

Рис. 12 Постоянная времени хранения нейтронов от стенки ловушки в зависимости от скорости нейтронов. Заполненные кружки – результаты измерения при комнатной температуре после откачки ловушки, квадраты - результаты измерения при комнатной температуре после прогрева ловушки при 150^{0}C в течении суток, пустые кружки - результаты измерения при температуре ловушки 150^{0}C.

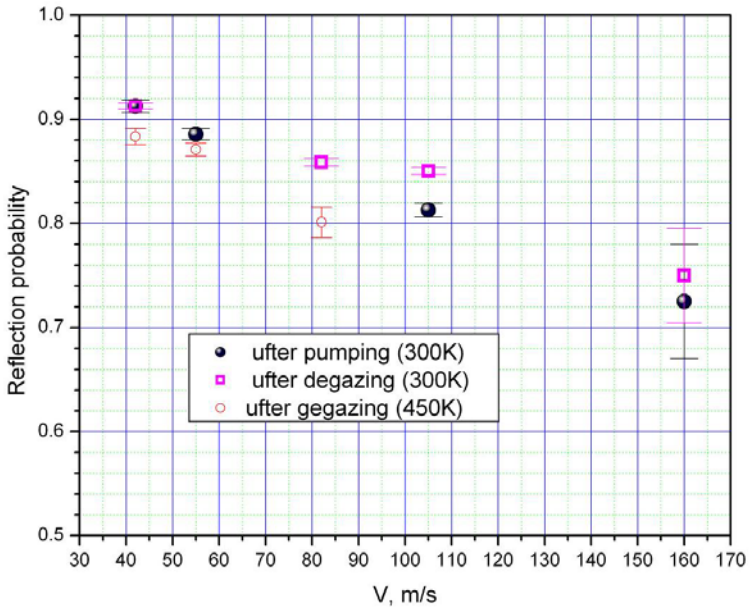

Рис. 13 Зависимость вероятности отражения от поверхности ловушки от скорости нейтрона. Заполненые кружки – результаты измерения при комнатной температуре после откачки ловушки, квадраты - результаты измерения при комнатной температуре после прогрева ловушки при 150^{0}C в течении суток, пустые кружки - результаты измерения при температуре ловушки 150^{0}C.

постоянная времени хранения нейтронов в ловушке как функция средней скорости нейтронов.

Ловушка была помещена в вакуумный кожух и откачена до вакуума лучше чем 10^{-3} мбар. После откачки была проведена первая серия измерений времён хранения. Вторая серия измерений была проведена после того как стенки ловушки были почищены от воды адсорбированной на поверхности алмазных частиц порошка (ловушка обезгаживалась при температуре 150^{0}C, в течение суток). Третья серия измерений была проведена в ловушке нагретой до 150^{0}C. Результаты измерений представлены на Рис. 12.

Из полученных зависимостей были вычислены зависимости вероятности отражения нейтрона на удар от скорости, приведённые на Рис. 13. При этих предварительных оценках брались простейшие газокинетические соображения для частоты соударений. Эти расчёты будут уточнены в дальнейшем соответствующим моделированием процесса диффузии ОХН в порошке с учётом геометрии ловушки методом Монте-Карло.

Полученные вероятности отражения ОХН согласуются с теоретическими оценками, полученными в рамке модели независимых частиц [5], принимая во внимание, что массовая доля примеси водорода в наноалмазах составляет ~1% [6].

Таким образом, экспериментально показано, что ОХН могут эффективно отражаться порошком алмазных наночастиц. Такой отражатель перекрывает провал в вероятности отражения в диапазоне энергий ОХН между эффективными отражателями тепловых и холодных нейтронов, используемых на реакторах, и эффективным отражением от потенциала Ферми для ультрахолодных нейтронов. Так же экспериментально показана возможность хранения ОХН, обсуждаемая в [7].

---

[5] V.V.Nesvizhevsky, G.Pignol and K.V.Protasov (2006). "Nanoparticles as a possible moderator for anultracold neutron source." International Journal of Nanoscience **6**(6)

[6] A.L. Vereschagin, G.V. Sakovich, V.F. Komarov, E.A. Petrov (1993). Diamond and Related Materials **3**: 160.

[7] V.V. Nesvizhevsky, E.V. Lychagin, A.Yu. Muzychka, A.V. Strelkov, G. Pignol, K.V. Protasov. “The reflection of very cold neutrons from diamond nanoparticles”, to be published in 2008.

В 2008 году планируется провести измерение индикатрисы рассеяния очень холодных нейтронов при однократном отражении от слоя наноалмазов для различных скоростей нейтронов.

1.4 Исследование нарушений пространственной и временной четности при взаимодействии нейтронов с ядрами

1.4.1 Измерение P-нечетной асимметрии вылета γ-квантов реакции $^{10}B(n,\alpha_1)^7Li^* \rightarrow ^7Li+\gamma$

В рамках экспериментов по поиску нейтральных токов в нуклон-нуклонных взаимодействиях и определению слабой π-мезонной константы связи проведены измерения (в коллаборации с ПИЯФ, ИЛЛ и ТУ Мюнхена) P-нечетной асимметрии γ-квантов реакции $^{10}B(n,\alpha_1)^7Li^* \rightarrow ^7Li+\gamma$ на пучке холодных поляризованных нейтронов PF1B (ИЛЛ, Гренобль).

Слабые взаимодействия в нуклон-нуклонных системах при низких энергиях описываются в приближении одно-мезонного обмена (обменами π, ρ, ω мезонами с передачей различного количества изоспина 0, 1, 2), где четность нарушается в одной из вершин NN-диаграммы. Слабый NN-потенциал параметризуется набором 6, в некоторых моделях 7, слабых мезон-нуклонных констант. Константы определяются на основе стандартной модели и кварковой структуры нуклонов, однако из-за неопределенностей при учете интерференции сильного взаимодействия, различные подходы дают существенно различные значения констант. Особенно чувствительна к модели π-мезонная константа связи f_π. С другой стороны, f_π полностью определяется обменом Z^0-бозоном между кварками, т.е. нейтральным током. Эксперименты по рассеянию поляризованных протонов на протонной мишени однозначно зарегистрировали заряженные токи в NN-взаимодействиях. Извлеченные из этих данных значения констант связи h_ρ^0 и h_ω^0 в пределах экспериментальной погрешности совпадают с теоретическими «лучшим значениям» Дипланка-Донахью-Нольстена (DDH «best values»). В то же время эксперименты, где были попытки определения слабой π-мезонной константы, дают несовпадающие значения в широком диапазоне (от 0 до ~$9\cdot10^{-7}$) Теоретическое «лучшее значение» $f_\pi = 4.6\cdot10^{-7}$. Наиболее строгие ограничения получены из экспериментов со ^{18}F ($f_\pi \le 1.2\cdot10^{-7}$) и нашего недавно завершенного эксперимента с ^6Li ($f_\pi \le 1.1\cdot10^{-7}$). Таким образом, до сих пор нет однозначного подтверждения нейтральных токов в слабых NN-взаимодействиях.

До этого было проведено 2 цикла измерений P-нечетной асимметрии γ-квантов реакции $^{10}B(n,\alpha_1)^7Li^* \rightarrow ^7Li+\gamma$ на пучке холодных поляризованных нейтронов PF1B (ИЛЛ, Гренобль). Было получено значение $\alpha_\gamma = (5.1 \pm 3.8)\cdot10^{-8}$. Согласно расчетам группы Чувильского асимметрия γ-квантов $\alpha_\gamma = 1.1\cdot10^{-8}$, если другие слабые мезон-нуклонные константы (главным образом h_ρ^0, поскольку дает наибольший вклад в величину асимметрии) равны теоретическим «лучшим значениям» Дипланка-Донахью-Нольстена.

В измерении этого года применялась новая система регистрации токовых сигналов. Метод позволяет производить процедуру, аналогичную интегрированию сигнала за значительно более короткие промежутки времени, чем аналоговые интеграторы. Это позволило уйти из низкочастотной области, где вклад флуктуаций мощности реактора и шумов максимален, и уменьшить погрешность определения эффекта более чем в 1.5 раза: $\alpha_\gamma = (3.9 \pm 3.9)\cdot10^{-8}$. Суммарное по трем циклам значение асимметрии (предварительное): $\alpha_\gamma = (4.5 \pm 2.7)\cdot10^{-8}$. Оценка слабой π-мезонной константы из полученных данных $f_\pi \le 4.7\cdot10^{-7}$. Таким образом, экспериментальной точности пока недостаточно для наблюдения эффекта асимметрии в реакции $^{10}B(n,\alpha_1)^7Li^* \rightarrow ^7Li+\gamma$, но полученное значение указывает на величину f_π, меньшую, чем «лучшее значение».

1.4.2 Поиск и исследование структуры подпороговых нейтронных p-резонансов на изотопах свинца методом комбинированной корреляционной гамма-спектроскопии

Завершён анализ экспериментальных данных, полученных в контрольных экспериментах 2005-2006г.г. на 1-м канале реактора ИБР-2 по поиску отрицательного нейтронного p-резонанса у изотопов свинца ^{204}Pb и ^{207}Pb.

Эти эксперименты проводились на усовершенствованном гамма-спектрометре COCOS с повышенной эффективностью и быстродействием с целью проверки полученных ранее данных о существовании отрицательного нейтронного p-резонанса у изотопа ^{207}Pb, вместо ^{204}Pb, как ожидалось на основании работ по наблюдению поворота спина тепловых нейтронов при взаимодействии со свинцом.

Результаты проведённого анализа не подтвердили наличие значительного отклонения сечения радиационного захвата от закона 1/v в области энергии нейтронов (1 – 5) эВ для изотопа ^{207}Pb, наблюдённого в экспериментах 2002-2003г.г. и свидетельствовавшего о существовании отрицательного p-резонанса у этого изотопа. Если такое отклонение имеет место, то оно незначительно и для этого изотопа вклад p-волны не превышает (5-6)% от s-волны.

Для изотопа ^{204}Pb искомое отклонение в пределах погрешности экспериментальных данных также не обнаружено. Это не может однозначно свидетельствовать об отсутствии отрицательного p-резонанса, так как в проведенных измерениях регистрируется гамма-переход, смешанный вблизи тепловой области энергий нейтронов от s- и p-резонансов, причём парциальная ширина такого перехода для p-волны неизвестна. Если она существенно меньше, чем у s-волны, то это может приводить к невозможности наблюдения отрицательного p-резонанса использованной методикой в пределах точности эксперимента (3-4)%.

1.4.3 Изучение возможности создания поляризованной лантановой мишени на основе LaS

Лантан является наиболее перспективным нуклидом для создания поляризованной мишени в эксперименте по проверке временной инвариантности при взаимодействии поляризованных нейтронов и ядер. LaS в отличии от монокристаллов $LaAlO_3$ или LaF имеет кубическую решетку и, в силу изотропности g-фактора, может использоваться в порошке. Поляризация La в LaS выполняется методом Оверхаузера.

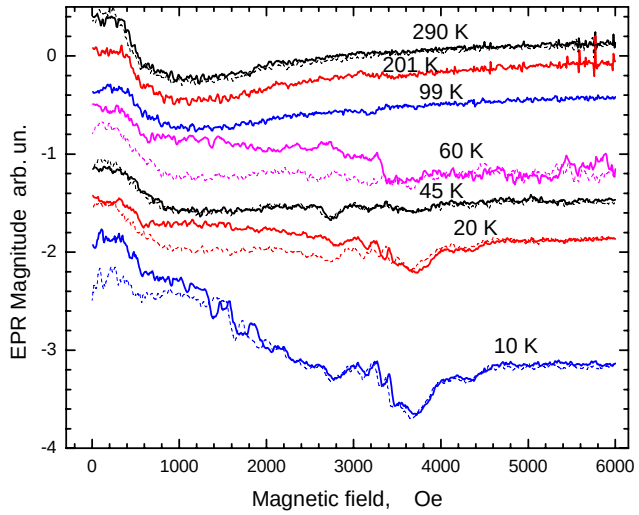

Рис. 14 Сигнал ЭПР в образце LaS.

Для проверки этой возможности в Институте Неорганической Химии СО РАН (Новосибирск) были изготовлены 4 образца LaS в виде таблеток из прессованного порошка. В Институте Радиоэлектроники РАН (Москва) были выполнены измерения формы линии парамагнитного резонанса с целью определения времени релаксации первичных носителей поляризации (свободных электронов). Выяснилось, что при 77 К скорость их релаксации столь велика, что линия ЭПР становится ненаблюдаемой. Такая ситуация типична для электронов проводимости в трехмерных системах. Была надежда, что при понижении температуры до 4 К релаксация замедлится и появится резонанс. Однако этого не произошло. Результаты для одного из образцов представлены на Рис. 14. Сплошные линии - запись при увеличении магнитного поля, штриховые линии - запись при уменьшении магнитного поля. Видны два типа сигналов. 1) При всех температурах наблюдается низкополевой сигнал. Этот сигнал связан с нерезонансным поглощением СВЧ и обусловлен соразмерностью скин-слоя и толщиной образца. Например, при повороте на 90^{o} градусов вокруг вертикальной оси этот сигнал пропадал. А ведь мы имеем дело с поликристаллом, где не должно наблюдаться структурных анизотропных эффектов. Следовательно, наблюдается анизотропия формы образца. 2) При температурах ниже 45 К появляются разнообразные широкие (от 500 Э) резонансные сигналы, разбросанные в широком диапазоне магнитных полей. Скоре всего это различные неконтролируемые примеси, которые, как правило, всегда присутствуют во всех образцах при первых попытках их изготовления. При внимательном рассмотрении свежих сколов на таблетках можно было легко видеть вкрапления другого цвета. Остальные образцы были аналогичны первому с одной лишь разницей: нерезонансного поглощения в низких полях у них не наблюдалось. Похоже, что не получалось "благоприятного" соотношения между скин-слоем и размерами образца. Таким образом, пока не удалось получить образцы LaS, пригодные для перехода к следующему этапу – поляризации La методом Оверхаузера.

1.4.4 Измерение параметров низковольтных нейтронных резонансов Xe

В экспериментах по оптической поляризации изотопов Xe выполненных в КЕК (2004) выяснилось, что табличные данные для резонансов 9.5 эВ (^{129}Xe) и 14.4 эВ (^{131}Xe) не описывают измеренные трансмиссионные данные. Кроме того, при сопоставлении данных различных библиотек (ENDF VII, JENDL 3.3, JEF 2.2) также были замечены значительные расхождения. В связи с этим, на Pohang Neutron Source (Республика Корея) были выполнены специальные измерения полного нейтронного сечения. Для этого был изготовлен баллон-мишень, схема которого показана на Рис. 15.

Баллон был заполнен естественной смесью изотопов Xe при давлении 1 атм. На Рис. 16 представлены измеренная трансмиссия и результаты подгонки. В таблицах 1 и 2 приведены полученные значения параметров. Результаты данной работы направлены для публикации в журнал Nuclear Instruments and Methods.

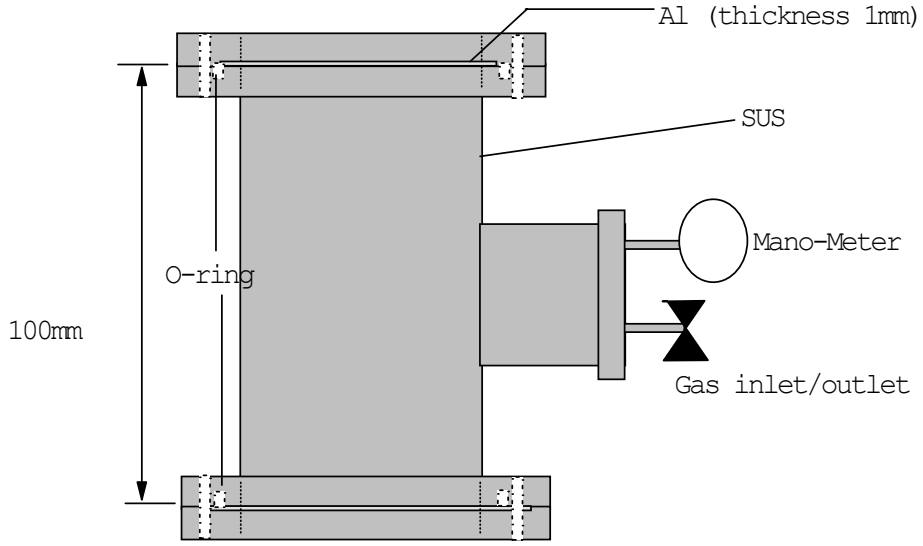

Рис. 15 Баллон-мишень для измерения полного нейтронного сечения Xe.

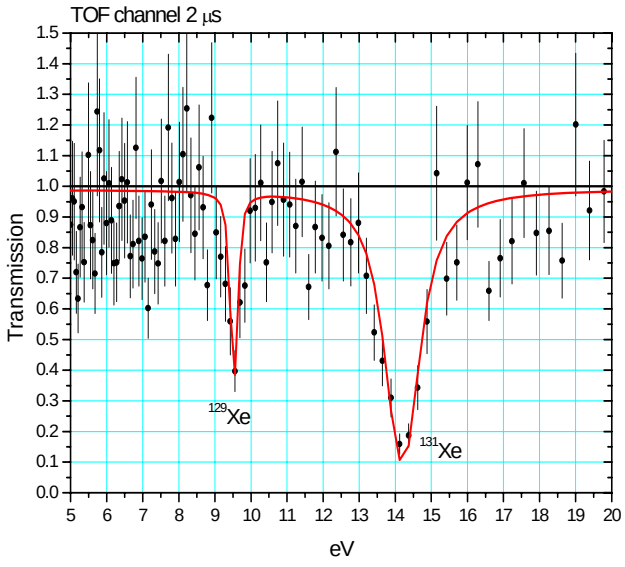

Рис. 16 Нейтронная трансмиссия натурального Xe. Кривая – результат подгонки.

Таблица 1. Параметры резонанса 9.5 эВ ^{129}Xe

Величина	Начальное[8]	Данная работа
E (эВ)	9.5	9.531±0.016
Γ_n (мэВ)	6.0	12.68±0.18
Γ_γ (мэВ)	110	114.2±1.7

Таблица 2. Параметры резонанса 14.4 эВ ^{131}Xe

Величина	Начальное[1]	Данная работа
E (эВ)	14.4	14.19±0.04

[8] Low Energy Neutron Physics, Subvolume B, Tables of Neutron Resonance Parameters, Edited by H. Schopper ISBN 3-540-63277-8, Springer-Verlag Berlin Heidelberg, 1998.

Γ_n (мэВ)	216	242.7±0.5
Γ_γ (мэВ)	94	419.7±0.5

1.5 Исследования свойств атомных ядер

1.5.1 Поиск экзотических мод деления на реакторе ИБР-2 с использованием установки «Мини-Фобос»

В предыдущих экспериментах, посвященных изучению спонтанного деления ^{252}Cf, были обнаружены многочисленные указания на существование необычного, по–крайней мере тройного, канала распада, названного тройным коллинеарным кластерным распадом[9]. Для исследования наблюдаемого эффекта планировалось изучение различных делящихся ядерных систем при различных энергиях возбуждения вплоть до порога выживания ядерных оболочек. Одной из выбранных для изучения реакций была реакция ^{235}U (n_{th}, f).

Эксперимент был выполнен на пучке тепловых нейтронов реактора ИБР–2 в Лаборатории нейтронной физики с помощью двухплечевого спектрометра время пролета-энергия миниФОБОС [10]. Детекторы спектрометра позволяют находить как первичные так и конечные массы фрагментов (т.е. до и после сброса нейтронов), вектор скорости (импульса), а также пробег фрагмента в газе ионизационной камеры в каждом плече спектрометра.

В экспериментах наблюдался специфический двумерный бамп в распределении масса-масса фрагментов деления [11] (см. Рис. 17a). Эффект проявляется только в одном плече спектрометра, а именно со стороны подложки мишени. Выход событий, образующих бамп, составляет около $5*10^{-3}$ на одно двойное деление. Эта оценка была получена после вычитания «хвоста» 2 из «хвоста» 1. Соответствующий разностный спектр (собственно бамп) показан на Рис. 17b. Максимум выхода в бампе лежит в окрестности масс 68–70, ассоциирующихся с магическими изотопами Ni.

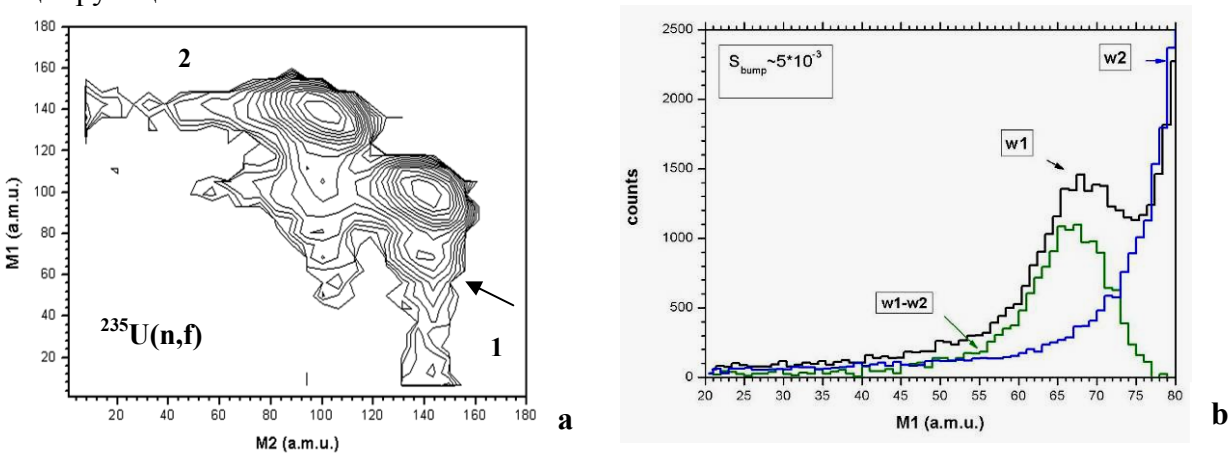

Рис. 17 Распределение масса-масса фрагментов (логарифмическая шкала), полученное в реакции ^{235}U(n,f) (a**). Обсуждаемая особенность спектра 1 обозначена стрелкой. Проекция распределения на ось M1 (**b**): «хвост» 1 дает спектр w1, «хвост» 2 – спектр w2, а результат их вычитания обозначен как w1-w2.**

Еще одно проявление кластеризации было получено в результате специальной обработки распределения масса-масса фрагментов. Был произведен отбор фрагментов деления по их

[9] Yu.V. Pyatkov et al., Phys. Atom. Nucl. V.66, 1631 (2003).
[10] D. V. Kamanin et al., International Symposium on Exotic Nuclei, Peterhof, Russia, 5-12 July 2004. Conference proceedings. Published by World Scientific Publishing Co. Pte. Ltd., 2005, p. 588-591.
[11] Yu. V. Pyatkov et al., Preprint JINR E15-2005-99, Dubna, 2005

скорости и импульсу. Отбирались события, имеющие приблизительно одинаковые скорости и лежащие одновременно вне «хвостов» рассеянных событий в распределении фрагментов по импульсам.

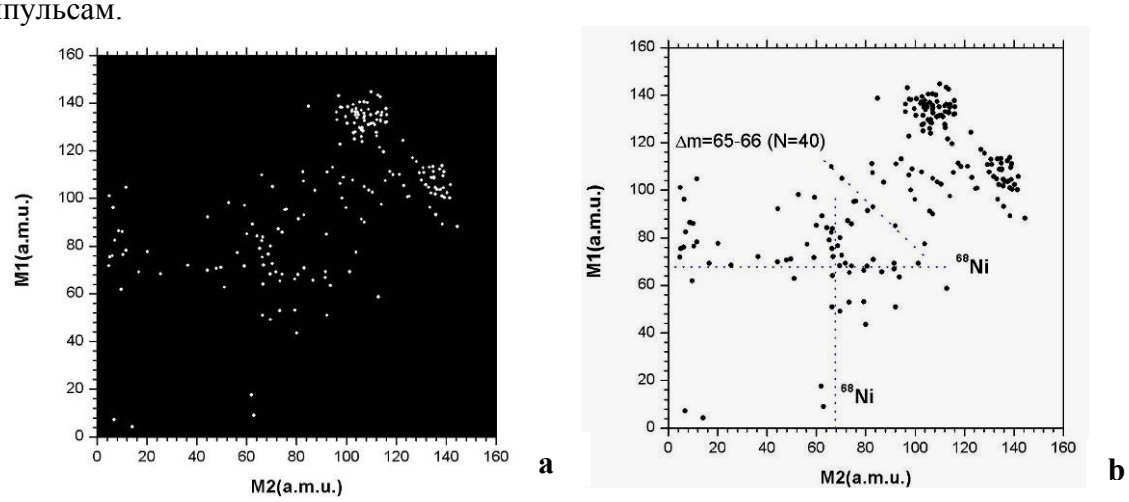

Рис. 18 Распределение масса-масса для событий деления с приблизительно равными скоростями, взятых вне «хвостов» рассеянных фрагментов в импульсном распределении (a**). Специфическая структура в форме прямого угла ясно видна в центре распределения. Вершина угла расположена в точке (68, 68), предположительно связанной с магическим изотопом ^{68}Ni (**b**).**

Обращает на себя внимание специфическая структура в центре распределения. Она выглядит подобно прямому углу с вершиной, лежащей в окрестности точки (68, 68) a.m.u., которая предположительно отвечает магическому ядру ^{68}Ni $_{40.}$ Используя такой же отбор, подобная структура (прямоугольник) была выявлена ранее в распределении масса-масса фрагментов спонтанного деления ядра ^{252}Cf [^{12}]. Некоторые точки на распределении лежат приблизительно на линии M1+M2=const (наклонная точечная линия на Рис. 18b). Соответствующий «потерянный фрагмент» также связан с известной нейтронной подоболочкой N=40.

Основное значение представленных результатов заключается в том, что они подтверждают, в основном, результаты, полученные ранее для различных делящихся систем.

1.5.2 Исследование вылета запаздывающих нейтронов на установке «ИЗОМЕР-М»

В продолжение исследований характеристик запаздывающих нейтронов деления главных и минорных реакторных изотопов в 2006-2007г.г. завершены измерения выхода запаздывающих нейтронов при делении изотопа ^{245}Cm тепловыми нейтронами на установке «Изомер-М» 11-б канала ИБР-2. Несмотря на высокое обогащение исследованного образца изотопом ^{245}Cm (95,46%) и большое сечение деления его тепловыми нейтронами (~2145 б), сопутствующие изотопы ^{244}Cm и ^{246}Cm создают постоянный фон мгновенных нейтронов спонтанного деления и определяют малость отношения эффект-фон при измерениях выхода запаздывающих нейтронов. Это обстоятельство потребовало провести модернизацию измерительного модуля для обеспечения максимальной стабильности работы, оптимизировать режим работы установки и тщательно учитывать все компоненты фона при проведении измерений.

По завершению обработки всех экспериментальных данных было получено значение полного выхода запаздывающих нейтронов при делении изотопа ^{245}Cm тепловыми нейтронами ν_d = (0,64±0,02)%. Это значение является вторым известным

[12] Yu. V. Pyatkov et al., Preprint JINR E15-2004-65, Dubna, 2004

экспериментальным результатом и выгодно отличается от него вдвое более высокой точностью. Проведённое сравнение этого результата с глобальной систематикой выходов запаздывающих нейтронов показало, что оно совпадает со значением, полученным в рамках упрощенного варианта этой систематики.

1.6 Гамма-спектроскопия нейтронно-ядерных взаимодействий

Комплексный анализ экспериментальных данных о процессе каскадного гамма-распада нейтронного резонанса позволяет получать принципиально новую информацию о свойствах ядерной материи ниже энергии возбуждения примерно 5-10 МэВ. Его наиболее важный результат – принципиально новая информация о динамике взаимодействия и перехода друг в друга сверхтекучего и обычного состояний ядерной материи. Аппроксимация большого набора экспериментальных значений плотности возбужденных уровней ядер из области масс $39<A<201$ показала, что возбуждения фононного типа определяют структуру возбужденных уровней ядра на 90% и более по крайней мере ниже половины энергии связи нейтрона. Выполненный в ЛНФ по оригинальной методике анализ опубликованных экспериментальных данных по интенсивностям первичных гамма-переходов захвата нейтронов с энергией около 2 кэВ позволил уточнить эти результаты и оценить их максимальную систематическую погрешность. Дополнительно был установлен факт отсутствия резкого изменения параметров каскадного гамма-распада от возможного изменения структуры нейтронного резонанса в этом интервале их энегий. Аппроксимация экспериментальных данных о парциальных ширинах первичных дипольных гамма-переходов в диапазоне энергии связи нейтрона подтвердила сильное влияние сверхтекучего состояния ядра и на этот параметр каскадного гамма-распада нейтронного резонанса. Таким образом продемонстрирована возможность и необходимость прямого экспериментального и теоретического изучения сверхтекучести нагретого ядра до его температуры не ниже 0.5 МэВ.

1.7 Исследование реакций (n,p) и (n,α)

Продолжались эксперименты по определению коэффициента корреляции вперед-назад в реакции $^{14}N(n,p)^{14}C$ на ускорителе ЭГ-5 ЛНФ ОИЯИ в области ближайших низко лежащих резонансов. По техническим причинам в 2007 г. пучковое время на ускорителе было ограничено. Были выполнены измерения в 5-ти энергетических точках, как для проверки полученных ранее результатов, так и при других энергиях. Тем не менее, для проведения теоретического анализа данных недостаточно.

На нейтронном источнике по времени пролета Московской мезонной фабрики ИЯИ РАН в Троицке проведены тестовые измерения при длительности вспышки 5 мкс для экспериментов по определению P-четных корреляций в реакции $^{35}Cl(n,p)^{35}S$. На основе полученых данных произведена оценка возможностей для исследования P-четных корреляций в реакции $^{35}Cl(n,p)^{35}S$. При тех параметрах пучка, что были в тестовом измерении (длительность вспышки 5 мкс, частота 50 Гц, средний ток протонов на мишени 1.5-1.7 мкА) за 3-е суток измерений можно достигнуть точности $5\cdot10^{-2}$ в интересующих энергетических интервалах.

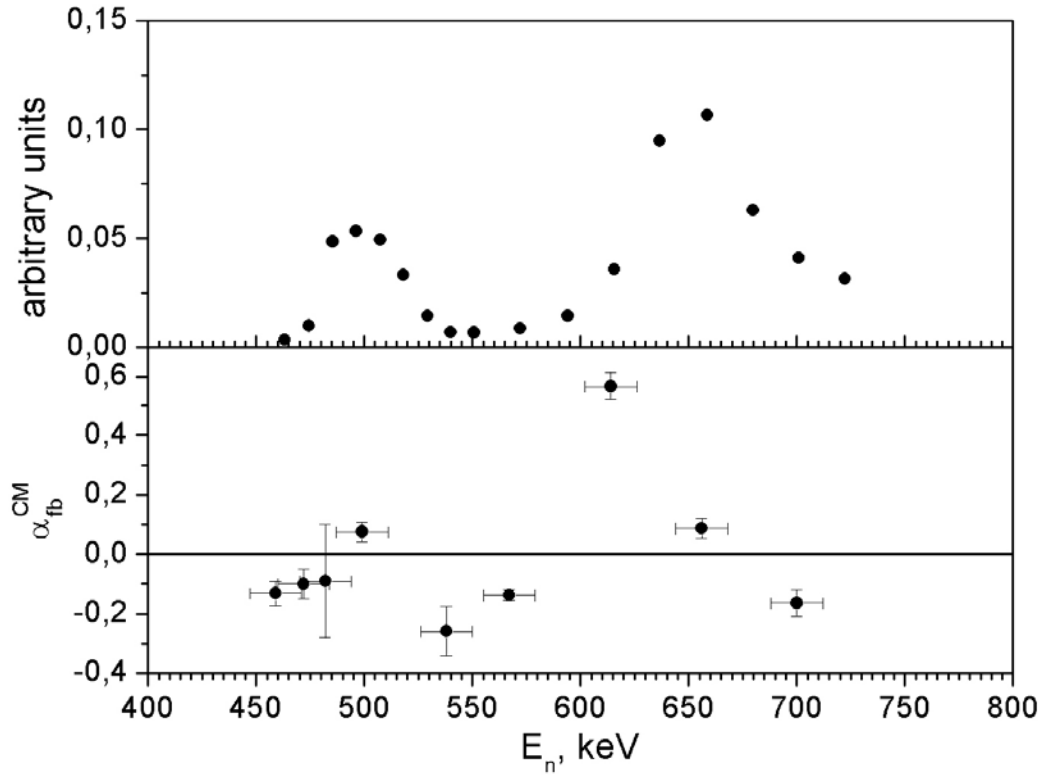

Рис. 19 Верхний график – относительный выход протонов из реакции $^{14}N(n,p)^{14}C$; нижний график – значения корреляции вперед-назад в системе центра масс.

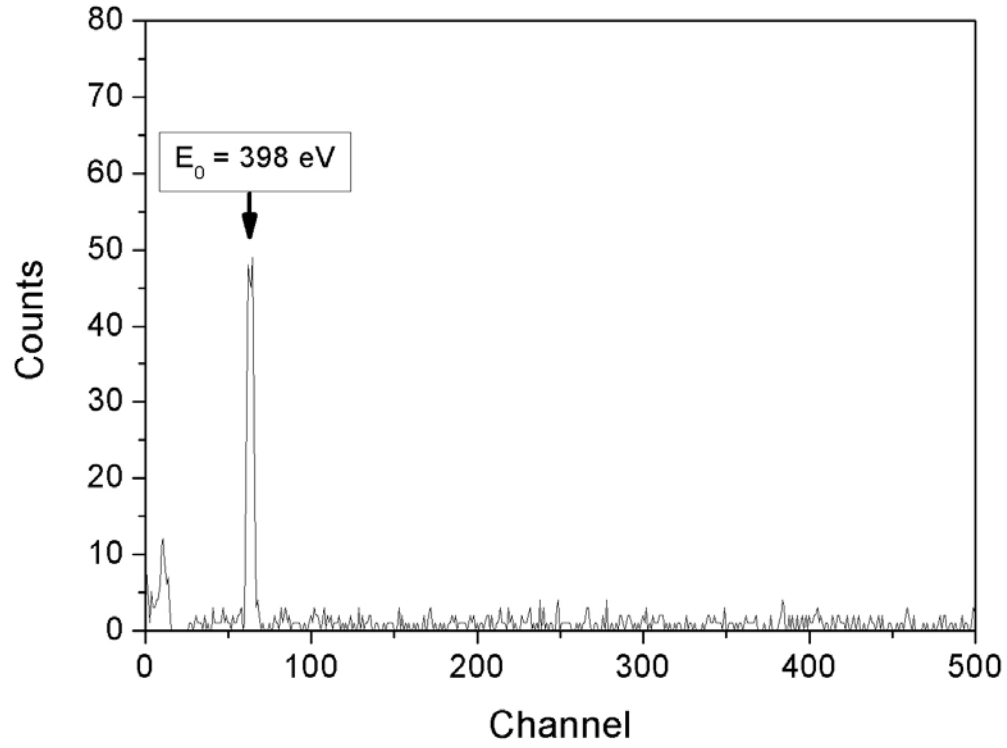

Рис. 20 Времяпролетный спектр реакции $^{35}Cl(n,p)^{35}S$ при длительности вспышки 5 мкс и частоте 50 Гц. Цена канала 1 мкс.

В рамках программы совместных исследований на ускорителе ЭГ-4.5 Института физики тяжелых ионов при Пекинском университете, Китай, проведены исследования реакции $^6Li(n,\alpha)^3H$ при E_n=1.23, 1.70, 2.05, 2.47 МэВ, получены энергетические спектры заряженных частиц (Рис. 21, Рис. 22). Данные в настоящее время обрабатываются. Данные для реакции

$^{6}Li(n,\alpha)^{3}H$ важны как для изучения механизмов ядерных реакций, так и для ядерной энергетики. Однако, в существующих на сегодняшний день экспериментальных данных и теоретических оценках в области энергий нейтронов несколько МэВ наблюдаются значительные расхождения.

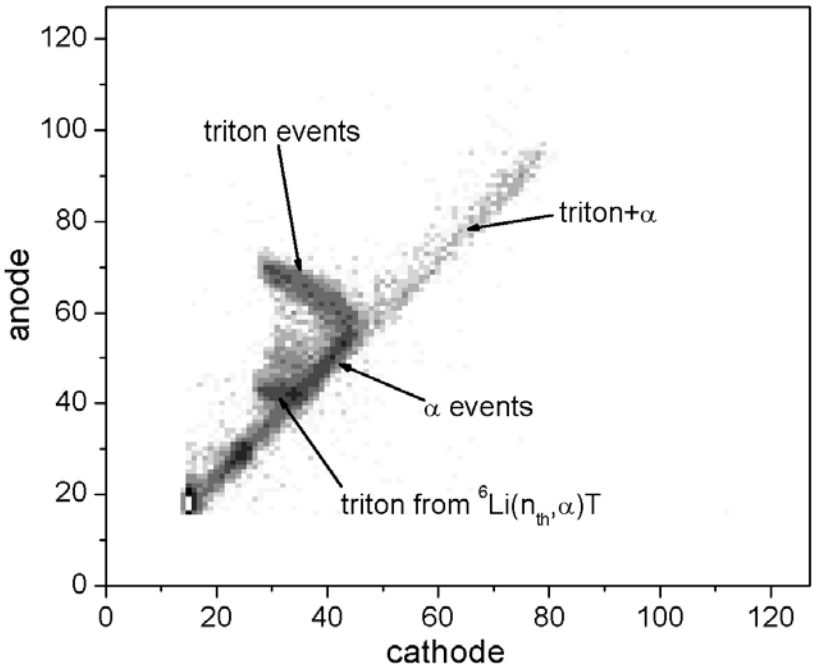

Рис. 21 Двумерный спектр заряженных частиц из реакции $^{6}Li(n,\alpha)^{3}H$ в направлении «вперед» при энергии E_n=1.23 МэВ

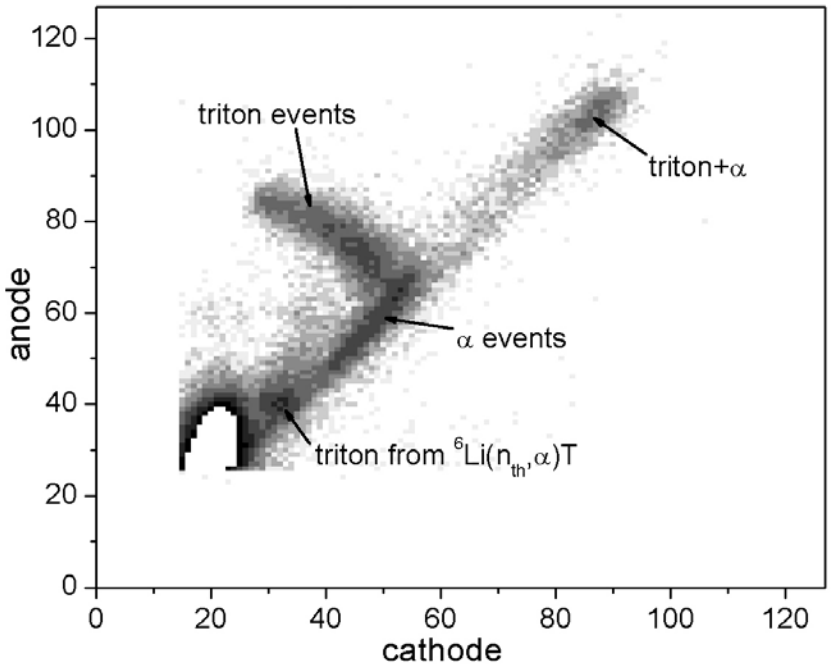

Рис. 22 Двумерный спектр заряженных частиц из реакции $^{6}Li(n,\alpha)^{3}H$ в направлении «вперед» при энергии E_n=2.47 МэВ

Проведена окончательная обработка результатов измерений реакции ^{64}Zn(n,α)^{61}Ni при E_n=4, 5.5 МэВ, а так же для более низкой энергии нейтронов 2.5 МэВ. Заметим, что в области энергии E_n ~2 МэВ из-за трудностей измерений, обусловленных малой величиной сечения и ростом фона, никогда ранее такие измерения не проводились. Полученные угловые распределения, дифференциальные и полные сечения приводятся на Рис. 23, Рис. 24 и в Таб. 3, где первая группа соответствует трем первым энергетическим ^{61}Ni (основное состояние, первое и второе возбужденные состояния 67 и 283 кэВ), вторая группа соответствует более высоким энергетическим состояниям ядра ^{61}Ni (656 кэВ, 909 кэВ, …).

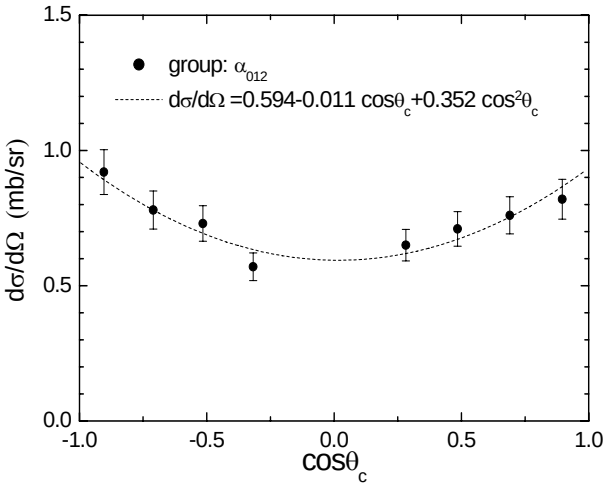

Рис. 23 Угловое распределение α-частиц из реакции ^{64}Zn(n,α)^{61} в системе центра масс при E_n = 2.5 МэВ

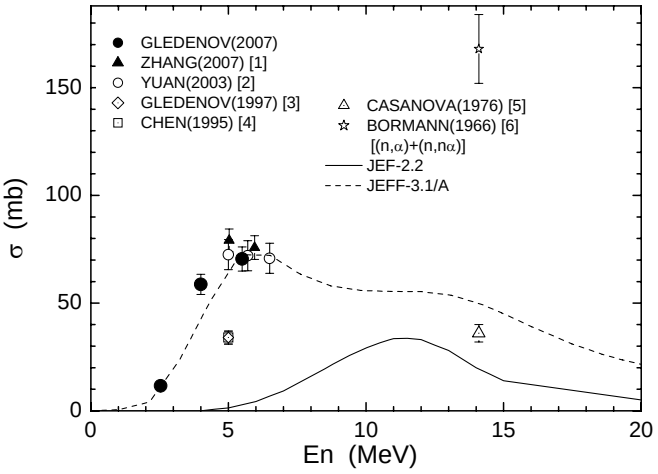

Рис. 24 Полученные сечения реакции ^{64}Zn(n,α)^{61} в сравнении с существующими данными

Таблица 3. Сечения реакций ^{64}Zn(*n, α_{012}*)^{61}Ni, ^{64}Zn(*n, $\alpha_{34...}$*)^{61}Ni, и ^{64}Zn(*n, α*)^{61}Ni

En (МэВ)	**σ (мб)**		
	Первая группа ^{64}Zn(*n, α_{012}*)^{61}Ni	Вторая группа: ^{64}Zn(*n, $\alpha_{34...}$*)^{61}Ni	Полное: ^{64}Zn(*n, α*)^{61}Ni
2.54 ± 0.03	9.0 ± 0.9	2.6 ± 2.0	11.6 ± 1.1
4.00 ± 0.21	40.9 ± 3.3	17.8 ± 1.4	58.7 ± 4.7
5.50 ± 0.13	30.9 ± 2.5	39.6 ± 3.1	70.5 ± 5.6

Работы проводятся совместно с Пекинским университетом (Китай), Лодзинским университетом (Польша) и Национальным университетом Монголии (Улан-Батор, Монголия).

2. Теоретические исследования

Экстраполяцией оптического потенциала взаимодействия нейтрона с веществом на область больших плотностей, имеющих место в нейтронной звезде, показано, что в нейтронной звезде имеют место силы нейтроно стрикции, которые сжимают звезду дополнительно к силам гравитации. Путем численных расчетов показано, что эффект оптических сил на массу, радиус зведы и распределение плотности в ней превосходит влияние эффектов общей теории относительности. Показано, также, что при наличии резонанса в нейтрон-нейтронном рассеянии в звезде могут возникать пульсации и звезда может взрываться с огромным выделением энергии.

Исходя из предположения, что нейтронная волновая функция представляется волновым пакетом, поставлен вопрос: изменяется ли ширина пакета с ростом энергии или нет? Для ответа на этот вопрос был проведен эксперимент по опре-делению температурной зависимости сечения рассеяния медленных нейтронов в газе He^4. Из результатов эксперимента следует, что ширина волнового пакета уменьшается с ростом энергии обратно пропорционально скорости нейтрона.

На основе алгебраического подхода к описанию процесса транспортировки ней-трона в однородной и мелкодисперсной среде получены новые формулы для альбедо нейтронов от слоев веществ заданной толщины. Новые формулы имеют преимущество перед известными, полученными ранее на основе диффузионной теории, поскольку применимы в более широкой области изменения параметров. Они могут использоваться для рассчета реакторов и радиационной защиты.

Разработан метод длинноволновой нейтронной голографии без опорного пучка, который позволяет записывать голографическое изображение магнитной и не-магнитной макроскопической структуры непрозрачных объектов и воспроизво-дить изображение в видимом свете. Метод основан на получении пучка нейтро-нов в когерентной суперпозиции состояний с двумя различными энергиями. Разность энергий и волновых векторов этих состояний создает в пространстве нейтронную волну прецессии, длина которой на несколько порядков больше длины волны де Бройля.

Получено полное решение задачи о взаимодействии нейтрона с веществами, имеющими геликоидальную магнитную структуру. Вычислены матричные амплитуды отражения и пропускания геликоидальных магнитных зеркал и обнаружен эффкт резонансного отражения с переворотом спина.

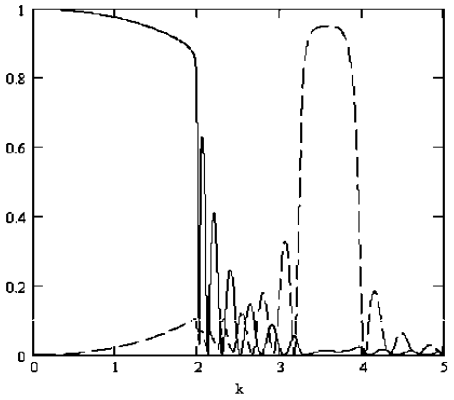

На рисунке показаны коэффициенты отражения с переворотом (пунктирная кривая) и без переворота спина (сплошная кривая) от геликоидального зеркала конечной толщины при поляризации падающего нейтрона антипараллельной геликоидальному вектору. По оси ординат отложен коэффициент отражения, а по оси абсцисс -- волновой вектор нейтрона в безразмерных единицах. Видно, что отражение с переворотом спина имеет резонансный характер, и резонанс имеет место при волновом векторе нейтрона равном геликоидальному.

3. Прикладные и методические исследования

3.1 Изучение свойств пиксельных полупроводниковых детекторов

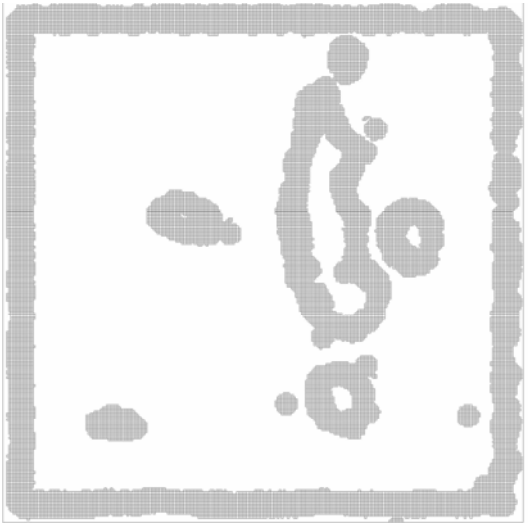

Рис. 25 Пиксели, исключенные из обработки.

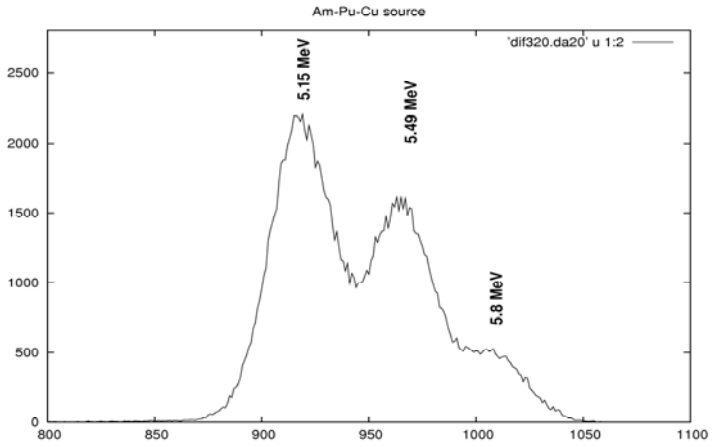

Рис. 26 Энергетический спектр для α-частиц от комбинированного источника после калибровки.

В коллаборации ЛНФ ОИЯИ – Политехнический Университет (г. Прага) ведутся работы по изучению возможности применения пиксельных полупроводниковых детекторов (MEDIPIX - MEDIPIX2 - TIMEPIX) для ядерно-физических исследований.

В 2007 году Институт Экспериментальной и Прикладной физики Чешского Политехнического Университета (г. Прага) получил первые экземпляры timepix детекторов. Timepix детектор - позиционно чувствительный детектор размером 1,5x1,5 $см^2$, представляющий матрицу 256x256 пикселей, каждый из которых имеет свой усилитель. Частица, попавшая в детектор, создает ионизацию, пропорциональную энергии частицы. Информация об ионизации считывается специальной системой считывания в компьютер.

Была поставлена задача провести калибровку такого детектора: найти наилучший коэффициент усиления для каждого пикселя для а-частиц с энергиями около 5 МэВ. Альфа-частица, попавшая в детектор, создает кластер размером около 80 пикселей. Надо считать информацию с каждого пикселя. Сумма всех значений пропорциональна энергии а-частицы.

В вакуумной камере были проведены 2 цикла измерений: измерение с источником Am-Pu-Cu и измерение с источником ^{241}Am, имеющем интенсивную α-линию 5486 кэВ. С комбинированным источником была набрана статистика около 5 событий на пиксель, а с источником ^{241}Am - около 37 событий на пиксель. Так как кластер от α-частицы имеет большой размер, прокалибровать краевые пиксели не представляется возможным. Задача калибровки осложнилась тем, что в некоторых частях детектора пиксели оказались или совсем нечувствительными, или имеют коэффициент усиления, очень отличающийся от среднего значения коэффициентов усиления для остальных пикселей. События, попадающие в эти пиксели, при обработке не учитывались. На Рис. 25 схематически показаны области, в которых находятся такие пиксели.

Из обработки данных измерений с источником ^{241}Am был получен первый вариант калибровочной матрицы, с использованием которой были обработаны данные с комбинированным источником и получен энергетический спектр, который приведен на Рис. 26.

3.2 Исследования элементного состава и структуры приповерхностных слоёв твердых тел на ускорителе ЭГ-5

На пучках заряженных частиц ускорителя ЭГ-5 проводились аналитические исследования с использованием неразрушающих ядерно-физических методик: RBS (метод резерфордовского обратного рассеяния) и ERD (метод ядер отдачи). Измерялись глубинные профили различных элементов, начиная от водорода и дейтерия вплоть до гадолиния и вольфрама.

В сотрудничестве с ЭИ САН (г.Братислава, Словакия) анализировались нанослои металлов и окислов металлов, нанесённые на кремниевые подложки. С помощью неразрушающей методики RBS выполнен элементный анализ слоя, содержащего $1{,}9 \times 10^{16}$ ат/см^2 гадолиния, $2{,}7 \times 10^{15}$ ат/см^2 скандия и $4{,}5 \times 10^{16}$ ат/см^2 кислорода. На Рис. 27 показан спектр ионов гелия с энергией 2,035 МэВ, рассеянных на угол 170 градусов на образце, толщиной которого составляет 17 нанометров. Толщина поверхностного слоя и его элементный состав были определёны в результате компьютерной обработки экспериментального спектра.

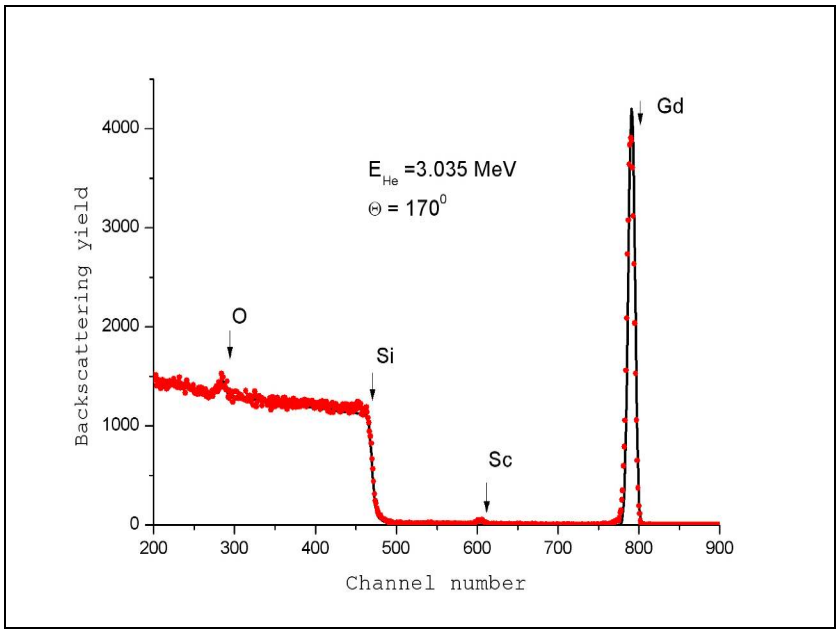

Рис. 27 Экспериментальный спектр (точки) и рассчитанный (линия) для оптимизированной модели образца.

Аналогичные исследования проводились в сотрудничестве с Воронежским Университетом. Был выполнен анализ образцов слоистых структур с толщинами слоёв от нанометров до 1-2 микрон. Для элементного анализа слоистых структур микронной толщины использовался также пучок протонов, получаемых от ускорителя ЭГ-5 ЛНФ. С помощью методики ERD был выполнен анализ кремниевых образцов, насыщенных водородом и дейтерием.

В сотрудничестве с УМКС и ЛУТ (г.Люблин, Польша), а также с СИМП (г. Сумы, Украина) анализировались образцы модифицированных конструкционных материалов. В частности выполнены детальные исследования изменения поверхностных свойств нержавеющей стали марки , имплантированной различными дозами азота. Выполнены также исследования процесса экстракции положительно заряженных ионов из плазмы в целях оптимизации ионных источников для имплантаторов.

3.3 Аналитические исследования с применением метода нейтронно-активационного анализа (НАА) на реакторе ИБР-2

Развитие экспериментальной базы сектора НАА

В период стоянки реактора ИБР-2 проводятся работы по усовершенствованию спектрометрического и сервисного оборудования установки РЕГАТА. В 2007 году

приобретены полупроводниковый германиевый детектор и ряд электронных блоков фирмы *Canberra*. Проведена калибровка детектора по эффективности с занесением полученных данных в программу расчета концентраций элементов. Совершенствуется пакет программ для обработки экспериментальных данных. Начаты работы по созданию спектрометра для проведения низкофоновых измерений.

По разработанной ранее в КБ ЛНФ конструкторской документации в Опытном производстве ОИЯИ в 2007 году были изготовлены новые каналы облучения для установки РЕГАТА на реакторе ИБР-2М. Проведен частичный демонтаж магистралей и устройств пневмотранспорта в кольцевом коридоре реактора для обеспечения возможности проведения работ по модернизации реактора. Изготовлена и смонтирована магистраль для заполнения детекторов жидким азотом.

Проведена теоретическая оценка возможности проведения НАА на новом источнике нейтронов ИРЕН, для чего были рассчитаны распределения плотностей потоков тепловых, резонансных и быстрых нейтронов вокруг мишени и выбрано оптимальное место расположения каналов облучения. Написано техническое задание на разработку системы пневмотранспорта для проведения активационного анализа на установке ИРЕН.

Экология

Биомониторинг

В марте 2007 года в Дубне на юбилейном XX Совещании комиссии ООН по трансграничному переносу воздушных загрязнений в Европе был подведен итог работам сектора НАА, проводимых в рамках международной программы «Атмосферные выпадения тяжелых металлов в Европе – оценки на основе анализа мхов-биомониторов». Эти работы охватывают некоторые регионы Центральной России, Южного Урала, Белоруссии, Болгарии, Словакии, Польши, Румынии, Сербии, Македонии, Хорватии и Греции, а также Монголии и Вьетнама, где были собраны и проанализированы более 2500 образцов мхов-биомониторов.

Результаты анализа для европейских стран по 13 элементам: Al, As, Cd, Cr, Cu, Fe, Hg, Ni, Pb, Sb, Ti, V и Zn – переданы в Европейский Атлас атмосферных выпадений тяжелых металлов, а полный спектр данных по 40–43 элементам, включая лантаниды (редкоземельные элементы) и актиниды (уран и торий), отражен в публикациях по соотвествующим регионам. Для оценки уровней загрязнения окружающей среды в промышленных районах России, подверженных сильному экологическому стрессу, качестве фоновых были результаты анализа мхов-биомониторов из биосферных заповедников (Приокско-Террасного и Воронежского), полученные в сотрудничестве с Институтом глобального климата и экологии (Москва).

В 2007 году намечены возможные пути сотрудничесива со Стелленбошским Университетом (ЮАР) в области биомониторинга (изучение распределения атмосферных выпадений метил-ртути с помощью мхов-биомониторов и НАА).

Оценка состояния экосистем

В рамках проекта РФФИ – Румынская Академия «Геохронология и изучение ретроспективных загрязнений незатвердевших донных отложений из кислородосодержащих и бескислородных акваторий западной части Черного моря» в 2007 году была завершена обработка результатов НАА донных отложений, отобранных на шельфе Черноморского побережья Румынии, и проведена оценка ретроспективного загрязнения этого региона. Совместно с румынской стороной подготовлены три публикации и отчет в РФФИ по проекту за 2007 год.

Завершена работа и представлены в печать результаты многоэлементного НАА коллекции аэрозольных фильтров разных лет, полученных из Братиславы, что позволило охарактеризовать динамику загрязнения атмосферы столицы Словакии тяжелыми металлами за последние 15 лет.

Совместно с Университетом в Ополе (Польша) выполнено комплексное исследование по оценке состояния окружающей среды на «аномальной территории» на западе Польши, характеризующейся повышенным радиоактивным фоном вследствие Чернобыльской аварии и техногенного воздействия промышленности. Первые результаты представлены в совместной статье, принятой в 2007 году к печати польским журналом «*Ecological Chemistry and Engineering*».

При участии университета «Дубна» завершено исследование распределения ряда тяжелых металлов вблизи транспортных развязок в Дубне и Москве (Щелковское и Минское шоосе). Работы доложены на двух международных конференциях и направлены в печать.

Результаты НАА (ОИЯИ) и ААС (Университет в Скопье) 200 образцов почв из района свинцово-цинкового комбината в Македонии послужили основой для Атласа карт распределения ряда тяжелых металлов, готовящегося к печати в Македонии.

Продукты питания и здоровье человека

В 2007 году на реакторе МИФИ (Москва) продолжены работы по анализу продуктов питания в связи с проектом сектора НАА с Корпорацией по атомной энергии Южной Африки (NECSA): «Сравнительное изучение воздействия на здоровье детей потребления продуктов питания, выращенных в некоторых промышленных районах России и Южной Африки, с использованием ядерно-физических аналитических методов».

Определение ряда короткоживущих изотопов в продуктах питания было проведено на реакторе Центра нейтронных исследований в Будапеште в октябре 2007 года. Результаты обрабатываются.

В рамках координационной программы МАГАТЭ «Воздействие токсичных и потенциально токсичных элементов на женщин репродуктивного возраста в развивающихся странах» совместно с Российским государственным медицинским университетом (Москва), Аналитическим центром Геологического института РАН и Медицинской Академией им. И.П. Сеченова продолжена работа по интерпретиции результатов многоэлементного анализа образов крови специально подобранных пациентов из одного из промышленных районов Москвы. Эти исследования подтвердили гипотезу о корреляции таких токсичных элементов, как свинец, цинк и сурьма, с индексом массы тела (Body Mass Index) обследуемых пациентов.

Биотехнологии

Продолжены исследования по биотехнологии очистки окружающей среды от токсичных элементов (ртуть, хром и др.), которые ведутся в секторе НАА совместно со специалистами Институтом физики им. Э. Андроникашвили (Тбилиси, Грузия). Новые результаты по использованию природных штаммов бактерий *Arthrobacter oxidans,* выделяемых из базальтов для восстановления токсичного Cr-VI в нетоксичную форму Cr-III, были представлены на международной конференции «Современные направления в активационном анализе» (17-21 сентября, Токио, Япония). Цикл из семи работ в области применения ядерно-физических методов в биотехнологии представлен на конкурс ОИЯИ научно-технических прикладных работ 2007 года.

Материаловедение

Синтез мелкокристаллических алмазов

Совместная работа с Институтом твердого тела и полупроводников Академии наук Беларуси по изучению влияния нейтронного облучения на свойства синтетических алмазов на примере системы Ni-Mn-C-Al_2O_3 в 2007 году направлена в российский журнал

«Кристаллография», а обобщенный материал о поведении дефектов в мелкокристаллических алмазах под воздействием нейтронного облучения в присутствии катализаторов представлен в виде отдельной главы в книге «Diamond and Related Materials» (США), находящейся в печати.

Археология

В рамках сотрудничества с Государственным Эрмитажем (Санкт-Петербург) был проведен статистический анализ ранее полученных результатов НАА образцов керамик из древних курганов (Сыртея Смоленской области и Северный Кавказ). Обсуждение результатов проходило на рабочем семинаре в Эрмитаже (23 ноября 2007 г), где были намечены направления дальнейших исследований.

Радиоэкология

Совместно с университетом Коменского в Братиславе в низкофоновой лаборатории физического факультета впервые были проведены радиометрические измерения 50 образцов мхов-биомониторов, собранных в Минской и Гомельской областях Беларуси спустя 20 лет после аварии на Чернобыльской АЭС. Результаты измерений показали, что уровень активности ^{137}Cs в Гомельской области в три раза превышает уровень активности в Минской области. Отмечено повышенное содержание ^{210}Pb, что, по всей вероятности, связано с мероприятиями по ликвидации последствий аварии на ЧАЭС в 1986 году. Готовится публикация в реферируемом журнале.

Учебный процесс

На базе установки РЕГАТА в 2007 году проводился Практикум для студентов старших курсов Университета «Дубна» и студентов Международных Летних Школ, организуемых УНЦ ОИЯИ. За отчетный период на базе сектора НАА были выполнены 2 курсовых и 3 магистерских работы.

Организация совещаний

XX Совещание комиссии ООН по трансграничному переносу воздушных загрязнений в Европе (5-9 марта 2007, Дубна).

Первое рабочее совещание в рамках проекта Технической кооперации сектора НАА ЛНФ с МАГАТЭ «Гармонизация системы контроля качества в лабораториях РФ, использующих ядерно-физические аналитические методы (9-15 декабря 2007, Дубна).

2. NEUTRON SOURCES

2.1. The IBR-2 pulsed reactor

Starting in December 2006 after the reactor shutdown the works on the modernization of IBR-2 were conducted in accordance with the "Program of activities on the IBR-2 reactor during its temporary shutdown (2007-2010)" in compliance with the quarterly plans approved by the FLNP chief engineer.

By now, work on the moving reflector PO-3, fuel elements and design documentation for all reactor equipment for the IBR-2M reactor has been completed.

1. Work on the dismantling of IBR-2:

1.1. The main task in 2007 according to the schedule of works on modernization is the defueling of the IBR-2 reactor core and the removal of sodium from the extracted fuel assemblies (FA). This work after thorough preparations started on March 12, 2007 and on June 22, 2007 it was successfully completed.

1.2. On July 6, 2007 sodium was drained from the Ist and IInd contours. The equipment and pipelines of sodium contours were filled with argon.

1.3. The actuating mechanisms of the safety control system (SCS) and ionization chambers were dismantled and placed in a storehouse.

1.4. The rolling shielding was moved away from the reactor.

1.5. The moving reflector was moved away from the reactor. Temporary service lines were laid for feeding helium and oil to PO-3 thus providing a temporary laying-up mode.

1.6. Water moderator and inclined moderator were dismantled.

1.7. Cooling pipes of stationary reflectors were dismantled.

1.8. The sodium cooling pipelines (pressure and outlet collectors) were cut off from the reactor vessel. A package of measures to remove the IBR-2 reactor vessel was carried out.

1.9. On December 12, 2007 the reactor vessel was placed in a standard depository in the reactor hall for long-term storage.

2. Safety Control System (SCS) of IBR-2M:

2.1. The manufacturing of a standard ASCS, reactor control panel (SNIIP-SYSTEMATOM) and CM system (INEUM) continued.

2.2. In JINR EW standard actuating mechanisms (AM) for control units of compensating regulators and manual regulators and a prototype model of AM of emergency shutdown system (ESS) were manufactured. The manufacturing of standard AM of ESS and AP is in progress.

2.3. On the FLNP test-bench the longevity tests of the prototype model of AM of CO and ESS were carried out.

3. In NIKIET the manufacturing of a new reactor vessel continued. The in-vessel FA reloading device was delivered to FLNP.

4. In JINR Experimental Workshops the manufacturing of rolling shielding, stationary reflectors and blocks of regulation for the stationary reflector was completed. The check assembly of this equipment complex was conducted. The specified equipment was accepted by the Commission with participation of NIKIET and Rostehnadzor (Federal Service for Supervision of Environment, Technology and Nuclear Management) and moved to the IBR-2 reactor hall.

5. Complex of cryogenic moderators (CM):

- CHF-700 (Heliymash) was manufactured;
- detail design of CM (NIKIET) was completed;
- the manufacturing of cryogenic pipelines in Heliymash is in progress;

- in NIKIET the design documentation for CM 202 (beams 7÷11) is being worked out;
- in JINR Experimental Workshops the manufacturing of water moderators started.

In 2007 for financing of works on the IBR-2 modernization a total of 915 k$ was spent as of January 1, 2008, which amounts to 106% of the plan for the year.

2.2. The IREN Project

The main tasks of the Frank Laboratory of Neutron Physics and the Laboratory of Particle Physics in 2007 were the development of engineering infrastructure and the installation of the available equipment of the 1st stage of the LUE-200 accelerator.

1. Development of engineering infrastructure

In 2007 in accordance with the approved plan-schedule the following works on the construction and installation of power supply systems, water-cooling and thermostabilization systems, control and alarm systems of the 1st stage of the IREN facility were performed:

- all electric equipment of the LUE-200 accelerator and auxiliary systems were installed and tested;
- systems of water-cooling, thermostabilization and of distillate preparation were installed;
- interlock and alarm systems were installed;
- repairs to control console and service rooms were done, the installation of equipment of AMCS (automated monitoring and control system) is underway;
- work to construct ARCS (automated radiation control system) started;
- installation of fire alarm and fire extinguishing systems is nearing completion.

2. The LUE-200 accelerator

In spite of the delay due to the accident with the klystron SLAC 5045, the installation of the accelerator systems is carried out in accordance with the corrected plan-schedule.

- The gun modulator charging system was started up on its regular place.
- The power supplies of the focusing magnets: UM-10, VC-25 (INP), Bruker D1 Bruker D2, Bruker Q1 were installed on their regular place and connected to the mains;
- The high-current power supplies of the focusing solenoids of the 1st accelerating section (Bruker D1) and of the SHF-buncher (Bruker Q1) were tested under real load conditions.
- Magnetic measurements and correction of magnetic field of the focusing solenoid were carried out. Magnetic field nonuniformity Br/Bz in the beam region is no worse than ± $5*10^{-3}$.
- At a full-scale test stand of the LUE-200 accelerator the power supply system of the SLAC 5045 klystron was adapted to the TH2129 klystron.
- Correcting coils of the first accelerating segment were installed.
- The first accelerating section was assembled.
- The installation of the SHF feeder was completed, vacuum tests of the accelerator comprising the electron source, the first accelerating segment and the first accelerating section were carried out.
- The installation of the magnetic spectrometer is nearing completion.
- The installation of the AMCS equipment is nearing completion.

2. НЕЙТРОННЫЕ ИСТОЧНИКИ

2.1. Импульсный реактор ИБР-2

Работы по модернизации ИБР-2, начиная с декабря 2006 г. после остановки реактора, ведутся в соответствии с «Программой работ на реакторе ИБР-2 в режиме временного останова (2007-2010 г.г.)» по квартальным планам, утверждаемым главным инженером ЛНФ.

К настоящему времени полностью готовы для реактора ИБР-2М:

- подвижный отражатель ПО-3;
- топливная загрузка;
- конструкторская документация по всему реакторному оборудованию.

1. Работы по демонтажу ИБР-2:

1.1. Главная задача 2007 г. по графику модернизации – разгрузка активной зоны ИБР-2 и отмывка выгруженных ТВС от натрия. Эта работа после тщательной подготовки была начата 12.03.2007 г. 22.06.2007 г. эта работа была успешно завершена.

1.2. 06.07.2007 г. был дренирован натрий из I^{го} и II^{го} контуров. Оборудование и трубопроводы натриевых контуров заполнены аргоном.

1.3. Исполнительные механизмы СУЗ и ионизационные камеры демонтированы и размещены в хранилище.

1.4. Удалены от реактора откатные защиты.

1.5. Подвижный отражатель удален от реактора. Смонтированы временные коммуникации для подачи в ПО-3 гелия и масла, что обеспечивает режим временной консервации.

1.6. Демонтированы водяной замедлитель и наклонный замедлитель.

1.7. Демонтированы трубы охлаждения стационарных отражателей.

1.8. Трубопроводы натриевого охлаждения (напорный и сливной коллекторы) отрезаны от корпуса реактора. Выполнен комплекс мер для удаления корпуса ИБР-2.

1.9. Корпус реактора 12 декабря 2007 г. удален в штатное хранилище реакторного зала для длительного хранения.

2. СУЗ ИБР-2М:

2.1. Продолжалось изготовление в СНИИП-СИСТЕМАТОМ штатного комплекта АСУЗ, а также пульта управления реактором, системы контроля технологических параметров (ИНЭУМ).

2.2. В ОП ОИЯИ изготовлены штатные исполнительные механизмы (ИМ) для органов регулирования КО и РР и опытный образец ИМ АЗ, ведется изготовление штатных ИМ АЗ и АР.

2.3. На стенде ЛНФ завершены ресурсные испытания опытного образца ИМ КО и АЗ.

3. В НИКИЭТ продолжалось изготовление нового корпуса. Внутрикорпусное перегрузочное устройство ТВС доставлено в ЛНФ.

4. В ОП ОИЯИ завершено изготовление откатных защит, стационарных отражателей и блоков регулирования в стационарном отражателе. Выполнена контрольная сборка этого комплекса оборудования. Указанное оборудование принято комиссией с участием НИКИЭТ и Ростехнадзора и перевезено в реакторный зал ИБР-2.

5. Комплекс криогенных замедлителей:

- изготовлена КГУ-700 (Гелиймаш);
- выпущен технический проект КЗ (НИКИЭТ);
- ведется изготовление криогенных трубопроводов в Гелиймаше;
- в НИКИЭТ ведется разработка КД для КЗ 202 (пучки 7÷11);

- в ОП ОИЯИ начато изготовление водяных замедлителей.

На обеспечение работ по модернизации ИБР-2 в 2007 г. было израсходовано на 01.01.2008 г. около 915 k$, что составляет 106 % от плана года.

2.2. Проект ИРЕН

Главными задачами Лаборатории нейтронной физики и Лаборатории физики частиц в 2007 году являлось создание инженерной инфраструктуры и монтаж имеющегося оборудования первой очереди ускорителя ЛУЭ-200.

1. Создание инженерной инфраструктуры

В течение 2007 года в соответствии с утвержденным планом-графиком были выполнены следующие работы по созданию систем электропитания, водоохлаждения и термостабилизации, управления и сигнализации первой очереди установки ИРЕН:

- Смонтировано и испытано все электрооборудование ускорителя ЛУЭ-200 и вспомогательных систем;
- Смонтирована система водоохлаждения, термостабилизации и подготовки дистиллята;
- Смонтирована система блокировок и сигнализации;
- Проведен ремонт пульта управления и вспомогательных помещений, идет монтаж оборудования системы АСКУ (автоматизированная система контроля и управления;
- Начаты работы по изготовлению системы АСРК (автоматизированная система радиационного контроля);
- Завершается монтаж системы автоматического пожаротушения и пожарной сигнализации.

2. Работы по ускорителю ЛУЭ-200

Несмотря на задержку, вызванную аварией с клистроном SLAC 5045, работы по монтажу систем ускорителя выполняются в соответствии с откорректированным планом-графиком.

- Запущена на штатном месте система зарядки модулятора пушки;
- Смонтированы на штатном месте и стационарно подключены к сети источники питания фокусирующих магнитов: УМ-10, ВЧ-25 (ИЯФ), Bruker D1 Bruker D2, Bruker Q1.
- Испытаны на реальную нагрузку сильноточные источники питания фокусирующих соленоидов 1-й ускоряющей секции (Bruker D1) и СВЧ–группирователя (Bruker Q1);
- Проведены магнитные измерения и коррекция магнитного поля фокусирующего соленоида. Неоднородность поля Br/Bz в области пучка не хуже, чем $\pm 5*10^{-3}$;
- На полномасштабном стенде ускорителя ЛУЭ-200 произведена адаптация системы питания клистрона SLAC 5045 к клистрону TH2129;
- Смонтированы катушки корректоры первого ускорительного промежутка;
- Установлена первая ускорительная секция;
- Завершен монтаж СВЧ фидера, проведены вакуумные испытания ускорителя в составе источника электронов, первого ускорительного промежутка и первой ускорительной секции;
- Завершается монтаж магнитного спектрометра;
- Завершается монтаж оборудования системы АСКУ.

3. DEVELOPMENT AND CONSTRUCTION OF ELEMENTS OF NEUTRON SPECTROMETERS FOR CONDENSED MATTER INVESTIGATIONS

In 2007 work in the framework of the theme was focused on the following main activities:

- construction of gas and scintillation neutron detectors;
- development of neutron beam-forming systems and sample environment systems;
- development of data acquisition systems and computing infrastructure.

1. Construction of neutron detectors

a) Gas detectors

Because of insufficiency of financial resources and in connection with the plans for 2008-2010 to develop a specialized readout ASIC for MWPC detectors within the frameworks of the EU project "DETNI" (Detectors for Neutron Instrumentation) it has been decided to postpone the commencement of works on construction of PSD with individual readout from each wire to 2008. At the first stage of this work the prototype of the detector with a limited number of wires (16-32) will be constructed.

In accordance with the plan the following works on the optimization of geometry and working parameters of the 2D detector with an active area of 225×225 mm² and delay line data readout (**Fig. 1**) were carried out:

- diameter of the anode wire was reduced from 15μm to 10 μm;
- tension and accuracy of positioning of cathode wires were improved;
- parallelism of anode and cathode wires (spread is less than 2 μm) was provided;
- length of the delay line was reduced by a factor of 1.5.

All these changes made it possible to improve the spatial resolution down to 2mm.

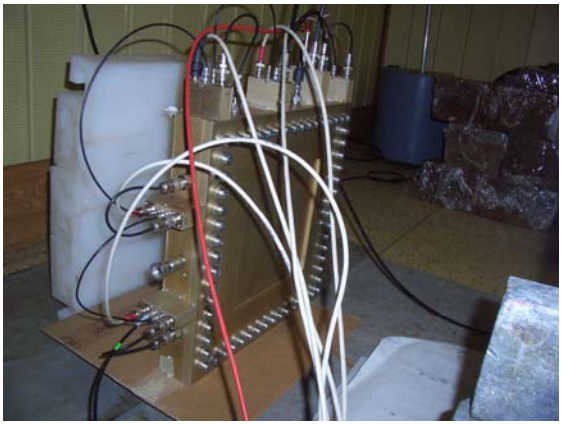

Fig. 1. 2D PSD with an active area of 225×225 mm².

Owing to the financial support of the Hungarian Academy of Sciences the development and manufacturing of a similar PSD detector for the GRAINS spectrometer started. In 2007 the design documentation for a PSD casing was worked out and the casing was produced; a high-voltage power supply, NIM crate and a constant fraction timing discriminator were purchased. Preamplifiers for signal readout from anode and cathode planes of the detector were made as well.

For the period of 2007-2008 a grant from the Federal Agency for Science and Innovations of the RF Ministry of Science and Education was received to design and create a system for monitoring cold moderators of new type based on a solid frozen mixture of aromatic hydrocarbons in the form of pellets at a temperature of 20-30 K (State Contract №02.518.11.7035 of 19.04.07). Within the framework of this contract the project of the monitoring system, whose main element is a 2D PSD with an active area of 200×200 mm^2, was developed. In 2007 the casing and electrodes of the detector were manufactured and standard electronic blocks were purchased.

In cooperation with INRNE BAS, Sofia, a gas-filled curved position-sensitive detector intended for studies in the area of X-ray structure analysis of solid-state samples is being designed.

A flow-type detector of cylindrical geometry, arc radius is 223.9 mm, occupied angle – 63º, height of the entrance window – 35 mm, has been designed. The spacing between anode wires is 1 mm, in cylindrical geometry it corresponds to 12 angular minutes. At such geometry the angular resolution of detected x-ray quanta is expected to be better than 10 angular minutes. Data on the place of detection are readout using delay lines with time spacing of 2 ns. The drawings of the detector have undergone a technological inspection and have been turned over for production to the JINR Experimental Workshops (**Fig. 2**).

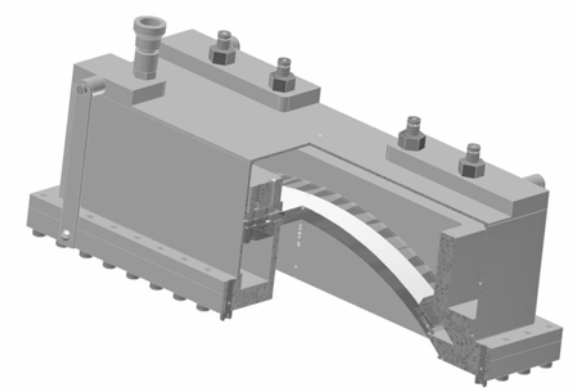

Fig. 2. Overall view of the curved PSD for X-ray diffraction measurements.

A chamber for the MiniFobos detector, which is intended for precise positioning of a fission fragment source, has been developed for FLNR JINR. The chamber **(Fig. 3)** allows micrometer movement along all three coordinate axes and rotation of the source through ±15º relative to the plane perpendicular to the MiniFobos axis. In addition, there is a possibility of preliminary positioning of the whole block. The drawings of the chamber have been turned over for production to the FLNP Experimental Workshops.

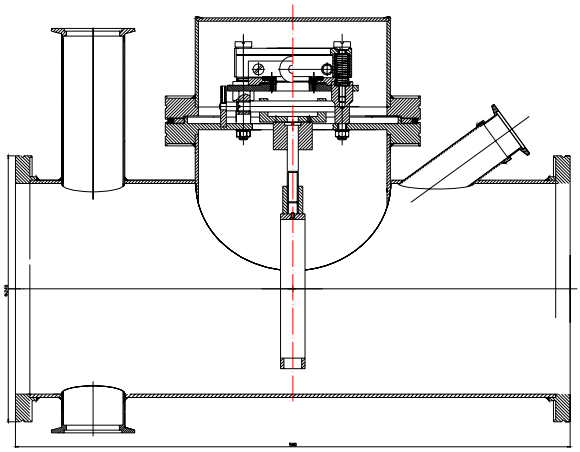

Fig. 3. Positioning chamber of the MiniFobos detector (front view).

Work to modernize the detector test stand **(Fig. 4)** has been carried out. A new block of moderators for working with the detectors with an active area of up to 200×200 mm^2 has been manufactured. Also, the re-layout of the room has been conducted to reduce human exposure to radiation and to improve the operators' working conditions. As a result of these measures, the total neutron and gamma-radiation dose rate at the operators' workplace with an installed source is no more than 0.5 μSv/h.

Fig. 4. Detector test stand.

To manufacture gas position-sensitive detectors with a large active area, a new winding machine (**Fig. 5**) has been constructed, making it possible to stretch fine gilded tungsten wires (up to 10 μm) across electrode frames of detectors. The machine comprises a platform rotating on a supporting stand. The plates intended to fix electrode frames are attached on both sides of the platform. The plates can be raised and lowered over the platform. The wire spacing is set by means of screws. The machine allows one to wind simultaneously one or two frames with an area of up to 800×800 mm^2. The maximum frame thickness is 12 mm. The wire spacing is a multiple of 1 mm, the minimum wire spacing is 1 mm.

Fig. 5. Winding machine.

2. Neutron beam-forming systems and sample environment systems

In 2007, in the framework of the BMBF-JINR project in cooperation with the German Institutes and PNPI (Gatchina) work to construct curved mirror neutron guides on beam 7a of the IBR-2 reactor and to radically modernize the EPSILON and SKAT spectrometers was started:

2.1. Calculations and simulation of the neutron guide elements were performed.

2.2. Positioning of the neutron guide constructions relative to real construction axes of channel N7 and building 117/2 (**Fig. 6**) was completed.

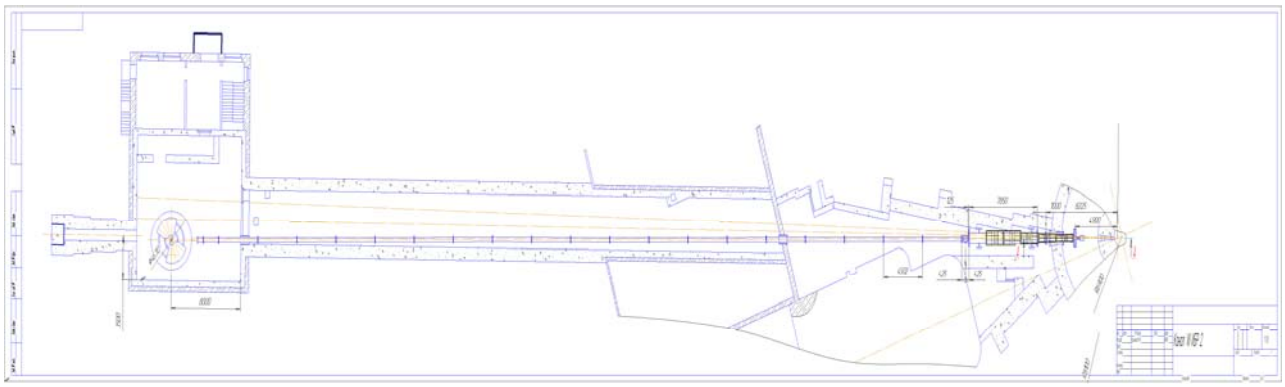

Fig. 6. Layout of mirror neutron guides on channel N7 of IBR-2.

2.3. Angular directions of axes of the direct part of neutron channels for neutron guides 7a-1 and 7a-2 relative to the geometrical axis of channel N7 for the SKAT and EPSILON spectrometers, respectively, were agreed upon and approved.

2.4. The entrance cross-sections for neutron guides 7a-1 and 7a-2 were determined and approved in accordance with the optimized calculated parameters of neutron beam transmission.

2.5. Draft and detail designs of vacuum housings for a three-channel optical collimator of the neutron guide system of channel N7 (**Fig. 7**) were developed.

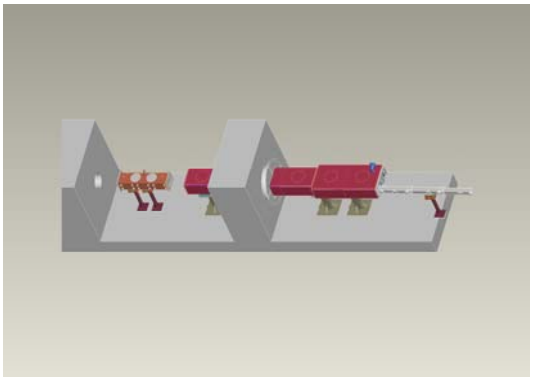

Fig. 7. Three-channel optical collimator of a neutron guide system.

2.6. Draft and detail designs of two types of vacuum housings with the necessary infrastructure for assembling and positioning of separate optical channels of neutron guides 7a-1 and 7a-2 (**Fig. 8**) were developed.

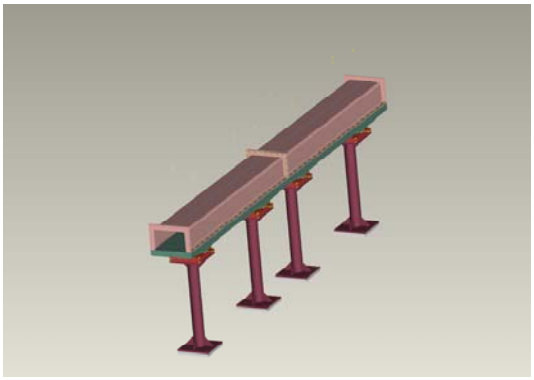

Fig. 8. Vacuum housing for two mirror channels.

2.7. Draft and detail designs of supporting piers and alignment tables for all types of vacuum housings of the neutron guide system of channel N7a (**Fig. 9**) were developed.

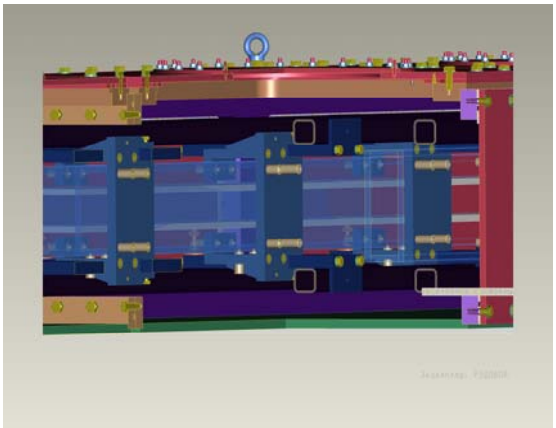

Fig. 9. Positioning mechanism on a supporting frame of vacuum housing.

2.8. The old neutron guide on channel N7a was dismantled and the biological shielding was partially disassembled (**Fig. 10**).

Fig. 10. Beam gallery of channel 7 of IBR-2 before and after dismantling.

The following activities were carried out to upgrade the control systems of actuating mechanisms of the spectrometers:

1. Controllers SMC-32-CAN for the control systems of actuating mechanisms of the IBR-2M spectrometers were developed and tested:

- Angular movement sensor (16 bits) and control block of DR-1.5RA direct-current motors were integrated into the control system;
- Controller program was designed to provide access to several blocks via a CAN line.

The above-mentioned blocks are in the CAN industrial standard. All spectrometers of IBR-2M will be equipped with these unified blocks.

2. The control block of the MOND spectrometer and the control block of 15 direct-current motors of the DISK spectrometer in the RRC «Kurchatov Institute» were put into operation.

A bore cryostat with a closed-cycle refrigerator SUMITOMO RP-062B (**Fig. 11**) was designed to carry out diffraction experiments with samples in high-pressure sapphire anvil cells on thermal neutron beams in the temperature range of 6-300 K. The cryostat has a vertical channel for inserting high-pressure cells into thermostatic temperature control area, and cells can be replaced without defrosting the cryostat. At present, the documentation is being processed in the JINR Experimental Workshops.

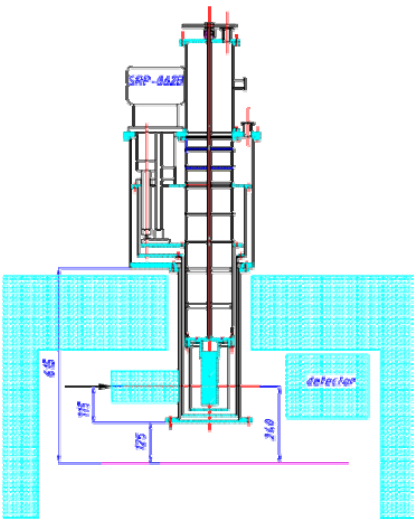

Fig. 11. Bore cryostat.

On the basis of the equipment received on account of the Romanian dues, a vacuum test-bench with a helium leak detector L200 (Leybold) intended to test various vacuum and cryogenic systems of the IBR-2 spectrometers was constructed and put into operation. Also, a contract with CRYOMECH (USA) to deliver cryorefrigerator PT 403, which is the main element of the cryogenic test stand, was concluded.

3. Development of data acquisition systems, computing infrastructure and software

The development of a DAQ block for multicounter systems (up to 64 channels in one block) was completed. The block was prepared for tests on the neutron source in PNPI (Gatchina). DAQ blocks for the system of acquisition and accumulation of data from 1D and 2D PSD were manufactured. These blocks will be tested on the BER-II reactor (HMI, Berlin) in early 2008. The expected count rate will be no less than 10^6 events/s.

The work on the construction of cable infrastructure of the network segment of the IBR-2 experimental halls (Gigabit Ethernet) was started. A contract to supply component parts was concluded with the “CONTACT” company. The work on the laying and welding of a fiber-optic cable was completed.

In the works on software, particular attention has been given to the development of the Sonix+ software package intended to operate at the IBR-2M reactor and to practical tests of the programs on the reactors of outside organizations (IPPE, Obninsk and RRC KI, Moscow). In particular,

- modules for control systems of actuating mechanisms with CAN interface were developed;
- spectrum visualization program was improved to operate in on-line and off-line modes;
- design of software for new electronic DAQ blocks connected to PC via USB-interface was started;
- first version of the Web Sonix system of remote supervision and control over the progress of the experiment at the spectrometers was prepared.

The Web Sonix system is intended for remote supervision and control over the experiments at the IBR-2M spectrometers. It should meet the requirements of all groups of users. The architecture of the system is independent of specific features of spectrometers and provides the user with:

- detailed information on parameters of the current measurement;

- contents of log files of measurements (current and previous);
- visualization of current spectra from all detectors.

The control assumes that the service provided by the Web site includes tools to read, edit and manipulate scripts.

In the FLNP network a special server is allocated to the Web Sonix system. The system is a client of Apache HTTP server 2.2.4 (**Fig. 11**). For generation of dynamical Web pages the language PHP 5.0 has been chosen. Command channel is realized at the socket level in the client-server model. FTP (SFTP) protocol is used to transfer files.

Preliminary tests of the Web Sonix system with a limited set of functions were carried out in December, 2006 on the spectrometers REMUR, NERA-PR and HRFD in the experiments using position-sensitive detectors. The tests have shown that the supervision system is serviceable and does not affect the reliability of operation of data acquisition systems. At present, the full version of Web Sonix is being tested.

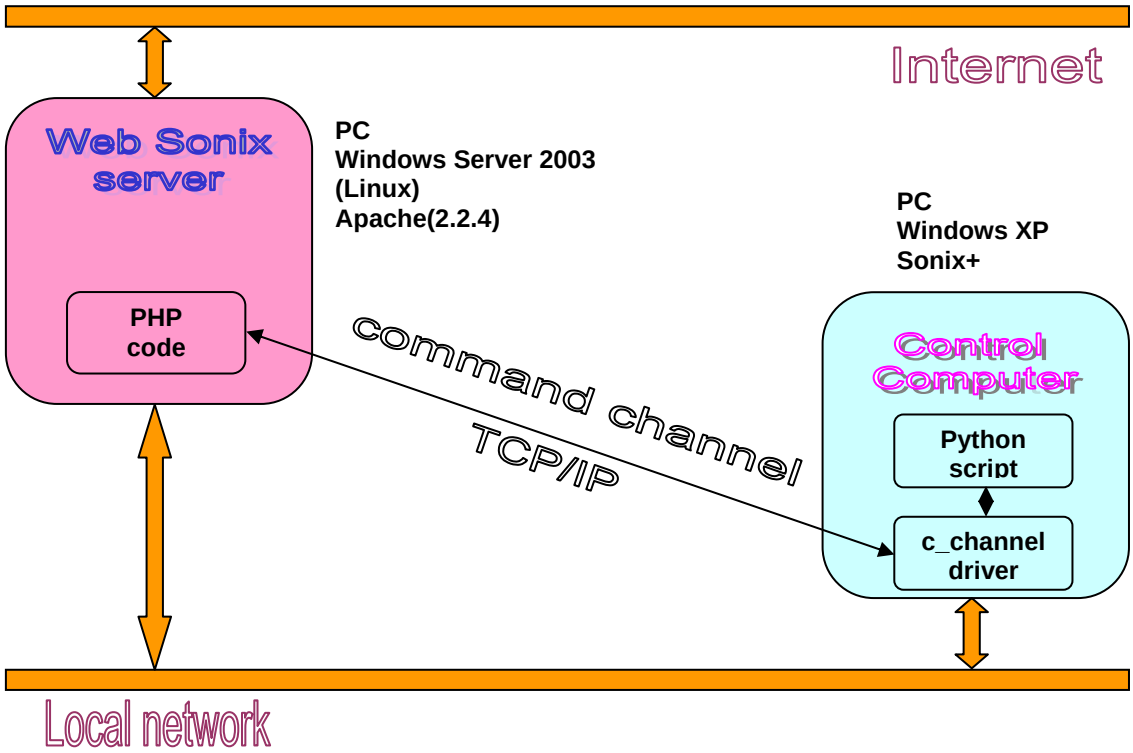

Fig.11. Scheme of command channel.

In collaboration with HMI, Berlin, a large amount of work to integrate the software (designed in FLNP) for the system of data acquisition from 2D PSD into the program system CARESS and to test its long-term stability was carried out. These activities were successfully completed at several spectrometers of the BER-II reactor and the synchrotron source of HMI.

In 2007, the development of the software package VITESS for simulation of new elements of spectrometers and neutron scattering methods was continued. As before, the Monte Carlo method (particle motion in three-dimensional space) was used. The modules were designed in the C/C++ programming language and for the graphical interface the TCL/TK interactive language was used.

The following modules for the VITESS package (**Fig. 12**) were designed, tested and put into service:

– Module for the refraction lens system with a set of accessory programs (bringing to a focus, etc.). The basic module includes visualization (**Fig. 13**).
– Module for simulation of neutron spin precession in pulsed magnetic fields (“triangle”, “saw” shapes).
– Module for analysis of polarization in time intervals (TIME GATE) for simulation of a spin-echo spectrometer.
– Module for simulation of multichannel polarizers (in the stage of testing and introduction). The module includes visualization.

Preliminary calculations were made and the following instruments were simulated:

1) Spin-echo spectrometer with time-dependent magnetic fields (“triangle”, “saw” shapes).
2) Systems of focusing refraction lenses and their application in the simplest small-angle setup to improve data quality.
3) Neutron beam polarizers (of N, V, Double V form).

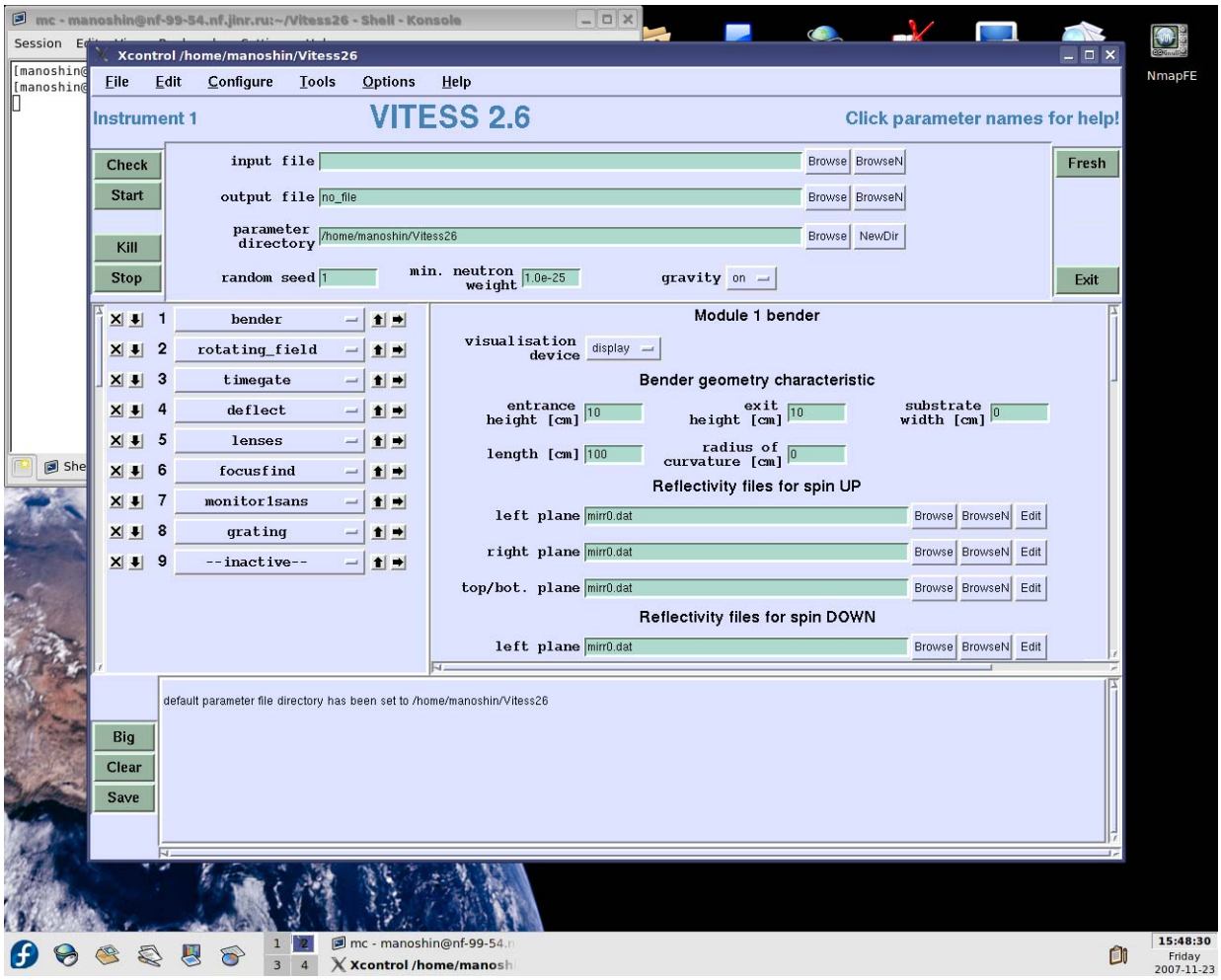

Fig. 12. Graphical shell for VITESS with new modules.

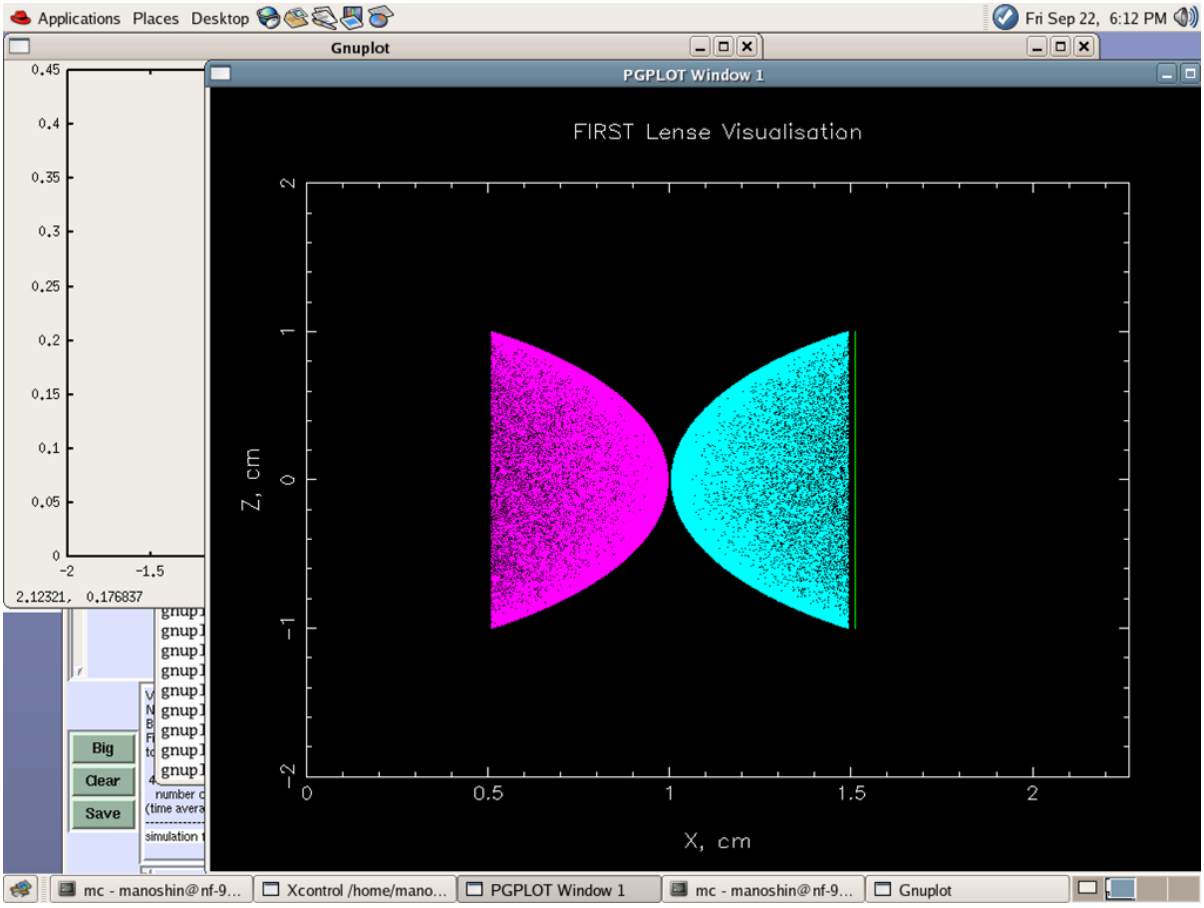

Fig. 13. Example of visualization of simulation of neutron concave refraction lens.

3. РАЗРАБОТКА И СОЗДАНИЕ ЭЛЕМЕНТОВ НЕЙТРОННЫХ СПЕКТРОМЕТРОВ ДЛЯ ИССЛЕДОВАНИЯ КОНДЕНСИРОВАННЫХ СРЕД

Работы по теме велись в следующих основных направлениях:
- создание газовых и сцинтилляционных нейтронных детекторов;
- системы формирования нейтронных пучков и системы окружения образца;
- развитие систем сбора данных и вычислительной инфраструктуры.

1. Создание нейтронных детекторов

а) Газовые детекторы

Из-за ограниченности финансовых ресурсов и в связи с планированием разработки в 2008-2010г.г. специализированной микросхемы ASIC для съема информации с MWPC детекторов в рамках проекта EU “DETNI” (Detectors for Neutron Instrumentation) было решено перенести начало работ по созданию ПЧД с индивидуальным считыванием информации с каждой нити на 2008г. На первом этапе этих работ будет создан прототип детектора с ограниченным числом нитей (16-32).

В соответствии с планом были выполнены работы по оптимизации геометрии и рабочих параметров двухкоординатного ПЧД с размерами чувствительной области 225×225 мм² и съемом информации с линий задержки (**Рис. 1**):

- диаметр анодной нити уменьшен с 15мкм до 10 мкм;
- повышены натяжение и точность монтажа катодных нитей;
- обеспечена параллельность анодных и катодных нитей (разброс менее 2 мкм);
- в 1,5 раза уменьшена длина линии задержки.

Все это позволило улучшить пространственное разрешение до 2 мм по обеим координатам.

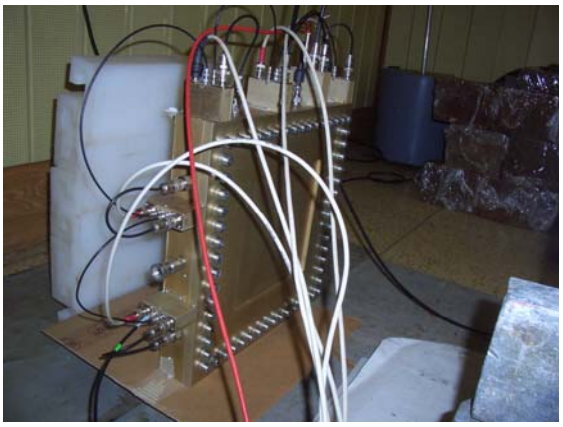

Рис.1 Двухкоординатный ПЧД с размерами чувствительной области 225×225 мм².

Благодаря финансовой поддержке Венгерской Академии Наук начата разработка и изготовление аналогичного ПЧД детектора для спектрометра «Горизонт». На этапе 2007 г. разработана конструкторская документация и изготовлен корпус ПЧД, приобретены в/в источник питания, NIM крейт и дискриминатор с точной временной привязкой. Изготовлены также предусилители для съема сигналов с анодной и катодных плоскостей детектора.

На период 2007-08 гг. получен грант Федерального агентства по науке и инновациям Минобрнауки РФ на разработку и создание системы мониторинга холодных замедлителей

нового типа на основе твердой замороженной смеси ароматических углеводородов в виде шариков при температуре 20-30 К (Государственный контракт № 02.518.11.7035 от 19.04.07). В рамках этого контракта разработан проект системы мониторинга, основным элементом которой является двухкоординатный PSD с чувствительной областью 200x200 мм². В 2007г. изготовлены корпус и электроды детектора и приобретены стандартные электронные блоки.

В сотрудничестве ИЯИЯЭ БАН, София разрабатывается газонаполненный изогнутый позиционно-чувствительный детектор, предназначенный для исследований в области рентгено-структурного анализа твердотельных образцов.

Детектор проточного типа цилиндрической геометрии, радиус дуги равняется 223.9 мм, занимаемый угол - 63º, высота входного окна – 35 мм. Расстояние между анодными нитями равняется 1мм, в цилиндрической геометрии это расстояние соответствует 12 угловым минутам. При такой геометрии угловое разрешение регистрируемых рентгеновских квантов ожидается лучше 10 угловых минут. Съем информации о месте регистрации производится с помощью линии задержки с временным шагом 2нс. Чертежи детектора прошли этап технологической проверки и переданы для изготовления в ОП ОИЯИ (**Рис. 2**).

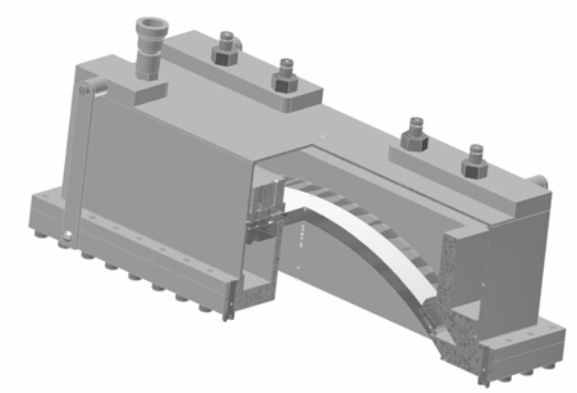

Рис.2. Общий вид изогнутого ПЧД для измерений рентгеновской дифракции.

Для ЛЯР ОИЯИ была разработана камера к детектору МиниФобос, которая предназначена для точной юстировки источника осколков деления. Камера (**Рис.3**) позволяет микрометрические передвижения по всем трем координатам, а также поворот источника на угол ±15º по отношению к плоскости, перпендикулярной оси МиниФобоса. Кроме того, имеется возможность предварительной юстировки всего блока. В настоящий момент чертежи камеры переданы для исполнения в ООЭП ЛНФ.

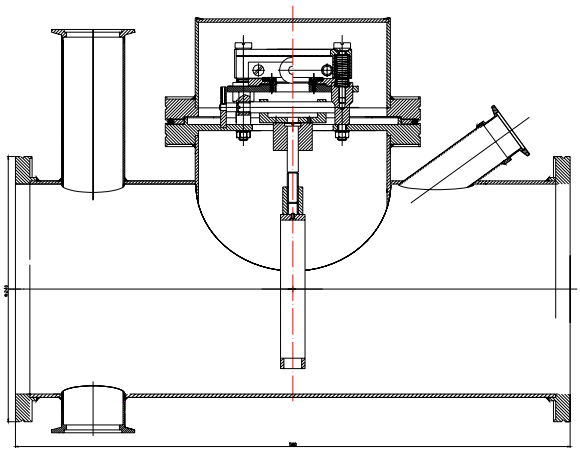

Рис. 3. Юстировочная камера детектора МиниФобос – фронтальная проекция.

Рис. 4. Детекторный стенд.

Были проведены работы по модернизации детекторного стенда (**Рис. 4**). Изготовлен новый блок замедлителей для работы с детекторами, имеющими чувствительную область до 200х200 мм^2. Также была произведена перепланировка помещения с целью усиления биологической защиты операторов и улучшения условий их работы. В результате этих работ, суммарная мощность дозы по нейтронам и гамма-излучению на рабочем месте операторов при установленном источнике составляет не более 0,5 мкЗв/час.

Рис. 5. Намоточный станок.

Для изготовления газовых ПЧД детекторов с большой чувствительной площадью создан намоточный станок (**Рис. 5**), позволяющий наматывать тонкие проволочки (до 10мкм) из позолоченного вольфрама на рамки электродов детекторов. Станок представляет собой плоскую основу, вращающуюся на укрепленной станине. С обеих сторон основы прикреплены пластины, предназначенные для крепления рамок электродов. Пластины могут подниматься и опускаться над основой. Шаг намотки проволочек задается с помощью дистанционных винтов. Станок позволяет наматывать одновременно одну или две рамки с размерами до 800х800 мм^2. Максимальная толщина рамки – 12 мм. Шаг намотки кратен 1 мм, минимальный шаг намотки составляет 1 мм.

2. Системы формирования нейтронных пучков и системы окружения образца.

В 2007 году в рамках проекта BMBF-JINR совместно с институтами ФРГ и ПИЯФ г. Гатчина начаты работы по созданию изогнутых зеркальных нейтроноводов на канале 7а реактора ИБР-2 и кардинальной модернизации спектрометров ЭПСИЛОН и СКАТ:

2.1. Выполнены расчеты и моделирование элементов нейтроновода.

2.2. Завершена привязка конструкций нейтроноводов к реальным строительным осям канала №7 и здания 117/2 (**Рис. 6**).

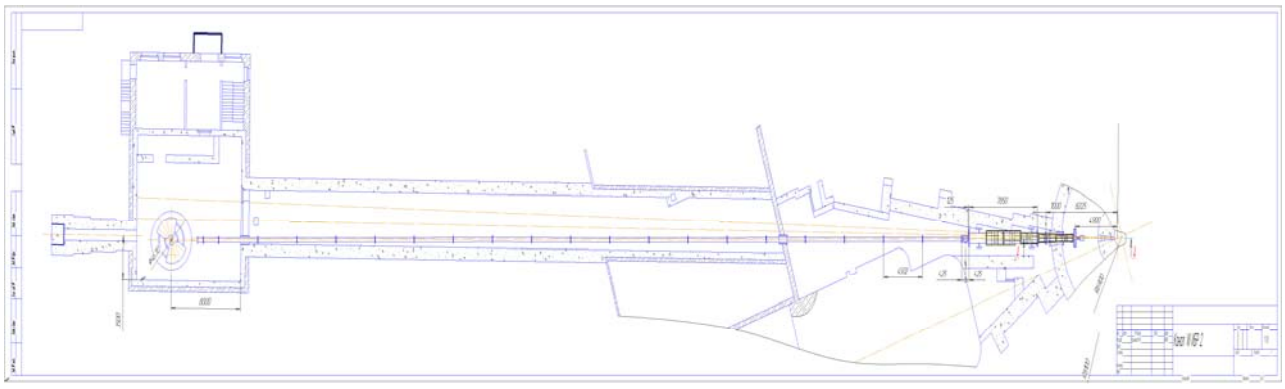

Рис. 6. Размещение зеркальных нейтроноводов на канале №7 ИБР-2.

2.3. Согласованы и утверждены угловые направления осей прямой части нейтроноводных каналов для нейтроноводов 7а-1 и 7а-2 по отношению к геометрической оси канала №7 реактора для установок SKAT и EPSILON соответственно.

2.4. В соответствии с оптимизированными расчетными параметрами по пропусканию нейтронного потока, согласованы и утверждены входные сечения для нейтроноводов 7а-1 и 7а-2.

2.5. Разработаны эскизный и рабочий проекты вакуумных кожухов входного трехканального оптического коллиматора нейтроноводной системы канала №7 (**Рис. 7**).

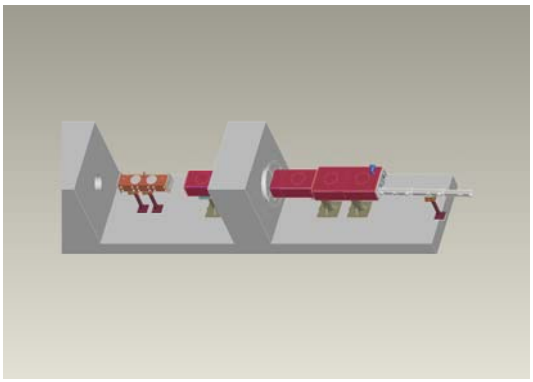

Рис. 7. Входной трехканальный оптический коллиматор нейтроноводной системы.

2.6. Разработан эскизный и рабочий проект для двух типов вакуумных кожухов с необходимой инфраструктурой, для сборки и юстировки раздельных оптических каналов нейтроноводов 7а-1 и 7а-2 (**Рис. 8**).

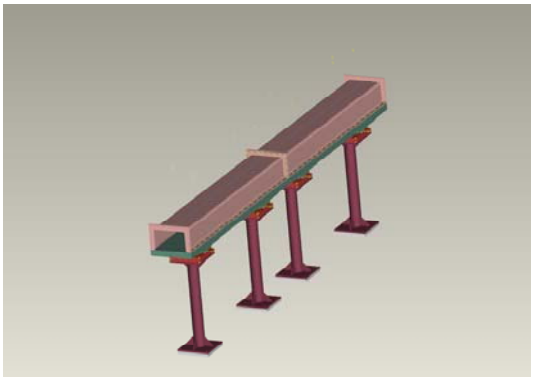

Рис. 8. Вакуумный кожух для двух зеркальных каналов.

2.7. Разработан эскизный и рабочий проект несущих опор и юстировочных столов для всех видов вакуумных кожухов нейтроноводной системы канала №7а (**Рис. 9**).

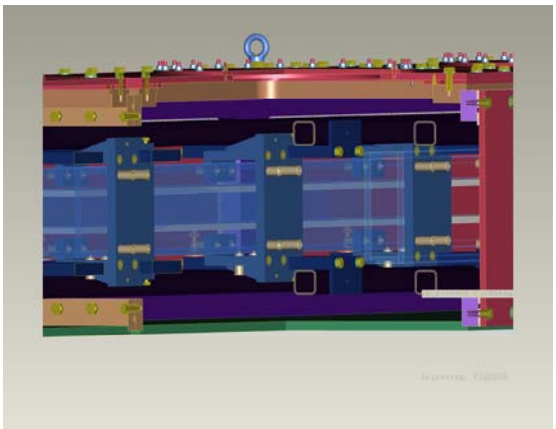

Рис. 9. Юстировочный механизм на несущем каркасе вакуумного кожуха.

2.8. Произведен демонтаж старого нейтроновода на канале №7а и частичная разборка биологической защиты (**Рис. 10**).

Рис. 10. Галерея вывода пучков 7 канала ИБР-2 до и после демонтажа

По системам управления исполнительными механизмами спектрометров выполнены следующие работы:

1. Разработаны и испытаны контроллеры SMC-32-CAN для систем управления исполнительными механизмами спектрометров на реакторе ИБР-2М:
   - в состав системы управления введены датчик углового перемещения (16 бит) и блок управления двигателями постоянного тока типа ДР-1,5РА;
   - разработана программа контроллера для доступа по линии CAN к нескольким блокам.

   Указанные блоки выполнены в промышленном стандарте CAN. Этими унифицированными блоками будут оснащаться все спектрометры ИБР-2М.
2. Сданы в эксплуатацию система управления спектрометра МОНД и система управления 15 двигателями постоянного тока спектрометра ДИСК в РНЦ «Курчатовский институт».

Разработан шахтный криостат с рефрижератором замкнутого цикла SUMITOMO RP-062B (**Рис. 11**) для проведения экспериментов по дифракции с образцами в камерах высокого давления с сапфировыми наковальнями на пучках тепловых нейтронов в диапазоне температур 6-300 К. Криостат содержит вертикальный канал для ввода камер высокого давления в зону термостатирования, причем замена камеры может производиться без размораживания криостата. Документация в настоящее время проходит технологическую обработку в ОП ОИЯИ.

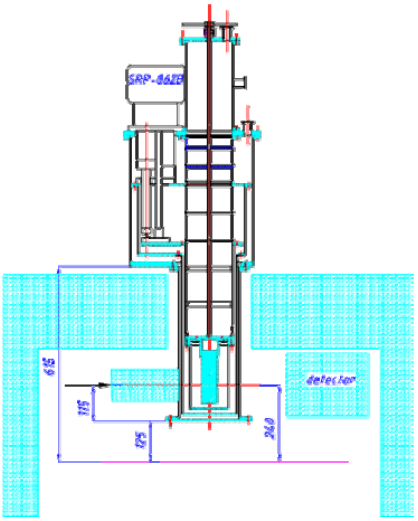

Рис. 11 Шахтный криостат.

На базе оборудования, полученного по долевому взносу Румынии, создан и запущен в работу вакуумный стенд с гелиевым течеискателем L200 (Leybold), предназначенный для испытаний различных вакуумных и криогенных систем спектрометров ИБР-2. Заключен также контракт с фирмой CRYOMECH (США) на поставку криорефрижератора PT 403, являющегося основным элементом криогенного стенда.

3. Развитие систем сбора данных и вычислительной инфраструктуры, разработка программного обеспечения

Завершена разработка блока сбора данных с многосчетчиковых систем (до 64 каналов в одном блоке). Блок подготовлен к испытаниям на нейтронном источнике в ПИЯФ (Гатчина). Изготовлены также блоки DAQ системы для сбора и накопления данных с 1D и 2D ПЧД. Тестирование этих блоков будет проводиться в начале 2008 г. на реакторе BER-II (ИГМ, Берлин). Ожидаемая скорость счета составит не менее no 10^6 событий/с.

Начаты работы по созданию кабельной инфраструктуры сетевого сегмента экспериментальных залов ИБР-2 (Gigabit Ethernet). Заключен контракт с компанией «Контакт» на поставку комплектующих изделий, выполнены работы по прокладке и сварке волоконно-оптического кабеля.

В работах по программному обеспечению основное внимание уделялось развитию комплекса Sonix+ для работы на реакторе ИБР-2М и практической проверке подготовленных программ на реакторах сторонних организаций ФЭИ, (Обнинск) и РЦКИ (Москва). В частности,

— разработаны модули для систем управления исполнительными механизмами с CAN интерфейсом;

— усовершенствована программа визуализации спектров для работы в on-line и off-line режимах;

— начата разработка программного обеспечения новых электронных блоков DAQ, подключаемых к компьютеру через USB- интерфейс;

— подготовлена к проверке первая версия системы удаленного слежения и управления ходом эксперимента на спектрометрах Web Sonix.

Система Web Sonix предназначена для удаленного наблюдения и контроля экспериментов на спектрометрах ИБР-2М. Она должна удовлетворять требованиям всех групп пользователей. Архитектура системы не зависит от специфических особенностей спектрометров и предоставляет пользователю:

- детальную информацию о параметрах текущего измерения;
- содержимое журнала регистрации измерений (текущее и предыдущее);
- визуализацию текущих спектров от всех детекторов.

Контроль предполагает, что сервис обеспечивается web сайтом и включает средства для чтения, редактирования и манипуляции скриптами.

В сети ЛНФ выделен специальный сервер для системы Web Sonix . Система является клиентом Apache HTTP server 2.2.4 (**Рис. 11**). Для генерации динамических web страниц выбран язык PHP 5.0. Командный канал связи сервера с управляющим компьютером спектрометра реализован по модели клиент-сервер с обменом на уровне сокетов. Для передачи файлов используется протокол FTP (SFTP).

Предварительное тестирование системы Web Sonix с ограниченным набором функций было выполнено в декабре 2006 г. на спектрометрах РЕМУР, НЕРА-ПР и ФДВР

в экспериментах с использованием позиционно-чувствительных детекторов. Тесты показали, что система наблюдения пригодна к эксплуатации и не влияет на надежность систем сбора данных. В настоящее время тестируется полная версия Web Sonix.

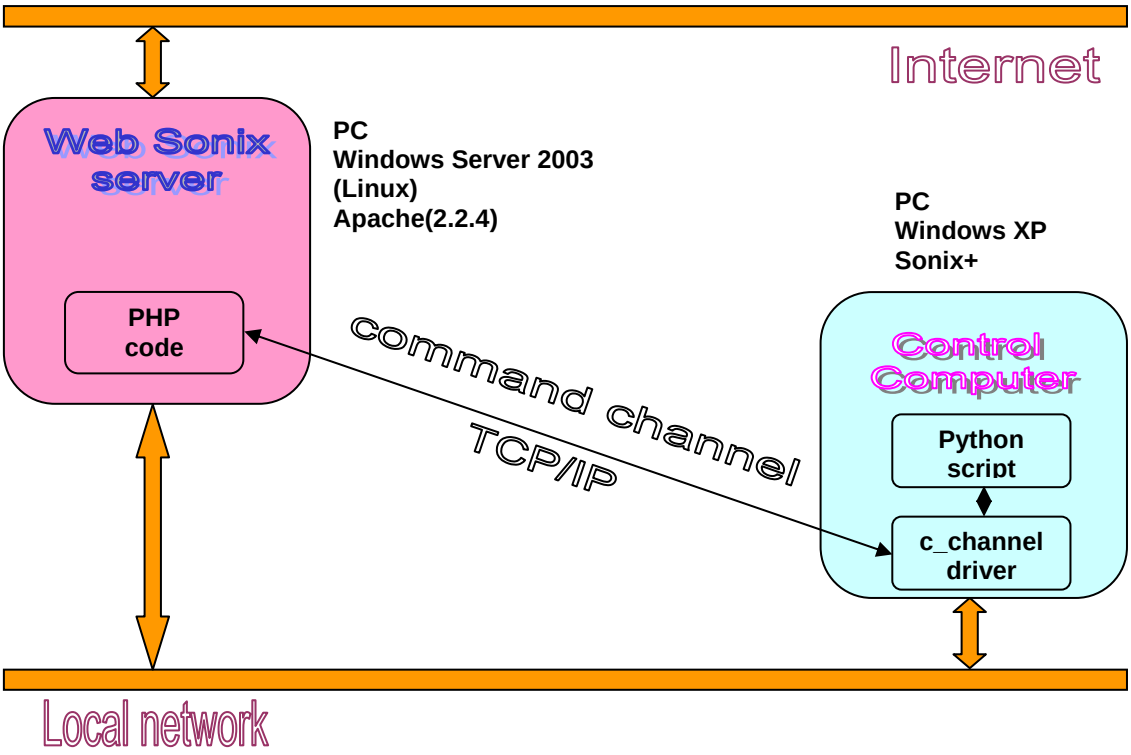

Рис. 11.Схема командного канала.

Совместно с ИГМ, Берлин выполнен большой объем работ по интеграции в программный комплекс CARESS и проверке долговременной стабильности разработанного в ЛНФ программного обеспечения системы сбора данных с двукоординатных ПЧД. Эти работы успешно завершены на нескольких спектрометрах реактора BER-II и синхротронного источника ИГМ.

В 2007 году продолжалось развитие программного комплекса VITESS для моделирования новых элементов спектрометров и методов нейтронного рассеяния. Как и ранее был использован метод Монте-Карло (движение частиц в трехмерном пространстве). Разработка модулей велась на языке программирования C/C++, а для графического интерфейса использовался интерактивный язык TCL/TK.

Были созданы, протестированы и внедрены следующие модули для пакета VITESS (**Рис. 12**):

– Модуль для системы рефракционных линз с комплектом вспомогательных программ (поиск фокуса и т.п.). В базовый модуль встроена визуализация (**Рис. 13**).

– Модуль для моделирования прецессии спина нейтрона в импульсных магнитных полях “треугольник”, “пила”.

– Модуль для анализа поляризации во временных интервалах (TIME GATE) для моделирования спектрометра спин-эхо.

– Модуль для моделирования многоканальных пропускающих поляризаторов (в стадии тестирования и внедрения). В модуль встроена визуализация.

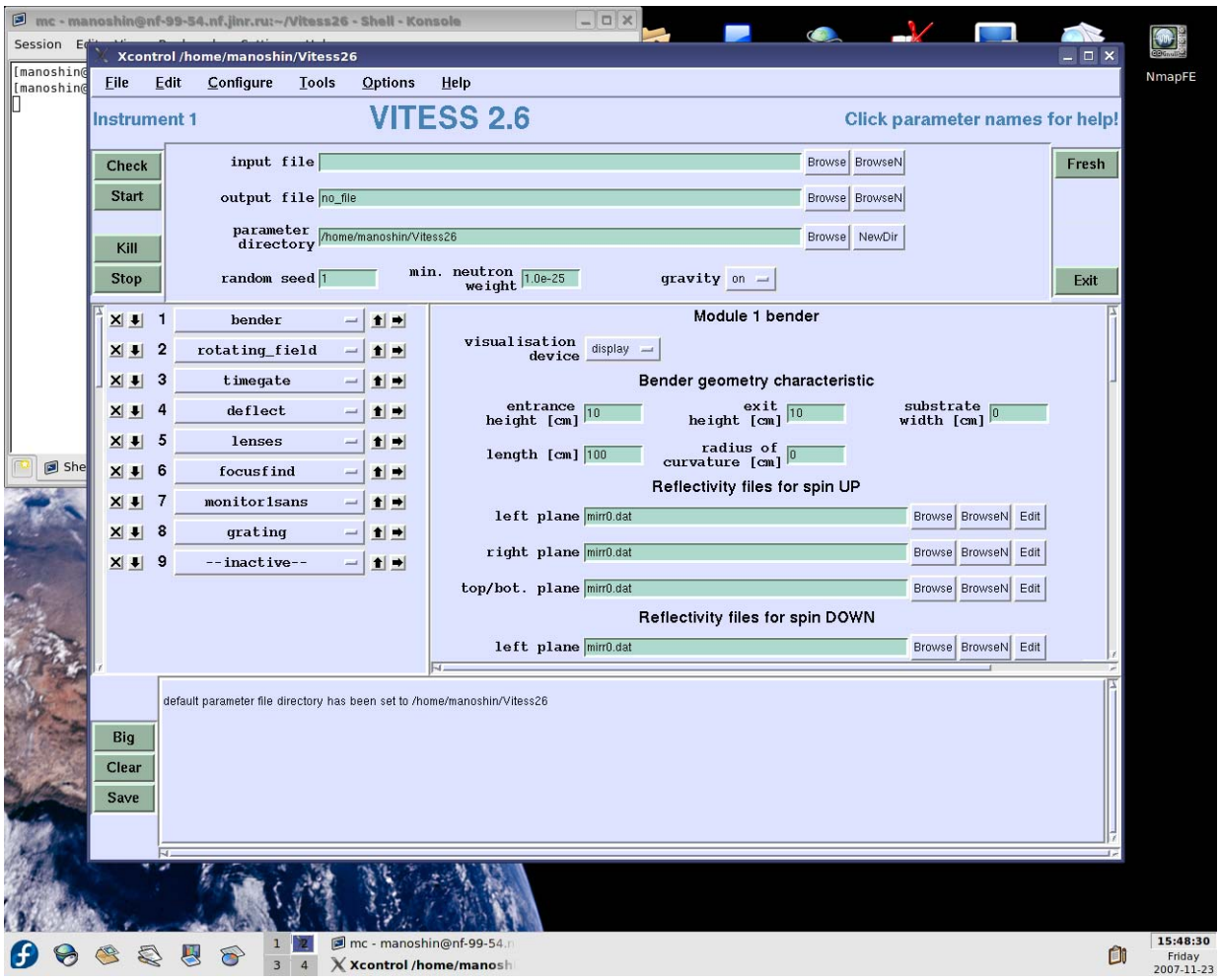

Рис. 12. Графическая оболочка VITESS с новыми модулями.

Были выполнены предварительные расчеты и промоделированы следующие установки:

1) Спектрометр спин-эхо с временно-зависимыми магнитными полями (“треугольник”, “пила”.)
2) Системы фокусирующих рефракционных линз и их применение в простейшей малоугловой установке для улучшения качества данных
3) Пропускающие поляризаторы нейтронного пучка (N, V, Double V вида).

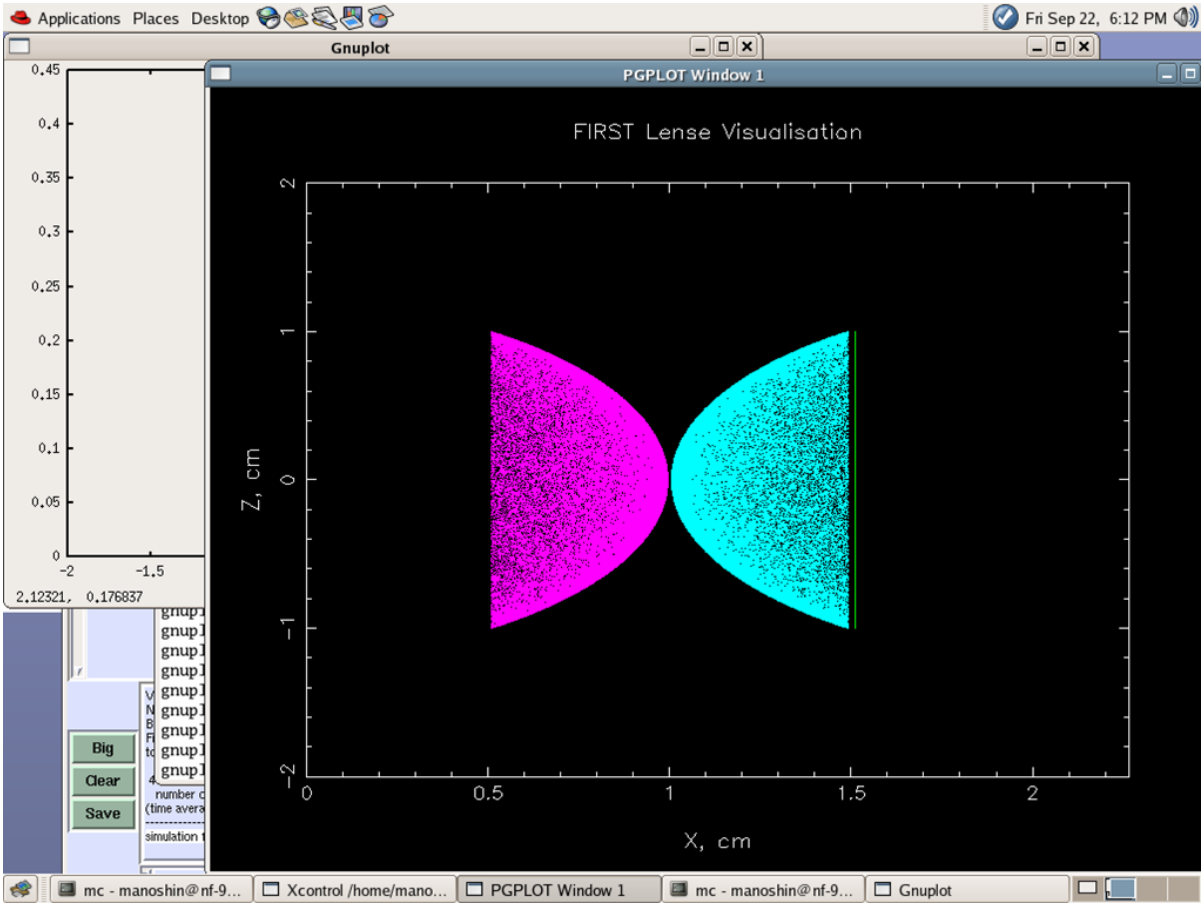

Рис. 13. Пример визуализации моделирования нейтронной вогнутой рефракционной линзы.

4. EXPERIMENTAL REPORTS

4.1. CONDENSED MATTER PHYSICS

Diffraction

Temperature and Pressure Driven Spin State Transitions in $LaCoO_3$
D. P. Kozlenko, N. O. Golosova, Z. Jirák, L. S. Dubrovinsky, B. N. Savenko, M. G. Tucker, Y. Le Godec and V. P. Glazkov

The Pyridinium Perrhenate Structure Study at High Pressure up to 15 GPa
S.E.Kichanov, D.P.Kozlenko, J.Wasicki, W.Nawrocik, P.Czarnecki, B.N. Savenko, L.S.Dubrovinsky

Neutron Texture Measurements and 3D Velocity Calculations on Strongly Foliated Biotite Gneisses from the Outokumpu Deep Drill Hole
T. I. Ivankina , H.M. Kern , A. N. Nikitin

Small-Angle Neutron Scattering

SANS Study of Magnetic Fluids Stabilized by Short Chain Length Mono-Carboxylic Acids
Mikhail V. Avdeev, Doina Bica, Ladislau Vékás, Maria Balasoiu, Victor L. Aksenov, László Rosta, Vasyl M. Garamus

SANS Contrast Variation in Ferrofluids as Polydisperse Multicomponent Superparamagnetic systems
Mikhail V. Avdeev, Artem V. Feoktystov, Vasyl M. Garamus

Behavior of Fatty Acids in d-Benzene by Small-Angle Neutron Scattering
V.I. Petrenko, M.V. Avdeev, L.A. Bulavin, V.L. Aksenov, L. Almásy, L. Rosta, V. Garamus

Partial Volume of Fatty Acids in Benzene by Molecular Dynamic Simulations
I.A.Bodnarchuk, V.I.Petrenko, M.V.Avdeev, Kh.T.Kholmurodov

Organization of Fullerene Clusters in the System C_{60}/N-Metyl-2-Pyrrolidone
O.A. Kyzyma, M.V. Avdeev, V.L. Aksenov, L.A. Bulavin, S.V. Snegir

On the inner structure of the polycarbosilane dendrimers
A.V. Rogachev, A.Yu. Chern, A.N. Ozerin, A.M. Muzafarov, E.A.Tatarinova, A.Kh. Islamov, V.I. Gordeliy, A.I. Kuklin

Measurements with New Type of Position Sensitive Detector in Backscattering and Small-Angle Scattering Arrangements
A.I.Kuklin, S.A.Kutuzov, A.Gabriel, G.Eckold, P.K.Utrobin, A.A.Smirnov, A.Ivankov, A.Kh.Islamov, Yu.S.Kovalev , A.Feoktistov, A.V.Rogachev, A.S.Kirilov, V.I.Gordeliy

Investigation of Intermembrane Interaction in Presence of Dimethylsulfoxide via SANS
J. E. Gorshkova and V. I. Gordeliy

Reflectometry, polarized neutrons

Coexistence of Superconductivity and Ferromagnetism in Nanostructure
Nb(500 Å)/Fe(39 Å)/[Si(34 Å)/Mo(34Å)]40/Si.
V.L. Aksenov, Yu.V. Nikitenko, Yu.N. Khaidukov, S.N. Vdovichev, N.N. Salashchenko, A.A. Fraerman, E.Kh. Mukhamedzhanov

Off-Specular Scattering in Magnetic Neutron Waveguides

S.V. Kozhevnikov, F. Ott, E. Kentzinger, A. Paul

Neutron Spin Turners with a Rotating Magnetic Field: First Experiments
V.I. Bodnarchuk, W.H. Kraan, M.T. Rekveldt and A.Ioffe

Inelastic Neutron Scattering

Dispersion Relation for Liquid Lithium Study by Means of Inelastic Neutron Scattering
N.M Blagoveshchenskii, A.G. Novikov, M.A.Pashnev,V.V. Savostin

4.2. NEUTRON NUCLEAR PHYSICS

Fundamental Research

New optical effect was firstly observed with UCNs
A.I.Frank, G.V.Kulin, D.V.Kustov, P.Geltenbort , M. Jentschel,. V.G.Nosov, A.N.Strepetov

Differential and Angle-Integrated Cross Section Measurement for the ^{64}Zn(n, α)^{61}Ni Reaction at 2.54, 4.00 and 5.50 MeV
Yu. M. Gledenov, M. V. Sedysheva, G. Khuukhenkhuu, P. J. Szalansk,i Jiaguo Zhang, Rongtai Cao, Li-an Guo, Jinxiang Chen, Jianyong Wang, Guohui Zhang

Temperature Dependence of Neutron Scattering He-4 Gas
V.Ignatovich

Character of Wear Process in Nitrogen-Implanted AISI 316L Stainless Steel
P.Budzynski, K.Polanski, A.P.Kobzev

Storage of Very Cold Neutrons in Bottles
E.V.Lychagin, A.Yu.Muzychka, G.V.Nekhaev, V.V.Nesvizhevsky, A.V.Strelkov

Applied Research

NAA and ESR for Biotechnology of Cr(VI) Detoxification
N. Tsibakhashvili, T. Kalabegishvili, L. Mosulishvili, E. Kirkesali, S. Kerkenjia, I. Murusidze, H.-Y. Holman, M.V. Frontasyeva, S.F. Gundorina

Epithermal NAA for Marine Geoecology
C. Cristache, O. Culicov, M. Toma, M.V. Frontasyeva, S.S. Pavlov, O.G. Duliu, G. Oaie

Observation of Pulsed Neutron Ramsey Resonance
Y. Masuda, V. Skoy, T. Ino, S.C. Jeong and Y. Watanabe

Ramsey Resonance for a Pulsed Beam
Yasuhiro Masuda, Vadim Skoy, Takashi Ino, Sun-Chang Jeong and Yutaka Watanabe

TEMPERATURE AND PRESSURE DRIVEN SPIN STATE TRANSITIONS IN $LaCoO_3$

D. P. Kozlenko[1], N. O. Golosova[1], Z. Jirák[2], L. S. Dubrovinsky[3], B. N. Savenko[1], M. G. Tucker[4], Y. Le Godec[5] and V. P. Glazkov[6]

[1] *Frank Laboratory of Neutron Physics, Joint Institute for Nuclear Research, 141980 Dubna Moscow Reg., Russia*
[2] *Institute of Physics, Cukrovarnická 10, 162 53 Prague 6, Czech Republic*
[3] *Bayerisches Geoinstitut, Universität Bayreuth, Bayreuth, D-95440, Germany*
[4] *ISIS Facility, Rutherford Appleton Laboratory, Chilton, Didcot, Oxon OX11 0QX, United Kingdom*
[5] *Physique des Milieux Condensés, Université P&M Curie, B77, 4 Place Jussieu, 75252 Paris, France*
[6] *Russian Research Center "Kurchatov Institute", 123182 Moscow, Russia*

The magnetic, transport and electronic properties of $LaCoO_3$ have been extensively studied with a growing interest from 1950s until now. At ambient pressure this compound exhibits unique behavior - it is a nonmagnetic semiconductor at low temperature and undergoes a phase transition to a paramagnetic insulating state at T = 100 K and paramagnetic metallic state at T = 500 K [1, 2]. These transitions are usually considered to be related to a change of the Co^{3+} spin state, from low spin state LS (t^6_{2g}, S=0) to intermediate state IS ($t^5_{2g}e^1_g$, S = 1) and from IS to high state HS ($t^4_{2g}e^2_g$, S=2), respectively. Both transitions are associated with anomalies in the magnetic susceptibility and thermal volume expansion.

The stability of different spin states of $LaCoO_3$ depend substantially on the geometry of CoO_6 octahedra which determines the crystal field splitting of t_{2g} and e_g energy levels and the strength of the hybridization between 3d orbitals of cobalt and 2p orbitals of oxygen [3, 4]. Lattice contraction under high pressure is thus very influential factor in the Co^{3+} spin-state equilibria. Due to strong correlation between spin state, magnetic and transport properties of this and related compounds, the knowledge of relationship between spin-state equilibria and crystal structure features (unit cell volume, interatomic distances and angles), which can be derived from high pressure investigations, is very essential for understanding the nature of physical phenomena observed in these compounds and constructing of theoretical models and ab-initio calculations.

In order to investigate the spin-state transitions in $LaCoO_3$ in 0-5 GPa pressure and 10-900 K temperature ranges, neutron diffraction experiments were performed at DN-12 spectrometer (IBR-2 pulsed reactor, FLNP JINR, Russia) and Pearl/HiPr diffractometer (ISIS spallation pulsed neutron source, RAL, UK).

The anomalous contribution to thermal volume expansion of $LaCoO_3$ at selected pressures is shown in fig. 1. It was analysed using three-level model with ground LS state and thermally activated IS and HS states [1,2].

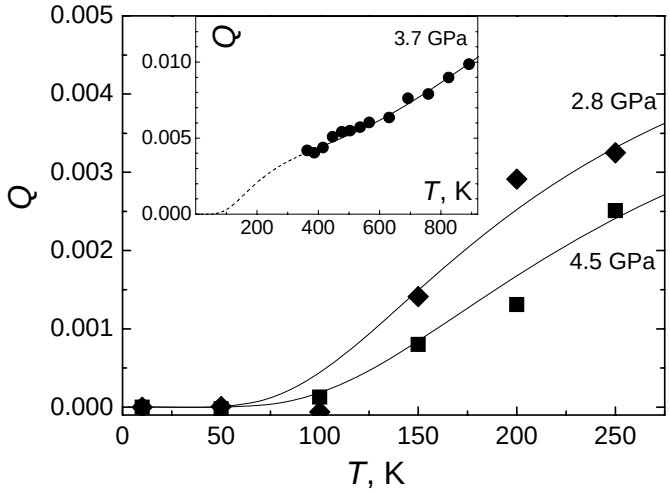

Fig. 1. The anomalous part Q of the thermal volume expansion for $LaCoO_3$ at different pressures obtained in the low temperature 16 – 250 K (DN-12 data) and high temperature 300 – 900 K (Pearl/HiPr data, inset) ranges. The solid lines represent the LS-IS-HS model fits. The dashed line in the inset is the expected low temperature behavior of Q at 3.7 GPa.

The obtained pressure and temperature dependences of LS-IS (E_1) and LS-HS (E_2) energy splittings and populations of LS, IS and HS states are shown in fig. 2.

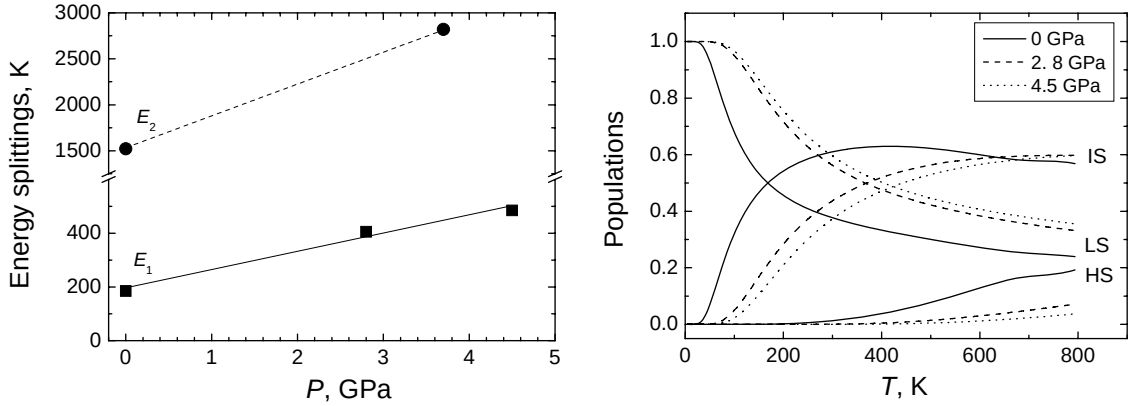

Fig. 2. Left: LS-IS (E_1) and LS-HS (E_2) energy splittings as functions of pressure. Right: Populations of LS, IS and HS states at different pressures.

Both LS-IS and LS-HS energy splittings increase substantially under high pressure with a larger $d\ln E_1/dP$ = 0.37 GPa^{-1} value in comparison with $d\ln E_2/dP$ = 0.23 GPa^{-1}. With increasing pressure the IS and HS states are depopulated in favour of the LS ground state. In the low temperatures region T < 250 K, where population of HS state is negligible, the population of the LS state progressively increases and that for the IS state decreases.

References:

[1] P.G.Radaelli and S.-W.Cheong, Phys. Rev. B 66, 094408 (2002).
[2] K.Asai, A.Yoneda, O.Yokokura, et al., J. Phys. Soc. Jpn. 67, 290 (1998).
[3] P.M.Raccah and J.B.Goodenough, Phys. Rev. 155, 932 (1967).
[4] K.Asai, O.Yokokura, M.Suzuku, et al., J. Phys. Soc. Jpn. 66, 967 (1997).

THE PYRIDINIUM PERRHENATE STRUCTURE STUDY AT HIGH PRESSURE UP TO 15 GPa.

S.E.Kichanov[a], D.P.Kozlenko[a], J.Wasicki[b], W.Nawrocik[b], P.Czarnecki[b], B.N. Savenko[a], L.S.Dubrovinsky [c]

[a]*Frank Laboratory of Neutron Physics, JINR, 141980 Dubna, Moscow Region, Russia*
[b]*Faculty of Physics, A.Mickiewicz University, Umultowska 85, 61-614 Poznań, Poland*
[c] *Bayerisches Geoinstitute, University Bayreuth, D-95440 Bayreuth, Germany*

Pyridinium salts belong to the group of molecular-ionic crystals with hydrogen bonds, which exhibit a reach variety of interesting phenomena such as structural phase transitions, ferroelectricity and dynamical orientational disorder of the pyridine cations [1-4]. Two latter compounds are of special interest because their Curie temperatures are above room temperature. The para-ferroelectric transition is accompanied by the structural phase transformation, resulting in the change of the disorder degree of pyridinium and perrhenate ions [5].

In the recent study of the *P-T* phase diagram of deuterated pyridinium perrhenate $(d_5PyH)ReO_4$ ($C_5D_5NHReO_4$) at high pressure up to 3.5 GPa and temperature by means of powder X-ray diffraction and neutron diffraction tree phases were observed [6]. At ambient conditions deuterated pyridinium perrhenate has orthorhombic structure of the $Cmc2_1$ symmetry (ferroelectric phase II). At T < 250 K a phase transition to the orthorhombic phase of the Pbca symmetry (paraelectric phase III) was observed. At P > 0.7 GPa the phase transition to orthorhombic phase with the Cmcm symmetry (paraelectric phase I) was observed at ambient temperature. At P = 2 GPa the phase I is stable in the temperature range 10-293 K, indicating a suppression of the ferroelectricity in $(d_5PyH)ReO_4$ by application of high pressure [6]. In order more complete investigate of structure changes of the deuterated pyridinium perrhenate $(d_5PyH)ReO_4$ at extended pressure range, we have performed X-ray diffraction measurements up to 15 GPa with a deuterated pyridinium perrhenate $(d_5PyH)ReO_4$ ($C_5D_5NHReO_4$).

X-ray powder diffraction measurements were made at high pressures up to 9.4 GPa and ambient temperature by means high pressure diffractometer at Bayerisches Geoinstitute (Bayreuth, Germany) [7]. The some parts of X-ray diffraction experiments at high pressures up to 15 GPa and ambient temperature with a diamond anvil cell were carried out using the powder diffractometer at experimental station “Mediana” [8] (KCSRNT, RRC “Kurchatov Institute”, Moscow, Russia).

At ambient conditions the orthorhombic phase II with space group $Cmc2_1$ was evidenced. At pressures appearance of the orthorhombic phase I with space group Cmcm and this result is good compared with Ref. [6] data. At pressure P>5 GPa the significantly changes in diffraction patterns were observed. This changes were correspond to the appearance new high pressure phase of the $(d_5PyH)ReO_4$. The peak indexing of diffraction patterns were carried out and parameters of new phase were obtained. The new phase is monoclinic with space group $P2_1$ and its parameters are: a=7.693(5) Å, b=13.265(7) Å, c=11.915(5) Å and β=94.9(5)^0.

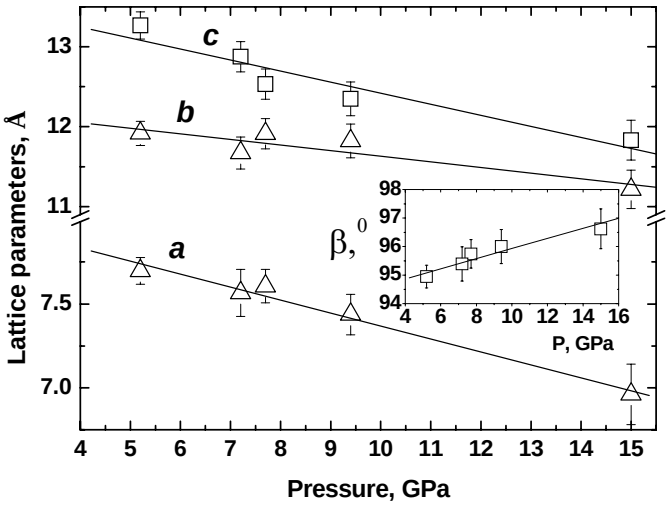

Figure 1. The pressure dependence of lattice parameters of the pyridinium perrhenate (for high pressure phase). The solid lines represent the linear fit of the experimental data.

The dependence of the lattice parameters of high pressure phase are shown in figure 1. The compressibility data were fitted by the third-order Birch–Murnaghan equation of state [9]:

$$P = 3/2B_0(x^{-7/3} - x^{-5/3})[1 + 3/4(B' - 4)(x^{-2/3} - 1)], \quad (1)$$

where $x = V/V_0$ is the relative volume change, V_0 is the unit cell volume at $P = 0$, and B_0 and B' are the bulk modulus $B_0 = -V\,(dP/dV)_T$ and its pressure derivative $B' = (dB_0/dP)_T$. The calculated values for high pressure phase are $B_0 = 21(8)$ GPa, $B' = 4(1)$.

[1] Czarnecki P, Nawrocik W, Pajak Z and Wasicki J 1994 *Phys. Rev.* B **49** 1511

[2] Czarnecki P, Nawrocik W, Pajak Z and Wasicki J 1994 *J. Phys.: Condensed Matter* **6** 4955

[3] Wasicki J, Czarnecki P, Pajak Z, Nawrocik W and Szczepanski W 1997 *J. Chem. Phys.* **107** 576

[4] Pajak Z, Czarnecki P, Wasicki J and Nawrocik W 1996 *J. Chem. Phys.* **109** 6420

[5] Czarnecki P, Beskrovny A I, Bobrovicz-Sarga L, Lewicki S and Wasicki J, 2005 *J. Phys.: Condensed Matter* **17** S3131

[6] S.E. Kichanov, D.P. Kozlenko, J. Wasicki, W. Nawrocik, P. Czarnecki, B.N. Savenko, V.P. Glazkov and C. Lathe, Journal of Molecular Structure, accepted for publication (2007).

[7] L. Dubrovinsky, N. Dubrovinskaia, I. Kantor, F. Nestola, D. Gatta, International Journal of High Pressure Research, 26, 137-143

[8] V.L.Aksenov, V.P.Glazkov, S.E.Kichanov, D.K.Pogoreliy, K.M. Podurets, V.A.Somenkov, B.N. Savenko, NIMA, 575, p. 266-268 (2007).

[9] F.J.Birch, J. Geophys. Res. 91, 4949 (1986).

NEUTRON TEXTURE MEASUREMENTS AND 3D VELOCITY CALCULATIONS ON STRONGLY FOLIATED BIOTITE GNEISSES FROM THE OUTOKUMPU DEEP DRILL HOLE

T. I. Ivankina [1], H.M. Kern [2], A. N. Nikitin [1]

[1] Joint Institute for Nuclear Research, Frank Laboratory of Neutron Physics, 141980, Dubna, Moscow Region, Russia
[2] Institut für Geowissenschaften, Universität Kiel, 24098 Kiel, Germany

Objectives

To characterize fabric-related anisotropy (lattice preferred orientation of minerals, LPO) neutron diffraction measurements were carried out on selected biotite gneisses of the Outokumpu deep drill hole. Measurements were done at the texture diffractometer SKAT at Dubna, Russia. Using the orientation distribution function (ODF) as a parameter characterizing the LPO of the constituent minerals, the seismic properties (3D velocity distribution of P- and S-waves) of bulk samples were calculated from the corresponding properties of major minerals.

Results and discussion

Eight core samples collected from the Upper and Lower gneiss series (depth range: 578 – 1093 m and 1609 – 2238 m) were used for the measurements. The strongly foliated biotite gneisses are mainly composed of biotite, muscovite, quartz and plagioclase with varying volume fractions.

Due to the high resolution of the SKAT neutron texture diffractometer at Dubna, Russia, a sufficient number of pole figures could be extracted from the diffraction spectra. In order to describe the complete mineral texture, we calculated the ODF and pole figures of the significant crystallographic planes.

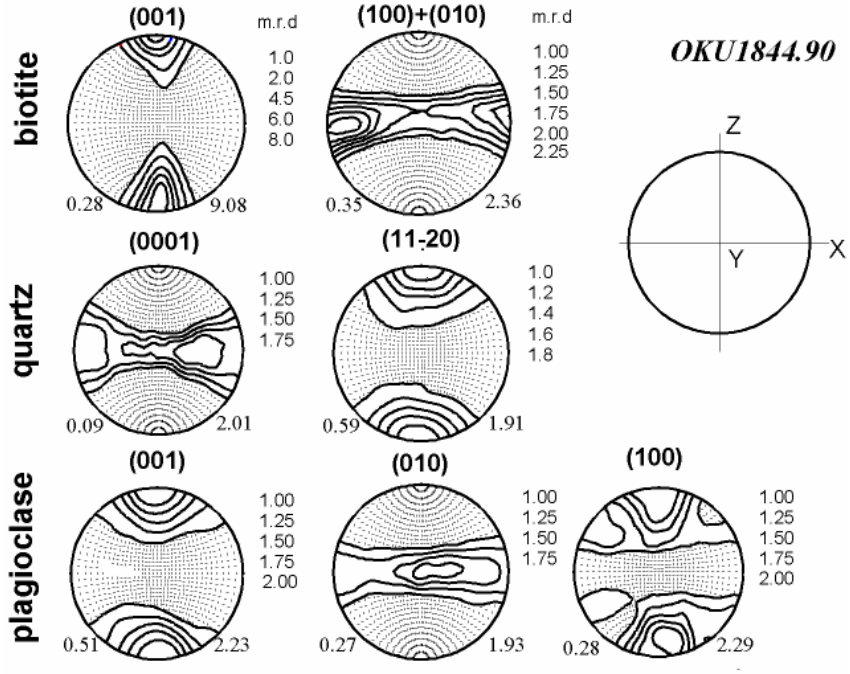

Fig.1. Complete quantitative texture analysis of the biotite gneiss sample OKU 1844.90. Principal pole figures of biotite, quartz and plagioclase (equal area projection, upper hemisphere). Counters in multiples of a random distribution. Grid points display intensities smaller than one time random. Minimum and maximum intensities are given at the bottom of the plots. XY-plane indicates foliation and X lineation.

As an example, the calculated pole figures of the sample OKU1844.90 (number indicates the depth of sample recovery in meters) are shown in Figure 1. Pole figures of biotite, quartz and plagioclase are recalculated based on the ODF's of the corresponding mineral textures. The biotite (001) pole figure is unimodal, the degree of preferred orientation is large; the intensity maximum parallels the foliation normal. The poles to the (100)+(010)-planes are concentrated on a great circle

within the foliation plane. A similar type of biotite preferred orientation is observed in all investigated samples. The textures of quartz and plagioclase are also well-pronounced, but are much weaker than those of biotite and muscovite. In general, the gneiss samples exhibit roughly the same quartz texture (LPO), whereas the LPO´s of plagioclase are different. It is worthy to note, that the pole figures of the phyllosilicates are in general symmetrically disposed to foliation and lineation.

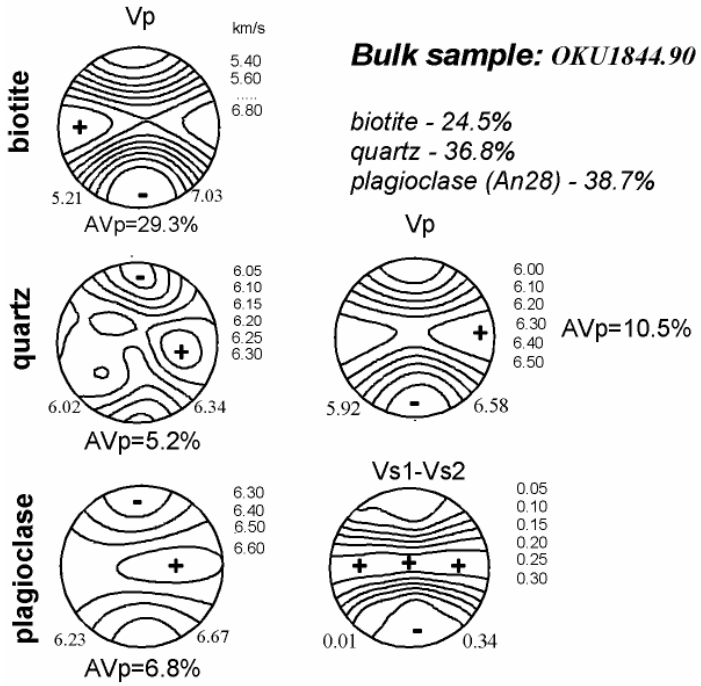

Fig.2. Texture-derived P-wave velocity distribution for the mineral aggregates and calculated velocity surfaces of Vp and Vs1-Vs2 for the whole rock sample OKU1844.90.

Figure 2 presents the LPO-based calculation of Vp and Vs velocity surfaces of biotite, quartz and plagioclase (100 vol.-%) and the resulting bulk Vp and Vs1 – Vs2 (shear wave splitting) for sample OKU 1844.90, according to the volume fractions of the constituent minerals. It is clear from Fig. 1 that the seismic anisotropy of the biotite gneiss (Fig.2) is dominated by the biotite preferred orientation. The directions of minimum and maximum Vp as well as the directions of minimum and maximum shear wave splitting (Vs1-Vs2) of the bulk rock correspond to the slow (001) and fast (100) + (010) directions of the biotite single crystal.

Conclusions

3D velocity calculations based on neutron diffraction texture measurements provide an important means to interpret the nature of the intrinsic (matrix) anisotropy and to assess the contribution of the LPO-related anisotropy to the bulk anisotropy measured on the cores sampled by the Outokumpu deep drill hole. The calculated bulk velocity anisotropy (average value of AVp ~ 10%) is generally smaller than the experimentally determined anisotropy (up to about 20 %). Obviously, shape preferred orientation (SPO) of the major minerals as well as oriented microcracks and grain boundary effects contribute to the bulk elastic properties of the Outokumpu core samples, in addition to the crystallographic orientation fabric.

SANS study of magnetic fluids stabilized by short chain length mono-carboxylic acids

Mikhail V. Avdeev[1], Doina Bica[2], Ladislau Vékás[2], Maria Balasoiu[3], Victor L. Aksenov[4,1], László Rosta[5], Vasyl M. Garamus[6]

[1]*Frank Laboratory of Neutron Physics, Joint Institute for Nuclear Research, Dubna, Russia*

[2]*Centre of Fundamental and Advanced Technical Research, Romanian Academy, Timisoara Division, Timisoara, Romania*

[3]*Horia Hulubei National Institute of Physics and Nuclear Engineering, Bucharest-Magurele, Romania*

[4]*Russian Research Center "Kurchatov Institute", Moscow, Russia*

[5]*Research Institute for Solid State Physics and Optics, Hungarian Academy of Sciences, Budapest, Hungary*

[6]*GKSS Research Centre, Geesthacht, Germany*

New tendencies in biomedical applications [1] of magnetic nanofluids—fine dispersions of magnetic materials in liquids—stimulate a search for effective and biocompatible surfactants used to stabilize these systems. In this paper the possibility to use short chain length mono-carboxylic acids (lauric, $C_{12}H_{24}O_2$, and myristic, $C_{14}H_{28}O_2$, saturated acids) for stabilizing magnetic fluids with organic carriers is reported. Such short chain length surfactants were experimented especially for water based magnetic fluids [2]. As a first step, these surfactants were probed to coat magnetite nanoparticles in non-polar organic liquids by the procedure described in [3, 4]. It is well known that the most effective stabilizing agent in such type of magnetic fluids is oleic acid, $C_{18}H_{34}O_2$, unsaturated carboxylic acid with a double bond kink in the middle of its tale. The kink plays a crucial role in the organization of the surfactant on the surface of magnetic particles, which results in proper steric repulsion [5]. This is confirmed by the fact that the saturated stearic acid of the same tail length, $C_{18}H_{34}O_2$, but without this kink, is a bad stabilizer. Nevertheless, as we show [6], shorter saturated mono-carboxylic acids provide high colloidal stability of organic magnetic fluids in respect both to the time factor and external magnetic field. The only significant difference compared to the classical fluids concerns the size distribution of stabilized magnetite particles, which is analyzed carefully including small-angle scattering of non-polarized and polarized neutrons.

The studied samples were synthesized at the Laboratory of Magnetic Fluids of the Center of Fundamental and Advanced Technical Research (LMF CFATR), Timisoara Branch of Romanian Academy of Sciences. Magnetite, Fe_3O_4, obtained by co-precipitation in aqueous solution of Fe^{2+} and Fe^{3+} ions in the presence of NH_4OH (temperature ~80^{o}C) was dispersed in light hydrocarbon (petroleum), using lauric (LA) or myristic (MA) acid as chemisorbed surfactant. Repeated flocculation with acetone and redispersion in petroleum were performed to remove free surfactant and to concentrate samples. Finally, magnetite nanoparticles with single layer surface coating were dispersed in different organic media, particularly, cyclohexane. It can be seen during the procedure that the preparation of magnetic fluids with short chain surfactants are characterized by a larger amount of non-dispersed material in comparison with the case of oleic acid (OA) and requires more cycles to achieve the same concentration. Nevertheless, in principle no difficulties to concentrate samples up to magnetic volume fraction φ_m = 20 % were found. The fluids show excellent stability in time (at least two years), as well as under effect of magnetic field (up to 2.5 T). The same procedure for stearic acid (SA) resulted in significantly less stable fluid.

Two-dimensional small-angle scattering patterns of scattering of polarized neutrons are shown in Fig.1. Changes for different neutron polarization states under effect of saturating magnetic field are

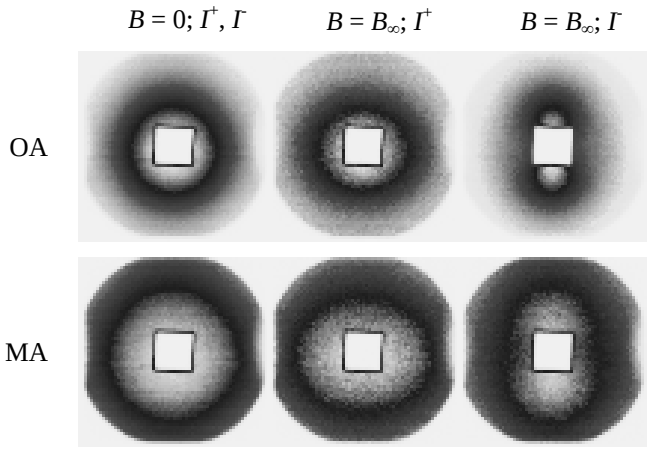

Fig.1. 2D experimental SANS patterns (SANS-1, GKSS) for two neutron polarizations in the case of magnetic fluids (φ_m = 2.8 %) based on d-cyclohexane and stabilized by oleic and myristic acids. Detector area is 55 × 55 cm^2. Sample-detector distance is 4.5 m. Wavelength of incident neutrons is 0.81 nm. White rectangle spot in the center of images is a shadow of the beam stop. Small side spots along the left and right edges are the shadows from the units of the magnetic system at the instrument.

demonstrated for the OA and MA ferrofluids based on d-cyclohexane. In the absence of the field there is no orientation of magnetic moments in the systems, so the scattering is isotropic over the φ-angle on the detector and both neutron polarizations result in similar pictures. Under the saturation field $I^+(q, \varphi)$ and $I^-(q, \varphi)$ are anisotropic. As one can see, the scattering differs depending on the used surfactants. It is more evident in Fig.2 where the $\langle F_N^2(q)\rangle_R$ function as a result of the separation of nuclear and magnetic scattering components is presented. The nuclear scattering curve for the OA fluid fits well (Fig.2) the model of non-interacting polydisperse core-shell spheres with the log-normal particle size distribution function of magnetite:

$$D_N(R) = (1/(2\pi)^{1/2}SR)\exp[-\ln^2(R/R_0)/(2S^2)], \quad (1)$$

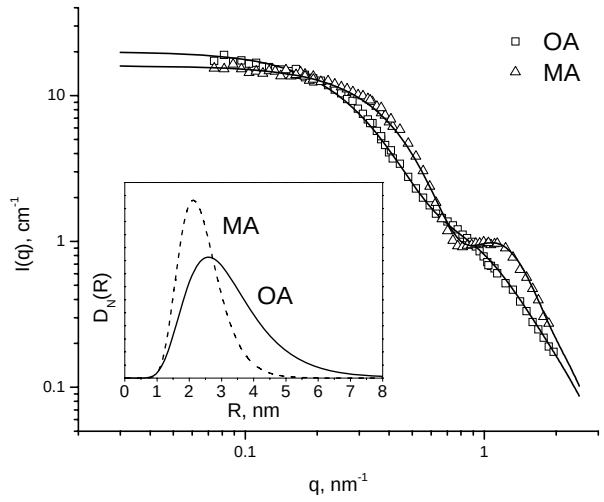

Fig.2. 1D curves for the nuclear scattering contribution $\langle F_N^2(q)\rangle_R$ (points) obtained as a result of treatment of 2D patterns (including those in Fig.1). Solid lines are the best fits of the model of non-interacting polydisperse core-shell spheres with log-normal distribution (1) of the magnetite core radius. Results of the fits are the following. **OA** – R_0 = 3.4 nm; S = 0.38; ($\langle R\rangle$ = 3.7 nm; σ = 1.4 nm) h = 1.38 nm; **MA** – R_0 = 2.3 nm; S = 0.28; ($\langle R\rangle$ = 2.4 nm; σ = 0.7 nm), h = 1.35 nm. The corresponding $D_N(R)$ functions are shown in the inset.

In caption to Fig.2 we give the resulting values of the varied parameters, which are the parameters of the $D_N(R)$ function (1) and the surfactant shell thickness, h. The MA fluid fits the above-mentioned core-shell model too (Fig.2). A great difference in the $D_N(R)$ function for the OA and MA samples can be seen.

The fact that MA is better stabilizer than SA can be explained by weaker van der Waals attraction between short chain length molecules. It provides higher solvation of surfactant tails and does not allow surfactants to collapse on the magnetite surface as was concluded for SA [5]. The resulting surfactant shell is closer by its properties to the OA case. Still, the effect is not the same in respect to compensation of magnetic attraction between particles, and if OA is proved to be highly efficient surfactant to stabilize nanomagnetite over the wide radius interval of 1-10 nm, MA stabilizes partially this interval dispersing in the carrier only a fraction of smaller particles. The same can be concluded about LA.

To summarize, we have shown that short chain length mono-carboxylic acids (lauric and myristic acids) can be used for the synthesis of highly stable magnetic fluids in organic non-polar media. The surfactant length is an important parameter, which determines the molecule organization on the surface of magnetic particles. In comparison with the classical surfactant oleic acid the shorter surfactants stabilize magnetite particles of smaller size and reduced polydispersity in organic media. The preparation of organic magnetic fluids is often the first stage in various techniques on synthesis of biocompatible magnetic carriers [1]. We believe that the given results determine a significant step in the understanding of this stage and development of these techniques.

This research project has been supported by the European Commission under the 6th Framework Program through the Key Action: Strengthening the European Research Area, Research Infrastructures. Contract nr: RII3-CT-2003-505925, GKSS, Germany, as well as by the AEROSPATIAL research program of the Romanian Ministry of Education and Research, contracts OALM nr.111/2004 and contract TRAMAG nr.173/2004.

References

[1] Book of abstracts of the 6th International Conference on Clinical and Scientific Applications of Magnetic Carriers, Krems, May 17-20, 2006.
[2] L. Shen, P.E. Laibinis, T.A. Hatton, Langmuir 15 (1999) 447.
[3] D. Bica, Rom. Rep. Phys. 47 (1995) 265.
[4] L. Vékás, et al., Progr. Colloid. Polym. Sci. 117 (2001) 104.
[5] R. Tadmor, R.E. Rosensweig, J. Frey, J. Klein, Langmuir 16 (2000) 9117.
[6] M.V.Avdeev, et al. J. Mag. Mag. Mater. 311 (2007) 6-9.

SANS contrast variation in ferrofluids as polydisperse multicomponent superparamagnetic systems

Mikhail V. Avdeev[1], Artem V. Feoktystov[1,2], Vasyl M. Garamus[3]

[1]*Frank Laboratory of Neutron Physics, Joint Institute for Nuclear Research, Dubna, Russia*

[2]*Physical Faculty, Kyiv Taras Shevchenko National University, Kyiv, Ukraine*

[3]*GKSS Research Centre, Geesthacht, Germany*

The organic non-polar magnetic fluids (magnetite dispersed in benzene and stabilized by single layer of myristic or oleic acid) were studied by the SANS contrast variation at the GKSS Research Rentre (SANS-1 set-up). The new approach of basic functions for polydisperse multicompnonet and superparamagnetic systems [1] was applied. The approach is the development of the classical method [2]. It employs the fact that in comparison with systems of monodisperse and non-magnetic particles for polydisperse and magnetic particles there is a residual scattering intensity around the effective match point, which can be reliably treated. Now, the effective match point takes the form:

$$\bar{\rho}_e = < \bar{\rho} V_c^2 > / < V_c^2 >, \tag{1}$$

and the scattering intensity can be written as

$$I(q) = \tilde{I}_s(q) + \Delta\tilde{\rho}\tilde{I}_{cs}(q) + (\Delta\tilde{\rho})^2 \tilde{I}_c(q), \tag{2}$$

$$\Delta\tilde{\rho} = \bar{\rho}_e - \rho_s . \tag{3}$$

where $\Delta\tilde{\rho}$ is the modified contrast and $\tilde{I}_c(q)$, $\tilde{I}_s(q)$, $\tilde{I}_{cs}(q)$ are the modified basic functions.

The expressions for integral parameters of the scattering (intensity in zero angle, radius of gyration, Porod volume) as a function of the modified contrast are also changed. For example, the behavior of the radius of gyration as a function of the modified contrast:

$$\tilde{R}_g^2 = \left(\frac{< V_c^2 R_c^2 >}{< V_c^2 >} + \frac{A}{\Delta\tilde{\rho}} - \frac{B}{(\Delta\tilde{\rho})^2}\right) / \left(1 + \frac{D}{(\Delta\tilde{\rho})^2}\right), \tag{4}$$

where R_c is the radius of gyration related to the whole particle shape and *A*, *B*, *D* are the parameters, differs qualitatively from the classical expression:

$$R_g^2 = R_c^2 + \alpha / \Delta\rho - \beta / (\Delta\rho)^2, \tag{5}$$

with parameters α, β. Particularly, Eq.4 has limit $-B/D$ at $\Delta\tilde{\rho} \to 0$. The similar qualitative difference can be found for the Porod volume as a function of contrast.

So, the given method allows us to exclude the effect of magnetic scattering and obtain the additional information about the particles in ferrofluids. Such parameters like *A*, *B*, *D* in Eq.4 can also be used to check out particle models. The given experiment is the first step in the detailed study of possibilities and limits of the proposed approach.

For the fluid stabilized with myristic acid, the initial sample in D-benzene (CFATR, Romania) with the magnetite volume fraction of 6 % was diluted down to 0.8 % with different mixtures of D- and H-benzene with variation of D-benzene in the final solution from 10 to 100 %. Measurements were made at twelve points over this interval. The special attention was given to the vicinity of the match point estimated as ~35 % of D-benzene. The obtained scattering curves for different contrasts are presented in Fig.1*a* with the visible squared radius of gyration (as obtained from the Guinier approximation to these curves). The effective match point is determined

(a) magnetite / myristic acid / benzene

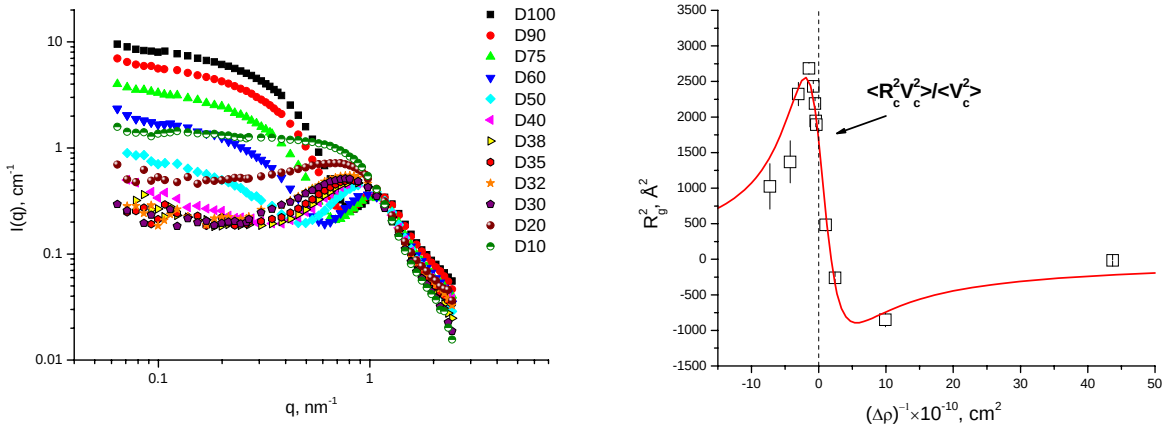

(b) magnetite / oleic acid / benzene

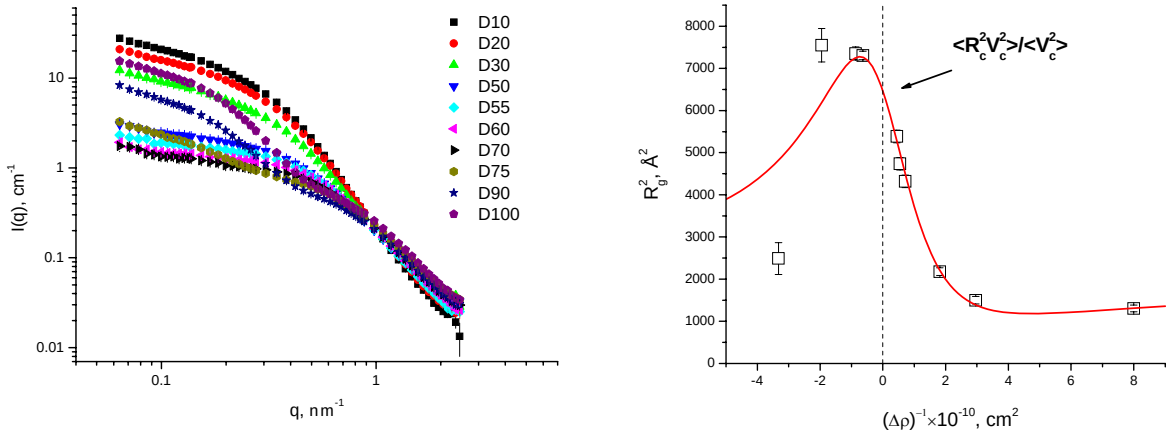

Fig.1. Contrast variation for two organic non-polar ferrofluids Graphs to the left show experimental curves at different content of deuterated component in the liquid carrier (indicated in the sample names). Graphs to the right show the behavior of the visible radius of gyration as a function of the inverse modified contrast. Lines correspond to calculations according to (4).

as 33.7 % of D-benzene, which corresponds to the scattering length density of 2.58×10^{10} cm^{-2}. The fit of Eq. (4) to the experimental data results in squared radius of gyration $R_c^2 = 1670 \pm 20$ Å^2, or $R_c = 40 \pm 3$ Å. Taking into account the quasi-spherical shape of particles one obtains for the characteristic radius of the whole particle the value of $(\langle R^2V^2\rangle/\langle V^2\rangle)^{1/2} = 52$ Å, which is consistent with the previous results obtained for this type of magnetic fluids with the use of polarized neutrons [3].

For the other fluid stabilized with oleic acid, the initial sample on D-benzene (CFATR, Romania) with the magnetite volume fraction of 10 % was diluted down to 0.7 % with different mixtures of D- and H-benzene. Measurements were made at ten points over this interval. The special attention was given to the vicinity of the match point estimated as ~0.6 of the D-benzene relative content. The obtained scattering curves for different contrasts are presented in Fig.1*b*. Some amount of aggregation in the fluids was detected, which we connect with the age effect (about one year after preparation). The intensity at zero angle and visible squared radius of gyration were obtained by the Guinier approximation to these curves over q–interval 0.1-0.25 nm^{-1}, where the effect of aggregates was small. The corresponding treatment of the dependence of the visible radius of gyration on the inverse modified contrast is also shown in Fig. 2*b*. The effective match point is determined as 0.63 ± 0.03 of the D-benzene relative content in the solvent, which corresponds to the scattering length

density of $(3.86 \pm 0.15) \times 10^{10}$ cm^{-2}. The fit of Eq. (4) to the experimental data results in the squared radius of gyration $R_c^2 = 6450 \pm 65$ Å^2, or $R_c = 80.3 \pm 0.4$ Å. Taking into account the quasi-spherical shape of particles one obtains for the characteristic radius of the whole particle the value of $(\langle R^2V^2\rangle/\langle V^2\rangle)^{1/2} = 103.3 \pm 0.5$ Å. It is twice larger compared to 52 Å in the previous experiment, which is in agreement with the results on the scattering of polarized neutrons [3]. Obtained parameters of (4) are to be compared with the values calculated by the polydispersity function from direct modeling of the curves.

The work is done in the frame of the project RFBR-Helmholtz (HRJRG-016).

References

[1] M.V.Avdeev, J. Appl. Cryst. 40 (2007) 56–70.
[2] H.B.Stuhrmann, In: Small-angle X-ray scattering, Eds. O.Glatter, O.Kratky, London: Acad. Press, 1982.
[3] M.V.Avdeev, D.Bica, L.Vékás, O.Marinica, M.Balasoiua, V.L.Aksenov, L.Rosta, V.M.Garamus, A.Schreyer, J. Mag. Mag. Mater. 311 (2007) 6-9.

Behavior of Fatty Acids in d-Benzene by Small-Angle Neutron Scattering

V.I. Petrenko[1, 2], M.V. Avdeev[1], L.A. Bulavin[2], V.L. Aksenov[3, 1], L. Almásy[4], L. Rosta[4], V. Garamus[5]

[1]*Frank Laboratory of Neutron Physics, Joint Institute for Nuclear Research, Dubna, Russia*

[2]*Physics Department, Kyiv Taras Shevchenko National University, Kyiv, Ukraine*

[3]*Russian Research Center "Kurchatov Institute", Moscow, Russia*

[4]*Research Institute for Solid State Physics and Optics, Hungarian Academy of Sciences, Budapest, Hungary*

[5]*GKSS Research Centre, Geesthacht, Germany*

The interaction of non-saturated (oleic acid) and saturated (stearic and myristic acids) mono-carboxylic acids in solutions of a non-polar organic solvent (deuterated benzene) is derived from the concentration dependence of the small-angle neutron scattering data. The study is related to different stabilization properties of these acids in ferrofluids. Oleic acid, a non-saturated mono-carboxylic acid, is a classical stabilizing agent used in the synthesis of ferrofluids for coating magnetic nanoparticles in non-polar organic liquids. The reason for high stabilization efficiency of oleic acid is often associated with its non-saturated bond, which results in a kink in the middle of the molecule. This conclusion comes from the fact that the linear saturated analog of oleic acid, stearic acid, exhibits extremely low stabilization efficiency in ferrofluids. This difference is not fully understood, and, after more than thirty years (first ferrofluids appeared in the middle of 1960s), still the problem is referred to as a "puzzle of stearic acid" [1]. The work was also initiated by recent discovery [2] of the fact that saturated mono-carboxylic acids with shorter chain length than stearic acid, namely myristic acid and lauric acid, reveal better possibility for stabilizing magnetite in non-polar organic liquids as compared to stearic acid.

Pure oleic, stearic and myristic acids were dissolved in d-benzene (C_6D_6) with ultrasonication. Several solutions of OA, MA and SA in d-benzene were obtained with the volume fraction of the surfactant within intervals of 5-35%, 3-25% and 2-7%, respectively.

SANS experiments were performed on the YuMO small-angle time-of-flight diffractometer at the IBR-2 pulsed reactor, JINR, Dubna and the Yellow Submarine small-angle instrument at the steady-state reactor of the Budapest Neutron Centre, Hungary.

As shown previously [3], for small molecules (characteristic radius ~ 1 nm) the concentration dependence of the forward scattering intensity can be approximated by a function:

$$\frac{I(0)}{\Phi} \sim C(1 + B\Phi), \qquad (1)$$

where C is a constant and B is the dimensionless analog of the second virial coefficient [4]. The sign of this coefficient corresponds to the repulsive ($B < 0$) or attractive ($B > 0$) type of interaction in the solution.

The Guinier plots of the experimental SANS curves for OA and MA at different volume fractions of the solute are presented in Fig.1. The data are well approximated by the Guinier formula. In both OA and MA systems the concentration dependences of the forward scattering intensity and the apparent radius of gyration (Fig.2) reveal negative slopes corresponding to the effective repulsion between the acid molecules.

Scattering curves for SA solutions (Fig. 3) reflect behavior drastically different compared to the OA and MA solutions. In the concentration range of Φ = 0.02-0.05, in contrast to the previous cases, the Guinier approximations for the SA solutions (Fig. 3a) reveal an increase both in normalized forward scattering intensity and in the apparent radius of gyration with the growth of the acid concentration (Fig.4). The positive sign of B shows effective attraction between the SA molecules in the solution. Above Φ = 0.05 this attraction results in aggregation of the acid molecules. At Φ = 0.07 the SANS signal from these aggregates is rather distinguished, allowing us to estimate their size roughly as 10 nm from the additional Guinier-type term.

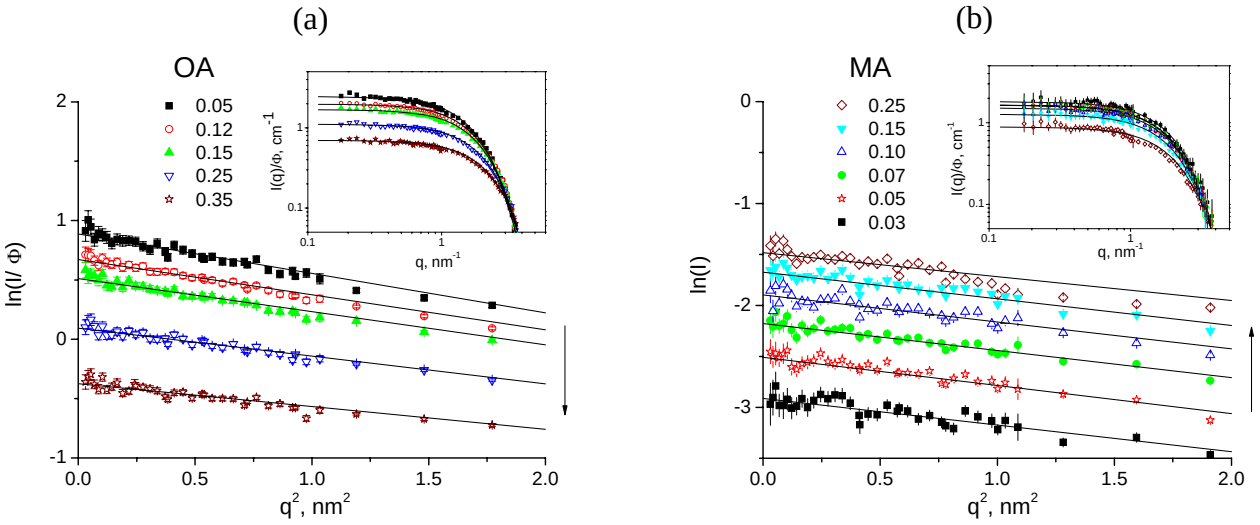

Figure 1. Guinier plots of experimental SANS curves from solutions of oleic (a) and myristic acids (b) in d-benzene referred to one volume fraction of solute. Arrow indicates the concentration growth. Inset shows the scattering intensity referred to one volume fraction of solute in the double logarithmic scale. Solid lines in both graphs correspond to Guinier approximations.

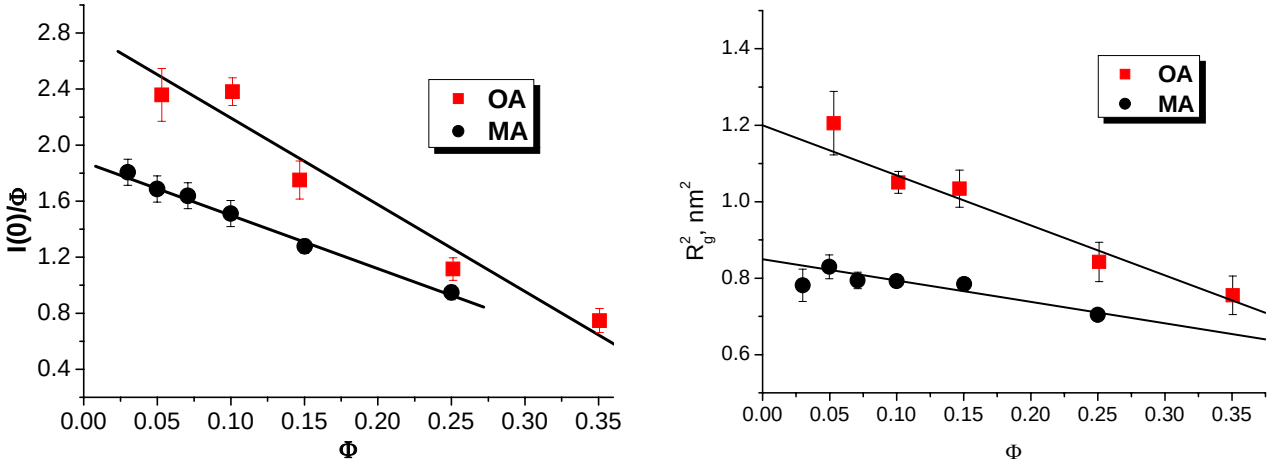

Figure 2. Forward scattering intensity referred to one volume fraction of solute (a) and squared radius of gyration (b) vs. acid volume fraction for solutions of oleic and myristic acids in d-benzene. Solid lines show linear fits.

The experimental molecular volumes of the acids molecules in solution were found from the constant C in (1) and are about 20 % larger than excluded volumes estimated by Tanford's formula [5], which was connected with fact that neutrons interact with nuclei and not with electrons.

Thus, OA and MA molecules show quite close behavior in benzene in terms of the second virial coefficient. Its value $B \sim -2$ is significantly larger than that for cases of rigid cylinders and hard-spheres, which means that besides the major excluded volume repulsion, an attractive component contributes significantly in the pair interaction potential. This component becomes strong enough in the SA solution to be the major contribution, which provides the effective attraction between the acid molecules.

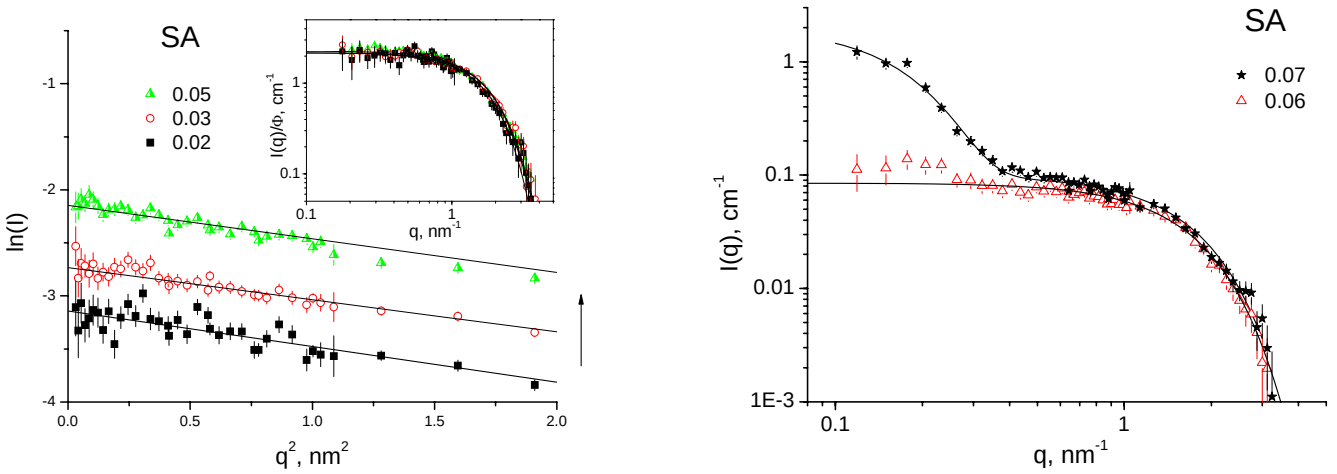

Figure 3. Experimental SANS curves from solutions of stearic acid in d-benzene with various volume fractions of the acid: Φ-interval of 0.02-0.05 (a) and $\Phi > 0.05$ (b).

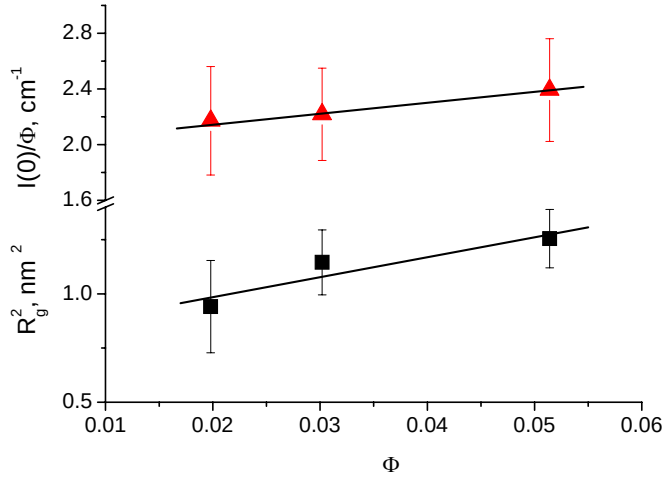

Figure 4. Forward scattering intensity normalized to concentration (triangle) and apparent radius of gyration (square) vs. SA volume fraction in d-benzene.

The possible origin of the discussed interaction component is solute-solvent interaction. The rate of solvation is concluded from the ratio V_{exp} / V_{excl}, which is the approximately the same for all molecules, and, hence, cannot explain the difference in the attraction of the acid molecules.

Thus, taking into account the colloidal size of the acid molecules (> 1 nm) one can assume that the observed attraction is a result of the van der Waals interaction. It increases with the effective molecular size, which explains why the behavior of OA and MA are close and differs from that of SA.

The van der Waals attraction observed in SANS experiments explains the shift of the transition into the liquid crystalline phase towards smaller acid concentrations.

The formation of the nematic phase in bulk solutions of mono-carboxylic acids can be important factor affecting the stabilization procedure of ferrofluids. This fact should be considered further in details with respect to poor stabilizing properties of SA in ferrofluids.

The work is partially done in the frame of the project RFBR-Helmholtz (HRJRG-016).

References

1. R. Tadmor, R.E. Rosensweig, J. Frey, J. Klein, Langmuir 16 (2000) 9117.
2. M.V. Avdeev, et al., J. Magn. Magn. Mater. 311 (2007) 6.
3. V.Yu. Bezzabotnov, et al., J. Phys. Chem. 96 (1992) 976.
4. F. Bonneté, D. Vivarès, Acta Cryst. D 58 (2002) 1571.
5. C. Tanford, J. Phys. Chem. 76 (1972) 3020.

Partial Volume of Fatty Acids in Benzene by Molecular Dynamic Simulations

I.A.Bodnarchuk[1], V.I.Petrenko[2,3], M.V.Avdeev[2], Kh.T.Kholmurodov[1]

[1]*Laboratory of Radiation Biology, Joint Institute for Nuclear Research, Dubna, Russia*

[2]*Frank Laboratory of Neutron Physics, Joint Institute for Nuclear Research, Dubna, Russia*

[3]*Physical Faculty, Kyiv Taras Shevchenko National University, Kyiv, Ukraine*

Molecular dynamic simulations (MDS) of limiting solutions of non-saturating mono-carboxylic acids - oleic (OA), stearic (SA), myristic (MA) acids - in benzene were carried out with the DL_POLY package [1]. The aim of this study was to conclude about the possible difference in the organization of benzene around the acid molecules in solutions. Since the size of the solvent molecule is comparable with that of the solute, such organization can result in a specific solute-solvent interaction, a significant contribution in the interaction potential for the acid molecules in solutions.

Solutions of fatty (mono-carboxylic) acids are of current interest from the viewpoint of stabilization of magnetic fluids. Non-saturated oleic acid $C_{18:1}$ is a classical surfactant used in synthesis of magnetic fluids for coating magnetic nanoparticles. Saturated stearic acid $C_{18:0}$ does not belong to good stabilizers, while stabilizing properties of shorter myristic acid $C_{14:0}$ are significantly better [2]. Recently, a great difference in the behaviour of these acids in benzene was revealed my means of small-angle neutron scattering (SANS) [3].

Molecular interaction in solution was modeled with the Lennard-Jones potential with cutoff radius 10 Å. Parameters of interaction between non-identical atoms were found according to the combination rule $\sigma_{ij} = (\sigma_i + \sigma_j)/2$ и $\varepsilon_{ij} = (\varepsilon_i\varepsilon_j)^{1/2}$, where σ_i, σ_j and ε_i, ε_j are parameters of the Lennard-Jones potential for atoms of *i*-s and *j*-s sorts taken from [4] for benzene and from [5] for acids.

Molecules of benzene and acids were of rigid atomic units. The initial configuration of benzene atoms was taken from the crystalline structure of benzene at 270 K [6]. One molecule of a fatty acid was put in the center of benzene cell of 1536 molecules with sizes 8*a*, 6*b*, 8*c* (Fig. 1). For imitation of infinite number of benzene molecules (limiting solution) orthorhombic periodical boundary conditions were used. After 20 ps of equilibration atoms coordinates were recorded every 0.1 ps in 150 ps trajectory of MDS at the constant both temperature (300 K) and cell volume.

Obtained radial distribution functions (RDFs) for pure benzene are shown in Fig.2. They agree well with the functions found experimentally and modeled by other research groups [7]. RDFs for benzene in solutions are close to those for pure benzene, i.e. acid molecules do not disturb much the structure of benzene. The comparison of the benzene organization at the

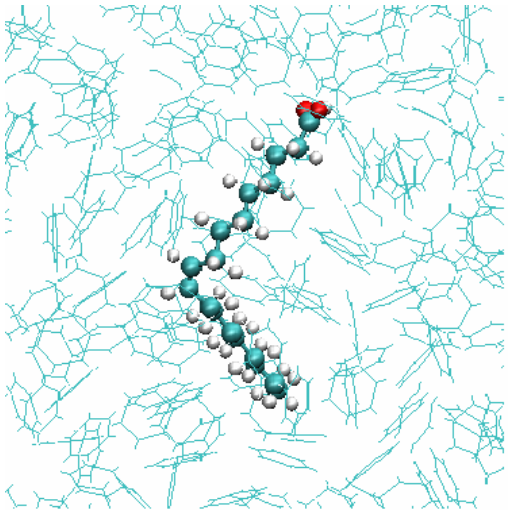

Fig.1. Snapshot of the equilibrium configuration for limiting benzene solution of oleic acid

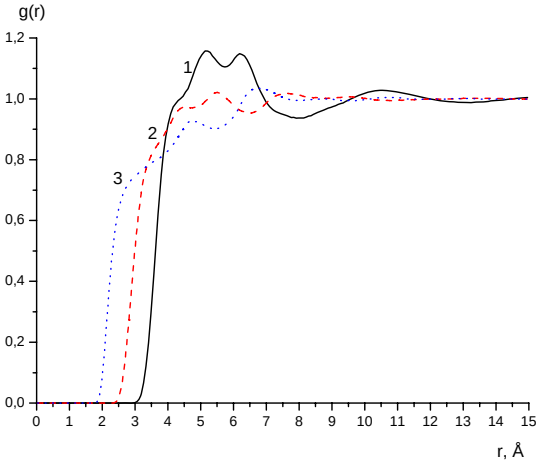

Fig.2. Partial RDFs for pure benzene. (1) C-C; (2) C-H; (3) H-H.

interface with acid molecules can be judged from the partial solute-solvent RDFs, which are given in Fig.3. Since no significant difference is seen for the three acids, there is strong evidence that the difference in the interaction of these molecules in solutions does not connect with solute-solvent interaction. The last is approximately the same for these molecules.

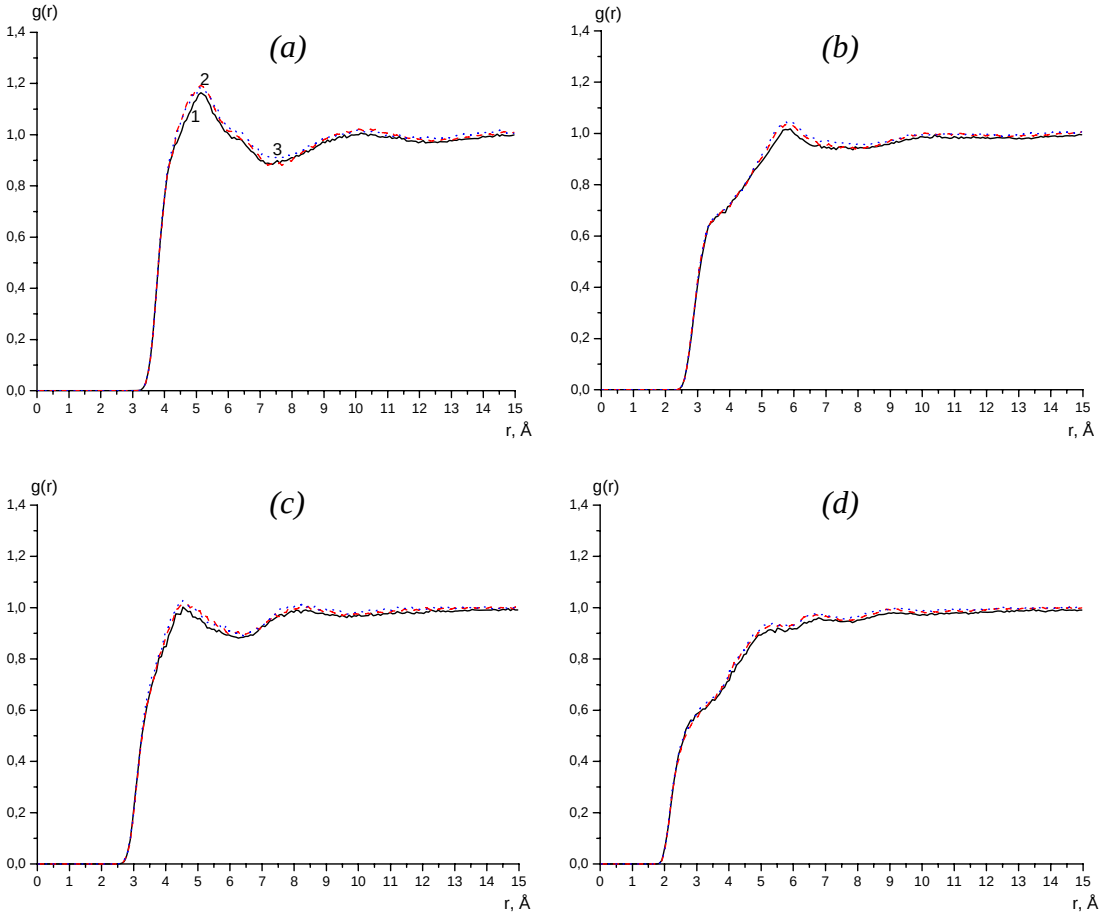

Fig.3. Partial RDFs for atoms of the solute acid (1 – OA, 2 – SA, 3 - MA) and benzene. (*a*) C benzene – C acid; (*b*) C benzene – H acid; (*c*) H benzene – C acid; (*d*) H benzene – H benzene.

In [8] it was shown that the limiting partial volume of the solute molecules, $\overline{V}^{\infty}$, can be found from the expression:

$$\overline{V}^{\infty} = \frac{\int_{|\vec{r}|<\lambda} (1 - g(\vec{r}))\, d\vec{r}}{1 - \frac{1}{V}\int_{|\vec{r}|<\lambda} g(\vec{r})\, d\vec{r}},$$

where $g(\vec{r})$ is any solute-solvent partial RDF, cutoff boundary $|\vec{r}| = \lambda$ around the solute beyond which the solvent properties would equal to their asymptotic limit, V is the volume of the modeled cell.

Results of calculations are given in Table 1. They are compared with the data of SANS [3]. As one can see, MDS give smaller values than SANS. We connect this difference with the fact that neutrons interact with nuclei, while $\overline{V}^{\infty}$ in our calculations is determined by the van der Waals radii of atoms. The difference of about 0.1 nm in the effective radius of the molecule cross-section is enough to explain why the volume is larger in neutron scattering experiments. The data of MDS are very close to $\overline{V}^{\infty}$ for oleic acid obtained from the vibration densitometry, $\overline{V}^{\infty} = 514 \pm 2$ Å^3 [9].

Table 1. Limiting partial molar volume $\overline{V}^{\infty}$ (Å^3) of fatty acids in benzene

Fatty acid	**MDS**	**SANS**
Oleic acid	522 ± 6	669 ± 50
Stearic acid	375 ± 5	644 ± 80
Myristic acid	311 ± 6	522 ± 50

References

1. Smith W., Forester T.R. // Molecular Graphics. 1993. 14. 136.
2. Avdeev M.V., Bica D., Vekas L. et al. // J. Magn. Magn. Mat. 2007. 311. 6.
3. Petrenko V.I., Avdeev M.V, Bulavin L.A. Aksenov V.L., Almásy L., Rosta L., Garamus V. Experimental report “Behavior of Fatty Acids in d-Benzene by Small-Angle Neutron Scattering” // this issue.
4. Jorgensen W.L., Severance D.L. // J. Am. Chem. Soc. 1990. V. 112. P. 4768.
5. Ryckaert J.P., Bellemans A. // Faraday Discuss. Chem. Soc. 1978. V. 66. P. 95.
6. Cox E.G., Cruickshank D.W.J., Smith J.A.S. // Proc. R. Soc. London, Ser. A. 1958. 247. 1.
7. Tassaing T., Cabaco M.I., Danten Y., Besnard M. // J. Chem. Phys. 2000. 113. 9. 3757.
8. Lockwood D.M., Rossky P.J. // J. Phys. Chem. B. 1999. V. 103. № 11. P. 1982.
9. Ramazanova A.G., Korolev V.V., Ivanov E.B. // Rus J Phys Chem 2007. 81. 4. 655.

Organization of fullerene clusters in the system C_{60}/N-metyl-2-pyrrolidone

O.A. Kyzyma[1,2], M.V. Avdeev[1], V.L. Aksenov[1, 3], L.A. Bulavin[2], S.V. Snegir[4]

[1]*Frank Laboratory of Neutron Physics, Joint Institute for Nuclear Research, Dubna, Russia*
[2]*Kyiv Taras Shevchenko National University, Kyiv, Ukraine*
[3]*Russian Research Center "Kurchatov Institut", Moscow, Russia*
[4]*Institute of surface chemistry, NAS of Ukraine, Kyiv, Ukraine*

Small-angle neutron scattering (SANS), UV-Vis spectroscopy and mass-spectroscopy experiments were performed on the solutions of C_{60} in N-methyl-2-pyrrolidone (NMP) and on the binary mixture NMP/water to improve the understanding of the cluster organization of C_{60} in nitrogen-containing solvents [1-3]. NMP is a comparatively good solvent for C_{60} (solubility is 1240 μM [4]) and is miscible with water. It can be used for fullerene transfer into aqueous media, which is important for employing biological activity of fullerenes in medical applications [5, 6].

Fullerene (Fullerenovye Tekhnologii, purity > 99.5%) was dissolved in NMP (Merck, purity > 99.5%) to obtain the C_{60}/NMP system. Then the solution was stirred for four days at room temperature. The solution was stored for one month after preparation in a dark place at room temperature. The solution concentration c = 1 μM was determined from the absorbance value at a wavelength of 342 nm, which was measured at Hitachi U-2000 spectrophotometer. Ternary solutions C_{60}/NMP/H_2O were obtained by addition of distilled water (Millipore) to the C_{60}/NMP solution.

Absorption spectra were obtained using Shimadzu UV-2401PC and Hitachi U-2000 UV/Vis spectrophotometers. SANS experiments were performed at the small-angle diffractometers at the research reactors of the Budapest Neutron Center (Hungary) and the Joint Institute for Nuclear Research (Dubna, Russia) according to standard procedures. The observable SANS signal was registered in the *q*-interval of 0.1-1 nm^{-1}. Mass spectrometry measurements were conducted using the Bruker Daltonics Autoflex II instrument at the Institute of surface chemistry, Kyiv, Ukraine.

Comparison of the SANS signals from systems C_{60}/NMP and C_{60}/NMP/H_2O are presented in Fig.1. One can see that the scattering from pure NMP solution is at the background level, while the addition of water results in its significant arise and reflects an effect of clusters within the size-interval of 10-100 nm corresponding to the covered *q*-range. The observed effect has a critical character in respect to the water relative content and takes place when later approaches 40 %, which is seen (Fig.2) in the behavior of the mean scattering intensity referred to one concentration. The rate

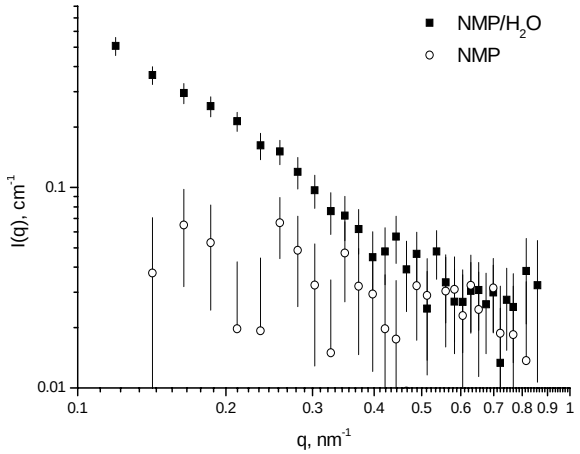

Fig.1. SANS signals from systems C_{60}/NMP and C_{60}/NMP/H_2O with water content of 50 vol. %. The concentration of C_{60} in both solutions is 500 μM.

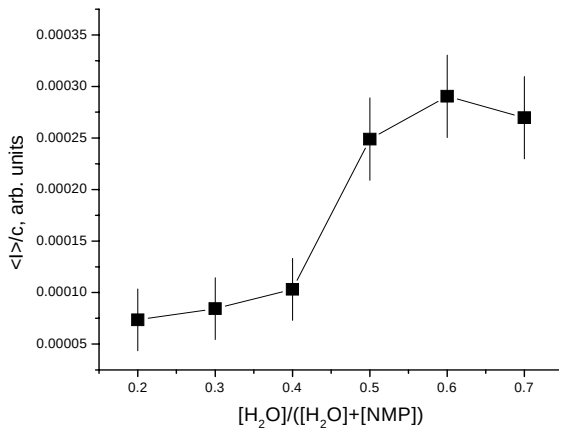

Fig.2. Mean scattering intensity of the SANS signal (over *q*-interval 0.14-0.44 nm^{-1}) from system C_{60}/NMP/H_2O as a function of relative water content.

of the intensity change depends on the age of the initial C_{60}/NMP solutions, and it is less for older solutions.

The appearance of the SANS signal makes it possible to apply the contrast variation procedure for estimating the inner structure of the clusters. To find out the match point of the mean cluster density we used the dependence of the mean scattering intensity on the D_2O content (Fig.3). The precision of the determined match point is poor, 0.8±0.3, however, its mean value corresponds well to the scattering length density $\rho \sim 5.6 \times 10^{10}$ cm^{-2} of packed fullerene structures (crystals or highly packed amorphous clusters).

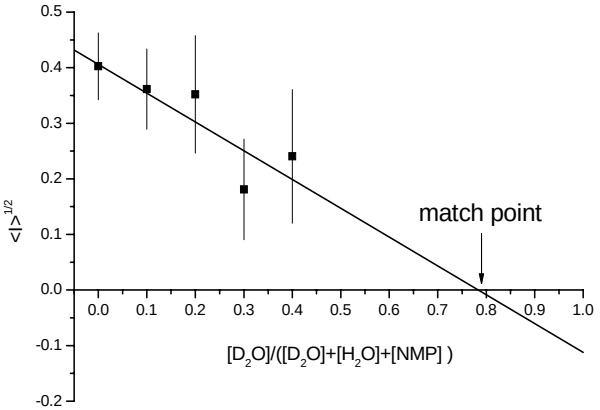

Fig.3. Contrast variation in the system C_{60}/NMP/H_2O/D_2O. The mean scattering intensity is determined for q-interval of 0.14-0.44 nm^{-1}.

Ternary solutions C_{60}/NMP/H_2O, which were obtained by addition of water to a fresh (type I) and old, age more than 1 month, (type II) C_{60}/NMP solutions was investigated by SANS (Fig. 4). For estimation of the clusters size in these systems, the scattering curves were processed using indirect Fourier transformation. The distribution functions of the pair distances p(r) for C_{60}/NMP/H_2O solutions are shown in Fig. 5.

A change of UV-Vis spectrum with time (temporal solvatochromic effect) within one month after preparation of the C_{60}/NMP system and sharp solvatochromic effect after water addition to the fresh C_{60}/NMP system was observed (Fig. 6). Addition of water to a two-component system with a smooth spectrum does not show change in the spectral curve.

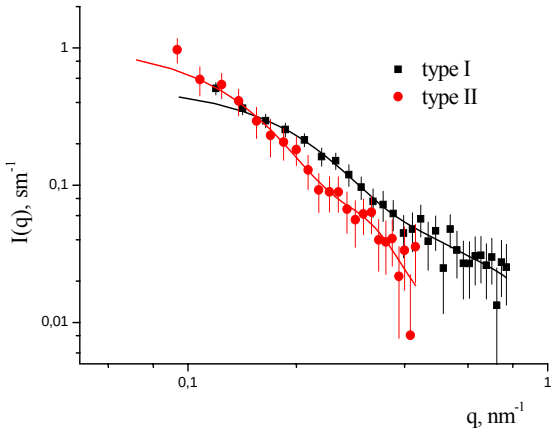

Fig.4. SANS curves from the system C_{60}/NMP/H_2O. The volume content of water in both solutions is 50% and the fullerene concentration is 500 μM. Solid lines are the model curves obtained by the indirect Fourier transformation.

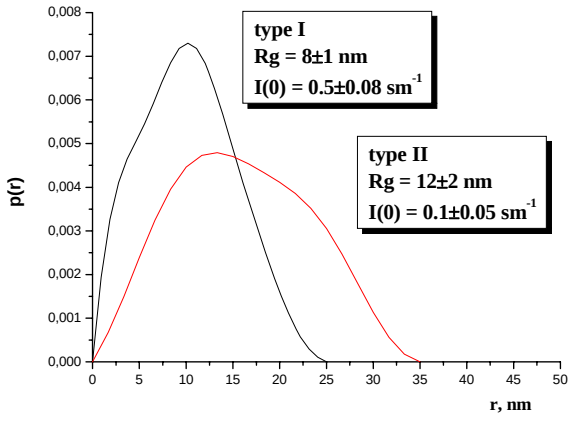

Fig.5. The distribution functions of pair distances as a result of treatment of the SANS curves by the indirect Fourier transformation.

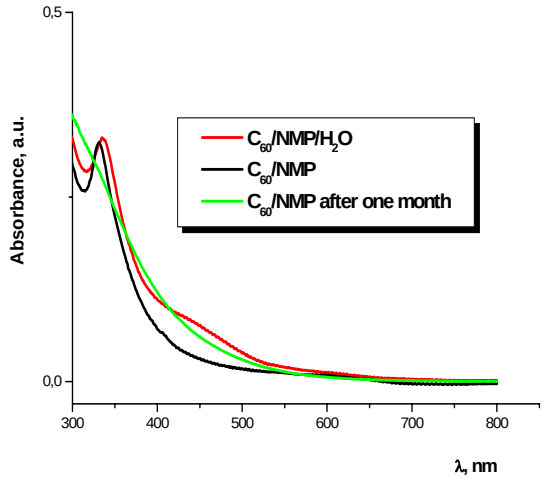

Fig.6. Change in the UV-Vis spectrum of the C_{60}/NMP solution (concentration 1 μM) with time and after addition of water.

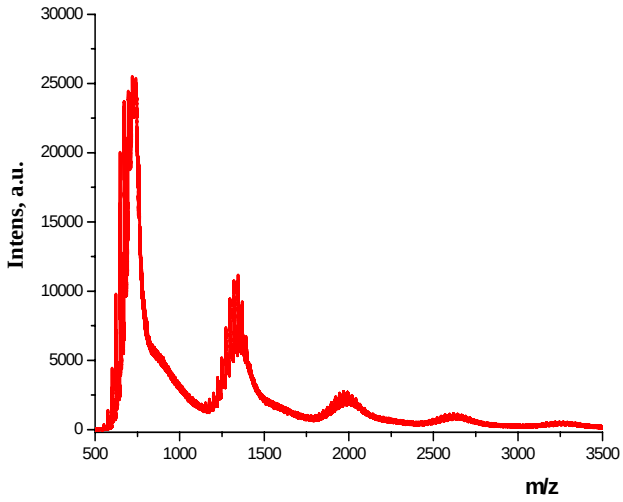

Fig.7. Mass-spectrum of fresh solutions C_{60}/NMP.

Mass-spectrum of fresh C_{60}/NMP solution is shown on Fig. 7. The fullerene clusters with number of monomers from 2 to 4 are present in the fresh solution. The ternary system C_{60}/NMP/H_2O has only clusters with 2 numbers of monomers (Fig. 8). Peaks, corresponding to the fullerene clusters as well as monomers were not observed in the case of old (age more than 1 month) solution C_{60}/NMP. This fact indicates that fullerenes form large scale clusters with strong bonds between molecules. However, the addition of water in this system leads to appearing of a monomer peak (Fig. 9). Therefore, the decomposition of clusters in solutions occurs as a result of the monomer detachment.

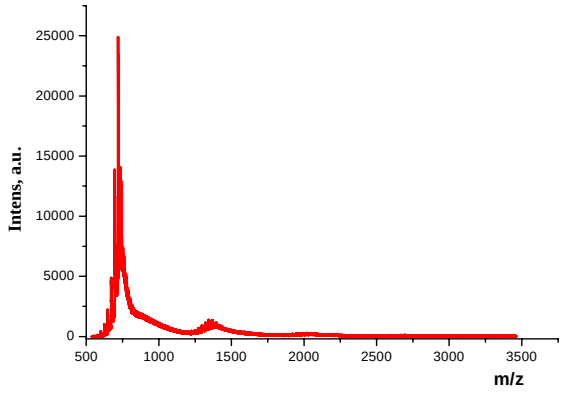

Fig.8. Mass-spectrum of fresh solution C_{60}/NMP after addition of water.

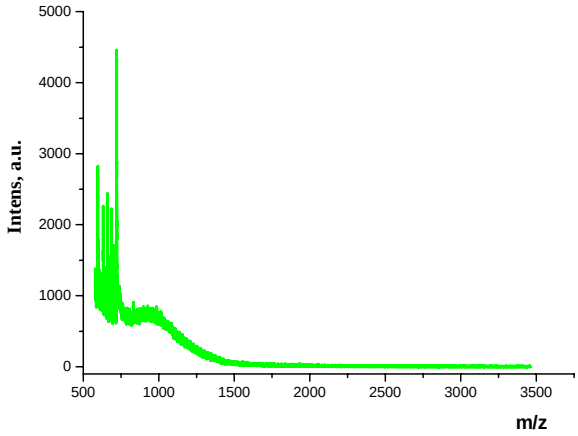

Fig.9. Mass-spectrum of old solution C_{60}/NMP after addition of water.

References

[1] A.Mrzel, A.Mertelj, A.Omerzu, M.Opi, D.Mihailovic, J. Phys. Chem. B 103 (1999) 11256.
[2] N.P.Yevlampieva, Yu.F.Biryulin, et al., Colloids and surfaces A 209 (2002) 167.
[3] M.Alfe, B.Apicella, R.Barbella, Chem. Phys. Lett. 405 (2005) 193.
[4] R.S.Ruoff, D.S.Tse, R.Malhotra, D.C.Lorents, J. Phys. Chem. 97 (1993) 3379.
[5] L.B. Piotrovsky et al., Mol. Mater. 13 (2000) 41.
[6] M. Gallego, Y.P. Pena, M. Valcarcel, Anal. Chem. 66 (1994) 4074.

On the inner structure of the polycarbosilane dendrimers

A.V. Rogachev[1,2], A.Yu. Cherny[3], A.N. Ozerin[4], A.M. Muzafarov[4], E.A.Tatarinova[4], A.Kh. Islamov[1], V.I. Gordeliy[1,5,6], A.I. Kuklin[1]

[1)] *Frank Laboratory of Neutron Physics, JINR, Dubna, Moscow reg., Russia*
[2)] *Skobeltsyn Institute of Nuclear Physics of Moscow State University, Moscow, Russia*
[3)] *Bogoliubov Laboratory of Theoretical Physics, JINR, Dubna, Moscow reg., Russia*
[4)] *Institute of Synthetic Polymeric Materials of the Russian Academy of Sciences, Moscow, Russia*
[5)] *Moscow Institute of Physics and Technology, Dolgoprudny , Moscow reg., Russia*
[6)] *IBI-2, Forshungszentrum, Juelich , Germany*

Dendrimers, tree-shaped acyclic macromolecules with a regular structure, form a new class of polymers [1, 2]. They were synthesized in the mid-1980s and studied by many methods [3–6]. However, some problems of dendrimer structure remain open: in particular, questions of internal hollows existence and penetration of solvent into the inner dendrimer volume [7]. Solution of these problems is important for practical using of dendrimer macromolecules as the functional carriers of universal purpose. The paper develops the previous investigations [8-13] to resolve that problem.

We experimentally investigate the structure of polycarbosilane dendrimers of the 9th generation G9Bu with 4-functional core and butyl end groups [1]. Synthesis of such kind of dendrimers is well controlled, and presence of the non-functional end groups provides long-term stability of the chemical structure, which is essential for investigating properties with various physical methods and long-term storing.

SANS experiments were performed with the two-detector system [14,15] at the YuMO instrument.

The dendrimers for the measurement were solved in mixture of benzene C_6H_6 and deuterated benzene C_6D_6 with the following volume ratio C_6H_6/C_6D_6: 0/1, 0.75/0.25, 0.5/0.5, 0.25/0.75, 1/0. Concentration of the dendrimers in solvent was 20 mg/cm^3. The solutions were placed into standard cells (Hellma) with thickness of 1 mm in the direction of neutron beam. The samples were kept at 20±0.03 °C in a special thermal box connected to a Lauda computer – controlled thermostat. The range of transferred momentum was 0.007 – 0.35 Å. The experimental data were treated with the SAS package [16], which makes it possible to sum the data for the same sample; calculate the instrumental resolution function for given experimental conditions; correct the data for the dead times of neutron detectors; and subtract the substrate background from the detector data, normalize the obtained spectrum to the spectrum of standard vanadium scatterer, and subtract the background sample data [17].

SANS data for dendrimers in mixtures of C_6H_6/C_6D_6 is shown in Fig 1. The behavior of curves does not change with contrast which is indirect evidence of homogeneity of scattering density inside the studied dendrimer.

The presents of two maximums on the scattering curve proves the assumption about monodispersion of dendrimers (Fig.2).

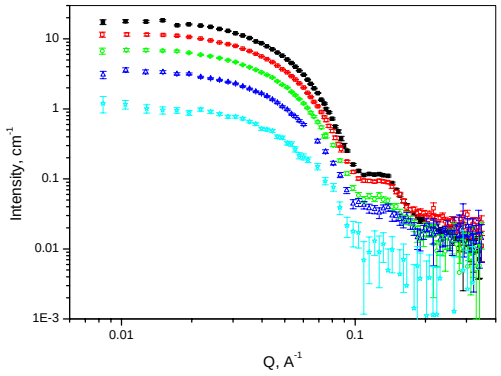

Fig. 1. SANS data for dendrimers in mixtures of C_6H_6/C_6D_6 from botton to top: 0/100, 75/25, 50/50, 25/75, 100/0, wt/wt %.

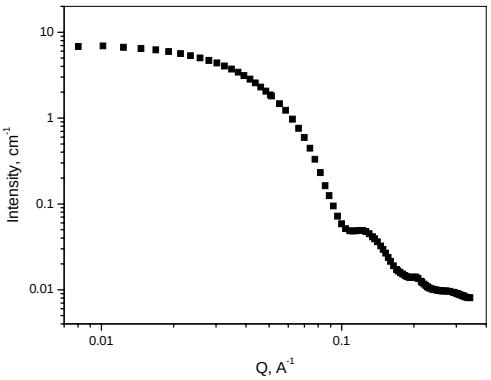

Fig. 2. SANS data for dendrimers in mixtures of C_6H_6/C_6D_6 with smoothing procedure.

Guiener approximation for experimental curves (Fig.1) is shown on Fig.3. Mean radius of gyration $\overline{R}_g$. is equal to $39.6(\pm 0.12)$ Å .

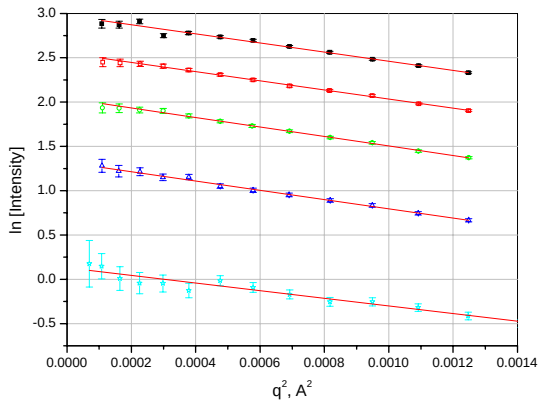

Fig. 3. Guinier approximation of SANS data of Fig. 1.

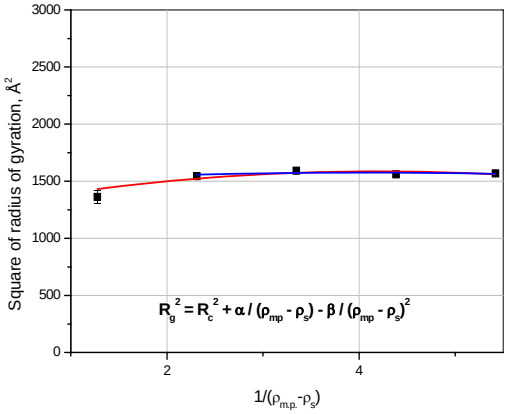

Fig. 4. Dependence of square of radius gyration on the reverse contrast.

The value R_g^2 does not depend on the contrast within experimental errors (Fig.4). This implies homogeneous distribution of scattering density inside the dendrimers.

In Fig. 5, the intensity in zero angle is shown as function of scattering length density. The fitting parabola attains the abscissa axis. This means [8-12] that dendrimers are monodispersive with respect to the scattering length density.

Concluding, the present experimentsal data can be consided as an evidence that first, the distribution of the scattering length density is homogeneous insides the dendrimers, and second, the dendrimers are identical in their inner structure.

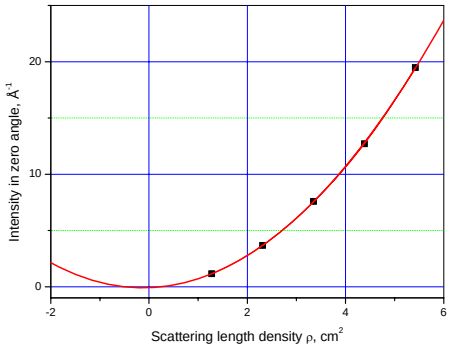

Fig. 5. Intensity in zero angle versus the scattering length density of the solvent.

References

1. A. M. Muzafarov and E. A. Rebrov, Polymer Sci. C 42 (1), 55 (2000).
2. D. A. Tomalia, A. M. Naylov, and W. A. Goddard, Angew. Chem., Int. Ed. Engl. 29 (2), 138 (1990).
3. R. Scherrenberg, B. Coussens, P. Vliet, et al., Macromolecules 31, 456 (1998).
4. T. J. Prosa, B. J. Bauer, and E. J. Amis, Macromolecules 34, 4897 (2001).
5. E. A. Tatarinova, E. A. Rebrov, V. D. Myakushev, et al., Izv. Akad. Nauk, Ser. Khim. No. 11 (2004).
6. B. V. Lebedev, M. V. Ryabkov, E. A. Tatarinova, et al., Izv. Akad. Nauk, Ser. Khim., No. 3 (2003).
7. P. de Gennes and H. Hervet, J. Phys. (Paris) 44, L351 (1993).
8. Kuklin A. I., Ignat'eva G. M., Ozerina L. A., et al., Polym. Sci. A, 44, 2124–2133, (2002).
9. Kuklin A. I., Ozerin A. N., Islamov A. Kh., et al., J. Appl. Cryst., 36, 679–683, (2003).
10. Ozerin A. N., Muzafarov A. M., Gordeliy V. I., et al., Macromol. Symp., 195, 171–178, (2003).
11. Ozerin A. N., Muzafarov A. M., Kuklin A. I., et al., Dokl. Chem., 395, 59–62 (2004).
12. Ozerin, A. N., Svergun D.I., Volkov V.V., et al., J. Appl. Cryst. 38, 996–1003, (2005).
13. Rogachev A.V., Cherny A.Yu., Ozerin A.N., et al., Crystallography Reports, 52, 3, 500–504, (2007)
14. Kuklin A.I., Islamov A.Kh., and Gordeliy V.I., Neutron News, vol. 16, 3, pp.16-18, (2005).
15. Куклин А.И, Исламов А.Х., Ковалев Ю.С. и др., Поверхность, №6, с.74-83, (2006).
16. A. G. Solov'ev, T. M. Solov'eva, A. V. Stadnik, et al., Report JINR R10-86 (2003).
17. Yu. M. Ostanevich, J. Macromol. Sci., Chem., Macromol. Symp. 15, 91 (1988).

Measurements with New Type of Position Sensitive Detector in Backscattering and Small-angle Scattering Arrangements

A.I.Kuklin[1], S.A.Kutuzov[1], A.Gabriel[2], G.Eckold[3], P.K.Utrobin[1,4], A.A.Smirnov[1], A.Ivankov [1,5], A.Kh.Islamov[1], Yu.S.Kovalev[1] , A.Feoktistov[1,5], A.V.Rogachev[1,6], A.S.Kirilov[1], V.I.Gordeliy[1,4,7].

[1]*FLNP, JINR Dubna, Russia;*[2]*EMBL, Grenoble, France;*[3]*Institute of Physics Chemistry Univ. Goettingen, Germany;*

[4] *Centre for Biophysics and Physical Chemistry of Supramolecular Structures, Moscow Institute for Physics and Technology, Dolgoprudny, Russia;*

[5]*Physical Faculty, Kyiv Taras Shevchenko National University, Kyiv, Ukraine;*

[6]*Skobeltsyn Institute of Nuclear Physics of Moscow State University, Moscow, Russia;*

[7]*IBI-2, Forshungszentrum Juelich , Germany.*

Two detector system (TDS) is the key element of a modernized YuMO spectrometer [1,2]. New setup of the instrument allows collecting SANS data in a wide interval of scattering vectors simultaneously. The momentum transfer dynamic range of the instrument has increased considerably to more than 90 and data acquisition time was reduced about two times. TDS has shown efficiency on ring wire detector basis. For the studies of anisotropic samples by SANS spectrometer it is necessary to use PSD with a central hole. The idea of this detector was created by the SAS group of FLNPh and the detector was developed in a tight cooperation with A. Gabriel and G. Eckold. First results with neutron were obtained at low pressure (1.1 atm) at the beam-line G5-6 in LLB [3]. In this paper we report about the results obtained in two experimental arrangements: diffraction (back scattering mode), as well as small-angle scattering using standard experimental setup.

In Fig.1. the main view of PSD detector is presented with the following parameters: external size diameter - 1070 mm, weigth is about 200 kg; size of the sensitive part of the detector is 580x580 mm^2; detector comprises 230 wires with the 2.5 mm gap; diameter of the central hole - 70 mm; type of the position encoding - delay-line readout .

Fig.1. Main view of the PSD with Vn-standard device and the special support for 3-D adjustments to neutron beam inserted in the detectors tube.

Fig.2. shows the setup of PSD for experiment in backscattering geometry. The results, obtained from Bi crystal can be observed in Fig.3. Resolution of the detector is better than 3 mm. Data acquisition system processes 1.7 Mevents/sec.

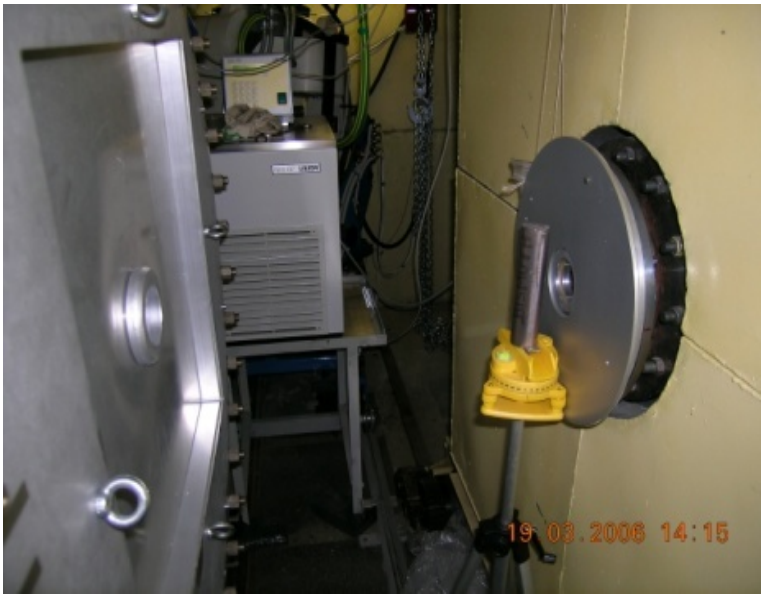

Fig.2. Setup of PSD for backscattering geometry.

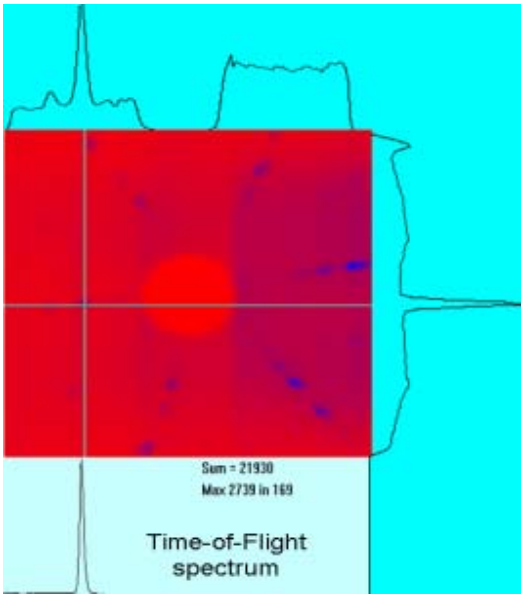

Fig.3. Raw data from PSD of Bi crystall.

Finally the detector was placed into the detector vacuum tube of the YuMO spectrometer (Fig.1) and the experimental tests were performed in the operational configuration of the instrument. Test of the PSD as TDS in working position in vacuum tube was made. Problems with vacuum and high voltage at the detector were resolved. The vanadium standard device was installed in front of the detector (Fig.1). Software for data acquisition and data treatment was prepared. The detector has a special support for 3 dimensional adjustments to neutron beam (Fig 1). Raw data of steel in space coordinate, time-of-flight and 1-dimensional spectrum and section through the middle part of space coordinate are presented in Fig.4.

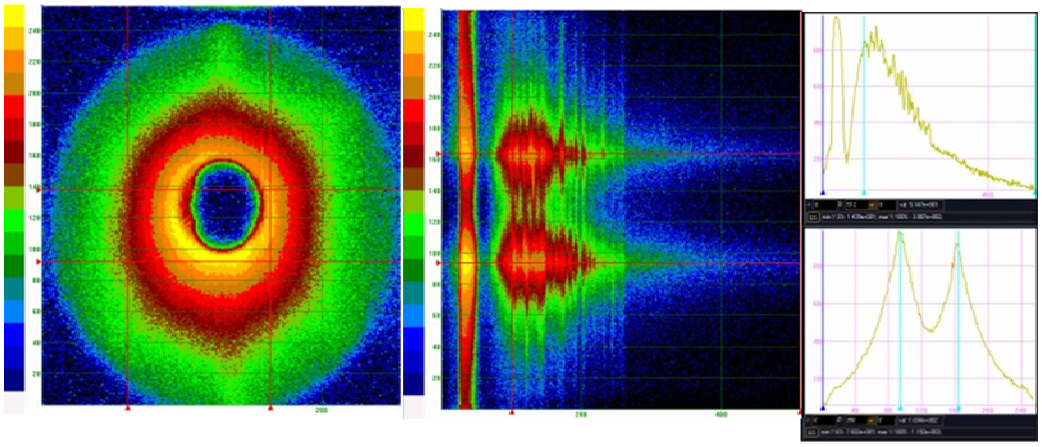

Fig.4. Raw data in space coordinate (left), time-of-flight (middle) and 1-dimensional spectrum (right top) and section through the middle part of space coordinate (right down).

In standard geometry, PSD was used during several cycles like second detector in TDS setup. The data from apoferritin, ferritin and silver behenate in q-space scale are presented in Fig.5.

The q-range of PSD is wide as the NEW circle detector in the same position.

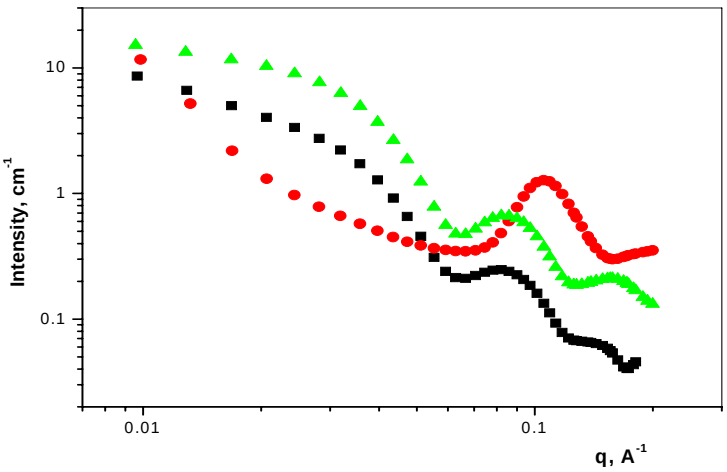

Fig.5. Scattering curves from ferritin(triangle), apoferritin (square)and silver behenate(circle), obtained by PSD

It has been shown that the PSD with a central hole can be used for diffraction experiments in the backscattering geometry as well as small angle neutron scattering arrangement. The experimental scattering curves collected with the PSD and a standard YuMO circle detector are in agreement within experimental errors.

References:

[1] A.I.Kuklin, A.Kh.Islamov, and V.I.Gordeliy, Two-Detector System for Small-Angle Neutron Scattering Instrument, Neutron News, Vol.16, Number 3, pp.16-18.

[2] A.I.Kuklin, A.Kh.Islamov, Yu.S.Kovalev, P.K.Utrobin, V.I.Gordeliy. Optimization of two detector system small angle neutron spectrometer YuMO for nanoobjects investigation. Surface.(in russian), 2006, №6, c.74-83.

[3] A. Kuklin, G.Eckold , V.Gordeliy, S.Kutuzov, A.Islamov, A.Smirnov, P.Utrobin, A.Bogdzel, N.Alekseev, V.Comparat, A.Pelissier, J. Ballon, J. Teixeira , G.Koskas, A.Gabriel. Report on a first neutron test of a new D position-sensitive detector of thermal neutrons LLB Sientific Report 2003-2004 http://www-llb.cea.fr/activ03-04/p165.pdf

[4] A. I. Kuklin, S. A. Kutuzov, A. Gabriel, G. Eckold, P. K. Utrobin, A. A.Smirnov, A. Kh. Islamov, A. S. Kirilov, A. A.Bogdzel, V. I. Gordeliy.The Parameters of Position Sensitive Detector with Central Hole and First Results in Small-angle and Backscattering Configurations. Book of abstracts 4-th European Conference on Neutron Scattering, 25-29 June 2007, Lund, Sweden, p.530.

This work was supported by the Federal Ministry of Education and Science (BMBF) of Federal Republic of Germany under grant № 03DU03G2

Acknolodgements: group of YuMO, M.Balasoiu, T.Murugova, A.Raevska, R.Erhan, A.Churakov, V.Vasko, V.Comparat, A.Pelissier, J.Ballon, A.Mennel, M.Moon, A.Polyakov, G.Andreev, D.A. Kudryavcev, E.Koberidze, G.A.Varenik, V.V.Ignatiev, A.Popov, A.Chernikov, V.Gaevskiy, V.Vstrechniy, A.Kurbakov, A.Balagurov, A.Beskrovniy, M. Kocsis, B.Guerard, G.Pepy, V.Sumin and institution: ILL, ESRF, LLB, ICC, EMBL.

INVESTIGATION OF INTERMEMBRANE INTERACTION IN PRESENCE OF DIMETHYLSULFOXIDE VIA SANS

J. E. Gorshkova[a] and V. I. Gordeliy[a, b, c]

[a] Joint Institute for Nuclear Research, ul. Zholio Kyuri 6, Dubna, Moscow oblast, 141980 Russia
[b] Moscow Institute of Physics and Technology, Institutski per. 9, Dolgoprudny, Moscow oblast, 141700 Russia
[c] Research Centre Jüelich, Jüelich, D-52425 Germany

Dimethyl sulfoxide (DMSO) is a solvent that has found wide application in cell biology, cryobiology, pharmacology, medicine, and agriculture. The influence of DMSO on the structures of lipid membranes was investigated early. However, a number of important properties exhibited by these systems are still not clearly understood. For example, there is no direct information regarding the influence of DMSO on the membrane thickness and the intermembrane distance (intermembrane interaction) in an excess of a water/DMSO solvent. It would be extremely important to obtain direct information on the interaction of DMSO with the membrane surface. In order to solve the above problems, we investigated the DMPC/DMSO/water ternary system.

The present work is devoted to analysis of dimethylsulfoxide (DMSO) influence on the structure of dimyristoylphosphocholine (DMPC) lipid membrane in wide-range DMSO mole fractions $0.0 \leq X_{DMSO} \leq 1.0$ at T=12.5$^{\circ}C$ and T=55$^{\circ}C$. The DMSO concentration influence on the repeat distance d of the multilayer membranes and intermembrane spacing d_b of the vesicles in gel $L_{\beta'}$ and liquid L_{α} phases was studied by Small-Angle Neutron Scattering (SANS). The intermembrane distance d_s was obtained using d and d_b values. It was shown that the intermembrane distance sharp decrease with increasing X_{DMSO} (Fig.1). At X_{DMSO} = 0.4 the neighboring membranes are in steric contact with each other. This results in the fusion of single membranes into multilamellar structures (Fig.2).

At first, we calculated a number of the DMSO molecules strong connective with membrane using DMSO-D6 and contrast variation method at X_{DMSO} = 0.2 (Fig.3). The number of these DMSO molecules is equal to 3.65, and their total volume amounts to 430 Å^3. This value is comparable to the volume of the polar head of the lipid molecule and accounts for the previously observed phase transition of the lipid membrane to the interdegitated phase.

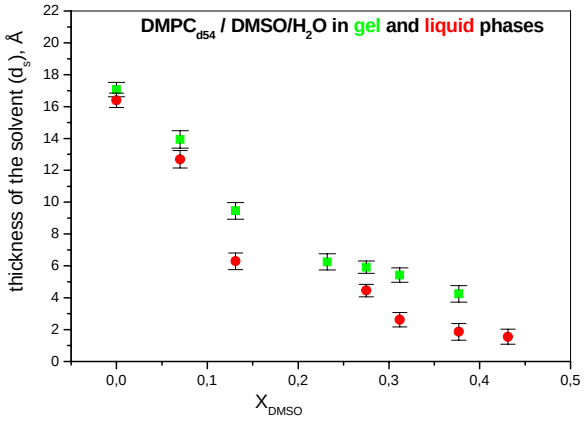

Fig.1. *Dependence of the solvent layer thickness d_s on the DMSO molar concentration for the DMPC-D54 (2%, wt/wt) multilamellar membranes in the water/DMSO solvent in the $L_{\beta'}$ ($T = 12.5^{\circ}C$) gel and L_{α} ($T = 55^{\circ}C$) liquid-crystalline phases.*

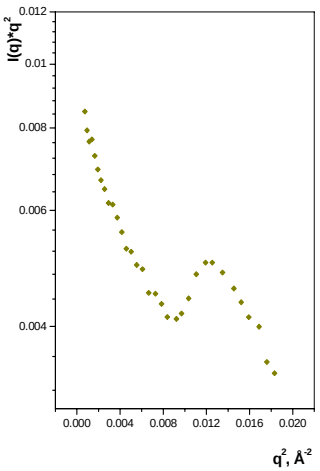

Fig.2. *Kratky-Porod plot for membranes prepared through extrusion of the DMPC-D54 2% wt/wt multilamellar membranes in the water/DMSO solvent in the liquid-crystalline L_{α} ($T=55^{\circ}C$) phase at the DMSO molar concentration X_{DMSO} = 0.43.*

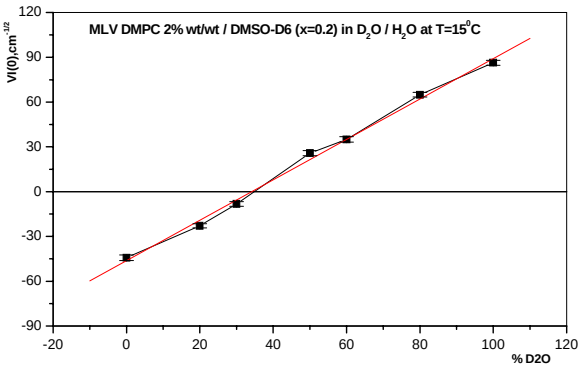

Fig.3. *Dependence of the quantity* $\sqrt{\mathrm{I}(0)}$ *on the D/2O percentage for single DMPC (2%, wt/wt) vesicles in the* H_2O/D_2O*/DMSO-D6 solvent in the* $L_{\beta'}(T=15^{\circ}C)$ *gel phase at the DMSO-D6 molar concentration* $\chi_{DMSO\text{-}D6}$ *= 0.2. The matching point (I(0)=0) corresponds to 34 %* D_2O *or* $\rho_{s,matching} = 3.53 \cdot 10^{10}\, см^{-2}$.

REFERENCES

1. J. E. Lovelock and M. W. H. Bishop, Nature (London) /183/, 1394 (1959).
2. S. Tristram-Nagle, T. Moore, H. Petrache, and J. F. Nagle, Biochim. Biophys. Acta /1369/, 19 (1998).
3. V. I. Gordeliy, M. A. Kiselev, P. Lesieur, et al., Biophys. J. /75/, 2343 (1998).
4. Z. W. Yu and P. J. Quin, Biochim. Biophys. Acta /1509/, 440 (2000).
5. V. I. Gordeliy, V. Cherezov, and J. Teixeira, Phys. Rev. E: Stat., Nonlinear, Soft Matter Phys. /72/ (1), 061913 (2005).
6. Z. W. Yu and P. J. Quin, Mol. Membr. Biol. /15/, 59 (1998).
7. A. M. Smondyrev and Max L. Berkowitz, Biophys. J. /76/, 2472 (1999).
8. Z. W. Yu and P. J. Quin, Biophys. J. /69/, 1456 (1998).

Coexistence of superconductivity and ferromagnetism in nanostructure Nb(500 Å)/Fe(39 Å)/[Si(34 Å)/Mo(34Å)]40/Si.

V.L. Aksenov[1,2], Yu.V. Nikitenko[1], Yu.N. Khaidukov[1], S.N. Vdovichev[3], N.N. Salashchenko[3], A.A. Fraerman[3], E.Kh. Mukhamedzhanov[2].

[1] *Joint institute for Nuclear Research, Dubna*

[2] *Russian Research Center "Kurchatov institute", Moscow*

[3] *Institute for physics of microstructures, Nizhniy Novgorod*

Study of influence of superconductivity (S) on ferromagnetism (FM) in layered nanostructures is an actual problem, both for fundamental science, and for practical applications. Theoretically predicted, that due to proximity effects between S and FM layers various scenarios of influence of superconductivity on ferromagnetism are possible: formation of domain structure (so-called cryptoferromagnetic state [1]), effect of magnetization "leakage" from FM to S layer [2, 3], change of direct and indirect exchange coupling of FM layers, etc. Practical importance studying of such systems is connected with perspective of creation of information record devices on two channels - electric resistance and intensity of a magnetic field. It is necessary to note, that number of experimental works in which influence of superconductivity on magnetism was observed is very small. For experimental study ferromagnetic resonance [4,5], synchrotron resonant reflectometry [6,7] , low energy muon spectroscopy [8] and polarized neutron reflectometry (PNR) [9,10,11,12] are used.

In this work study of structure Nb(500 Å)/^{57}Fe(39 Å)/[Si(34 Å)/Mo(34Å)]$_{40}$/Si was done. The sample has been prepared in the Institute for physics of microstructures (Nizhniy Novgorod) [13].Test of the superconductivity for the prepared sample was done by a contactless method as a third-harmonic nonlinear response of superconducting substance to the excitation by microwave frequencies in helium cryostat (Nizhniy Novgorod). The temperature of superconducting transition of niobium according to these measurements makes $T_{C\text{-}Nb}$ = 9.2K. The periodic Si/Mo structure (PS) is also a superconductor with critical temperature $T_{C\text{-}Si/Mo}$ = 4.5K. Presence of the second superconductor in layered structure allows us to compare behavior of systems $N_1/F/N_2$ at $T > T_{C\ Nb}$, $S_1/F/N$ at $T_{C\text{-}Si/Mo} < T < T_{C\text{-}Nb}$ and $S_1/F/S_2$ at $T < T_{C\text{-}Si/Mo}$.

Structural properties of system were investigated at the station for high-precision X-ray optics at the Kurchatov center for synchrotron radiation and nanotechnology [14]. Measurements specified high quality of structure - four Bragg peaks from periodic Si/Mo system and well resolved Kiessig oscillations were observed.

Neutron measurements have been lead on time-of-flight spectrometer of polarized neutrons REMUR of reactor IBR-2 in Dubna.

For change of polarization of incoming beam one spin-flipper was used : at switched off (on) spin-flipper intensity of the scattered neutrons with polarization «+» («-») was measured (sign specifies a projection of a neutron to external magnetic field). Measurements were done at fixed grazing angle θ_1 = 9.9 mrad with divergence $\Delta\theta \approx 0.4$ mrad in a range of scattering angles θ_2 = 5.3-28.4 mrad and in the range of neutron wavelengths λ = 1-11 Å with resolution $\Delta\lambda$ = 0.019 Å. Altogether it was done three measurements at temperatures 2, 5 и 15K in magnetic field H = 0.5 кGs applied parallel to surface.

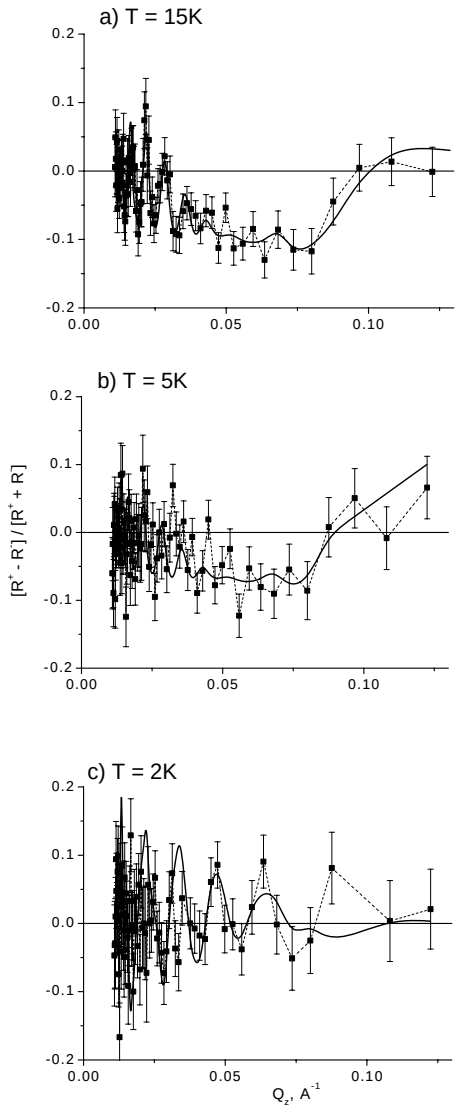

Fig.1. Experimental (dots) and model (solid lines) spin asymmetries at different temperatures.

Spin asymmetry $S = (R^+ - R^-)/ (R^+ + R^-)$ at given temperatures is shown on fig. 1. At T = 15K curve is characterized by presence of 10% deep at Q = 0.03 - 0.1 $Å^{-1}$. At downturn of temperature up to T = 5K there is a reduction of the deep up to 7 %. At the further downturn of temperature up to 2K spin asymmetry changes much. The deep in the specified range disappears and S (Q) oscillates about zero with the period $dQ \approx 0.02$ $Å^{-1}$. Such a period coincide to size $2\pi/dQ \approx 300$ Å in real space. The analysis of data of neutron experiment was done within the frame of supermatrix formalism [15]. At the first stage the specular reflectivity R (Q) was fitted at variation of nuclear potential. Thickness of layers, sizes of roughness were taken from fit of x-ray data. Such co-processing has allowed to define nuclear profile of structure more reliably. At the second stage fit of spin asymmetry was done at variation of magnetic profile $4\pi M(z)$. Fit results are shown on fig. 2. At T = 15K only FM layer is magnetic with magnetization 1.9 ± 0.3 kGs. At downturn of temperature up to 5K there is a reduction of average magnetization of iron up to 1.3 ± 0.2 kGs and appearance of the small diamagnetic moment in niobium -20 Gs. The small size of the diamagnetic moment is explained by the fact that thickness of the film is compared with penetration

depth of magnetic field in superconducting niobium. The behavior of a curve at T = 2K can be described by introduction in the center of Nb film magnetic layer with the thickness of the order 100 Å with positive magnetization 1.5 ± 0.5 кGs. In other part of niobium magnetization also positive, monotonously decreasing from the center to interfaces. Magnetization of Fe layer and Si/Mo system make 0.1 kGs и -0.2 kGs corresponding.

Appearance of magnetic layer with positive magnetization at 2K in niobium can be explained by Abrikosov vortices. In-plane averaged core of the vortex has the linear size of the order 100 Å, that less than coherence length in Nb ξ_S ~ 400 Å and reflects also linear density of distribution of vortices in Nb layer. Let's note, that, despite of quite high positive magnetization in niobium, all structure as a whole has the diamagnetic moment. The absolute size of the diamagnetic moment in Si/Mo is 2.5 times less than intensity of external magnetic field. This allows us to estimate penetration depth of magnetic field inside superconducting PS as $\lambda_{Si/Mo}$ ~ 800 Å. Absence of a vortex state at 5K is probably connected by that a layer of iron with nonzero magnetization shunts a magnetic flux, reducing intensity of a magnetic field in Nb layer. Estimations give H ≈ 150 Oe, that it is much less than H_{C1} ≈ 360 Oe.

Thus, it is established, that average magnetization in FM layer falls at downturn of temperature below critical on 30 % at 5K and 95 % at 2K. As decrease of diffuse scattering intensity with temperature decrease was detected it is possible to conclude that reduction of absolute size of local value of magnetization in the magnetic domain takes place. Calculations show, that observable falling of diffuse scattering can be described by reduction of local magnetization till 0.97 at 5K and 0.91 at 2K (magnetization at T = 15K is taken as unit). Authors express their gratitude for A.V.Petrenko, V.V.Proglyado, A. Kh. Islamov and A.I. Ivankov (FLNP JINR) for their help in measurements and M.A.Andreeva (Moscow State University) for fruitful discussion.

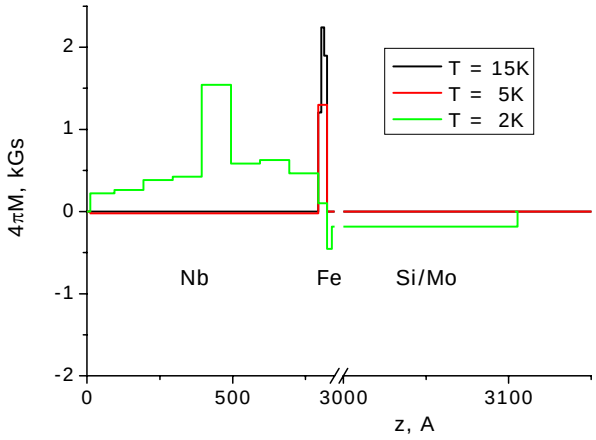

Fig.2. Magnetic profile of the structure at different temperatures.

1. P.W.Anderson, H. Suhl, Phys. Rev.,V.116 p. 898 (1959)
2. V.N. Krivoruchko and E.A. Koshina, Phys. Rev. B 66, 014521 (2002)
3. F. S. Bergeret, A. F. Volkov and K. B. Efetov, Phys. Rev. B 69, 174504 (2004)
4. Th. Muhge, et.al, Physica C 296 (1998) 325-336
5. I.A. Garifullin et al., Appl. Magn. Reson. 22, 439 (2002)
6. M.A. Anrdeeva et al., NIM B 266, 187-196 (2008)
7. M.A. Andreeva L. Haggstrom, B. Lindgren et. al., Hyperfine Interactions, 2004, v. 156-157, p. 607-613
8. A.J. Drew, S.L. Lee, D. Charalambous et. al, PRL 95, 197201 (2005)
9. V.L. Aksenov, K.N. Jernenkov, Yu.N. Khaidukov, et.al, Physica B 356, 9-13 (2004).
10. V. L. Aksenov, Yu.V. Nikitenko, A.V. Petrenko et. al, Crys. Rep. 52 pp. 381-386 (2007).
11. J.P. Goff, P.P. Deen, R.C.C. Ward et al., JMMM 240 (2002) 592-594
12. J. Stahn, J. Chakhalian, Ch. Niedermayer et al., PRB 71, 140509 (2005)
13. M.A. Anrdeeva et al., NIM B 266, 187-196 (2008)
14. http://www.kcsr.kiae.ru/stations/k6.6.php
15. N.K. Pleshanov, V.M. Pusenkov Z.Phys.B 100,p. 507, 1996

OFF-SPECULAR SCATTERING IN MAGNETIC NEUTRON WAVEGUIDES

S.V. Kozhevnikov[a], F. Ott[b], E. Kentzinger[c], A. Paul[c]

[a]*Frank Laboratory of Neutron Physics, JINR, 141980 Dubna, Moscow Region, Russian Federation*
[b]*Laboratoire Léon Brillouin, CEA/CNRS, UMR12, CEA Saclay, 91191 Gif sur Yvette Cedex, France*
[c]*Institut für Festkörperforschung, Forschungszentrum Jülich, D-52425 Jülich, Germany*

In order to produce submicron neutron beams [1], we are developing neutron waveguides (NWG). The large magnetic neutron cross section allows to fabricate guides in which the optical index can be dynamically modulated [2]. We produced NWG with the following tri-layer structure: Py(10-20nm)/Ti(10-80nm)/Py(10-50nm)//glass. The samples are produced by RF sputtering. The top permalloy layer acts as the coupling layer with the incident beam, the Ti layer as the guiding layer and the bottom layer as the reflecting layer (see Fig. 1). We have characterized our systems by polarized neutron reflectometry (specular and off-specular) on the reflectometer HADAS [3] at the FZ Jülich in order to probe the effect of the different imperfections (interface roughness, magnetic non-collinearity, dispersion of the layers thickness) on the reflectivity. A polarized neutron beam (λ = 4.52 Å) is sent onto the sample with an incident glancing angle α_i. A position sensitive detector is set after the sample and the scattered intensity is recorded as a function of α_f.

The neutron wave function (WF) density for ‘‘+’’ spin state is shown in Fig. 2 as a function of the sample depth z and the incident angle α_i. In the Ti guiding layer there are three resonance states (order m = 1, 2, 3) in the total reflection region. The zero order resonance m = 0 is absent for this system. The WF density is enhanced, at the interfaces in the Ti layer, by a factor of 10 – 30. The magnetic reflection of the waveguide has been measured in a saturating field of 100 Oe (see Fig. 3). At the resonance conditions, one observes marked dips in the total reflection. The reflectivities have been fitted with the program SimulReflec [4]. The fitted structure is PyOx(1.7nm)/Py(16.5)/Ti(79)/Py(46)//*glass* with an interface roughness σ = 1 nm. The regular dynamical reflectivity calculation cannot account for the large resonance dips (10 – 15 %). The diffuse off-specular scattering at one resonance position only represents 1 % of the specular signal and also cannot account for the dips. Thus to fit the data, we introduced an artificially high absorption in the Ti guiding layer (60 times the tabulated value of 6.09 b). However, we think that the neutrons are actually lost because they channel along the sample (over a distance up to 3 mm), exit at the edge of the sample and are lost for the specular reflectivity [5].

In the saturating field (Fig. 3) the magnetic Py layers are collinear and no spin-flip signal is observed $\left(R^{+-} = R^{-+} = 0\right)$. The magnetization M is 0.8 μB/at. or the upper Py layer and 0.9 μB/at. for the bottom one. Off-specular scattering in the saturated state is presented in Fig. 4 (left) in the axis coordinates (α_i, α_f). The diagonal $\alpha_i = \alpha_f$ corresponds to the specular reflectivity. Along the lines α_i = const and α_f = const one can observe the large off-specular scattering corresponding to the resonance modes (m = 1, 2, 3). The amplitude of off-specular reflection intensity normalized on specular reflection decreases from 10^{-2} near specular reflection to 10^{-3} for the larger angles. The off-specular reflection intensity integrated in the intervals $\Delta\alpha_i = \Delta\alpha_f$ = 1 mrad and along the off-specular angles α_i and α_f for one resonance mode consists of about 10^{-2} of the specular reflection intensity in the corresponding interval ($\Delta\alpha_i$, $\Delta\alpha_f$).

The signal has been modelled using the program sdms [6-7] based on the DWBA approximation [8]. It is possible to qualitatively account for the data by describing the system with magnetically collinear homogeneous layers (see Fig. 4 right). The shape and position of the diffuse scattering due to the guide effects (along the white lines) are easy to reproduce: it is simply necessary to introduce an in-plane roughness correlation length ξ of the order of 100 μm. It is thus possible to reproduce the spots of enhanced intensity corresponding to the intersections of 2 resonant modes. However, the roughness parameter σ cannot be evaluated. The modelling does not account for the

absolute value of the diffuse scattering and thus the absolute intensities cannot be adjusted to obtain a value for σ.

In conclusion, with these measurements, we have shown: (i) neutron resonance states in magnetic neutron waveguides lead to enhanced off-specular scattering up to 1 %; (ii) the amplitude of resonances on the reflectivity (10 %) mainly depends on wave guiding effect in Ti guiding layer and only a negligible part is connected to off-specular reflection; (iii) off-specular scattering can be observed without any micro-magnetic structure.

More detailed results of this investigation are published in [9].

This research project has been supported by the European Commission under the 6th Framework Programme through the Key Action: Strengthening the European Research Area, Research Infrastructures. Contract n°: RII3-CT-2003-505925.

[1] F. Pfeiffer et al., Phys. Rev. Lett. 88 (2002) 055507-1.
[2] S.P. Pogossian et al., Phys. Rev. B 53 (1996) 14359.
[3] U. Rücker et al., Physica B 297 (2001) 140.
[4] SimulReflec : http://www-llb.cea.fr/prism/programs/simulreflec/simulreflec.html
[5] V.K. Ignatovich, F. Radu, Phys. Rev. B 64 (2001) 205408-1.
[6] E. Kentzinger et al., Physica B 335 (2003) 89.
[7] E. Kentzinger et al., Physica B 335 (2003) 82.
[8] B.P. Toperverg, Physica B 297 (2001) 160.
[9] S.V. Kozhevnikov et al., Physica B (2007) 68-70.

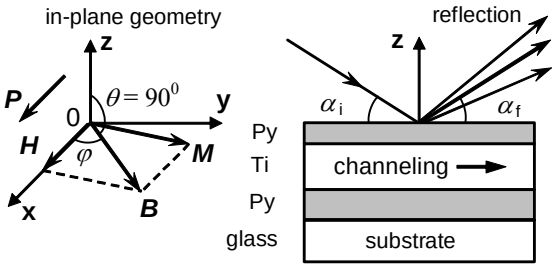

Fig. 1. Reflection from a magnetic neutron waveguide.

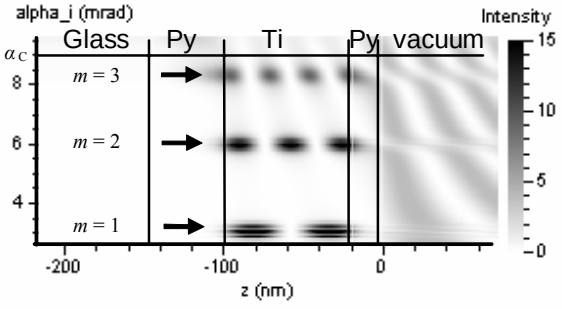

Fig. 2. Wave function density "+" inside the waveguide structure vs the incidence angle α_i and the sample depth z (calculated using SimulReflec [4]). The Ti guiding layer is 80 nm thick.

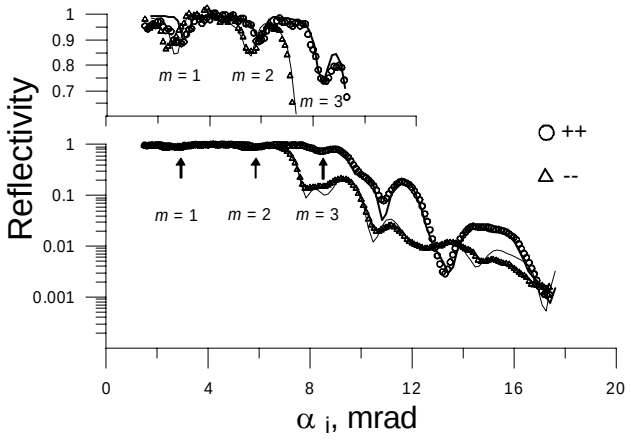

Fig. 3. Specular reflectivity for the waveguide Py(20nm)/ Ti(80)/Py(50)//*glass* (points are experiment, lines are fit, insets are linear scale for total reflection).

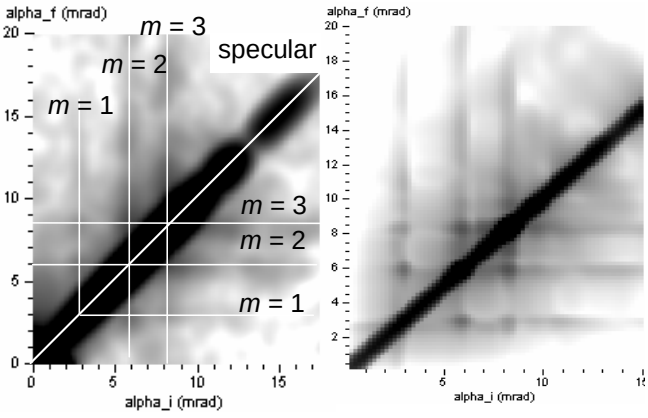

Fig. 4. Off-specular scattering (UP-UP) in the saturated state: (left) experiment – (right) simulation.

Neutron Spin Turners with a Rotating Magnetic Field: First Experiments

V I Bodnarchuk[1], W H Kraan[2], M T Rekveldt[2] and A Ioffe[3]

[1]*Frank Laboratory of Neutron Physics, Joint Institute for Nuclear Research 141980 Dubna, Russia.*

[2]I*nterfaculty Reactor Institute, Delft University of Technology, Mekelweg 15, 2629JB, Delft, The Netherlands.*

[3]*Institut für Festkörperforschung, Forschungszentrum Jülich GmbH, Jülich Centre for Neutron Science at FRM II, Lichtenbergstr. 1, 85747 Garching, Germany*

In the neutron resonance flipper [1] the neutron spin (seen in the rotating frame) rotates around the angle of π around the resonance magnetic field created by the superposition of two perpendicular magnetic fields: a constant field along the z-axis and a rotating in the x-y plane. However, it is possible to achieve the same effect using a magnetic field rotating in the y-z plane of a thin spin turner. If the neutron procession (Larmor) frequency $\omega_L=\gamma \boldsymbol{B}$ defined by the magnetic field strength $\boldsymbol{B}$ (γ is the gyromagnetic ratio for the neutron) is much higher than the frequency ω of the field rotation and the spin turner is thin enough, so that the vector $\boldsymbol{B}$ is not rotated significantly during the neutron propagation across the spin turner, then, after the π-procession of the neutron spin around vector $\boldsymbol{B}$, it will again arrive in the y-z-plane, i.e. effectively rotating with the frequency 2ω around an instant position of the magnetic field vector. Using such spin turners, it is possible to build a new type of the spin-echo spectrometer [2].

As the working material for the spin turner we chose the thin foil of the metallic glassy alloy $Fe_{78}B_{13}Si_9$ of thickness 25 μm (fabricated by the Goodfellow) that features a high frequency susceptibility (300-500 kHz) and an extreme magnetic softness, so that the external magnetic field smaller than 50 mG is required to control the film magnetization.

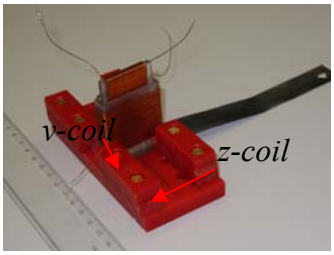

***Fig 1**. The coil configuration containing the foil.*

We put the foil into the field composition generated by the y-coil inside the z-coil, with fields $B_y=A_y cos(\omega t)$ and $B_z = A_z sin(\omega t)$ (see Fig. 1). When added, they produce the field rotating in the y-z plane at the circular frequency ω. Currents in these coils are generated by two KEPCO amplifiers, controlled by the software of the spectrometer PANDA (TU Delft) [3]. The phase of KEPCO-y is delayed by 90° with respect to KEPCO-z. Data are collected in "dynamic mode" in N_{chan} = 100 channels per revolution, coupled to the rotation of the field. When energising y- and z-coils simultaneously, the currents are carefully adjusted to be equal and shifted by $\pi/2$ by an oscilloscope.

The response of a monochromatic (λ=0.2 nm) polarised neutron beam is measured by 3D polarisation analysis [3]. While the neutron beam propagates across the coil system, the polarisation subjected to the rotation $R^{(z)}(\varepsilon)$ around z by the field of the outer coil before and after the inner coil, where $\varepsilon = c\lambda B_z((l_z - l_y)/2)$ with $B_z=B_z^{max}cos(\omega t)$. We transform the argument ωt into the time channel n by means of $\omega t = 2\pi(n/N)$. (N - the total number of time channels). To account for the

delay $\tau = l_{foil\text{-}det}/v$ between the foil and the detector, ωt is diminished by φ. Hence, the rotation ε in the z-field before and after the inner coil is given by

$$\varepsilon = \left(c\lambda |B| \frac{l_z - l_y}{2} \right) cos\left(2\pi \frac{n}{N} T - \varphi \right) \equiv \varepsilon' cos\left(2\pi \frac{n}{N} T - \varphi \right) \quad (1)$$

When entering the inner coil *(y),* the polarisation vector is subjected to the rotating magnetic field denoted $\tilde{B}$. We describe the rotation in this field in the coordinate system, where the vector **B** remains pointing along the z direction by the (3x3) matrix $R^{(z)}(\Phi)$, and

$$\Phi = c|\tilde{B}|\lambda\, l_y. \quad (2)$$

Transformed into the laboratory system this matrix becomes:

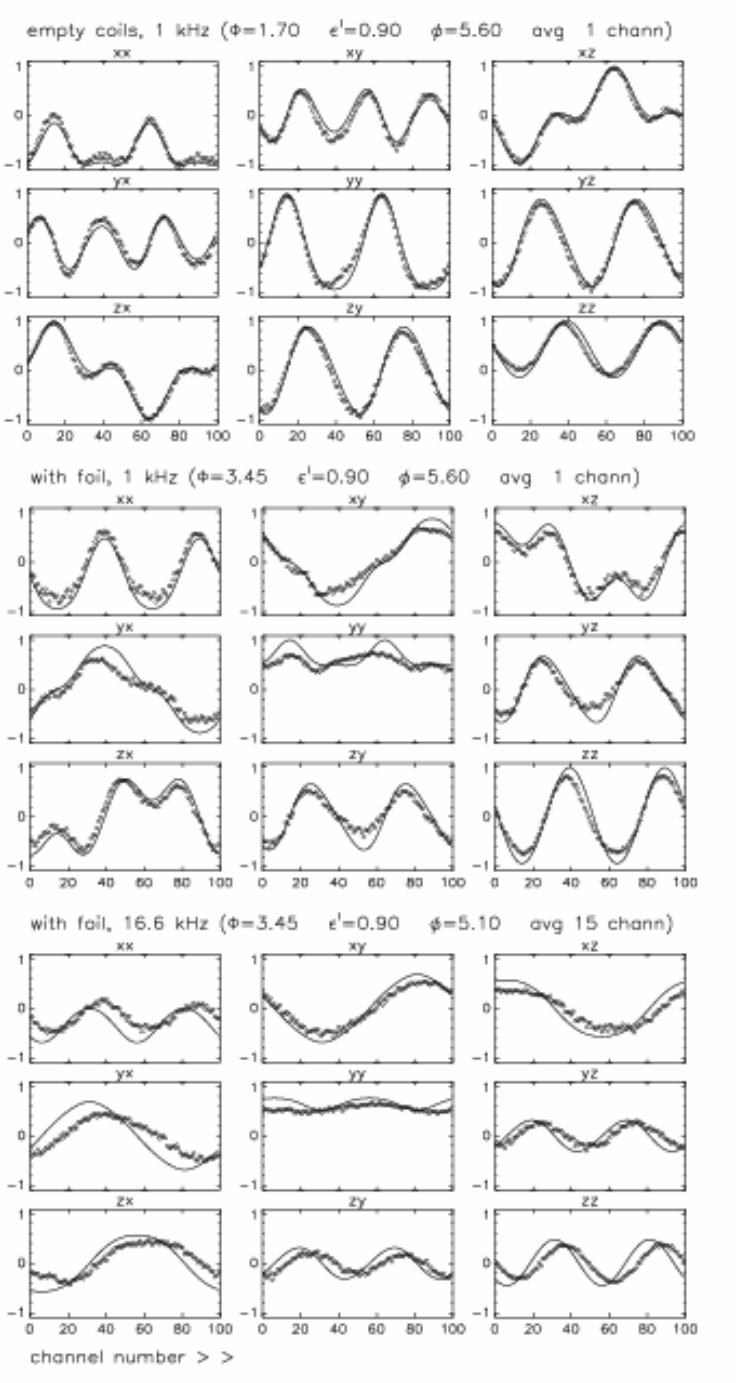

$$R^{(x)}(\theta)R^{(z)}(\Phi)R^{(x)}(-\theta) \quad (3)$$

where the angle $\theta = \omega t$ between the positive z-axis and the rotating field, in analogy with the phase of B_z, is written:

$$\theta = 2\pi \frac{n}{N} T - \varphi \quad (4)$$

Here we neglect the field component along the rotation axis x $B_x = \omega/\gamma$. Hence, the complete transformation undergone by the polarisation vector reads:

$$R(\varepsilon, \Phi, n, \varphi) = R^{(z)}(\varepsilon)R^{(x)}(\theta(n,\varphi))R^{(z)}(\Phi) \times \times R^{(x)}(-\theta(n,\varphi))R^{(z)}(\varepsilon), \quad (5)$$

where ε, Φ and $\theta(n,\varphi)$ are given by eqs. (1), (2) and (3). They contain ε', Φ and φ as parameters. Eq.(1) for the lengths l_y and l_z given above, combined with $|B|$=16 G gives ε'=0.9. Eq.(2) in the case of empty coil gives Φ=1.7, when the foil is mounted Φ=3.45. Above we found for 1 kHz: φ=5.6 rad.

Fig 2. *Elements of the depolarisation matrix with rotating magnetic fields, measured (circles) and calculated according to Eq.(5) (lines) as the function of the time channel in one cycle of the field: (a) empty coil system, 1 kHz; (b) with the foil 1 kHz, (c) idem, 16.6 kHz. It is seen at 16.6 kHz that the measured matrix elements "lag behind" the calculated elements by about 7 channels.*

Figure 2(a) contains the depolarisation matrix elements for the empty coil system at 1 kHz; Figure 2(b) gives the same, with the foil in the coil

system. The lines refer to the results calculated according to Eq.(5) with properly chosen ε', Φ and φ as parameters. The simulation gives a rather consistent description of the observed matrices, especially at low frequencies. This is seen from comparing the data points at 1 kHz (circles) with the full lines (simulations). At higher frequencies the phenomena become smeared over time channels, as to be expected from the wavelength spread of PANDA. For the simulation at frequencies above 10 kHz, the values for the parameter φ, is more than 10 times 2π within the precision of 5%. Reduced between 0 and 2π, this parameter gets an uncertainty corresponding to the half field period. To obtain a more precise value we carried out simulations for the empty beam measurements, choosing φ in a such way that the simulations coincide with measurements. These values of φ were used to simulate measurements with the foil; Figure 2(c) (see parameters below) shows the result for 16.6 kHz. Measured matrix elements appear to be shifted by about 7 channels (~4μs) towards the calculated data. This means that the magnetization in the foil "lags behind" the imposed rotating field. At 20 kHz this effect amounts to 6μs. Simultaneously, we observe that the determinant decreases with an increasing frequency. Both phenomena indicate the presence of a domain structure, which becomes increasingly difficult to eliminate at higher frequencies, so the much stronger field is required to achieve the foil's saturation at higher frequencies. We have shown that the intended field configuration is reasonably realised and the behaviour of the observed polarization vector corresponds to the calculations. The increasing depolarisation and the fact that the magnetisation lags behind the rotating field at 16 kHz suggests that the proposed concept of a ferromagnetic foil with rotating magnetization for a spin turner has a limited range (5-10 kHz) of frequencies. From the point of view of applications of such foils, for purposes of the rotating magnetic field neutron spin-echo spectroscopy it means a limited range in the spin-echo time; in SESANS a limited maximum spin-echo length. Perhaps the reason of high depolarisation is the domain structure in the studied amorphous ferromagnetic foil. Indeed, the present alloy needs much stronger field (>30 G) to get fully magnetised, so for our practical purposes another alloy may be required.

Acknowledgement

The project has been supported by the European Commission under the 6th Framework Programme through the Key Action: Strengthening the European Research Area, Research Infrastructures. Contract n°: HII3-CT-2003-505925 .

The full text of this work is available in Meas.Sci.Technol.19 (2008) 034012.

References

[1]. Gähler R, Golub R 1984 *J. Phys.* C **3-229** 45; Golub R, Gähler R 1987 *Phys. Lett* A**123** 43.
[2]. Ioffe A 2003 *Physica B* **335** 169-173.
[3]. Rekveldt M Th 1973, *Z.Physik* **259** 391; Rekveldt M Th, 1971 *J.de Physique* **32** 579
[4]. Mezei F 1972, *Z.Phyzik* 255, 146

DISPERSION RELATION FOR LIQUID LITHIUM STUDY BY MEANS OF INELASTIC NEUTRON SCATTERING

N M Blagoveshchenskii, A G Novikov, M.A.Pashnev,V V Savostin

State Scientific Center of the Russian Federation, Institute for Physics and Power Engineering, 1 Bondarenko Sq., 249033 Obninsk, Kaluga region, Russian Federation

We report here the main results for liquid lithium obtained with the help of experiment held on the neutron TOF-spectrometer DIN-2PI incorporated with the pulsed reactor IBR-2 [1]. The first set of these results is accumulated in the detailed study of frequency spectrum inferred from the incoherent part of neutron scattering (E_0=31 meV) by liquid lithium at T=227C, 397C, and 557C [2]. The aim of present communication is to demonstrate some collective modes of motions in liquid lithium medium, in contrary with individual atoms motions studied in paper [2] where essentially the incoherent scattering of neutrons has been taken into account.

To separate the coherent one-phonon component from incoherently scattered component, and to evaluate the quasielactic, multiple and multiphonon content in the resulting double-differential scattering (DDS) cross-section, the computer code SLOWN [3] has been used. Typical coherent DDS in the energy scale after subtraction of incoherent component and multiple and multiphonon pattern in "Q=*const*" representation is shown at fig.1 together with its decomposition onto two lorentzians. Fig.2 demonstrates a degree of advantage to use the "Q=*const*" representation in the comparison of case "Θ=*const*". A very close resemblance is due to high extent of vertical-like behaivour of scattering conservation laws for the 31 meV initial energy.

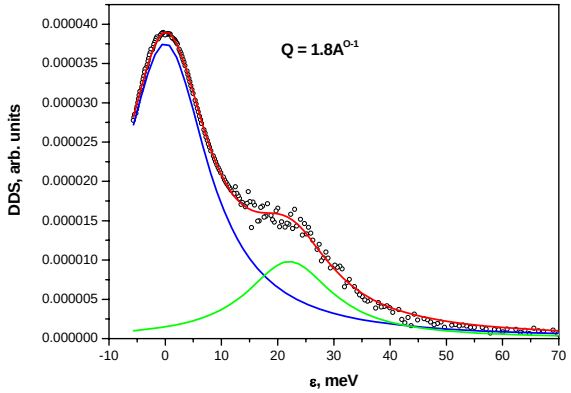

Fig.1 DDS's for Q=1.8A^{O-1} for subtracted quasielastic(incoherent) peak as well as multiple and multiphonon patterns. Two-lorentzian decomposition marks the quasielastic and inelastic coherent peaks

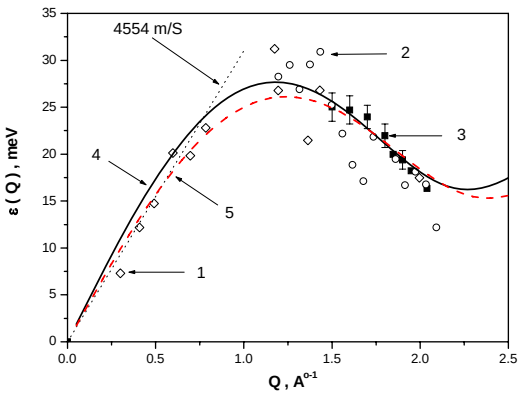

Fig.2 Primary dispersion curves. Dash – - for data 1 and 2 [4].4-first iteration data of present study (3). Our points without errorbars illustrate approach where the condition Θ=*const* is held

Dispersion curves obtained were evaluated by correctly taking into account the coherent component, in accord with the formula [5]:

$$S(Q,\omega)=\frac{S(Q)}{\pi}\cdot\frac{\tau\omega_0^2\left[\omega_L^2-\omega_0^2\right]}{\left[\omega\tau(\omega^2-\omega_L^2(Q))\right]^2+\left[\omega^2-\omega_0^2(Q)\right]^2} \qquad (1)$$

Here S(Q)-the structure factor of liquid lithium,

$\tau(Q) = \frac{1}{2}\left(\frac{\pi}{\omega_L^2 - \omega_0^2}\right)^{1/2}$, and ω_0 and ω_L obey the following expressions:

$$\omega_0^2(Q) = \frac{k_B T Q^2}{MS(Q)}, \qquad \omega_L^2(Q) = \frac{3k_B T Q^2}{M} + \omega_K^2(Q), \text{ where}$$

$$\omega_K(Q) = \omega_E\left[1 - \frac{3\sin(Qr_0)}{Qr_0} - \frac{6\cos(Qr_0)}{(Qr_0)^2} + \frac{6\sin(Qr_0)}{(Qr_0)^3}\right]^{1/2}, \quad \omega_E = \left[\frac{4n\pi}{3M}\int g(r)\frac{\partial^2 U(r)}{\partial r^2} r^2 dr\right]^{1/2} \qquad (2)$$

The dispersion curve expression (2) is correct for longitudinal oscillations [6], and is applied for next iterations. Full-component result of development is depicted by fig.3 and fig.4.

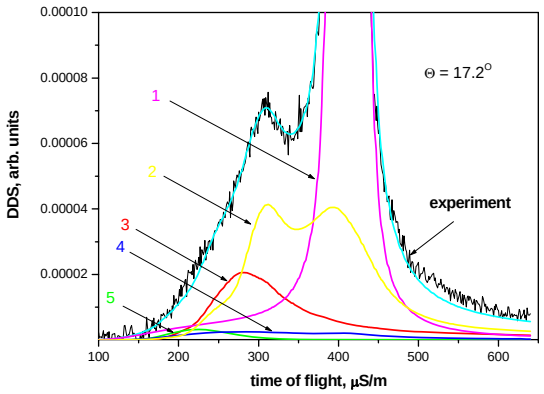

Fig.3 The typical decomposition of experimental data into following components:
1- quasielastic (QE) incoherent;
2- coherent inelastic and QE by (1);
3- incoherent inelastic (see fig.1);
4- total (coherent and incoherent) multiple;
5- multiphonon component

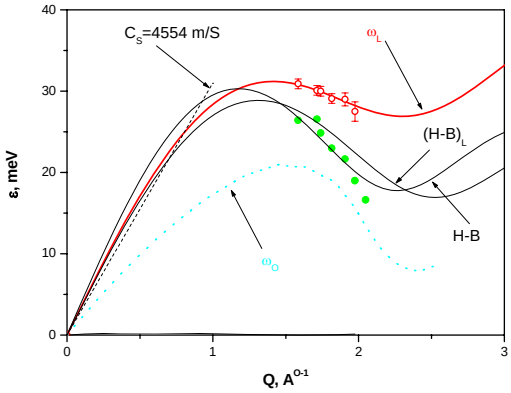

Fig.4 Final values of ε(Q) data obtained by iterations using SLOWN(fulled symbols) and its fit by (2) (H-B). Up and down curves - ω_L and ω_0; $(H\text{-}B)_L$- the component (2) of ω_L in the representation of S(Q,ω) in form of longitudinal currents

Remark that curves (H-B) and $(H\text{-}B)_L$ corresponding to the usual and current dispersion relations do not coincide. One can take the averaged value of interatomic distance and E_E, namely:

$$r_0 = 3.12 \pm 0.08 A^0, \qquad E_E = 22.4 \pm 0.4 meV \qquad (3)$$

Note that interatomic distance (3) coincides with doubled radius of atom, 2R = 2*1.56 = 3.12A^O. It should be noted also a good accordance of the slope of obtained ε(Q) at Q→0, and the hydrodynamic sound velocity, with a slightly revealed anomalous positive dispersion (fig.4).

Another way to use data on dispersion relation is possible extraction of the interatomic potential U(r) on the basis of estimated dependence U(Q). On the one hand, we have for ε(Q) the expression (2), fitting the experimental data. On the other hand, there are a lot of theoretical formulas linking the kinetic and potential energy of atoms onto the elementary excitation's energy. For example, a very simple expression of this type is represented as follows [7]:

$$\varepsilon(Q) = \left[\left[\frac{Q^2}{2M}\right]^2 + nU(Q)\frac{Q^2}{M}\right]^{1/2} \qquad (3)$$

This expression gives linear behavior at small values of Q, ε(Q→0) = CQ, $C = \left[nU(Q)/M\right]^{1/2}$,

appearance of local maximum and minimum of $\varepsilon(Q \sim 2\pi / r_0)$ for $Q = 1 - 2A^{O-1}$ and asymptotic form of free-atom dispersion, $\varepsilon(Q>>1) = Q^2/2M$ for very large values of Q.

From theoretical expression (3) and experimental (2) one can infer the Fourier-component of interatomic potential U(Q). Next, using the inverse Fourier transform, one obtains:

$$U(r) = \frac{1}{2\pi^2 nr}\int_0^\infty U(Q)Q\sin(Qr) \qquad (4)$$

This radial distribution has a first pronounced minimum at $r = 3.15A^O$. This value agrees very well with mean interatomic distance estimated previously, $r_0 = 3.12A^O$. Unfortunately, the second derivative of U(r) at minimum point has overestimated value. However, if one regards somewhat modified the dispersion relation $\varepsilon(Q)$ as asymptotically approaching the free atom dispersion at $Q \geq 4A^{O-1}$, while having the first minimum of the same type as depicted at fig.4, the agreement between result to be obtained and estimated value of $d^2U(r)/dr^2$ [2] will be better. The value of $d^2U(r)/dr^2$ at minimum point becomes ~ 18.0 n/m, and minimum depth $U_{min} \sim 80$ meV, in accord with other theoretical estimation [8]: $d^2U(r)/dr^2 = 18.5$ n/m; $U_{min} \sim 75$ meV.

Note that this mentioned form of U(Q) leads also to the almost total absence of Friedel oscillations in radial dependence of U(r), tending the potential shape to the Lennard-Jones kind.

REFERENCES

1. User Guide. Neutron Experimental Facilities for Condensed Matter Investigation at JINR. Ed. by Sikolenko V. Dubna: JINR Press, 1997. P. 25.
2. N.M. Blagoveshchenskii, V.A. Morozov, A.G. Novikov, M.A. Pashnev, V.V. Savostin, A.L. Shimkevich. Crystallography Reports. 52 (2007) 460.
3. Лисичкин Ю.В. и др. Учет конечных размеров образца при обработке измерений дважды-дифференциальных сечений рассеяния медленных нейтронов: ВАНТ.-Сер. Ядерные константы.-1979.-Вып.2.-С.12-24
4. P.H.K. de Jong, P.Verkerk and L.A. de Graaf. Collective Modes at Very Short Wavelengths in Liquid Lithium. Journ. of Non-Crystalline Solids 156-158, 1993, 48
5. S. Lovesey. J. Phys. C, 4 (1971) 3057.
6. J.Hubbard and J.L.Beeby. Phys.Rev. C 2,1969, 556
7. Н.Н.Боголюбов, Д.Н.Зубарев. Волновая функция нижнего состояния системы взаимодействующих бозе-частиц. ЖЭТФ, 28(2), 1955, 129-139
8. M.Canales, J.A.Padro, L.E.Gonzalez and A.Giro. Molecular dynamics simulation of liquid lithium. J.Phys.:Condens.Matter 5, 1993, 3095

New optical effect was firstly observed with UCNs

A.I.Frank, G.V.Kulin,

Frank Laboratory of Neutron Physics, Joint Institute for Nuclear Research, Dubna, Russia

D.V.Kustov,
Frank Laboratory of Neutron Physics, Joint Institute for Nuclear Research, Dubna, Russia
and
Institute for Nuclear Research, Kyiv,Ukraine

P.Geltenbort , M. Jentschel,.
Institute Laue Langevin,Grenoble, France

V.G.Nosov, A.N.Strepetov
Russian scientific center "Kurchatov Institute", Moscow, Russia

Abstract

As that was recognized recently after the wave of any nature passed through the spatially restricted medium volume which is moving with linear acceleration, the wave frequency and correspondent energy change. This effect is universal and seems was not been detected till recently. Using of UCN allowed us to demonstrate it in neutron experiment.

It is well known for any wave that the wave number k in a medium is related to its vacuum value k_0 by the index of refraction. The generally recognized understanding is when the wave leaves the medium back to vacuum the absolute value of its wave number is exactly equal to the incident wave number, although the propagation direction may be different. This statement is valid for all types of waves, but only for the case of a medium in rest or moving with constant velocity. In the latter case a sample movement may only result in the change of the phase of the transmitted wave due to the change of the effective length $\Delta L = v\tau$ of the sample. Here $\tau = L/nc$ is the passage time through the sample of length **L,** and **c** – wave speed in vacuum.

However, at the end of the last century it was found theoretically, that wave number and frequency change when the wave passes through an accelerating sample of a refractive medium. That was firstly shown by K.Tanaka [1] for the case of light optics. Later the same result was derived for neutron waves [2,3].

More generally, a refractive index may be introduced for waves of any nature and the only requirement is the presence of scattering centers in the medium. Therefore particles of any nature should change their energy passing through the bounded volume of accelerating medium [4].

It is worth noting that the Tanaka effect is so small, that despite the fantastic sensitivity of modern optical methods it hasn't been observed yet. However, the neutron-optics experiment of this kind appeared to be feasible and was performed recently.

If a neutron passes through a refractive sample, which is moving with acceleration **a**, it changes its energy by $\Delta E = \left(\frac{1-n}{n}\right) maL$. Using of **U**ltra **C**old **N**eutrons (UCN) limits the sample thickness *L* due to the strong absorption in matter. However, this disadvantage is completely compensated by two factors: i) In the case of UCNs the factor $(1-n)/n$ is rather high and its value may be as high as 0.5. For cold neutrons with wavelength, for instance, 2 nm, this value is of order 10^{-3}. ii) UCN spectrometry methods based on neutron Fabri-Perot interferometers have extraordinary sensitivity.

Namely such a spectrometer based on two Fabri-Perot wave length filters (see for instance Annual Report 1999) was used for detecting the effect of accelerating medium in neutron optics. Samples of silicon wafers of thickness 0.6 mm and 1.85 mm were placed between the two filters. The Si-Samples were oscillated with frequencies 40 Hz and 60Hz, which gave a periodically modulated acceleration achieving maximum values of about 10g (g – free fall acceleration).

The value of energy change to be detected was about 0.2÷0.6 neV. The periodical modulation of the acceleration imposes a periodical change of neutron energy. Due to the narrow band pass properties of the spectrometer this should lead to an oscillation of the neutron count rate. Additionally the total neutron count rate is influenced by other effects. However, measuring the phase of the count rate oscillation provided the unambiguous way to select the effect of accelerating medium from other systematical effects. Picture 3 shows results of one of these measurements. Drawn results are in a quite good agreement with theoretical predictions and are in a drastic contradiction with the assumption when effect is absent.

So, using UCN gave one the possibility to show new optical effect that is of universal nature.

References

1. K.Tanaka. Phys.Rev.A. 25 (1982) 385.
2. F.V. Kowalski. Phys. Lett.A. 182 (1993) 335.
3. V.G.Nosov, A.I.Frank. Phys. of Atomic Nuclei. 61 (1998) 613.
4. A.I. Frank, P.Geltenbort, G.V.Kulin, D.V. Kustov, V.G. Nosov and A. N. Strepetov. JETP Letters. 84 (2006) 363.

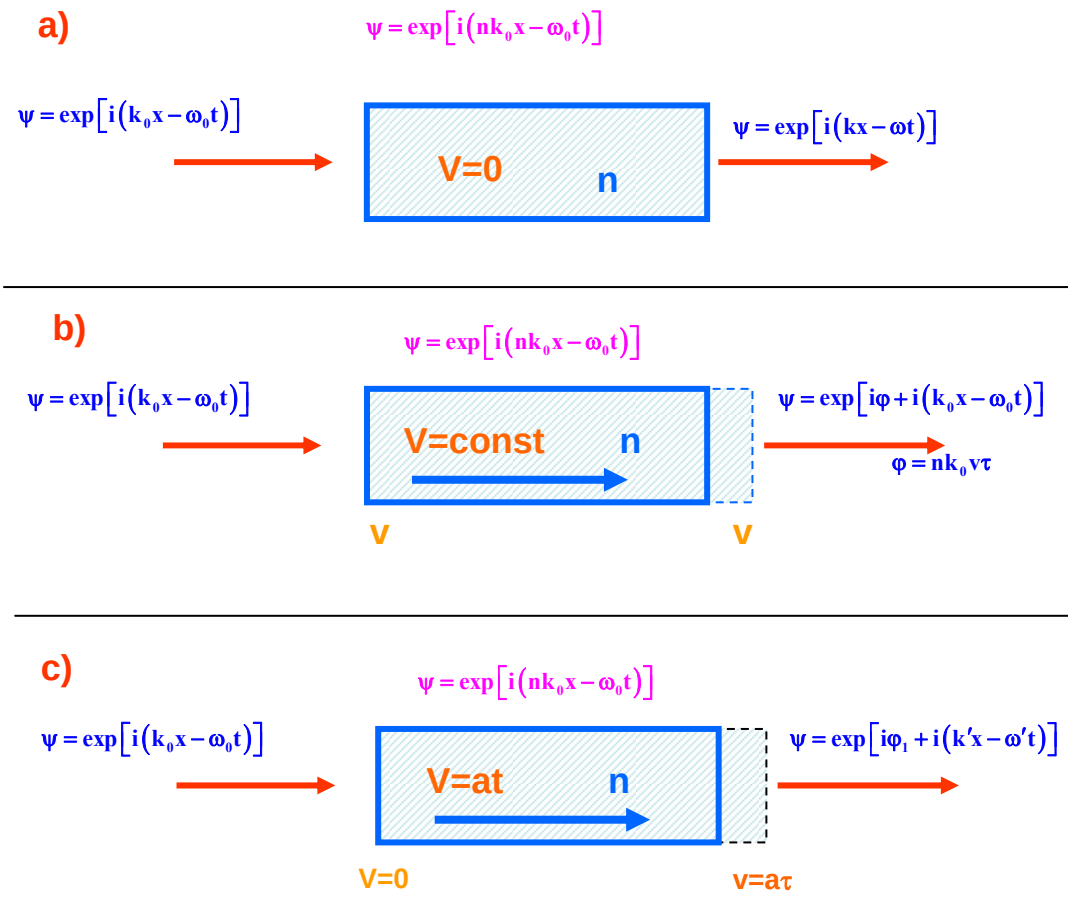

Fig.1. When the sample is in rest a) or moving with permanent velocity b) the wave vector and frequency of the transmitted wave are the same as for the initial wave. The motion of the sample with permanent acceleration c) causes the change of the wave frequency and of the corresponding wave number. In the case of the matter wave the particle energy $\mathbf{E' = \hbar\omega'}$ also differs from the initial value $\mathbf{E_0 = \hbar\omega_0}$

Fig.2. Gravity UCN spectrometer. An electro-magnet driver inducing a harmonical motion to the sample is installed at the upper flange.

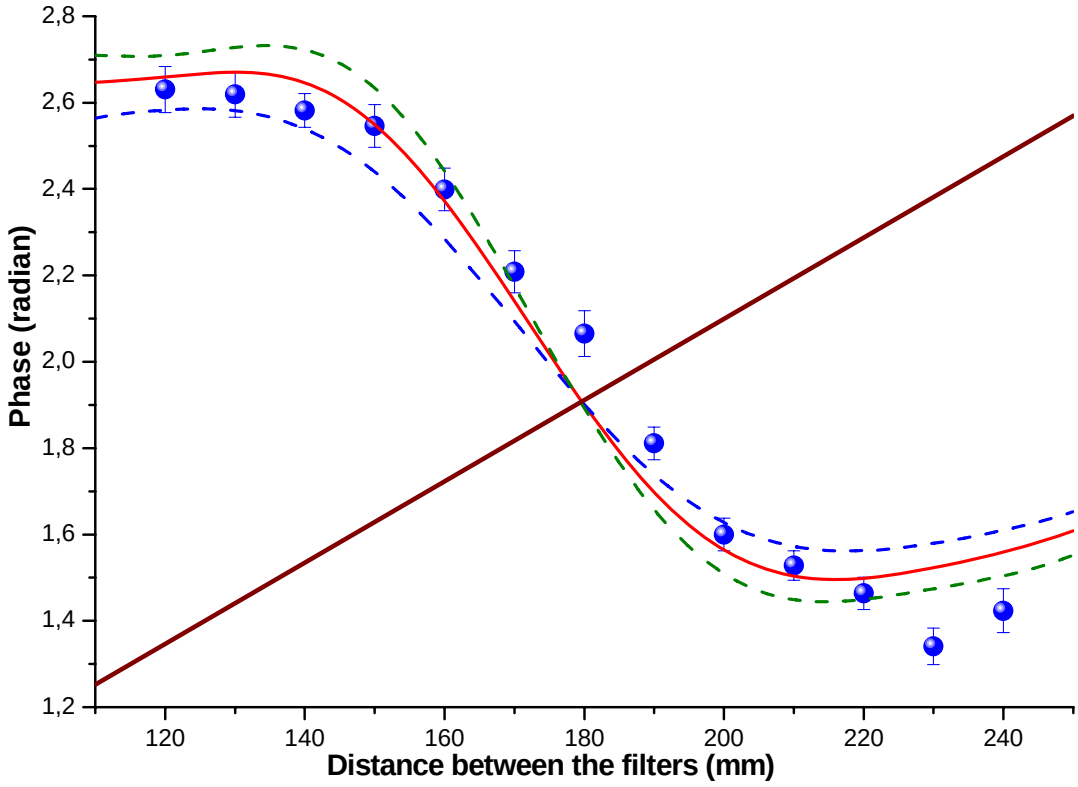

Fig.3. Phase of the count rate oscillation as a function of the distance between the two Fabri-Perot interferometers. Blue points – experimental results. Red curve – theoretical prediction. Wine straight line is the result of simulation in the assumption of the absence of the accelerating matter effect.

Differential and Angle-Integrated Cross Section Measurement for the $^{64}Zn(n, \alpha)^{61}Ni$ Reaction at 2.54, 4.00 and 5.50 MeV.

Yu. M. Gledenov, M. V. Sedysheva
Frank Laboratory of Neutron Physics, JINR, Dubna,141980, Russia
G. Khuukhenkhuu
Nuclear research Centre, National University of Mongolia, Ulaanbaatar, Mongolia
P. J. Szalanski
University of Lodz, Institute of Physics, Poland
Jiaguo Zhang, Rongtai Cao, Li-an Guo, Jinxiang Chen, Jianyong Wang, Guohui Zhang
Key Laboratory of Heavy Ion Physics, Ministry of Education and School of Physics, Peking University, Beijing 100871, China

Introduction

There are large discrepancies among the few existing evaluations and measurements for the $^{64}Zn(n,\alpha)^{61}Ni$ reaction cross sections [1-5]. The activation method is not feasible for this cross section measurement because the residual nucleus ^{61}Ni is stable. In our previous work, differential and angle-integrated cross sections of the $^{64}Zn(n,\alpha)^{61}Ni$ reaction were measured at 5.03 and 5.95 MeV by using a twin-gridded ionization chamber (GIC) [1]. Now we extended our measurements to 2.54, 4.00 and 5.50 MeV to get the near threshold and systematic behavior of this reaction.

Experiment

The experiment was performed at the 4.5 MV Van de Graaff accelerator of Peking University, China. Quasi- monoenergetic neutrons were produced through the $T(p,n)^3He$ reaction with the solid Ti-T target (0.80 mg/cm^2). The energy of the accelerated protons before enter the solid target was 3.35 MeV, and the corresponding neutron energy was 2.54 ± 0.03 MeV.

The deuterium gas target was used to produce neutrons through the $D(d,n)^3He$ reaction. The gas cell was separated from the vacuum tube by a 5 μm thick molybdenum film. The length of the cell was 2.0 cm, and the deuterium gas pressure was 2.65~2.80 atm. The energies of the accelerated deuterons before entering the film were 1.77 and 2.84 MeV, and the corresponding neutron energies were 4.00 ± 0.21 and 5.50 ± 0.13 MeV, respectively.

The twin GIC was constructed at Frank Laboratory of Neutron Physics, Dubna Russia. The detailed structure of the chamber was described in [6]. The working gas of GIC was Kr +2.68%CO_2. The pressures of the working gas were 0.90, 1.25 and 1.55 atm for 2.54, 4.00 and 5.50 MeV measurements.

Two ^{64}Zn samples (mass 4.05 ± 0.05 mg and thickness 266.3 μg/cm^2 each) back-to-back attached to the common cathode were used for forward (0 to 90°) and backward (90 to 180°) alpha event measurement simultaneously. The abundance of the ^{64}Zn isotope material was 99.4%. Each sample was evaporated on a tantalum backing 4.8 cm in diameter and 50 μm in thickness. The absolute neutron flux was determined by a ^{238}U foil (7.85 ± 0.10 mg, ∅4.50 cm, abundance 99.999%). The $^{238}U(n, f)$ cross section was taken from the ENDF/B-VI.8 library. Two compound alpha sources were used for the adjustment of electronics and energy calibration of the data acquisition system. It is suitable to change sample positions using the sample changer without opening the chamber.

A BF_3 long counter was used as neutron flux monitor. The axis of the BF_3 long counter and the center of the GIC was placed at 0° to the beam line (fig.1). The electrodes of the chamber were perpendicular to the beam line. The distance from the front side of the BF_3 long counter to the neutron target was about 2.9 m. For E_n=2.54 MeV measurement, the distance from the solid Ti-T target to the common cathode of the twin chamber was 23.9 cm. For E_n=4.00 and 5.50 MeV measurements, the distance from the center of the gas cell to the cathode was 18.4 cm.

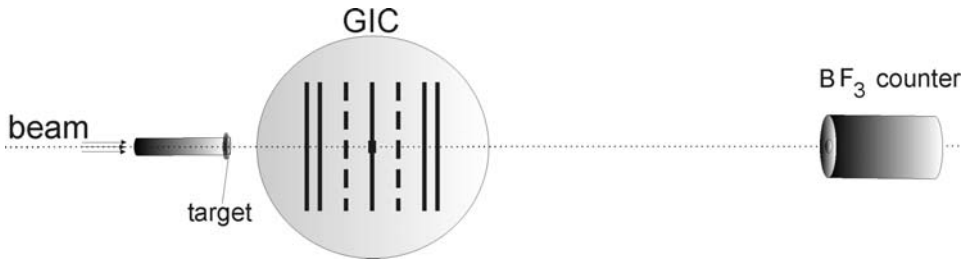

Fig. 1. Experimental setup.

Results

The cathode-anode two-dimensional spectrum for forward α-particles and differential energy spectrum ($0.8 \le \cos\theta_L < 0.9$) at E_n=5.50 MeV are shown in Fig. 2. and Fig. 3.

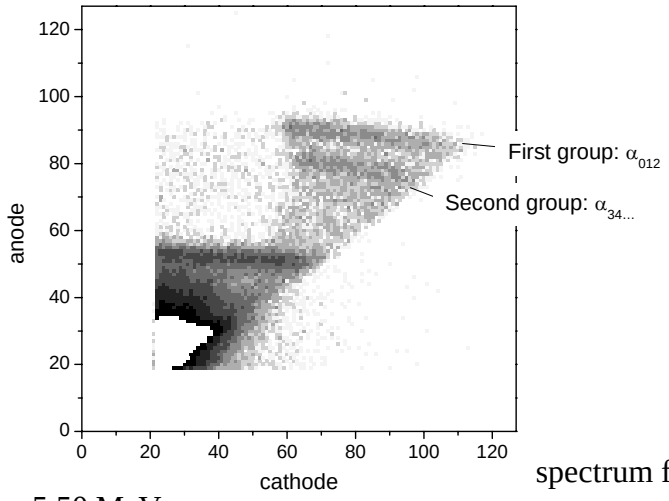

Fig. 2. Two-dimensional spectrum for forward α-particle measurement at E_n= 5.50 MeV

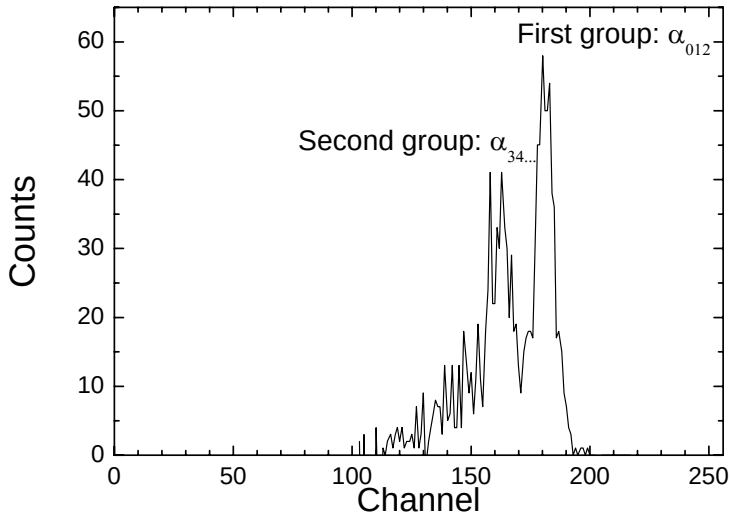

Fig. 3. Alpha-particle differential energy spectra for En = 5.50 MeV ($0.7 \le \cos\theta_L < 0.8$)

Two major groups of alpha particles can be found from the figures. The first group (with higher energies) corresponds to three energy levels of ^{61}Ni (ground state, the first and the second excited states of 67 and 283 keV). The second group corresponds to higher excited states of ^{61}Ni.

The measured differential cross sections for the ^{64}Zn(n, α_{012})^{61}Ni and ^{64}Zn(n, $\alpha_{34...}$)^{61}Ni reaction (correspond to the first and the second group of alpha particles) in the center of mass system are plotted in Figs. 4 - 6. Even though the beam time for E_n=2.54 MeV was 56.5 h, there were still too less $\alpha_{34...}$ particles to get the differential cross sections of the ^{64}Zn(n, $\alpha_{34...}$)^{61}Ni reaction at this energy point.

In Fig.7 the present cross sections are compared with existing data.

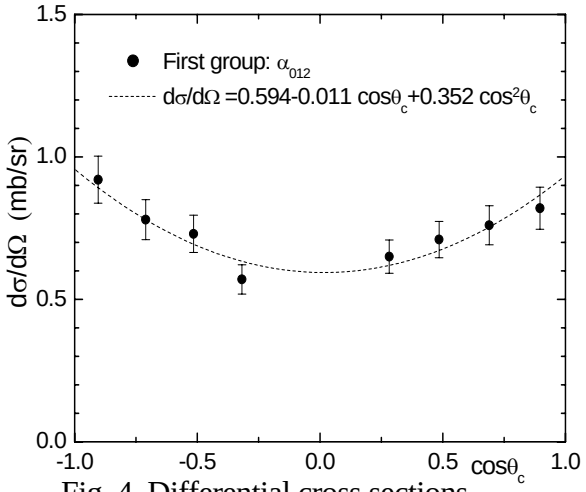

Fig. 4. Differential cross sections of the first group of α particles in the c.m. system at E_n = 2.54 MeV

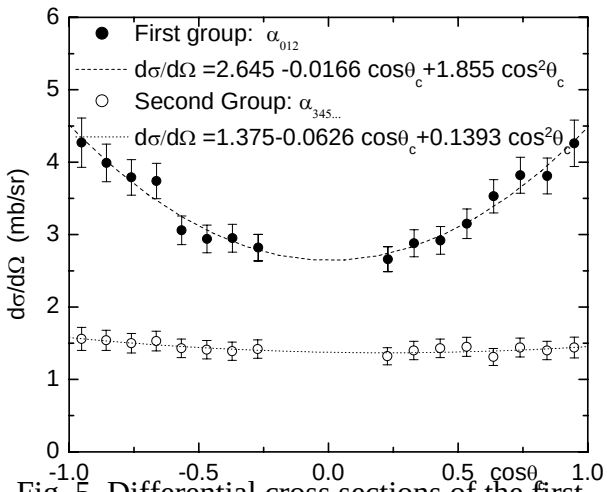

Fig. 5. Differential cross sections of the first and the second group of α particles in the c.m. system at E_n = 4.00 MeV

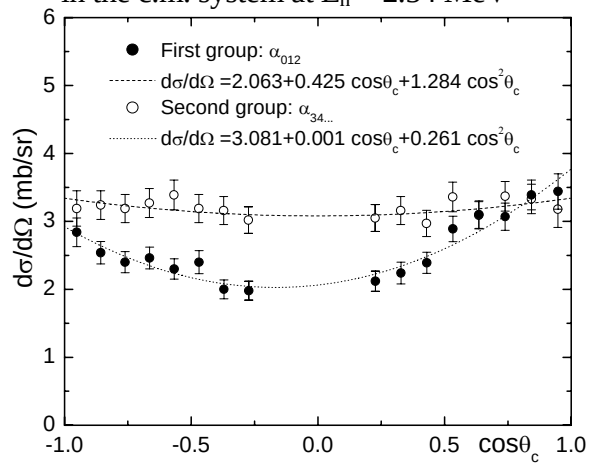

Fig. 6. Differential cross sections of the first and the second group of α particles in the c.m. system at E_n = 5.50 MeV

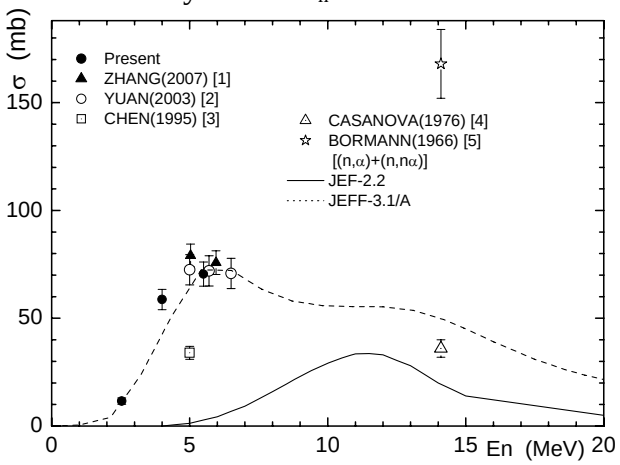

Fig. 6. Present cross sections of the ^{64}Zn(n,α)^{61}Ni reaction compared with existing data

The cross section data for the first group, second group, and total alpha particles are shown in Table I.

Table I Angle-Integrated Cross Sections for the ^{64}Zn(n, α)^{61}Ni Reaction

E_n (MeV)	σ (mb)		
	First group: ^{64}Zn(n, α_{012})^{61}Ni	Second group: ^{64}Zn(n, $\alpha_{34...}$)^{61}Ni	Total: ^{64}Zn(n, α)^{61}Ni
2.54 ± 0.03	9.0 ± 0.9	2.6 ± 2.0	11.6 ± 1.1
4.00 ± 0.21	40.9 ± 3.3	17.8 ± 1.4	58.7 ± 4.7
5.50 ± 0.13	30.9 ± 2.5	39.6 ± 3.1	70.5 ± 5.6

References

1. G. Zhang, R. Cao, J. Chen, et al., *Nucl. Sci. Eng.*, **156** (2007)115.
2. J. Yuan, Z. Chen, G. Tang, et al., *Nucl. Sci. Eng.*, **144** (2003)108.
3. Y. Chen, Z. Chen, H. Qi, et al., *Chin. J. Nucl. Phys.*, **17** (1995)167.
4. J. L. Casanova and M. L. Sanchez, *Anales de Fisica y Quimica* **72** (1976)186.
5. M. Bormann, U. Seebeck, W. Voights, G. Woelfer, *Zeitschrift fuer Naturforschung, Section A*, **21** (1966) 988.
6. G. Zhang, G. Tang, J. Chen et al., *Nucl. Sci. Eng.*, **134**, 312 (2000).

Storage of Very Cold Neutrons in Bottles

E.V.Lychagin, A.Yu.Muzychka, G.V.Nekhaev, A.V.Strelkov
Frank Laboratory of Neutron Physics, JINR, Dubna, Russia

V.V.Nesvizhevsky
ILL, Grenoble, France

Abstract Ultra cold (UCN) neutrons and very cold neutrons (VCN) interact strongly with nanoparticles due to similarity of their wavelengths and nanoparticle sizes of the order of a few nanometres; which provides a huge enhancement of the coherent elastic interaction cross-section. We have examined in detail the total cross-section of the interaction of VCN with nanoparticles using macroscopically thick samples of nanoparticles, both theoretically and experimentally. This study allowed us to conclude that the extremely short diffusion length of VCN observed in such a nano-structured medium as well as rather small losses of VCN during their diffusion motion inside the nano-structured medium (under the condition that the medium is produces from low-absorbing materials) would allow us to obtain the reflection coefficient from such a nano-structured wall close to a unity in a broad range of initial neutron velocities from nearly zero to approximately 100 m/sec. We are going therefore to investigate a possibility to store VCN in a closed trap with nano-power walls with the thickness of one of a few centimeters.

We carried out a first experiment on storage of very cold neutrons (VCN) in a trap (with the volume of ~100 liters) with walls (with the thickness of ~2,5 cm) made of powder of diamond nanoparticles (with the typical nanoparticle diameter of 5-10 nm). The entrance window size was equal to 2 by 2 cm2 The VCN beam (with the initial velocity 40-160 m/s) was collimated by diaphragms (with the diameter of 13 mm) and was shaped using a velocity selector installed in front of the trap entrance window.

VCN can be stored in this trap for a certain period of time, and some of them can be counted using a neutron detector installed at a top trap wall. A whole (with the diameter of 6 cm) in the trap wall in front of the neutron counter allowed VCN to pass through. The whole area is much smaller than the total surface area of the trap, therefore the corresponding VCN losses in the neutron counter do not change considerably the VCN storage time and can be corrected for, The VCN detection probability depends on the probability of their reflection by the trap walls.

The VCN beam was chopped in front of the trap entrance window (with the frequency of ~1 Hz). The VCN storage time in the trap is measured in such an experimental configuration as a characteristic time of exponential decrease of the VCN count rate after closer of the entrance valve. The velocity selector allows to measure the VCN storage time in the trap as a function of the average VNC velocity.

The VCN trap was placed inside a vacuum chamber and pumped to the residual pressure of lower than 10-3 mbar, then the first set of measurements of the VCN storage times was carried out. The second set of measurements was carried out with the trap, in which the nanopowder had been cleaned from water absorbed at surfaces of the nanoparticles using the following procedure: the trap was heated to 150° C, this temperature was kept constant for ~24 hours, and then it was lowed down to the room temperature. The third set of measurements was carried out while the trap temperature was kept constant at 150°C. The results are shown in fig. 1.

We used the data shown in fig. 1 in order to calculate the probabilities of VCN reflection per bounce, shown as a function of the VCN velocity in fig. 2. This preliminary estimation is based on simple gas-kinetic calculation for the bounce frequency and has rather good accuracy. It will be improved in future calculations using Monte Carlo model of VCN diffusion inside powder.

The obtained VCN reflection probabilities agree with theoretical expectations within the model of independent diamond nanoparticles at rest [1], taking into account a mass admixture of hydrogen of ~1% [2].

Thus, we have proven experimentally the feasibility of efficiently reflecting VCN at a powder of diamond nanoparticles, thus bridging the energy gap between efficient reactor reflectors for thermal and cold neutrons, and the effective Fermi potential for ultracold neutrons and the feasibility of VCN storage in traps as discussed in [3].

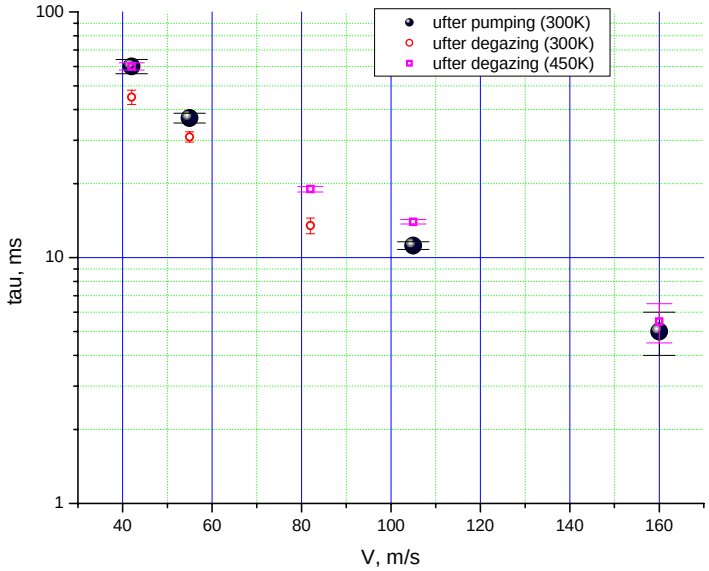

Fig. 1. The VCN storage time in the nanoparticle trap as a function of VCN velocity. The solid circles indicate the data measured at room temperature just after pumping the trap. The squares show results obtained at room temperature after degassing of the trap at the temperature of 150°C for ~24 hours. The empty circles indicate the data measured at the trap temperature of 150°C.

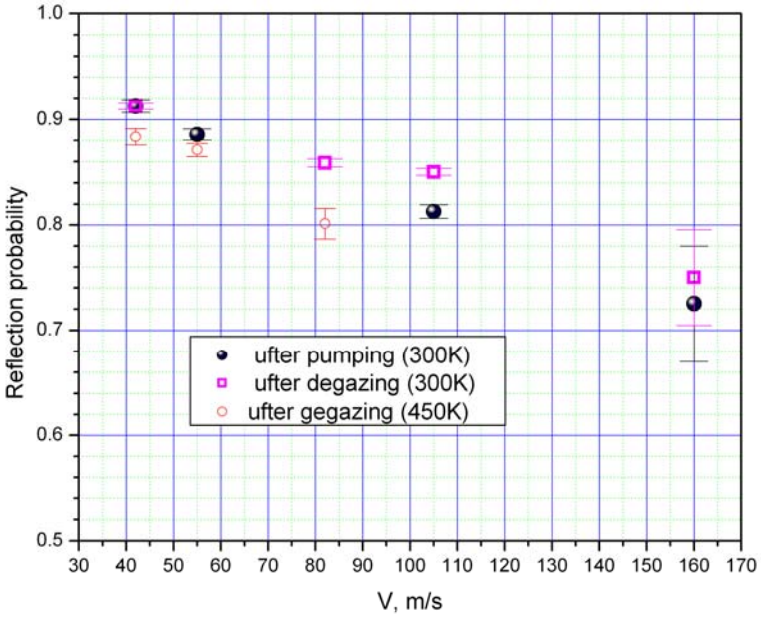

Fig. 2. The probability of VCN reflection as a function of VCN velocity. The solid circles indicate the data measured at room temperature just after pumping the trap. The squares show results obtained at room temperature after degassing of the trap at the temperature of 150°C for ~24 hours. The empty circles indicate the data measured at the trap temperature of 150°C.

[1]_V.V.Nesvizhevsky, G.Pignol and K.V.Protasov (2006). "Nanoparticles as a possible moderator for an ultracold neutron source." International Journal of Nanoscience 6(6): 1-15.
[2] A.L. Vereschagin, G.V. Sakovich, V.F. Komarov, E.A. Petrov (1993). Diamond and Related Materials 3: 160.
[3] V.V. Nesvizhevsky, E.V. Lychagin, A.Yu. Muzychka, A.V. Strelkov, G. Pignol, K.V. Protasov. “The reflection of very cold neutrons from diamond nanoparticles”, to be published in 2008.

Observation of pulsed neutron Ramsey resonance

Y. Masuda[a], V. Skoy[b], T. Ino[a], S.C. Jeong[a] and Y. Watanabe[a]

[a]High Energy Accelerator Research Organization, 1-1 Oho, Tsukuba Ibaraki 305-0801, Japan
[b]Joint Institute for Nuclear Reasearch, 141980 Dubna, Moscow Region, Russia

Ramsey resonance makes use of Larmor precession in a static field, H_0, between two separated oscillatory fields for a precision nuclear magnetic resonance [1]. A rotating field about H_0 is produced from the first oscillatory field. The effective field on the neutron spin disappears in a rotating frame of the resonance frequency, ω_0, and then the neutron spin sees only H_1 as a static field. As a result, neutron spin rotates about H_1 by $\pi/2$ from the parallel direction to the transverse direction to H_0 in the Ramsey resonance. After $\pi/2$ rotation, the neutron spin rotates about H_0. If the phase of the second oscillatory field is the same as the first oscillatory field, then the neutron spin is also perpendicular to the second rotating field, which is produced from the second oscillatory field. The neutron spin continues to rotate by $\pi/2$ from the transverse direction to the anti-parallel direction, as if there is no space between the two oscillatory fields. When the oscillatory field frequency, ω, is deviated from ω_0, the frequency difference, $\omega-\omega_0$, is enhanced by the time duration, t, between the two separated oscillatory fields. At the second oscillatory field, the neutron spin direction is deviated by $(\omega-\omega_0)t$ from the perpendicular direction. After the second oscillatory field, the projection angle of the neutron spin on the static field becomes $\pi+(\omega-\omega_0)t$, which is analyzed in the Ramsey resonance. Neutron spin echo is similar technique to the Ramsey resonance. The neutron spin also rotates in a static field after $\pi/2$ rotation. The neutron spin rotation phase, which has velocity dependence via the neutron time of flight (TOF) in the static field, is compensated with a precession in another static field after π rotation. Neutron inelastic scattering is observed as a deviation from the compensation [2] and [3].

The experimental apparatus is shown in Fig. 1 [4]. The neutrons pass through a polarized ^{3}He neutron spin polarizer. After polarization, the neutrons enter the first oscillatory field. Higher energy neutrons from the pulsed neutron source come to the oscillatory field earlier than lower energy neutrons. The oscillatory field is synchronized with the neutron motion. The amplitude of H_1 is modulated so that $\gamma H_1 t_r$ becomes $\pi/2$ for all of the neutrons in some particular neutron energy region from E_h to E_l [5] and [6]. The parameter t_r is the neutron TOF in the RF coil. The oscillatory field is switched on when neutrons of energy E_h arrive at the RF coil and switched off when neutrons of energy E_l leave the RF coil. After $\pi/2$ rotation, the neutrons pass through a static field and then enter the second oscillatory field. The neutron spins rotate in the same way as in the first oscillatory field. After the second oscillatory field, the neutron spins are analyzed by means of a polarized ^{3}He neutron spin analyzer.

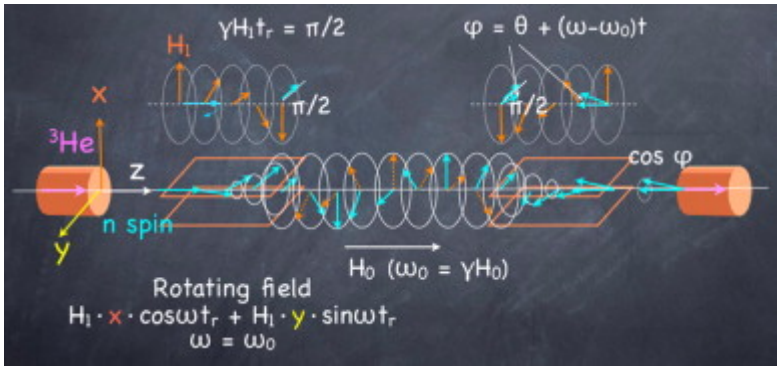

Fig. 1. Ramsey resonance apparatus. Neutrons from a pulsed neutron source are polarized upon passing through a ^{3}He neutron spin polarizer. Neutron spins rotate from the longitudinal direction to the transverse direction in the rotating field which is produced from oscillatory fields in the RF

coils. After the first rotating field, the neutron spins rotate about the longitudinal static field, and then rotate from the transverse to the longitudinal direction in the second rotating field. Finally the neutron spins pass through a ^{3}He neutron spin analyzer.

The neutron transmission through the apparatus when the oscillatory fields are switched on is obtained as

$$T_{on}=T_1T_2(1+\alpha(E)P_{n1}P_{n2}). \quad (1)$$

From a density matrix formalism [7] and [8]. Here, T_1 and T_2 are the neutron transmissions, and P_{n1} and P_{n2} are the polarizing and analyzing powers of the polarized ^{3}He neutron spin polarizer and analyzer, respectively, which are represented as [9]

$$T_1=A_1\exp(-n_{He1}o_0d_1)\cosh(P_{He1}n_{He1}o_0d_1), \quad (2)$$

$$T_2=A_2\exp(-n_{He2}o_0d_2)\cosh(P_{He2}n_{He2}o_0d_2), \quad (3)$$

$$P_{n1}=\tanh(P_{He1}n_{He1}o_0d_1), \quad (4)$$

$$P_{n2}=\tanh(P_{He2}n_{He2}o_0d_2). \quad (5)$$

Here P_{He1} and P_{He2} are the ^{3}He polarizations, n_{He1} and n_{He2} the ^{3}He number densities, and d_1 and d_2 the ^{3}He thicknesses of the polarizer and analyzer, respectively. The parameter σ_0 is the neutron-capture cross section of ^{3}He, which is proportional to $1/v$. A_1 and A_2 are neutron attenuation factors by other processes. The effect of the neutron spin rotation during transmission through the first $\pi/2$ coil, the static field, and the second $\pi/2$ coil is represented as $\alpha(E)$, which is the projection component of the neutron polarization on the static field. Here, E is the neutron energy. Near resonance, $\alpha(E)$ is approximately represented as

$$\alpha(E)=\cos\{\pi+(\omega-\omega_0)t+\theta\}. \quad (6)$$

Here, we assume the phase of the second oscillatory field is shifted b θ with respect to the first oscillatory field. The neutron spin is deviated by $(\omega-\omega_0)t+\theta$ from the perpendicular direction to the second rotating field. The Ramsey resonance is analyzed by means of a transmission ratio, which is defined as $R=T_{on}/T_{off}-1$. Here, T_{off} is the transmission without the oscillatory fields. When the oscillatory fields are switched off, $\alpha(E)$ becomes 1. Therefore, the neutron transmission ratio becomes

$$R=(1+\alpha(E)P_{n1}P_{n2})/(1+P_{n1}P_{n2})-1. \quad (7)$$

We measured the transmission ratio at $\omega=\omega_0$ and $\theta=0$. Here, the neutron spins are reversed after the second oscillatory field, and then $\alpha(E)$ becomes -1. The transmission ratio is represented as

$$R=(1-P_{n1}P_{n2})/(1+P_{n1}P_{n2})-1. \quad (8)$$

We set the energy E_h at 80 meV, and E_l at 23.6 meV. The result of the transmission ratio is shown in Fig. 2. The effect of the oscillatory fields was clearly observed at neutron energies from E_l=23.6 meV to E_h=80 meV. No effect was observed at other neutron energies. The solid curve is the result of a least square fitting. The neutron energy dependence of the solid curve arises from the $1/v$ dependence of the ^{3}He cross section.

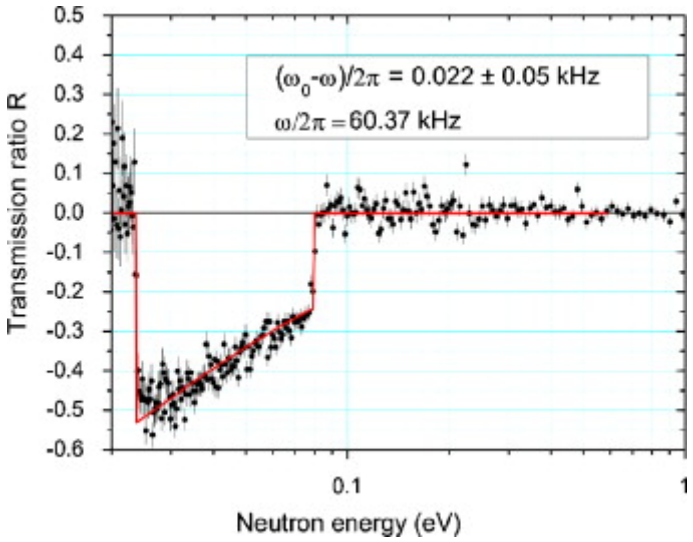

Fig. 2. Neutron transmission ratio at an oscillatory field frequency of 60.37 kHz. The static field was 20.78±0.02 G. This value was obtained from the neutron TOF dependence of the ratio *R*.

References

[1] N.F. Ramsey, *Phys. Rev.* **76** (1949), p. 996.
[2] F. Mezei, *Z. Physik* **255** (1972), p. 146.
[3] R. Golub and R. Gahler, *Phys. Lett. A* **123** (1987), p. 43
[4] Y. Masuda, V. Skoy, T. Ino, S.C. Jeong and Y. Watanabe, *Phys. Lett. A* **364** (2007), p. 87.
[5] W.M. Snow *et al.*, *Nucl. Instrum. Methods A* **440** (2000), p. 729.
[6] R. Maruyama *et al.*, *Nucl. Instrum. Methods A* **530** (2004), p. 505.
[7] L. Stodolsky, *Nucl. Phys. B* **197** (1982), p. 213.
[8] S.K. Lamoreaux and R. Golub, *Phys. Rev. D* **50** (1994), p. 5632.
[9] Y. Masuda *et al.*, *Appl. Phys. Lett.* **87** (2005), p. 053506.

Ramsey resonance for a pulsed beam

Yasuhiro Masuda[a], Vadim Skoy[b], Takashi Ino[a], Sun-Chang Jeong[a] and Yutaka Watanabe[a]
[a]High Energy Accelerator Research Organization, Oho 1-1, Tsukuba, Ibaraki 305-0801, Japan
[b]Joint Institute for Nuclear Research, 14980 Dubna, Moscow Region, Russia

We discuss here the Ramsey resonance for a pulsed beam, for example a pulsed neutron beam. [1-4]. From a pulsed neutron source, higher energy neutrons come to the oscillatory fields earlier than lower energy neutrons. In the present method, oscillatory fields for NMR are synchronized with these neutron motions. The oscillatory fields are applied to neutron spins in a time interval, which corresponds to the TOF of some particular neutron energies, by use of the start timing of the neutron pulse for triggering oscillatory field generation. The amplitudes of the oscillatory fields are modulated as a function of the neutron TOF so that the condition of $\pi/2$ spin rotation is satisfied for all of the neutrons in this energy region [5] and [6]. In addition, the phase of the second oscillatory field is modulated. The result of the Ramsey resonance is observed as a neutron-beam intensity modulation as a function of the neutron TOF. A square-wave phase modulation was tried before for the frequency stabilization of an atomic clock [7]. The present method is different from this. The phase is modulated as a function of the neutron TOF by use of the start timing of the neutron pulse. The neutron velocity can be measured by the neutron-beam intensity modulation.

The experimental apparatus comprises a ^{3}He neutron spin polarizer, a first radio frequency (RF) coil set for $\pi/2$ rotation, a Larmor precession path, a second RF coil set for $\pi/2$ rotation and a ^{3}He neutron spin analyzer, which are placed in a static magnetic field of solenoids, as shown in Fig. 1. Each RF coil set has two pairs of 20 cm long and 7 cm wide rectangular coils. Each pair of coils has a gap of 3 cm for a neutron beam, which is collimated in the z direction. One coil pair induces a transversely oscillating field in the x direction and the other coil pair in the y direction. The neutron beam size is 1.5 cm in diameter. The apparatus is placed in a neutron beam line at the KEK pulsed neutron source, KENS. The neutron pulse width depends on the neutron energy, E, as $1.3/\sqrt{E/\mathrm{eV}}$ μs. Neutrons from the pulsed neutron source are longitudinally polarized upon passing through the ^{3}He neutron spin polarizer [17], [18] and [19]. After polarization, the neutrons enter the first RF coil set. An oscillatory field in the x direction is switched on when neutrons of higher energy, E_h, arrive at the RF coil, and is then switched off when neutrons of lower energy, E_l, leave from the RF coil, as shown in Fig. 2, where the start timing of the neutron pulse is used for RF switching. When the frequency of the oscillatory field, ω, is at the Larmor frequency, $\omega_0=\gamma H_0$, namely at the resonance, neutron spins rotate about a rotating field, H_1, which is produced by the oscillatory field. H_0 denotes the strength of the static magnetic field and γ the gyro magnetic ratio. The rotation axis of H_1 is in the H_0 direction.

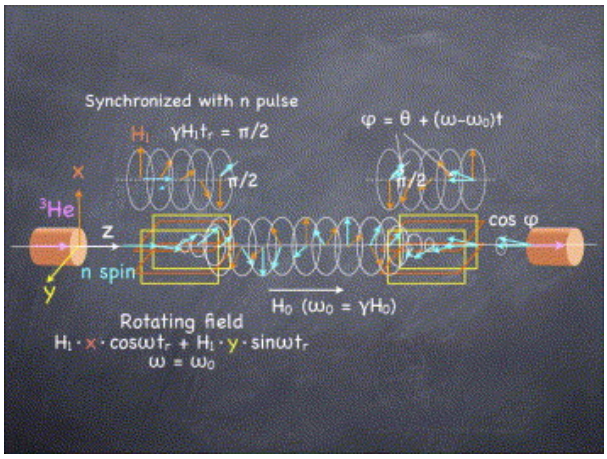

Fig. 1. Ramsey resonance apparatus. The apparatus comprises a ^{3}He neutron spin polarizer, an RF coil set, a Larmor precession path, another RF coil set and a ^{3}He neutron spin analyzer. Each RF coil set has two pairs of 20 cm long and 7 cm wide

rectangular coils. Each coil pair has a gap of 3 cm for a 1.5 cm diameter neutron beam in the z direction. One coil pair induces a transversely oscillating field in the x direction and the other coil pair in the y direction. From the oscillatory field in the x or y direction, a rotating field in the xy plane is produced together with another rotating field in opposite direction. If we switch on the oscillatory field in the y direction with a $\pi/2$ phase shift, in addition to the oscillatory field in the x direction, one rotating field is induced without the opposite component.

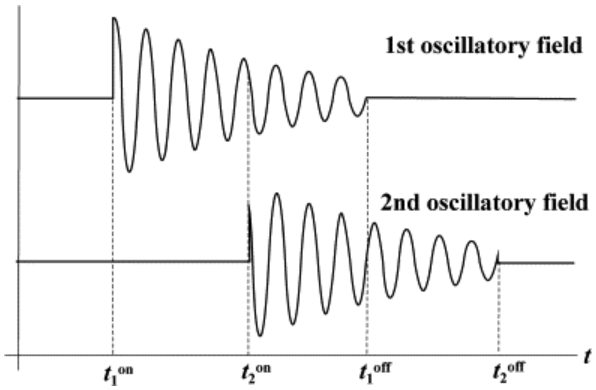

Fig. 2. Timing of RF pulses. The first oscillatory field is switched on at $t = t_1^{on}$ and off at $t = t_1^{off}$, and the second on at $t = t_2^{on}$ and off at $t = t_2^{off}$, respectively. Here, $t_1^{on} = l_1/v(E_h)$, $t_1^{off} = (l_1 + l_{\pi/2})v(E_l)$, $t_2^{on} = l_2/v(E_h)$, $t_2^{off} = (l_2 + l_{\pi/2})v(E_l)$. Parameters $\boldsymbol{l_1}$ and $\boldsymbol{l_2}$ are the neutron TOF lengths from the pulsed neutron source to the fronts of the first and second RF coils, respectively, $\boldsymbol{l_{\pi/2}}$ is the length of the RF coils and $\boldsymbol{v(E_h)}$ and $\boldsymbol{v(E_l)}$ are neutron velocities at $\boldsymbol{E=E_h}$ and $\boldsymbol{E=E_l}$.

The oscillatory field is represented as a linear combination of two rotating fields, which are rotating in opposite directions. The opposite component can be neglected in NMR, if the condition, $H_1 \ll H_0$ is satisfied. If we switch on the oscillatory field also in the y direction with a $\pi/2$ phase shift, one rotating field is induced without the other rotating field in opposite direction, and the condition, $H_1 \ll H_0$ does not apply. In the latter case either the amplitude of H_1 can be increased or the amplitude of H_0 decreased.

The neutron spin rotation angle in the RF coil becomes $\gamma H_1 t_r$. The parameter t_r is the neutron TOF in the RF coil, which is represented in terms of the RF coil length, $l_{\pi/2}$, and the neutron velocity, v, as $l_{\pi/2}/v$. The amplitude of the rotating field, H_1, is modulated as a function of the neutron TOF so that all of the neutron spins in the energy region from E_h to E_l rotate by $\pi/2$, and then become perpendicular to H_0. After the first RF coil set, the neutron spins rotate about H_0 with a Larmor frequency of ω_0. After Larmor precession, the neutrons enter the second RF coil set, and then another oscillatory field in the x direction is switched on and off in the same way as in the first RF coil set. The neutron spins are always perpendicular to the first rotating field before entering the second RF coil set. When the phase of the second oscillatory field is the same as the first one, the neutron spins continue to rotate about the second rotating field, H_1, by $\pi/2$ in exactly the same way as in the first RF coil set, as if there is no space between the two RF coil sets. As a result, the neutron spins rotate by π. If the phase of the second oscillatory field is shifted by θ, this phase shift is transformed to the projection angle of the neutron spin on the direction of H_0 after the second RF coil set and is then detected by means of the ^{3}He neutron spin analyzer. If the oscillatory field frequency is deviated from the resonance frequency, any phase difference, $(\omega-\omega_0)t$, is transformed to the projection angle of the neutron spin on the static magnetic field after the second RF coil set. The variable t denotes the neutron TOF between the two RF coil sets.
Neutron transmission can be analyzed by means of the density matrix formalism [8] and [20]. The neutron transmission becomes $T_{on}=T_1T_2\{1+\alpha(E)P_{n1}P_{n2}\}$, when the oscillatory fields are switched

on. Here, T_1 and T_2 are the neutron transmissions of the polarized ^{3}He neutron spin polarizer and analyzer, which are represented as

$$T_1=A_1\exp(-n_{He1}\sigma_0 d_1)\cdot\cosh(P_{He1}n_{He1}\sigma_0 d_1)$$

and

$$T_2=A_2\exp(-n_{He2}\sigma_0 d_2)\cdot\cosh(P_{He2}n_{He2}\sigma_0 d_2),$$

respectively [19]. P_{He1} and P_{He2} are ^{3}He polarizations, n_{He1} and n_{He2} the ^{3}He number densities, and d_1 and d_2 the ^{3}He thicknesses. The parameter σ_0 is the neutron capture cross section of ^{3}He, which is proportional to $1/v$. In terms of σ_0, the neutron cross section of polarized ^{3}He is represented as $\sigma_\pm=\sigma_0(1\mp P_{He})$ for parallel and antiparallel neutron spin states to ^{3}He polarization, respectively [21]. Here, the polarization cross section is the same as the neutron capture cross section for ^{3}He. A_1 and A_2 are neutron attenuation factors by other processes. P_{n1} and P_{n2} are the polarizing and analyzing powers of the polarizer and analyzer, which are represented as $P_{n1}=\tanh(P_{He1}n_{He1}\sigma_0 d_1)$ and $P_{n2}=\tanh(P_{He2}n_{He2}\sigma_0 d_2)$, respectively. The effect of the neutron spin rotation during transmission through the first $\pi/2$ coil, the static field and the second $\pi/2$ coil is represented as $\alpha(E)$, which is the projection component of the neutron polarization on the static field. Here, E is the neutron energy. Near resonance, $\alpha(E)$ is approximately represented as $\cos\{\pi+(\omega-\omega_0)t+\theta\}$. When the oscillatory fields are switched off, $\alpha(E)$ becomes 1, then the neutron transmission becomes $T_{off}=T_1T_2\{1+P_{n1}P_{n2}\}$.

The ^{3}He polarizations and the thicknesses of the neutron spin polarizer and analyzer were measured by means of neutron transmission. The results of the polarizations were $P_{He1}=31\%$ and $P_{He2}=51\%$, respectively. The two ^{3}He polarizations were in the same longitudinal direction. The ^{3}He gas pressures were 2.32 atm and 2.13 atm at 300 K, respectively. The length of the ^{3}He gas in the neutron beam direction was 5 cm for both the polarizer and the analyzer. The neutron energies, E_h and E_l, were set at 80 meV and 23.6 meV, respectively. The amplitude of H_1 was modulated from 1.7 G to 0.9 G. The value of H_0 was 20.7 G. Therefore, the condition, $H_1 \ll H_0$ was satisfied. We counted the neutrons that passed through the apparatus shown in Fig. 1 as a function of the neutron TOF.

We changed the frequency of the oscillatory fields around the resonance frequency. When we switched on the oscillatory fields, the neutron counts were greatly changed at neutron energies from 80 to 23.6 meV. No effect was observed at other neutron energies. For normalization of the incident neutron spectrum, we calculated the neutron transmission ratio, which was defined as $R=T_{on}/T_{off}-1$. In the transmission ratio, the transmission factors, T_1 and T_2, were also removed, since it is described as $R=(1+\alpha(E)P_{n1}P_{n2})/(1+P_{n1}P_{n2})-1$. The experimental results of the transmission ratio are shown in Fig. 3, Fig. 4, Fig. 5, Fig. 6 and Fig. 7 from lower to higher oscillatory field frequencies. We modulated the phase of the second oscillatory field proportionally to the neutron TOF, t, between the two RF coil sets from 2π to 0 for the energy region from E_h to E_l. The transmission ratio with the phase modulation becomes $R_{mod}=[1+\cos(\pi+\theta)\cdot P_{n1}P_{n2})]/[1+P_{n1}P_{n2}]-1$. Here, $\theta=2\pi(t(E_l)-t)/(t(E_l)-t(E_h))$, which is a function of the neutron velocity. The parameters $t(E_h)$, $t(E_l)$, and t are the neutron TOF at neutron energies, E_h, E_l, and E, which are represented in terms of the TOF length between the two RF coil sets, l_{12}, and the neutron velocities, $v(E_h)$, $v(E_l)$ and $v(E)$ as $l_{12}/v(E_h)$, $l_{12}/v(E_l)$ and $l_{12}/v(E)$, respectively. We set the energies E_h and E_l at 80 meV and 23.6 meV, respectively. The result of the transmission ratio is shown in Fig. 8 as a function of the neutron energy. Here, the neutron energy was obtained from the neutron TOF. At E=80 meV and 23.6 meV, the phase differences of the second oscillatory field from the first oscillatory field were adjusted to 2π and 0, respectively. At some particular energy E between 80 meV and 23.6 meV, the phase difference was adjusted to θ. A sinusoidal beam intensity modulation is found in Fig. 8, as expected. The solid curve was obtained from the least square fitting by using the phase modulation θ and the neutron TOF. The result shows the neutron velocity obtained from the phase modulation is consistent with the value from the neutron TOF.

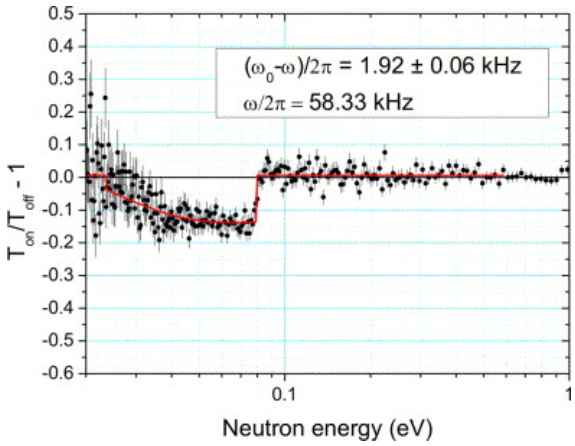

Fig. 3. Neutron transmission at an oscillatory field frequency of 58.33 kHz.

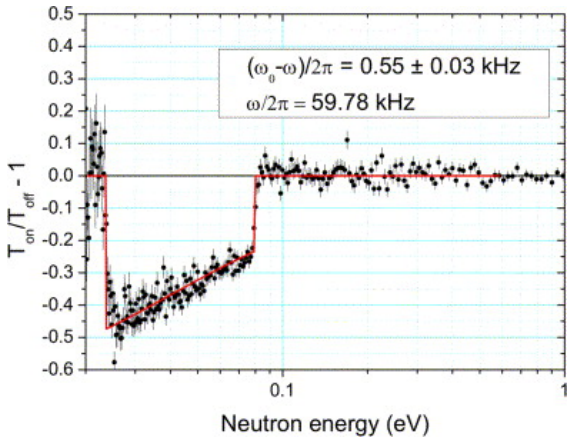

Fig. 4. Neutron transmission at an oscillatory field frequency of 59.79 kHz.

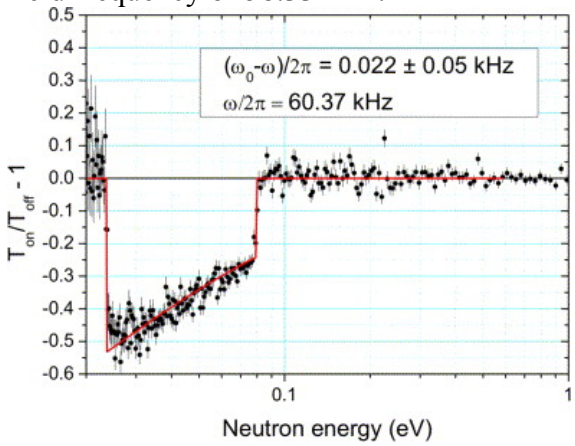

Fig. 5. Neutron transmission at an oscillatory field frequency of 60.37 kHz.

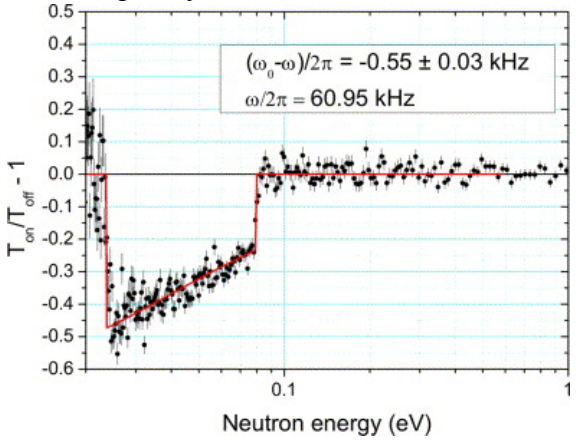

Fig. 6. Neutron transmission at an oscillatory field frequency of 60.95 kHz.

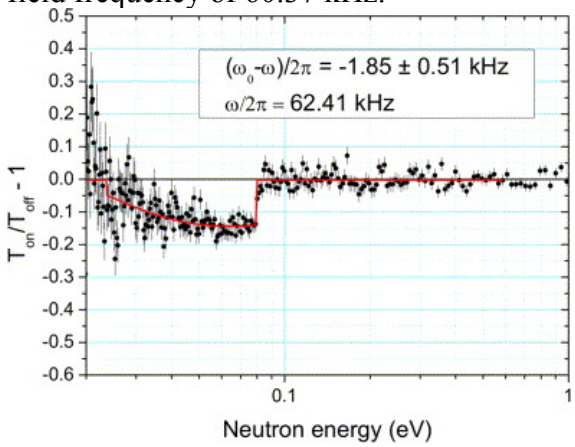

Fig. 7. Neutron transmission at an oscillatory field frequency of 62.41 kHz.

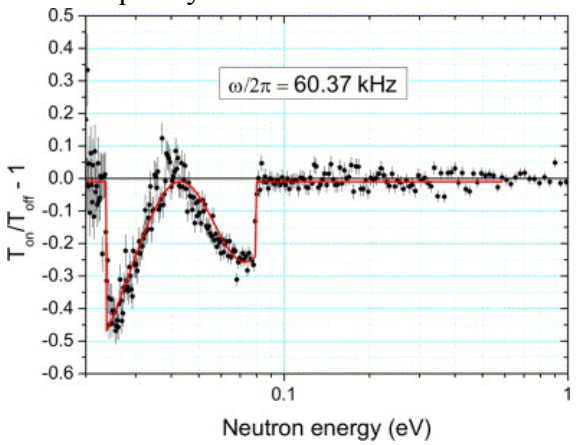

Fig. 8. Ramsey resonance with a phase modulation. The oscillatory field frequency was set at the resonance, and then the phase of the second RF was modulated as a function of the neutron TOF with respect to the first RF.

References

[1] N.F. Ramsey, *Phys. Rev.* **76** (1949), p. 996.
[2] E.L. Hahn, *Phys. Rev.* **80** (1950), p. 580.
[3] F. Mezei, *Z. Phys.* **255** (1972), p. 146.
[4] R. Golub and R. Gähler, *Phys. Lett. A* **123** (1987), p. 43.
[5] W.M. Snow *et al.*, *Nucl. Instrum. Methods A* **440** (2000), p. 729.
[6] R. Maruyama *et al.*, *Nucl. Instrum. Methods A* **530** (2004), p. 505.

[7] R.S. Badessa, V.J. Bates and C.L. Searle, *IEEE Trans. Instrum. Meas.* (1964), p. 175.
[8] L. Stodolsky, *Nucl. Phys. B* **197** (1982), p. 213.
[9] P.K. Kabir, *Phys. Rev. D* **25** (1982), p. 25.
[10] V.E. Bunakov and V.P. Gudkov, *Z. Phys. A* **308** (1982), p. 363.
[11] J.D. Bowman, Tests of Time Reversal Invariance in Neutron Physics, World Scientific, Singapore (1987) p. 121.
[12] Y. Masuda *et al.*, *Hyperfine Interact.* **74** (1992), p. 149., Y. Masuda *et al.*, Dark Matter in Cosmology, Clock and Tests of Fundamental Laws, Editions Frontiers, Dreux (1995) p. 14.
[13] V.R. Skoy, *Phys. Rev. D* **53** (1996), p. 4070.
[14] Y. Masuda, *Nucl. Instrum. Methods A* **440** (2000), p. 632.
[15] H. Glättli *et al.*, *J. Phys.* **40** (1979), p. 629.
[16] F. Mezei, *Nucl. Instrum. Methods* **164** (1979), p. 153.
[17] J. Mayers *et al.*, *J. Phys. D* **18** (1985), p. 156.
[18] K. Coulter *et al.*, *Nucl. Instrum. Methods A* **270** (1988), p. 90.
[19] Y. Masuda *et al.*, *Appl. Phys. Lett.* **87** (2005), p. 053506.
[20] S.K. Lamoreaux and R. Golub, *Phys. Rev. D* **50** (1994), p. 5632.
[21] M. Rose, *Phys. Rev.* **75** (1949), p. 213.

Temperature dependence of neutron scattering on He-4 gas

V. Ignatovich
Frank Laboratory of Neutron Physics of Joint Institute for Nuclear Research, 141980, Dubna
Moscow region, Russia

Abstract

A suggestion [**?**] that temperature dependence of the total neutron-^{4}He cross section can be proportional to $T^{3/2}$ is checked. The experiment is described. The temperature dependence was found to be $T^{1/2}$ in agreement with the standard scattering theory (SST). The consequence of this result for the scattering theory is discussed.

1 Introduction

Experiments on storage of ultracold neutrons (UCN) reveal [1] anomalously high loss coefficient at a single collision of neutrons with material walls of storage vessels. After many unsuccessful attempts to explain this anomaly, a hypothesis was spoken out [2] that the cause of high losses is related to wave packet form of the free neutron wave function. It was supposed (there are also other arguments that lead to the same hypothesis [3]) that the wave packet can be of the de Broglie singular form [4]:

$$\psi_{dB}(\boldsymbol{r},t)=\sqrt{\frac{s}{2\pi}}\exp(i\boldsymbol{v}\boldsymbol{r}-i\omega t)\frac{\exp(-s|\boldsymbol{r}-\boldsymbol{v}t|}{|\boldsymbol{r}-\boldsymbol{v}t|}, \tag{1}$$

where $\omega=[v^2-s^2]/2$, s determines the packet width, and $\boldsymbol{v}$ is wave packet velocity, which in our units $m=\hbar=1$ coincides with the wave vector $\boldsymbol{k}$.

The wave packet can be representable in Fourier expansion form. Because of its width s a particle incident on a mirror surface at grazing angles θ less than critical θ_c can go through the mirror with probability $w\propto s\lambda_c$, where λ_c is critical wavelength of the mirror substance. A problem, which arises here is: what is the parameter s? Is it a fundamental constant or some function, which depends on neutron energy? At first sight it should be proportional to the neutron speed v. However in such a case the transmission probability at subcritical incidence angles should increase with the neutron energy. Experiments searching for such a transmission [5] did not reveal a dependence on energy, and it was concluded that parameter s is some fundamental constant.

However, if s does not depend on speed, then neutron transmission through gases would decrease with the gas temperature proportionally to $T^{3/2}$. So, it was necessary to check this temperature dependence. Experiments of such type were performed long ago [6]. However that time it was measured not the temperature dependence but dependence of cross section on energy of incident neutrons, and temperature dependence was deduced from it.

It was possible to make direct measurement of the temperature dependence of neutron transmission through ^{4}He gas, and thanks to kind permission and help of P.Geltenbort and T. Brenner these measurements were done. Below we describe the experiment, its results and discuss the consequences of the obtained temperature dependence.

2 Description of the experiment and its results

The experiment, scheme of which is shown in fig. 1, was performed at the PF2/TEST beam port. Ultra-cold neutrons (UCN) pass through an electropolished stainless steel tube of length

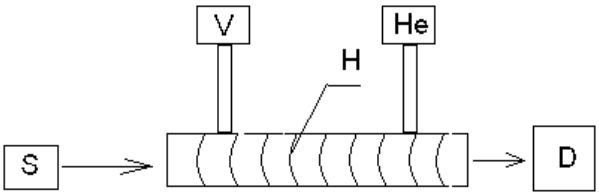

Figure 1: Scheme of the experiment. S — source of the neutrons, D — detector, V — system for vacuum, He — helium tank, H — heating wire.

$d = 0.5$ m, which has at both ends stainless steel or Al windows of 0.1 mm thickness. Therefore, either only neutrons with energies above the limiting energy of stainless steel or only those with energies above the limiting energy of Al are transmitted. When the tube was evacuated and kept at room temperature the average neutron count rate was 6700 n/s for stainless steel windows and 34000 n/s with Al windows. For the detector we used a strip ^{3}He counter. Without any special shielding the background count rate (exit shutter of PF2/TES closed) was 2.3 n/s for both window types.

When the stainless steel tube is filled with ^{4}He gas the neutron count rate of the detectors decreases. For small He pressures the decrease of count rate is proportional to $\Delta J = JN\sigma d$, where N is the density of the He gas, J is the count rate for the evacuated bottle, d is the length of the tube and σ is the total neutron scattering cross section in He. At pressures P up to 1000 mbar the count rate decreased linearly: $\Delta J \propto P$. When the tube was filled with 1000 mbar of He at room temperature, the count rate was only 20% less than for evacuated tube.

The main idea of the experiment was to check the dependence of ΔJ on P when P increased not because of amount of He, but because of the gas temperature increase, which was achieved with the heating wire H shown in fig. 1.

The results of measurements for Al windows (the results for stainless steel windows were the same) are demonstrated in fig. 2. Curve 1 shows the dependence of $\Delta J = JN\sigma d$ on P at room temperature, when the He pressure is increased by pumping He into the tube. The branch 2 of the curve 1 shows the same dependence, when the pressure is increased by heating the stainless steel tube with fixed amount of He. In this case $JN\sigma d$ increases not because of increase of the density N of the He gas, but due to increase of the total cross section σ. The graph shows that the increase of σ with P is about two times slower than the increase of N with P. Such a behavior is predicted by the standard scattering theory where $\sigma \propto T^{1/2} \propto P^{1/2}$.

We were not able to measure whether the power of T is really 1/2, because we had no monitor, and the decrease of count rate with increase of temperature by $\approx 60^\circ$ C, was only several %, while reactor intensity[1] was fluctuating at the level 1.5%. Nevertheless, since the fluctuations were sufficiently slow, we could find an interval of time where the measurements were reproducible, and they show that the temperature dependence is below the linear one and not above it. This dependence testifies in favor of $T^{1/2}$ and against $T^{3/2}$.

3 Conclusion

This experiment definitely shows that the packet width s is proportional to the relative speed v of the neutron with respect to scattering nucleus, and we now must resolve the contradiction, which arises between this work and the results of the experiment [5] on subcritical transmission.

[1]It was reported by reactor staff.

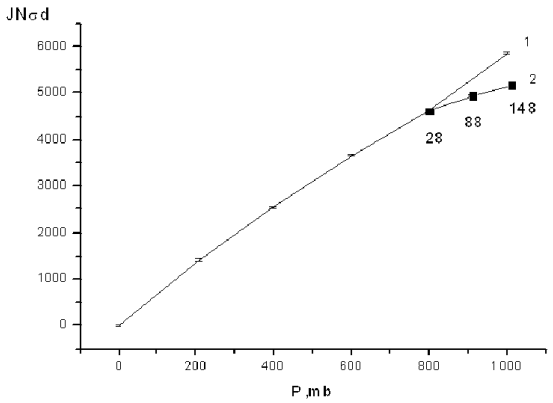

Figure 2: Dependence of $JN\sigma d$ on the pressure P of ^{4}He-gas in stainless steel tube with Al windows: 1 - at room temperature (28^{o}C); 2- for a constant number N of atoms, but different temperatures. The numbers indicate the gas temperature in °C. All the other points correspond to room temperature.

We think that the experiment [5] should be repeated with more careful search of the transmitted neutrons, when grazing angle of incident beam is below the critical one.

Acknowledgement

The author is very grateful to P.Geltenbort and T. Brenner of ILL staff for their help and excellent preparation of the experiment, to Prof. J-F. Bloch of IFPG (Grenoble), and Dr. E.P.Shabalin of JINR (Dubna) for their interest and support.

References

[1] V.K.Ignatovich. The Physics of Ultracold Neutrons. Oxford Clarendon Press. 1990.

[2] V.K. Ignatovich, M. Utsuro, Phys. Lett. **A225**, 195-202 (1997.)

[3] V.K. Ignatovich, Concepts of Physics, **1**, 51 (2004).

[4] L. de Broglie, *Non-Linear Wave Mechanics: A Causal Interpretation*, (Elsevier, Amsterdam, 1960.)

[5] M. Utsuro, V. Ignatovich, P. Geltenbort, Th. Brenner, J. Butterworth, M. Hino, K. Okumura, M. Sugimoto, *Proceedings of VII International Seminar on Interaction of Neutrons with Nuclei: Neutron Spectroscopy, Nuclear Structure, Related Topics, Dubna, May 25-28, 1999*, **E3-98-212**, 110, JINR, Dubna, 1999.

[6] R. Genin, H. Beil, C. Signarbieux a. o., Le Journal de physique et le radium **24** 21 (1963).

Character of wear process in nitrogen-implanted AISI 316L stainless steel

P. Budzynski [1], K.Polanski [2], A.P.Kobzev [3]

[1]*Mechanical Faculty, Lublin University of Technology, Nadbystrzycka str. 36, 20-618 Lublin, Poland.*
[2] *Department of Solid State Physics, University of Lodz, Poland.*
[3] *Frank Laboratory of Neutron Physics, Joint Institute for Nuclear Research, 141980 Dubna, Moscow Region, Russia*

Abstract

The effects of nitrogen ion implantation into AISI316L stainless steel on friction, wear, and microhardness have been investigated at an energy level of 125 keV at a fluence of 1×10^{17}–1×10^{18} N/cm^2. The composition of the surface layer was investigated by RBS, XRD (GXRD), SEM and EDX. The friction coefficient and abrasive wear rate of the stainless steel was measured in atmospheres of air, oxygen, argon, and vacuum. As follows from the investigations, there is increase in resistance to frictional wear in the studied samples after implantation; however, these changes are of different characters in the various atmospheres. The largest decrease in wear was observed during the tests in air, and the largest reduction in the value of the friction coefficient for all implanted samples was obtained during tests in the argon atmosphere. Tribological tests revealed larger contents of nitrogen, carbon, and oxygen in the products of surface layer wear than in the surface layer itself of the sample directly after implantation.

1. Introduction

Surface modification of stainless steels by nitrogen ion implantation is a well-established process. The possible mechanisms of such modification are not fully understood, but the formation of new nitride phases in the implanted layers is expected to have a large effect on tribological properties. The microstructure of the implanted layer has attracted much attention because of its important influence on the surface properties of a work piece implanted with nitrogen ions.

In austenitic stainless steels (304, 304L, 316, 316L), ion implantation treatments are able to produce a modified surface layer consisting of metastable phase, known as supersaturated or expanded austenite γ_N [1-4]. However, the authors of [5] concluded that the ion implantation did not create any new phase and did not influence the crystallographic texture that they observed before the implantation. Implantation at the fluence 6×10^{16}–1.2×10^{17} (N/cm^2) to the steel of types 304 and 316 is responsible for precipitation of CrN [6].

Changes in the surface layer due to nitrogen implantation may be larger than those observed so far. Paper [7] shows that the high-fluence carbon ion implantation modified the microstructure of the steel, as demonstrated by the presence of two amorphous layers separated by a layer of extended austenite. The divergent opinions about the effect of nitrogen implantation on properties of the steel AISI 316L inspired us to study the crystalline structure of steel, formation of the compounds Fe-N and Cr-N, as well as change of steel tribological properties after implantation.

As mentioned before, implantation with nitrogen ions is a well-recognized technique of surface modification that improves the tribological properties of machine tools and is frequently used for steels. However, there is lack of information concerning the influence that the type of atmosphere has on the course of development of tribological process of ion-implanted metals. Changes of steel tribological properties after implantation are rarely studied. Paper [8] studied the effect of implantation on the change of steel wear in air and nitrogen atmospheres. Nitrogen implantation at high fluence has been shown to increase microhardness [1], but friction and wear tests show no significant change of the friction coefficient, whatever the relative humidity during the tests; however, an important wear resistance improvement was observed.

In this paper, friction tests in various atmospheres—air, oxygen, argon, and vacuum—show a considerable influence of the atmospheric environment on the rate and character of wear, which indicates the importance of the modified ion-implanted layer and its reaction with the environment. The aim of the experiments was to test the changes in tribological properties caused by various kinds of atmospheres in which the friction process takes place.

2. Experimental details and discussion

AISI316L stainless steel samples were used in this study. The chemical composition of the samples was: (wt %) (0.1% C, 0.16% Al, 0.29% Si, 0.52% S, 17.58% Cr, 10.32% Ni, 0.36% Cu, Fe = balance). The specimens were the discs of 25 mm diameter and 4 mm thickness, mechanically polished to a mirror finish to obtain a roughness parameter R_a = 0.08 μm.

The subsequent implantation with 125 keV N^+ ions was carried out using the standard ion accelerator. The beam current density was 3μA/cm^2. The samples were implanted over the fluence range 1×10^{17} to 1×10^{18} N/cm^2.

Depth profiles of the nitrogen distribution were measured in the JINR Dubna via the RBS technique, using a He beam with the energy 2.04 MeV scattered at the angle 170º. The depth distribution profiles of the implanted nitrogen atoms, evaluated from the Rutherford Backscattering Spectrometry (RBS) measurements at different fluences, are presented in Fig.1.

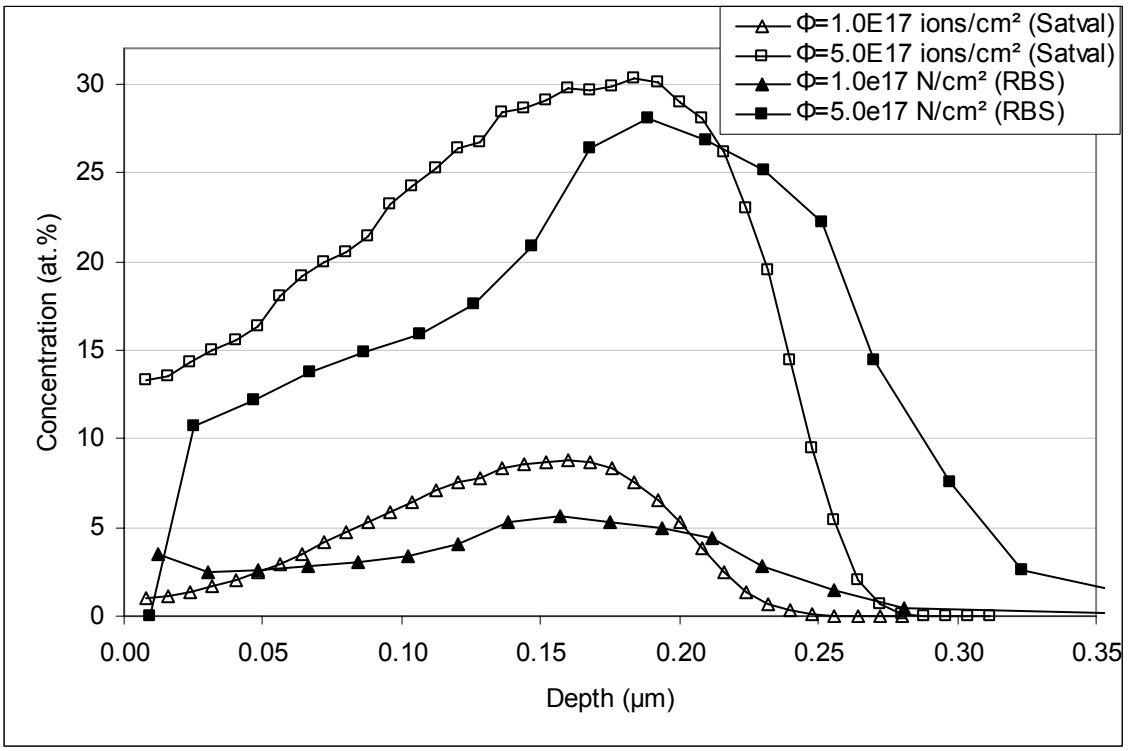

Fig. 1. RBS and simulated by SATVAL code depth profiles for AISI316L stainless steel implanted with nitrogen at the energy 125 keV.

The figure shows also the predicted distribution of nitrogen atoms calculated by means of the program SATVAL [9]. As follows from RBS measurements with the increase of the implanted ions fluence, more nitrogen atoms are found in farther layers of the sample than predicted from the theoretical distribution. However, after implantation of the fluence 5×10^{17} N/cm^2, their amount diminishes significantly in the surface layer. This situation is attributable to the two factors—diffusion of nitrogen atoms, both deep down into the sample and towards the surface, as well as sputtering of the sample surface layer during implantation. With the increase of the

fluence, the thickness of the sputtered layer containing larger nitrogen atoms concentration increases.

X-ray diffraction (XRD) experiments were performed using a CuK_α source (0.15406 nm) over the 2θ range from 20º to 100º. Grazing incidence X-ray diffraction (GXRD) was performed for 1º and 5º incidence angles. Unimplanted 316 L stainless steel showed the characteristic spectra of face-centred-cubic austenite a = 0.3601(5) nm. After implantation with the fluence of 1×10^{17} N/cm^2, the lattice constant increases to reach the value a = 0.3719(5) nm. Implantation with the fluence of 5×10^{17} N/cm^2 causes a to increase up to the value of 0.3887(5) nm. Further increase in implanted ions fluence does not result in lattice changes.

Friction and wear testing for the stainless steel samples was performed on a ball-on-disc tribotester, using a tungsten carbide ball of a diameter 0.5 mm at the indentation load 491 mN and velocity about 56 mm/s. The friction measurements for the stainless steel samples were carried out under the technically dry friction. The environment temperature was about 20^{o}C and relative humidity 25–30%; the atmospheric pressure value was about 1000 hPa. A hermetic cover was used over the measurement area to produce a controlled atmosphere for friction tests. A vacuum pump was used to obtain pressures of 10^{-4} Pa in the bench measurement chamber and various gases could also be admitted to produce a test environment at normal atmosphere.Ball on disc wear tracks were analyzed by means of a Taylor Hobson profilometer. Sets of about 20 profilograms were made for each wear track.

Energy dispersive X-ray spectroscopy (EDX) has been obtained to measure the chemical composition of the surface layers. The relative contents of nitrogen and oxygen as well as carbon increase in worn out fragments of the sample compared to the portion surrounding the track.

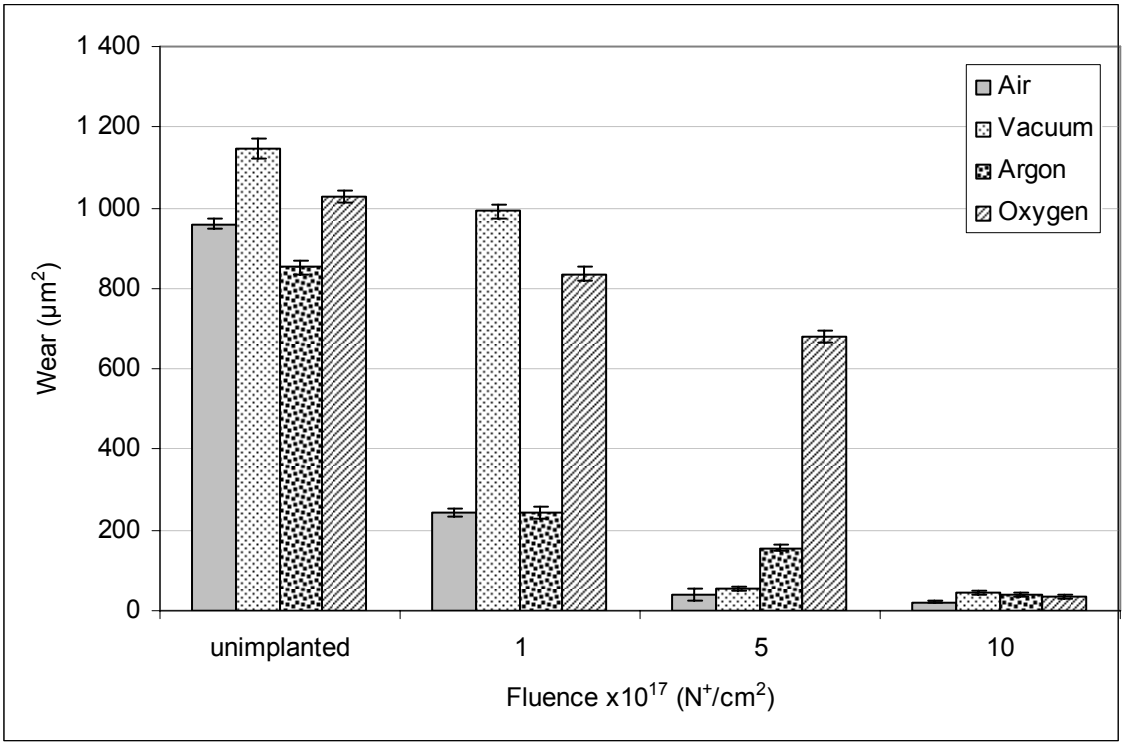

Fig. 2. Sample wear as a function of nitrogen dose for the AISI316L steel in addition to the unimplanted sample at energy 125keV.

The large friction coefficients in the vacuum for the unimplanted sample and for that implanted with the smallest fluence is probably a result of local welding with the countersample owing to the Fe-C bonds. A small amount of carbon (~0.1%) is contained in the sample material and the rest comes from the countersample (WC). This interaction leads to significant wear of

these samples in vacuum (Fig. 2). This mechanism confirms the increase of carbon content on the track surface by 0.04(2)%.

In the studies of wear products formed during friction, larger amounts of nitrogen, carbon, and chromium were observed compared to their contents in the track and in the surface layer of the sample.

3. Summary and conclusion

The depth distribution of nitrogen implanted into the steel AISI 316L departs from that predicted theoretically because of diffusion. Nitrogen implantation leads to a change of crystalline structure and chemical changes in the surface layer. The new phase-expanded austenite CrN inserts as well as crystalline lattice defects formed during implantation improve the steel's tribological properties.

The lower wear rate after implantation is a result of the lower coefficient of friction, which, in turn, is probably ascribable to the increase in surface hardness, leading to a smaller contact area and possibly a change in the mode of wear, from adhesive (unimplanted) to abrasive (after implantation).

The largest decrease of friction coefficient for all implanted samples was observed in the argon atmosphere. When the modified surface layer was rubbed off, the friction coefficient has a value characteristic of the unimplanted sample. Oxidizing wear found in the oxygen and air atmospheres does not occur in the argon atmosphere. Moreover, tribocorrosion caused by water vapour occurs in air.

The large friction coefficient in the vacuum for the unimplanted sample and that implanted with the smallest fluence is probably attributable to local tacking with the countersample owing to the Fe-C bonds. The wear products contain larger contents of nitrogen, carbon, and chromium than do the surface layer of the sample.

Finally, one can conclude that:

- Implantation of nitrogen into AISI 316L stainless steel forms the new phase—expanded austenite, precipitation of CrN, and increase of lattice constant by ~8%.
- Increase of sample temperature during implantation and formation of the phase γ_N are responsible for large nitrogen mobility.
- Nitrogen implantation improves tribological properties of the steel AISI 316L and changes the character of wear. Adhesive wear decreases and abrasive wear increases. Mild oxidizing wear remains one of kind of wear in the air and oxygen atmosphere.
- Local increase of temperature during friction promotes mobility of nitrogen, chromium, and carbon.

References

[1] J.P. Riviere, P. Meheust, J.A. Garcia, r. Martinez, R. Sanchez, R. Rodriguez, Surf. Coat. Technol. 158-159 (2002), 295-300.

[2] G.S. Chang, J.H. Son, S.H. Kim, K.H. Chae, C.H. Whang, E. Menthe, K.T. Rie, Y.P. Lee, Surf. Coat. Technol. 112 (199) 291-294.

[3] D.L. Williamson, O. Ozturk, S. Glick, R. Wei, P.J. Wilbur, Nucl. Instr. Meth. B59/60 (1991) 737-741.

[4] R. Wei, J.J. Vajo, J.N. Matossian, P.J. Wilbur, J.A. Davis, D.L. Williamson, G.A. Collions, Surf. Coat. Technol. 83(1996) 235-242.

[5] P. J. Marques, J. Pina, A.M. Dias, J.L. Lebrun, J. Feugeas, Surf. Coat. Technol. 195(2005)8-16.

[6] M. Baron, A.L. Chang, J. Schreurs, R. Kossowsky, Nucl. Instr. Meth.182/183 (1981) 531-538.

[7] M.E. Murphy, G.M. Insley, M.T. Laugier, S.B. Newcomb, Nucl. Instr. Meth. B 234 (2005) 256-260.

[8] A. Kluge, K. Langguth, R. Ochsner, K. Kobs, H. Ryssel, Nucl. Instr. Meth. B39 (1989) 531.
[9] J. Sielanko, W. Szyszko, Nucl. Inst. Meth B. 16 (1986) 340.

NAA and ESR for biotechnology of Cr(VI) detoxification

N. Tsibakhashvili[1,2], T. Kalabegishvili[2], L. Mosulishvili[2], E. Kirkesali[2],
S. Kerkenjia[1], I. Murusidze[1], H.-Y. Holman[3], M.V. Frontasyeva[4], S.F. Gundorina[4]

[1] *Chavchavadze State University, Tbilisi, Georgia,*
[2] *Andronikashvili Institute of Physics, Tbilisi, Georgia*
[3] *Lawrence Berkeley National laboratory, Berkeley, USA*
[4] *Joint Institute for Nuclear Research, Dubna, Russia*

Contamination with chromium is widespread throughout the environment because of its use in dyes, pigments, refractory material, leather tanning, and electroplating [1]. As an environmental contaminant, chromium is found mostly in its oxidized, hexavalent form. Cr(VI) is a toxic, soluble species that moves fairly rapidly in the subsurface and that can readily enter a cell, whereas the reduced form, trivalent chromium Cr(III), is relatively insoluble, and thus not bioavailable and nontoxic. Some indigenous microorganisms, especially those residing at heavy metal contaminated sites, have developed abilities to co-exist with the toxic metals. Among these microorganisms are common soil bacteria of *Arthrobacter* that can not only grow in the presence of Cr(VI), but they can also reduce it to Cr(III). Bacterial reduction of Cr(VI) into less toxic Cr(III) is one of the most promising strategies for the bioremediation of contaminated environments [2].

The present study is focused on dose-dependent formation of Cr(III) complexes and accumulation of chromium by these bacteria exposed to high concentrations of Cr(VI). For this purpose three Gram-positive basalt-inhabiting bacterial strains of *Arthrobacter* genera have been isolated from the most polluted regions in the Republic of Georgia (*Arthrobacter sp.* and *Arthrobacter globiformis)* and in the USA from polluted Columbia basalt rocks (*Arthrobacter oxydans)* [3].

Instrumental neutron activation analysis (INAA) was used to track accumulation of chromium in the bacterial cells. To monitor and identify Cr(III) complexes in these bacteria**,** the electron spin resonance (ESR) spectrometry was employed.

Sample cultivation and preparation for analysis. The bacteria were grown in the following nutrient medium: 10 g of glucose, 10 g of peptone, 1 g of yeast extract, 2 g of caseic acid hydrolysate, 5 g of NaCl, and 1 liter of distilled water. To provide the chromium concentration within the range of 50–1000 mg/L**,** Cr(VI) [as K_2CrO_4] was added to the nutrient medium at the early stationary phase of growth. After being cultivated for 5 days the cells were harvested by centrifuging (10,000 rpm, 15 min, 4 °C), rinsed twice in a 20 mM phosphate buffer and analyzed by both NAA and ESR methods. To prepare bacterial samples for NAA**,** wet biomass was placed in an adsorption-condensation lyophilizer, dried, and pelletized to 5 mm pieces (~0.5 g) by means of titanium press form.

INAA at the reactor IBR-2 in FLNP, JINR, Dubna, was applied for determination of chromium in the bacterial cells. Samples were irradiated for 100 h and gamma-spectra of induced activity measured for 30 min – 2 h to provide counting statistics in the peak of Cr with error no worse than 10%. Quality assurance was achieved by certified reference materials Lichen-336 and Bottom Sediments SDM-2T (International Atomic Energy Agency, Austria).

ESR measurements of Cr(III) complexes were carried out in the Andronikashvili Institute of Physics, Tbilisi, at the RE 1306 radiospectrometer with computer-based digital systems for data acquisition and processing. ESR signals were measured at liquid nitrogen temperature (T=77 K) [4].

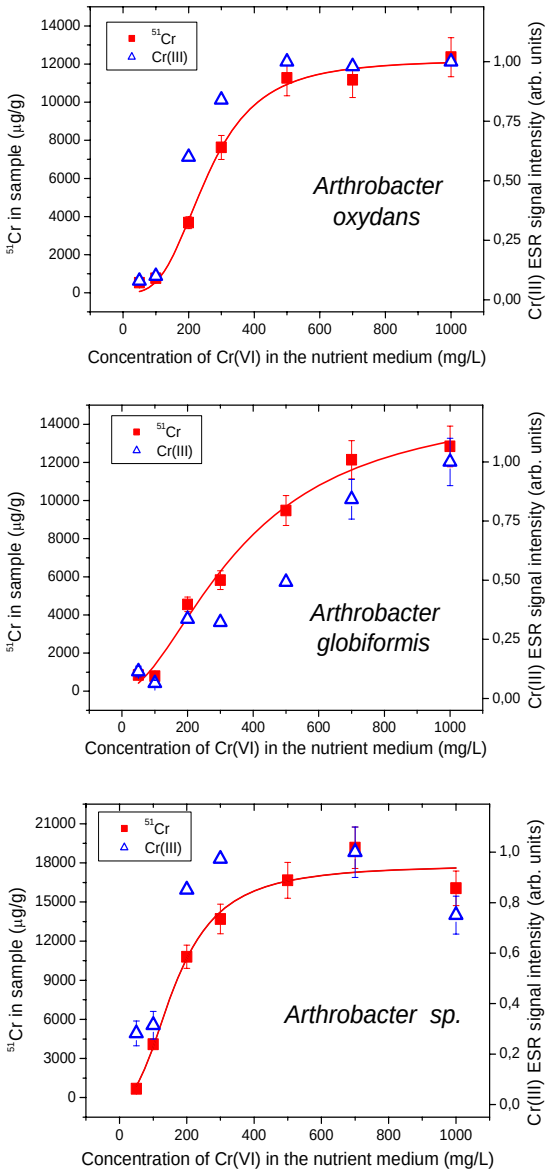

Fig. 1. A dose-dependent accumulation of chromium and formation of Cr(III) complexes in different basalt-inhabiting bacteria of *Arthrobacter* genera

Fig. 1 illustrates that for all bacteria the accumulation of chromium, pronounced in the beginning, is followed by its slower uptake. The relative intensity of Cr(III) ESR signal (with a g-factor of 2.02 and line width of 650 Gauss corresponding to Cr(III) hydroxide), directly proportional to the concentration of Cr(III), behaves similarly. Besides, the concentration of Cr(III) in bacterial cells is of the same order of magnitude as that of total chromium, evidencing that the main amount of accumulated Cr(VI) has been transformed into Cr(III).

To quantify Cr uptake by bacteria, the Langmuir-Freundlich (LF) model (solid lines) was successfully applied [5]:

$$q = \frac{q_{\max}(bc)^n}{1+(bc)^n}$$

Here c is the concentration of metal ions; qmax represents the maximum metal accumulation, b is an affinity parameter of the isotherm reflecting the high affinity of the biosorbent for the sorbate, and n is an empirical parameter that varies with the degree of heterogeneity. As follows from the Table, all tested bacteria are heterogenous (n<1) with a similar ability of chromium accumulation. In case of *Arthrobacter globiformis* the maximum Cr accumulation is reached at the concentrations higher than 1000 mg/L of Cr(VI). In comparison with other bacterial strains, *Arthrobacter sp.* shows

Table. The R^2 and fitting parameters for the LF fit to the accumulation curves of tested bacteria

Bacteria	q_{max} [mg/g]	b [L/mg]	n	R^2
A. oxydans	12.2 ± 0.41	0.004 ± 0.00018	0.32 ± 0.05	0.99
A. globiformis	15.3± 1.88	0.003± 0.0005	0.56 ± 0.11	0.99
Arthrobacter sp.	17.8± 1.05	0.006±0.0007	0.42 ± 0.09	0.98

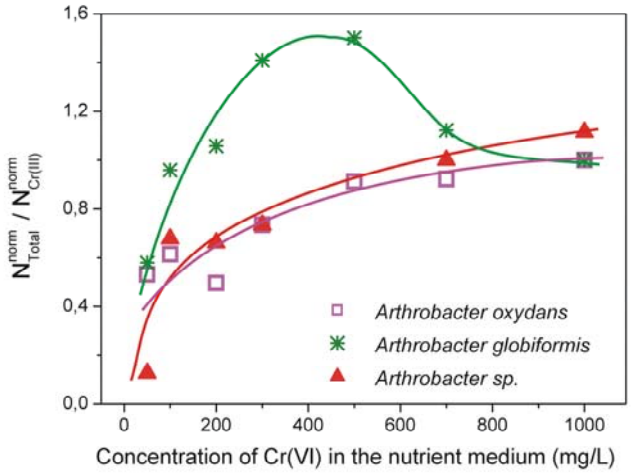

Fig. 2. A comparison between chromium accumulation and formation of Cr(III) complexes in different basalt-inhabiting bacteria of *Arthrobacter* genera exposed to high concentrations of Cr(VI). N_{Total}^{norm} and $N_{Cr(III)}^{norm}$ are, respectively, the total Cr and Cr(III) concentrations in arbitrary units

Figure 2 illustrates that the transformation mechanism of Cr(VI) to Cr(III) is different in each particular bacteria.

Conclusions

By combined application of INAA and ESR spectrometry the behaviour of chromium in basalt-inhabiting bacteria of *Arthrobacter* genera exposed to high concentrations of Cr(VI) was studied. It was shown that the tested bacteria of *Arthrobacter* genera can efficiently detoxify high concentrations of Cr(VI).

NAA measurements revealed that under aerobic conditions the accumulation of chromium in bacteria is dose-dependent and its character changes significantly at higher concentrations of Cr(VI). The chromium accumulation process fits well with the Langmuir-Freundlich model.

By ESR method it was established that the main part of accumulated chromium consists of Cr(III) complexes (in general, Cr(III) hydroxide).

Comparative analysis of dose-dependent formation of Cr(III) complexes and uptake of chromium revealed that Cr(VI) transformation mechanism is rather similar in *Arthrobacter oxydans* and *Arthrobacter sp.*, and is different in *Arthrobacter globiformis.*

References

1. J. Nriagu, J. Pacnya. Nature, 333 (1988) 134.
2. Y. Suzuki, J. Banfield. 2006. Geomicrobiology J. 113.
3. H.-Y. Holman, D. Perry, M. Martin, G. Lamble, W. Mckinney, J. Hunter-Cevera. Geomicrobiology J., 16 (1999) 307.
4. T. Kalabegishvili, N. Tsibakhashvili, H.-Y. Holman, Environ. Sci. Technol. 37 (2003), 4678.
5. V. I. Slaveykova, K. J. Wilkinson, Environ. Chem. 2 (2005) 9

Epithermal NAA for marine geoecology

C. Cristache[a], O. Culicov[b,e], M. Toma[a], M.V. Frontasyeva[b], S.S. Pavlov[b], O.G. Duliu[c], G. Oaie[d]

[a] *Horia Hulubei National Institute for Physics and Nuclear Engineering, Magurele, Romania*
[b] *Joint Institute for Nuclear Research, Dubna, Russia*
[c] *University of Bucharest, Romania*
[d] *National Institute of Marine Geoecology and Geology, Bucharest, Romania*
[e] *National Institute for Research and Development in Electrical Engineering "ICPE – CA", Bucharest, Romania*

The Black Sea represents a remnant of the Mesozoic Tethys Ocean. A continuous layer of almost biologically dead water saturated with dissolved hydrogen sulfide is found between 180 m beyond sea level and the deepest bottom of 2,210 m. Only some anaerobic bacteria inhabit this medium, and for this reason, bottom sediments are completely voided of bioturbation that makes them ideal object for various stratigraphic investigations.

Some of the largest European rivers such as the Danube, Dnieper and Don via the Sea of Azov, flow into the Black Sea, carrying a considerable amount of pollutants, collected from industrial countries [1]. Both atmospheric nuclear weapon tests and the Chernobyl accident released into atmosphere a considerable amount of the radioactive ^{137}Cs which presence in sediments, due to its half-life of 30.4 years represents suitable marker for a recent absolute geochronology [2]. Thus the investigation of the vertical distribution of pollutants in correlation with the ^{137}Cs profile in sediments [3] could be very useful in reconstructing the history of pollution process affecting the Black Sea.

Sediments. The unconsolidated sediment core (a total length of 50 cm) has been collected from the abiotic zone of the Romanian Continental Shelf of the Black Sea, in the vicinity of the town of Constanta, at depth of 600 m below sea level. A digital radiography showed the presence of about 265 distinct layers, 1 to 3 mm thickness. For further investigations, the core was sliced into 45 fragments which thickness gradually increased from 5 mm at the surface to 4 cm at the bottom. Each section was dried at 105 ºC, ground and homogenized. The vertical distribution of five potential pollutants Zn, As, Br, Sn and Sb as well as Sc as a reference natural element in the core collected from the abiotic zone of the Black Sea was examined along with the ^{137}Cs content.

ENAA measurements. An amount of about 0.100 g of bottom sediment material was used for multi-element epithermal NAA carried out at the reactor IBR-2, FLNP, JINR, Dubna. Experimental procedure is described elsewhere [4]. Software developed at FLNP was used for acquisition and processing of gamma spectra of induced activity [5]. Quality assurance was provided by using IAEA standard reference materials SL-1, SL-3, and Sl-7.

^{137}Cs measurements. The ^{137}Cs activity of the uppermost 20 samples were measured at Horia Hulubei National Institute of Physics and Nuclear Engineering -Bucharest for 20 h, using a HPGe detector (Canberra) with a FWHM of 1.9 keV at ^{60}Co 1332 keV and a relative efficiency of 30%. Standard PC software OS2/Gennie for gamma spectra processing was used.

^{137}Cs vertical profile. Radiocesium vertical profile showed two maxima, one of them vas very sharp and localized at a depth of 1 cm and the other very broad, almost undistinguished at about 8 cm depth. As the two major radiocesium aerial pollutions took place in 1963 (atmospheric nuclear bombs tests) and 1986 (Chernobyl accident) and by taking into account

the existence of a vertical migration of Cs ions in sediments, one could conclude that the upper maximum corresponds to the 1986 Chernobyl accident. As the core has been collected in 2004, a sedimentation rate could be assessed as ~ 0.5 mm/year.

To be unambiguously considered as a pollutant, a potentially harmful compound must fulfill two criteria: (i) to exceed the legal limits, and (ii) to present an increased concentration near the sediment surface [6]. Only five of 45 determined elements follow these criteria. The results for these elements are given in the Table.

Table. Max (C_{max}), min (C_{min}), UCC (Upper Continental Crust), normal (C_{norm}); min ($C_{alert,min}$) and max ($C_{alert,max}$) alert concentrations (μg/kg)

Element	C_{max}	C_{min}	UCC [6]	C_{norm} [7]	$C_{alert,min}$ [7]	$C_{alert,\ max}$ [7]
Zn	145	53	71	100	300	700
As	16	8	1.5	5	15	25
Br	149	52	–	50	100	100
Sn	4.8	2.1	5.5	20	35	100
Sb	7.8	1.4	0.2	5	12.5	20

Heavy elements vertical profile. To exclude influence of mineral component of sediments, the concentrations of elements in question were normalized to the relevant Sc concentration considered as a naturally occurred element [8]. The distributions of these ratios along the vertical profile of the core are presented in Fig. 1.

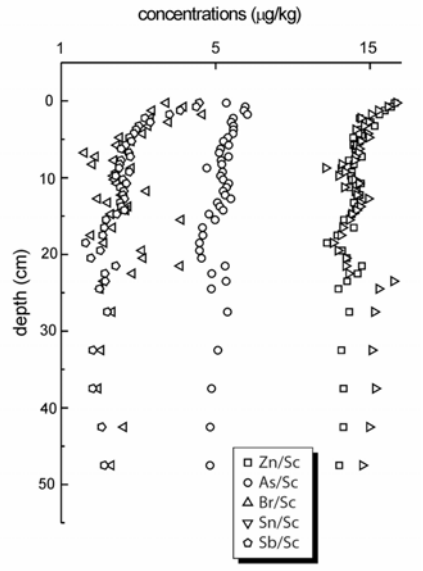

Fig. 1. The vertical distributions of concentrations of Zn, As, Br, Sn and Sb normalized to Sc

It is obviously seen that all of them demonstrate a sharp increase in the concentration range corresponding to the last 5–6 cm below the sediment surface. Taking into account the sedimentation rate discussed above, this interval could be attributed to the last 90–100 years, *i.e.* to the period of rapid industrialization of the European countries.

It should be pointed out that in case of Sn and As, their maximal concentrations are observed at 1 cm below the sediment surface that roughly corresponds to the year of 1990, while the concentrations of other three elements monotonously increases up to the sediment surface. Thus the first criterion is fulfilled for all five elements.

A box and whisker diagram for both average and extreme numerical values of the elemental concentrations is given in Fig.2. It follows from the analysis of the data collection that none of the elemental concentrations reached the intervention threshold. The normal concentrations of Zn, As, Br and Sb are slightly transcended, while the minimal alert concentrations are surpassed only in few cases by As and Br. Therefore, only As and Br satisfy the second criterion. The increased concentration of halogen Br is hardly be attributed to any pollution process, but most probably to its “marine” origin” [9].

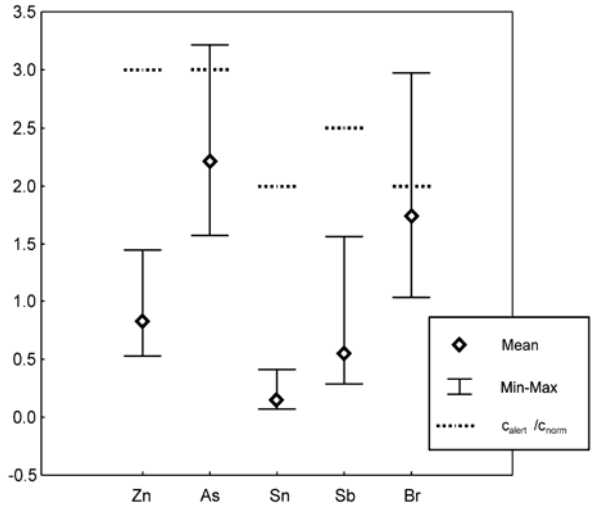

Fig. 2. Box and whiskers diagram for experimental and literature data set

This figure represents the maxim, minimum as well as the average concentrations of considered elements along the entire core. The concentrations of each element were normalized to their normal concentrations taken from [7].

The same procedure we have used for the minimum alert concentrations which positions are marked by the dashed lines.

Correlation analysis applied to the obtained experimental data set revealed strong correlation between the following elements: Zn and Sb (0.97), As and Zn (0.79) and As and Sb (0.78).

This fact could be interpreted more rather by having a common source of pollution than having similar chemical properties.

Conclusion. Epithermal Neutron activation analysis was used to investigate the vertical distribution of the concentrations of potential polluting Zn, As, Br, and Sb in the upper 50 cm of the sediments collected 600 m below sea surface from abiotic zone of the Black Sea.
All these elements presented towards superior limit of sediments increased concentration that in the case of Zn, As and Sb were, in accordance with Romanian Environment Regulations, greater than the normal ones, elements concentrations reached the intervention threshold.
By using Chernobyl ^{137}Cs as time marker it was possible to establish that the region with increased concentrations corresponds to the last 100 years. *i.e.* the period of the steadily industrialization process in Europe.

Acknowledgement. The authors acknowledge the Protocol on Scientific and Technical Cooperation between the University of Bucharest and JINR, Dubna (Reg. No. 06-4-1036-2001/2007) and the grant of RFBR–Romanian Academy (Project No. 07-05-91681).

References

1. S. Reschke, V. Ittekkot, N. Panin. Estuarine, *Coast. Sci*, 54 (2002) 563.
2. R. A. Ligero, M. Barrera et al. *Env. Poll*., 118, (2002), 97.
3. W. Penington, R.S. Cambray, E.M. Fisher. *Natur*e, 242 (1973) 342.
4. M.V. Frontasyeva, S.S. Pavlov. In «Problems of Modern Physics». Edts: A.N. Sissakian, D.I. Trubetskov. Dubna, JINR, 1999, p. 152-158.
5. T.M. Ostrovnaya et al. In Activation Analysis in Environment Protection, D-14-93-325, Dubna (1993) 319-326.
6. S.R. Taylor, S.M. McLennan. The Continental Crust: Its Composition and Evolution. Geoscience Texts, Blackwell, Oxford, 1985.
7. Monitorul Oficial al Romaniei 303 bis, 1997, p. 23 (in Romanian).

8. L.C. Dinescu, O.G. Duliu, M.Badea, N.G. Mihailescu, I.M. Vanghelie, *J. Radioanal. Nucl. Chem.*, 238 (1998) 75.
9. E. Steinnes, M.V. Frontasyeva. *J. Radioanal. Nucl. Chem.*, 253 (2002)173-177.

5. PUBLICATIONS

CONDENSED MATTER PHYSICS

Atomic and magnetic structures

1. Aksenov V.L., Glazkov V.P., Kichanov S.E., Pogoreliy D.K., Podurets K.M., Somenkov V.A., Savenko B.N. Powder diffractometer for microsamples at the Kurchatov Synchrotron Radiation Source, Nucl. Instr. and Meth. A, 2007, v.575, pp.266-268.
2. Antonov V.E., Beskrovnyy A.I., Fedotov V.K., Ivanov A.S., Khasanov S.S., Kolesnikov A.I., Sakharov M.K., Sashin I.L., Tkacz M. Crystal structure and lattice dynamics of chromium hydrides, J. Alloys and Compounds, 2007, v.430, pp.22-28.
3. Dmitriev A.I., Radchenko M.V., Lashkare G.V.v, Butorin P.E., Sichkovskyi V.I., Kovalyuk Z.D., Beskrovny A.I., Aleshkevych P., Szymczak R., Dobrowolski W., Minikaev R. Neutron Diffraction Researches of Magnetic Transformation for Layered semiconductor InSe<Mn>, submitted in Journal of Magnetism and Magnetic Materials.
4. Hall P., Hall E., Houtmann S., Salazar J., Natkanec I., Smirnov L.S., Ivanov A., Beskrovnyy A., Vasilovskiy, S. Butorin P. Study of nanocrystalline substances with sorbed hydrogen by neutron scattering, Communication JINR, E14-2007-65.
5. Kessner D., Kiselev M., Dante S., Hauss T., Lersch P., Wartewig S., Neubert R.H.H. Arrangement of ceramide[EOS] in a stratum corneum lipid model matrix -new aspects revealed by neutron diffraction studies. Submitted to Chem&Phys Lipids, 2007.
6. Kessner D., Kiselev M.A., Hauss T., Dante S., Wartewig S., Neubert R.H.H. Localisation of partially deuterated cholesterol in quaternary SC lipid model membranes. A neutron diffraction study, European Biophysical Journal (Biophysics Letter) submitted, 2007
7. Kessner D., Ruettinger A., Kiselev M.A., Wartewig S., Neubert R.H.H. Properties of ceramides and their impact on the stratum corneum structure. A review, Part II: Stratum corneum lipid mixtures. Skin Pharmacology and Physiology, 2007, in press.
8. Kichanov S.E., Kozlenko D.P., Wasicki J., Nawrocik W., Czarnecki P., Savenko B.N., Glazkov V.P. and Lathe C. Structural phase transitions in pyridinium perrhenate at high pressure, Journal of Molecular Structure, accepted for publication, 2007.
9. Kiselev M.A., Zemlyanaya E.V., Ryabova N.Y., Hauss T., Dante S., Lombardo D. Water distribution function across the curved lipid bilayer: SANS study. Chemical Physics, 2007, in press.
10. Kiselev M.A., Gutberlet T., Hoell A., Aksenov V.L., Lombardo D. Orientation of the DMPC unilamellar vesicle system in the magnetic field: SANS study. Chemical Physics, 2007, in press.
11. Kiselev M.A., Lombardo D., Lesieur P., Kisselev A.M., Borbely S., Simonova T.N., Barsukov L.I. Membrane Self Assembly in Mixed DMPC/NaC Systems by SANS. Chemical Physics, 2007, in press.
12. Kozlenko D.P., Dubrovinsky L.S., Goncharenko I.N., Savenko B.N., Voronin V.I., Kiselev E.A. and Proskurnina N.V. Pressure-induced monoclinic distortion and charge and orbital ordering in $La_{0.5}Ca_{0.5}MnO_3$, Phys. Rev. B, 2007, v.75, pp.104408-1-6.
13. Kozlenko D.P., Dubrovinsky L.S., Jirak Z., Savenko B.N., Martin C., Vratislav S. Pressure-induced antiferromagnetism and compression anisotropy in $Pr_{0.52}Sr_{0.48}MnO_3$ Phys. Rev. B, 2007, v.76, pp.094408-1-6.

14. Kozlenko D.P., Golosova N.O., Jirák Z., Dubrovinsky L.S., Savenko B.N., Tucker M.G., Godec Y. Le and Glazkov V.P. Temperature and pressure driven spin state transitions in $LaCoO_3$, Phys. Rev. B, 2007, v.75, pp.064422-1-12.
15. Kozlenko D.P., Kichanov S.E., Lee S., Park J.-G. and Savenko B.N. Pressure-induced spin fluctuations and spin reorientation in hexagonal manganites" J. Phys.: Condensed Matter, 2007, v.19, pp.156228-1-9.
16. Kozlenko D.P., Trukhanov S.V., Lukin E.V., Troyanchuk I.O., Savenko B.N. Pressure-induced modifications of crystal and magnetic structure of oxygen deficient $La_{0.7}Sr_{0.3}MnO_{3-d}$ manganites, Eur. Phys. J. B, 2007, v.58., pp.361-365.
17. Mirmelstein A., Clementyev E., Voronin V., Akshentsev Yu., Kozlenko D., Kutepov A., Petrovtsev A., Zuev Yu. Effect of chemical and external pressure on the structure of intermetallic compound CeNi", J. Alloys and Compounds, 2007, v.444-445, pp.281-284.
18. Nietz V.V., Osipov A.A. Ball solitons and kinetics of the first order magnetic phase transition, admitted in Journal of Magnetism and Magnetic Materials.
19. Nietz V.V., Osipov A.A. Ball solitons in kinetics of the first order magnetic phase transition, Communication JINR, 2007, E17-2007-63, Dubna.
20. Nietz V.V., Stavisskiy Yu.Ya. Prospects for neutron research of magnetism with a pulsed magnetic field at powerful pulsed neutron sources, in press Journal of Neutron Research, 2007.
21. Pomjakushin V.Yu., Sheptyakov D.V., Conder K., Pomjakushina E.V., Balagurov A.M. Effect of oxygen isotope substitution and crystal microstructure on magnetic ordering and phase separation in $(La_{1-y}Pr_y)_{0.7}Ca_{0.3}MnO_3$, Phys. Rev. B, 2007, v.75, pp.054410-1-12.
22. Ruettinger A., Kiselev M.A., Hauss Th., Dante S., Neubert R.H.H. Fatty acid interdigitation in the stratum corneum model membranes: A neutron diffraction study. Submitted to European Biophys. J., 2007.
23. Балагуров А.М., Бобриков И.А., Помякушин В.Ю., Шептяков Д.В., Бабушкин Н.А.а, Горбенко О.Ю., Картавцева М.С., Кауль А.Р. Влияние изотопического состава и микроструктуры на кристаллическое и магнитное фазовое состояние в $R_{0.5}Sr_{0.5}MnO_3$ ЖЭТФ, принята в печать.
24. Биккулова Н.Н., Бескровный А.И., Ядровский Е.Л., Скоморохов А.Н., Степанов Ю.М., Миколайчук А.Н., Сагдаткиреева М.Б., Каримов Л.З. Динамика решётки и ионный перенос в структурно-разупорядоченных халькогенидах меди и серебра. Кристаллография, 2007, том 52, №3, с.474-476.
25. Дмитриев А.И., Лашкарев Г.В., Буторин П.Е., Сичковский В.И., Радченко М.В., Ковалюк З.Д., Бескровний А.И., Алешкевич П., Шимчак Р., Добровольский Д., Миникаев Р. Нейтронографические исследования магнитных превращений слоистого полупроводника InSe<Mn>, направлена в печать в Украинский физический журнал.
26. Злоказов В.Б., Бобриков И.А., Балагуров А.М. Анализ данных магнитного дифракционного рассеяния нейтронов на поликристаллах с помощью программы VMRIA, Сообщение ОИЯИ, 2007, Р10-2007-118, ОИЯИ, Дубна.
27. Киселев М.А. Комбинированное применение нейтронного и синхротронного излучения для исследования влияния диметилсульфоксида на структуру и свойства везикул из дипальмитоилфосфатидилхолина. Кристаллография, 2007, т.52, с.554-559.
28. Киселев М.А. Конформация молекул церамида 6 и chain-flip переходы в липидной матрице верхнего слоя кожи - Stratum Corneum. Кристаллография, 2007, т.52, с.549-553.

29. Кичанов С.Е., Козленко Д.П., Вонсицки Я.В., Чернецки П., Глазков В.П., Наврочик В., Савенко Б.Н., Лате К. Исследование структуры молекулярного кристалла $PyHReO_4$ под высоким давлением, Кристаллография, 2007, т.52, с.468-471.
30. Козленко Д.П., Воронин В.И., Глазков В.П., Савенко Б.Н. Влияние высокого давления и химического замещения на кристаллическую структуру и магнитное состояние $R_2Fe_{17-x}Si_x$ (R = Lu, Y; x =0, 1.7), Письма в ЖЭТФ, 2007, т. 86, стр. 675-680.
31. Козленко Д.П., Кичанов С.Е., Ли С., Парк Дж.-Г., Глазков В.П., Савенко Б.Н. Гексагональные фрустрированные манганиты $RMnO_3$ (R=Y, Lu) при высоких давлениях, Кристаллография, 2007, т.52, с.441-445.
32. Козленко Д.П., Овсянников С.В., Щенников В.В., Воронин В.И., Савенко Б.Н. Термоэлектрические свойства манганита $La_{0.75}Ca_{0.25}MnO_3$ при сверхвысоких давлениях до 20 ГПа, Письма в ЖЭТФ, 2007, т.85, с.242-246.
33. Козленко Д.П., Труханов С.В., Лукин Е.В., Троянчук И.О., Савенко Б.Н., Глазков В.П. Влияние дефицита кислорода и высокого давления на магнитную и кристаллическую структуры манганитов $La_{0.7}Sr_{0.3}MnO_{3-d}$, Письма в ЖЭТФ, 2007, т.85, с.123-127.
34. Лушников С.А., Балагуров А.М., Бобриков И. А., Вербецкий В.Н., Глазков В.П., Соменков В.А. Структура и особенности химической связи в дейтеридах $CeNi_3$. Неорг. мат., 2007, т.43(7), с.1-8. Lushnikov S.A., Balagurov A.M., Bobrikov I.A., Verbeckii V.N., Glazkov V.P., Somenkov V.A. Structure and chemical bonds peculiarities in $CeNi_3$ deuterides.
35. Нитц В.В. Мощные импульсные источники нейтронов для исследований с импульсным магнитным полем, Кристаллография, 2008, т.54, № 2.
36. Нитц В.В., Осипов А.А. Шаровые солитоны в кинетике магнитных фазовых переходов первого рода. Новый механизм фазовой перестройки, Кристаллография, 2008, т.53, № 1, с.130-134.
37. Труханов С.В., Троянчук И.О., Бобриков И.А., Симкин В.Г., Балагуров А.М., Структурное исследование анион-дефицитных манганитов $La_{0.70}Sr_{0.30}MnO_{3-\delta}$ Кристаллография, 2007, т.52(5), с.834 - 839.

Applied research (diffraction)

38. Frischbutter A., Janssen Ch., Scheffzük Ch., Walther K., Ullemeyer K., Behrmann J.H., Nikitin A.N., Ivankina T.I., Kern H. & Leiss B. Strain and texture measurements on geological samples using neutron diffraction at IBR-2, Joint Institute for Nuclear Research Dubna (Russia), Dedicated to the 50th anniversary of the Joint Institute for Nuclear Research Dubna. ЭЧАЯ (Physics of Particles and Nuclei), 2007, v.37 (Suppl.7), S91-S128.
39. Ivankina T.I., Kern H., Lokajicek T., Nikitin A.N., Pros Z. The effect of oriented microcracks and crystallographic and shape preferred orientation on bulk elastic anisotropy of a strongly foliated biotite gneiss. Tectonophysics. 2007. (submitted).
40. Lychagina T.A., Nikolayev D.I., Wagner F. Using Individual Spectra Simulation for a Pole Figures Errors Study, Physica Status Solidi, accepted.
41. Nikolayev D., Siegesmund S., Mosch S. and Hoffmann A. Model-based prediction of unfractured rock masses, ZDGG, 2007, v.158/3, pp.483-490.
42. Nikolayev D., Siegesmund S., Mosch S. and Hoffmann A. Quantification of nfractured rock masses, LITOS, 2007, v.92/5, pp.94-111.
43. Scheffzük Ch., Siegesmund S., Nikolayev D.I. & Hoffmann A. Texture, spatial and orientation dependence of internal strain in marble: A key to understand the bowing of

marble panels? In: Přikryl, R. & Smith, B.J. (eds.): Building Stone Decay: From Diagnosis to Conservation. Spec. Publs Geol. Soc. London, 2007, v.271, pp.237-249.

44. Scheffzük Ch., Walther K., Frischbutter A. & Naumann R.: Residual strain and texture of an anhydrite-dolomite-specimen, sampled in the Piora-syncline (Central Switzerland). Z. Geol. Wiss., 2007, submitted.
45. Siegesmund S., Mosch S., Scheffzük Ch. & Nikolayev D.I. The bowing potential of granitic rocks: Rock fabrics, thermal properties and residual strain, Environment Geology, 2007, in print.
46. Taran Yu.V. To the 40th anniversary of the first nuclear experiment with a polarized deuteron target, In: Proc. XIV International Seminar on Interaction of Neutrons with Nuclei "Neutron Spectroscopy, Nuclear Structure, Related Topics", 2007, JINR E3-2007-23, Dubna, pp.22-29.
47. Taran Yu.V., Schreiber J., Balagurov A.M., Stuhr U., Kockelmann H., Zlokazov V.B. Triaxial residual stresses in composite tube from austenitic stainless steel with welded ferritic steel cladding, Zeitschrift fur Kristallographie, 2007, Supplement Issue no. 26, pp.355-360.
48. Walther K., Scheffzük Ch., Frischbutter A., Naumann R. & Brovkin I.V. A "Zuckerdolomit"-sample from the Piora Mulde (Switzerland), studied by an in situ applied load experiment using neutron time-of-flight diffraction, Z. geol. Wiss. (submitted).
49. Walther, K., Frischbutter, A., Scheffzük, Ch., Kenkmann, T. & Eichhorn, F. Diffraction measurements with synchrotron radiation on superimposed deformed composite of quartzite and dunite, Z. Geol. Wiss., 2007, v.35 (1/2), pp.17-26.
50. Базалеев Н.И., Воробьев И.Б., Иванкина Т.И., Клепиков В.Ф., Литвиненко В.В., Лонин Ю.Ф., Никитин А.Н. и др. Радиационные методы оценки рисков захоронения радиоактивных отходов в горных породах, Письма в ЭЧАЯ, 2007 (сдано в печать).
51. Лычагина Т.А., Николаев Д.И. Исследование ошибок экспериментальных полюсных фигур с помощью моделирования индивидуальных спектров, Кристаллография, 2007, т.52, с.804-810.
52. Никитин А.Н., Иванкина Т.И., Уллемайер К., Васин Р.Н. Аналогичные кристаллографические текстуры кварца в горных породах континентальной земной коры по данным нейтронографии. Часть I. Типизация текстур в мономинеральных горных породах. Кристаллография, 2007, принята в печать.
53. Никитин А.Н., Иванкина Т.И., Уллемайер К., Васин Р.Н. Аналогичные кристаллографические текстуры кварца в горных породах континентальной земной коры по данным нейтронографии. Часть II. Типизация текстур в многофазных горных породах, Кристаллография. 2007. Принята в печать.
54. Никитин А.Н., Иванкина Т.И., Уллемайер К., Васин Р.Н. Аналогичные кристаллографические текстуры кварца в горных породах континентальной земной коры по данным нейтронографии. Часть III. Связь типов текстур кварца с механизмами и условиями текстурообразования, Кристаллография, 2007, принята в печать.
55. Никитин А.Н., Кулаковский А.Л., Родкин М.В., Юрченко О.Ю., Иванкина Т.И., Васин Р.Н. О некоторых механизмах проницаемости горных пород в связи с геоэкологической безопасностью хранилищ высокорадиоактивных отходов, Геофизические исследования, Сб.науч.тр./ Институт физики Земли РАН. – М.: ИФЗ РАН, 2006, вып.6, с. 85-95.
56. Никитин А.Н., Маркова Г.В., Балагуров А.М. и др. Исследования структуры и свойств кварца в облсти α-β перехода методами нейтронной дифракции и

механической спектроскопии, Кристаллография, 2007, т. 52, № 3, с. 450-457. Nikitin A.N., Markova G.V., Balagurov A.M., Vasin R.N., Alekseeva O.V. Investigation of the structure and properties of quartz in the α-β transition range by neutron diffraction and mechanical spectroscopy, Crystallography Reports, 2007, v.52, pp.428-435.

57. Смирнов Ю.П., Горбацевич Ф.Ф., Никитин А.Н., Тюремнов В.А. Характеристики текстуры, структуры, анизотропии пород по разрезу Кольской сверхглубокой скважины. Вестник МГТУ. Сб.науч.тр. «Глубинное вещество: Структура, свойства и состояние в геопространстве Кольской сверхглубокой скважины. Результаты исследований по проекту МПГК-408 ЮНЕСКО», 2007, т.10, № 2, с.285-295.
58. Уваров В.Т., Уваров В.В., Робук В.Н., Пономарев А.Г., Никитин А.Н., Лонин Ю.Ф., Литвиненко В.В., Иванкина Т.И. и др. Процессы массопереноса в образцах горных пород под действием импульсных сильноточных пучков электронов, Письма в ЭЧАЯ, 2007 (сдано в печать).

Nanostructures (SANS)

1. Aksenov V.L., Avdeev M.V., Kyzyma O.A., Rosta L., Korobov M.V.. Age effect of solution C_{60}/N-methilpyrrolidone on the cluster structure in the system C_{60}/N-methilpyrrolidone/water, Crystallography reports 52 (2007) 479-482.
2. Avdeev M.V., Aksenov V.L., Rosta L., Pressure induced changes in fractal structure of detonation nanodiamond powder by small-angle neutron scattering, Diamond and Related Mater. 16 (2007) 2050-2053.
3. Avdeev M.V., Bica D., Vékás L., Marinica O., Balasoiu M., Aksenov V.L., Rosta L., Garamus V.M., Schreyer A. On the possibility of using short chain length mono-carboxylic acids for stabilization of magnetic fluids, J. Mag. Mag. Mater., 2007, v.311, pp.6-9.
4. Avdeev M.V., Contrast variation in small-angle scattering experiments on polydisperse and superparamagnetic systems: basic functions approach, J. Appl. Cryst., 2007, v.40, pp.56-70.
5. Avdeev M.V., Tropin T.V., Aksenov V.L., Rosta L., Kholmurodov M.T., On the question of fullerene cluster formation and growth in carbon disulfide solutions. Small-angle neutron scattering and molecular dynamics data, J. Surf. Investigation. X-ray, Synchrotron and Neutron Techniques (2007) accepted.
6. Balasoiu M., Avdeev M. V., Aksenov V. L., SANS Study of Clusters in Aqueous Magnetic Fluids, Review, Crystallography Reports, 52 (2007) 505–511.
7. Balasoiu M., Barsov S.G., Bica D., Vekas L., Vorobyev S.I., Gritsaj K.I., Duginov V.N., Zhukov V.A., Komarov E.N., Koptev V.P., Kotov S.A., Mamedov T.N., Mikirtychyants C.M., Petrescu C., Shcherbakov G.V. Influence of magnetic nanoparticles on behaviour of polarized positive muons in ferrofluid on the Fe_3O_4 base in carrier medium D_2O, 2007, Preprint PNPI No. 2745 (in Rus.)
8. Balasoiu M., Bica D., Vekas L., Gritsaj K.I., Duginov V.N., Zhukov V.A., Mamedov T.N., Olshevsky V.G., Petrescu C. Magnetic properties investigation of the magnetite ferrofluids by mSR spectroscopy at the Phasotron in function at LNP JINR, 2007, JINR Comunication P14-2007-21, Dubna (in Russian).
9. Feoktystov A.V., Avdeev M.V., Aksenov V.L., Bulavin L.A., Bica D., Vekas L., Garamus V.M., Willumeit R., Small-angle neutron scattering contrast variation on ferrofluid magnetite/myristic asid/benzene, J. Surf. Investigation. X-ray, Synchrotron and Neutron Techniques (2007) accepted.
10. Haramagatti C.R., Islamov A., Gibhardt H., Gorski N., Kuklin A. and Eckold G. Pressure induced phase transitions of TTAB-micellar solutions studied by SANS and Raman spectroscopy, Phys. Chem. Chem. Phys., 2006, v.8, pp.994–1000.

11. Here M., Islamov A., Kuklin A., Gago M., Gruszecki W.I. Effect of antibiotic amphotericin B on structural and dynamic properties of lipid membranes formed with egg yolk phosphatidylcholine, Chemistry and Physics of Lipids, 2007, v.147, pp.78–86.
12. Ioffe A., Bodnarchuk V., Bussmann K.. R.Müller, Larmor labeling by time gradient magnetic fields, Physica B 397 (2007) 108-111.
13. Jernenkov M., Klimko S., Llauter-Pasyuk V., Toperverg B., Milyaev M., Romashev L., Ustinov V., Aksenov V., Lauter H., Larmor precession reflectometry for magnetic film studies, Nucl. Instr. Meth. A (2007), in print.
14. Khokhryakov A.O., Avdeev M.V., Kyzyma O.A., Len A., Bulavin L.A., Aksenov V.L., Colloidal structure and nature of stabilization of nonmodified fullerene water solutions, Crystallography Reports 52 (2007) 487–491.
15. Kovalev Yu.S., Kuklin A.I., Novikov A.G., Savostin V.V., Shimkevich A.L., Jadrovsky E.L. The microstructure of Pb–K liquid alloy from small-angle neutron scattering experiments, Journal of Non-Crystalline Solids, 2007, v.353, pp.3532-3534.
16. Krainova E.A., Avdeev M.V., Merkushina K.V., Rodionov A.I., Garamus V.M., Willumeit R., Structural Studies of a Carbonizate Obtained from Solid Cellulose-containing Waste by Sulfuric Acid Carbonization, Rus. J. Appl. Chem. 80 (2007) 1670
17. Kyzyma O.A., Avdeev M.V., Aksenov V.L., Bulavin L.A., Snegir S.V., Reorganization of fullerene clusters in the system C_{60}/N-metyl-2-pyrrolidone/water, J. Surf. Investigation. X-ray, Synchrotron and Neutron Techniques (2007) accepted.
18. Kyzyma O.A., Bulavin L.A., Aksenov V.L., Avdeev M.V., Tropin T.V., Korobov M.V., Snegir S.V., Rosta L.. Organization of fullerene clusters in the system C_{60}/N-metyl-2-pyrrolidone, Materials structure in Chemistry, Biology, Physics and Technology (2007) accepted.
19. Kyzyma O.A., Bulavin L.A., Aksenov V.L., Avdeev M.V., Tropin T.V., Korobov M.V., S.V. Snegir, L. Rosta, Aggregation in C_{60}/NMP, C_{60}/NMP/water and C_{60}/NMP/Toluene mixtures, Fullerenes, Nanotubes and Carbon Nonstructures. (2007) in print.
20. Lauter-Pasyuk V.V., Neutron grazing incidence techniques for nano-science, Journal de Physique IV (2007) in print.
21. Molchanov V.S., Philippova O.E., Khokhlov A.R., Kovalev Y.A., Kuklin A.I. Self-Assembled Networks Highly Responsive to Hydrocarbons, Langmuir, 2007, v.23, pp.105-111.
22. Novosylna O., Kanibolotsky D., Serdyuk I., Timchenko A., Tiktopulo E., Negrutskii B., Analysis of conformation differences of the normal and oncogenic isoforms of eEF1A1, Acta Biochimica Polonica, 54 (2007) 24.
23. Petrenko V.I., Avdeev M.V., Aksenov V.L., Bulavin L.A., Rosta L., Structure of magnetic fluids with surfactant excess by small-angle neutron scattering, J. Surf. Investigation. X-ray, Synchrotron and Neutron Techniques (2007) accepted.
24. Toperverg B., Kampmann R., Lauter-Pasruk V., Lauter H., Tietze U., Solina D., Schreyer A., Larmor encoding and Fourier reconstruction for wavelength dispersive reflectometry, Physica B 397 (2007) 141.
25. Tropin T.V., Avdeev M.V., Aksenov V.L., Small-angle neutron scattering study of C_{60}/CS_2 solutions, Fullerenes, Nanotubes and Carbon Nanoclusters, (2007) in print.
26. Vekas L., Bica D., Avdeev M.V., Magnetic nanoparticles and concentrated magnetic nanofluids: Synthesis, properties and some applications, Review, China Particuology 5 (2007) 43–49.
27. Авдеев М.В., Структурные особенности магнитных жидкостей, УФН 177 (2007) 1139-1144.
28. Боднарчук В.И., Ярадайкин С.П., Поиск неупругого рассеяния тепловых нейтронов на планарных магнитных возбуждениях, Кристаллография 52 (2007) 573-575.

29. Боднарчук И.А., Холмуродов Х.Т., Петренко В.И., Авдеев М.В. Определение предельного парциального молярного объема растворов монокарбоксильных кислот в бензоле методом молекулярно-динамического моделирования, направлено в Ж. Хим. Физ.
30. Горшкова Ю.Е., Горделий В.И. Исследование взаимодействия диметилсульфоксида с липидными мембранами с помощью малоуглового рассеяния нейтронов, Кристаллография, 2007, т.52, № 3, с.584–588.
31. Докукин М.Е., Перов Н.С., Докукин Е.Б., Исламов А.Х., Куклин А.И., Калинин Ю.Е., Ситников А.В. Изменение магнитных свойств гранулированных пленок на основе Со при перколяционном переходе, Известия РАН. Серия Физическая, 2007, т.71, №11, с.1643-1644.
32. Жерненков М., Климко С., Лаутер–Пасюк В., Топерверг Б. П., Миляев М., Рамашев Л., Устинов В., Лаутер Х., Аксенов В., Рефлектометрия с Ларморовской прецессией для исследования многослойных структур, Кристаллография (2007) в печати.
33. Муругова Т.Н., Горделий В.И., Куклин А.И., Ковалев Ю.С., Юрков В.И., Нюренберг А., Исламов А.Х., Ягужинский Л.С. Обнаружение новых двумембранных структур в нативных митохондриях с помощью метода малоуглового рассеяния нейтронов Биофизика, 2006, т.51, №6, с.1001-1007.
34. Муругова Т.Н., Горделий В.И., Куклин А.И., Солодовникова И.М. и Ягужинский Л.С. Регистрация трехмерно упорядоченных структур в интактных митохондриях с помощью метода малоуглового рассеяния нейтронов, Кристаллография, 2007, т.52, №3, с.545-548.
35. Новосильная А.В., Тимченко А.А., Тиктопуло Е.И., Сердюк И.Н., Негруцкий Б.С., Ельская А.В., Характеристика физических свойств изоформ фактора элонгации трансляции eEF1A, Биополимеры и клетка 23 (2007) 386-391.
36. Рогачев А.В., Черный А.Ю., Озерин А.Н., Горделий В.И., Куклин А.И. Модель шаровых секторов для описания экспериментальных данных малоуглового рассеяния нейтронов на дендримерах, Кристаллография, 2007, т.52, №3, с.546-550.
37. Селиванова О.М., Федорова Ю.Ю., Сердюк И.Н., Протеолиз рибосомного белка S1 из Escherichia coli и Thermus thermophilus приводит к образованию двух разных фрагментов, Биохимия, 72 (2007) 1112-117.
38. Сердюк И.Н., Галзитская О.В., Неупорядоченные области в элонгационных факторах трех Надцарствах Живого Мира, Молекулярная биология 41 (2007) 134-138.
39. Сердюк И.Н., Структурированные белки и белки с внутренней неупоеядоченностью, Молекулярная биология, 41 (2007) 297-313.
40. Тропин Т.В., Авдеев М.В., Аксенов В.Л., Немонотонное поведение концентрации в кинетике растворения фуллеренов, Кристаллография 52 (2007) 528-531.
41. Федотов Г.Н., Пахомов Е.И., Поздняков А.И., Куклин А.И., Исламов А.Х., Путляев В.И. Структура и свойства почвенных органико-минеральных гелей, Почвоведение, 2007, № 9, с.1071–1077.
42. Феоктистов А.В., Авдеев М.В., Аксенов В.Л., Булавин Л.А., Бика Д., Векаш Л., Гарамус В.М., Виллумайт Р. Вариация контраста в малоугловом рассеянии нейтронов на магнитной жидкости магнетит/миристиновая кислота/бензол, Поверхность, принято к печати.

Nanostructures (reflectometry)

1. Аксенов В.Л., Игнатович В.К., Никитенко Ю.В. Отражение нейтронов от геликоидальных систем, Поверхность, рентгеновские, синхротронные и нейтронные исследования, 2007, № 9, с.40-48.
2. Аксенов В.Л., Никитенко Ю.В. Нейтронная поляризационная рефлектометрия на импульсном реакторе ИБР-2, Кристаллография, 2007, т.52, с.564-572.
3. Aksenov V.L., Nikitenko Yu.V., Osipov A.A. Neutron Nano-Spin-Echo Spectrometer Based on Magnetic Nanostructures, Crystallography Reports, 2007, 52, No.5, pp.901-905.
4. Аксенов В.Л., Никитенко Ю.В., Петренко А.В., Уздин В.М., Хайдуков Ю.Н., Цабель Х. Особенности магнитного состояния слоистой наноструктуры ферромагнетик-сверхпроводник Fe-V, Кристаллография, 2007, т.52, №3, с.403-409.
5. Аксенов В.Л., Никитенко Ю.В., Проглядо В.В., Хайдуков Ю.Н., Гаврилов В., Райтман Э., Боттян Л., Надь Д. Исследование влияния ультразвукой упругой волны на магнитное упорядочение в слоистой структуре 20х[Fe(1.99нм)/Cr(1.2нм]/MgO. Сообщение ОИЯИ, 2007, Р14-2007-109, Дубна.
6. Deak L., Spiering H., Bottyan L., Nagy D.L., Khaidukov Yu. N., Yoda Y. Perturbative Theory of Grazing-Incidence Diffuse Nuclear Resonant Scattering of Synchrotron Radiation, Phys. Rev. B, accepted.
7. Wolff M., Zhernenkov K., Zabel H. Neutron reflectometry with ADAM at the ILL: Present status and future perspectives, 2007, Thin Solid Films, v.515, pp.5712-5715.
8. Vadalà M., Nefedov A., Wolff M., Zhernenkov K., Westerholt K., Zabel H. Structure and magnetism of Co_2MnGe – Heusler multilayers with V, Au and AlO_x spacer layers, Journal of Physics D: Applied Physics, 2007, v.40(5), pp.1289-1292.
9. Kozhevnikov S.V., Ott F., Kentzinger E., Paul A. Enhanced off-specular scattering in magnetic neutron waveguides, Physica B, 2007, v.397, pp.68-70.

Inelastic Scattering

1. Bator G., L.Sobczyk, A.Pawlukojc, J.Nowicka-Scheibe, E.Grech, J.Krawczyk, M.Nowina-Konopka, I.Natkaniec, I.V.Kalinin and O.Steisvoll, Inelastic and quasielastic neutron scattering and IR and R spectroscopic studies of 1,2,4,5-tetracyanobenzene(TCNB)-1,2,4,5-tetramethylbenzene (durene) complex' Phase Transitions, Vol. 80, No 6–7, June–July 2007, 489–500.
2. Bator G., Sobczy L.k, Рчяawlukojc A., Nowicka-Scheibe J., Grech E., Krawczyk J., Nowina-Konopka M., Natkaniec I., Kalinin I.V. and Steisvoll O. Inelastic and quasielastic neutron scattering and IR and R spectroscopic studies of 1,2,4,5-tetracyanobenzene(TCNB)-1,2,4,5-tetramethylbenzene (durene) comple Phase Transitions, 2007, v.80, pp.489–500.
3. Blagoveshchenskii N.M., V.A.Morozov, A.G.Novikov, D.V.Savostin, V.V.Savostin, A.L.Shimkevich, Na-Pb liquid alloy structure at low lead concentrations: Neutron-diffraction studies. J. Non-Cryst. Solids, 353(2007)3032-3034.
4. Juszynska E., Massalska-Arodz M., Natkaniec I., Krawczyk J. Neutron scattering studies of solid-state polymorphism in dimethyl butanol glass formers, Physica B, 2007, v.403, pp.109-114.
5. Kolesnikov A.I., Antonov V.E, Markushin Yu.E., Natkaniec I., Sakharov M.K. Lattice dynamics of α-AlH_3 and α-AlD_3 by inelastic neutron scattering: High-energy band of optical bond-stretching vibrations, Phys. Rev. B, 2007, v.76, pp.643002-1-7.

6. Kovalev Yu.S., A.I.Kuklin, A.G.Novikov, V.V.Savostin, A.L.Shimkevich, E.L.Jadrovsky, The Microstructure of Pb-K Melt from Small Angle Neutron Scattering Experiments. J. Non-Cryst. Solids, 353(2007)3532-3534.
7. Migdal-Mikuli A., Holderna-Natkaniec K., Mikuli E., Hetmanczyk L., Natkaniec I. Phase transitions and NH_3 motions in $[Zn(NH_3)_4](ClO_4)_2$ studied by incoherent neutron scattering and ^1H NMR methods, Chemical Physics, 2007, v.335, pp.187-193.
8. Natkaniec I., Holderna-Natkaniec K. and Nowak D. Neutron Scattering Studies of Molecular Dynamics in Solid Phases of Neohexane and Diisopropyl, in Quasi-Elastic Neutron Scattering Conference 2006 (QENS2006), edited by Paul E. Sokol, Helmut Kaiser, David Baxter, Roger Pynn, Dobrin Bossev, Mark Leuschner, Mater. Res. Soc., Warrendale, PA, 2007, pp.117-122.
9. Natkaniec I., Holderna-Natkaniec K., Nowak D., Majerz I. and Prager M. Molecular Dynamics in Crystalline and Glassy State of 2,4,6-trimethyl-pyridine, in Quasi-Elastic Neutron Scattering Conference 2006 (QENS2006), edited by Paul E. Sokol, Helmut Kaiser, David Baxter, Roger Pynn, Dobrin Bossev, Mark Leuschner, Mater. Res. Soc., Warrendale, PA, 2007, pp.131-136.
10. Pawlukojć A., Starosta W., Leciejewicz J., Natkaniec I., Nowak D. The molecular structure and dynamics of 2-aminopyridine-3-carboxilic acid by X-ray diffraction at 100K, inelastic neutron scattering, infrared, Raman spectroscopy and from first principles calculation, Chem. Phys. Lett., 2007, v.437, pp.32-37.
11. Pokotilovski Yu. N., Natkaniec I., Holderna-Natkaniec K. The experimental and calculated density of states and UCN loss coefficients of perfluoropolyether oils at low temperatures, Physica B, 2007, in print.
12. Prager M., Desmedt A., Allgaier J., Russina M., Janses A., Natkaniec I., Pawlukojc A., Press W. Methyl group rotations and whole molecule dynamics in methyl bromide hydrate, Phase Transitions, 2007, v.80. No.6-7, pp. 473-488.
13. Reehuis M., Wozniak K., Dominiak P., Smirnov L.S., Natkaniec I., Baranov A.I., Dolbinina V.V. X-ray and neutron single crystal diffraction on $(NH_4)_3H(SO_4)_2$. II. Refinement of phase II crystal structure at room temperature, Поверхность, рентгеновские, синхротронные и нейтронные исследования, 2007, №11, с.21-28.
14. Skomorokhov A.N., D.M.Trots, I.L. Sashin, H.Fuess, E.L.Jadrowskii, S.G.Ovchinnikov, Phonon density of states in γ-, β- and α- AgCuS, Физика Твердого Тела, 2007, в печати.
15. Skomorokhov A.N., D.Trots, S.Ovchinnikov, H.Fuess, Lattice vibrations in an α- and β-AgCuS superionic conductor: experimental time-of-flight inelastic neutron scattering studies, Journal of Physics: Condensed Matter 2007, V.19., p.186228 - 186240
16. Skomorokhov A.N., Trots D.M., Sashin I.L., Fuess H., Jadrowskii E.L., Ovchinnikov S.G. Phonon density of states in γ-, β- and α- AgCuS, ФТТ, 2007, в печати.
17. Smirnov L.S., Melnyk G., Zink N., Wozniak K., Dominiak P., Pawlukojc A., Shuvalov L.A., Loose A. Refinement of hydrogen positions in $(NH_4)_2SeO_4$, Journal of Surface Investigation, X-ray, Synchrotron and Neutron Techniques, 2007, v.1, No.1, pp.113-119, Поверхность, рентгеновские, синхротронные и нейтронные исследования, 2007, №2, с.73-79.
18. Sobolev O., A.Novikov, J.Pieper, Quasielastic neutron scattering and microscopic dynamics of liquid ethylene glycol, Chemical Physics 334(2007)36-44.
19. Биккулова Н.Н., А.И.Бескровный, Е.Л.Ядровский, А.Н.Скоморохов, Ю.М.Степанов, А.Н.Миколайчук, М.Б.Сагдакириева, Л.З.Каримов, Динамика решетки и ионный перенос в структурно-разупорядоченных халькогенидах меди и серебра // Кристаллография, 2007, том 52, №3, с.474-476.

20. Благовещенский Н.М., В.А.Морозов, А.Г.Новиков, В.В.Савостин, Д.В.Савостин, А.Л.Шимкевич. Изучение микродинамики жидкого лития и расплава литий−водород методом неупругого рассеяния нейтронов. Кристаллография, 2007, т. 52, № 3, с. 498 – 504 (англ. вариант: Crystallography Reports. 52 (2007) 406).
21. Благовещенский Н.М., Н.И.Логинов, В.А.Морозов, А.Г.Новиков, А.В.Пучков, В.В.Савостин, Д.В.Савостин, А.Л.Шимкевич, Исследования жидкометаллических композиций на основе свинца методом нейтронного рассеяния, Известия вузов. Ядерная энергетика, 2007, №1, с.129-137.
22. Дубовский О.А., Орлов А.В. / Периодическая взаимная конверсия солитонных волн сжатия и разрежения в кристаллах с межатомным потенциалом Леннарда – Джонса, направлено в Письма в ЖЭТФ.
23. Дубовский О.А., Орлов А.В. / Солитоны сжатия двух типов в кристаллах с межатомным потенциалом взаимодействия Леннарда – Джонса, направлено в Письма в ЖЭТФ
24. Дубовский О.А., Орлов А.В. /Бесфононные солитонные волны – ранние предвестники разрушения кристаллических материалов//Препринт ФЭИ – 3103, 2007 г., 24 стр.
25. Калинин И.В., Лаутер Х., Коза М., Лаутер-Пасюк В.В., Пучков А.В. Поверхностные возбуждения в нано-пленках жидкого гелия, Кристаллография, 2007, т.52, №3, с.505-510.
26. Калинин И.В., Х.Лаутер, А.В.Пучков «Исследование особенностей спектра возбуждений сверхтекучего гелия методом неупругого рассеяния нейтронов», ЖЭТФ, 2007, т.132, вып.1, с.157.
27. Калинин И.В., Х.Лаутер, М.Коза, В.В.Лаутер-Пасюк, А.В.Пучков «Поверхностные возбуждения в нано-пленках жидкого гелия», Кристаллография, 2007, т. 52, № 3, с. 505-510.
28. Семенов В.А., Ж.А.Козлов, И.Крэчун, Г.Матиеску, В.М.Морозов, А.Опре, К.Опре, И.Падуреану, А.В.Пучков, Неупругое рассеяние медленных нейтронов ванадием при температурах 293-1773К, Препринт ФЭИ-3098, 2007 г., 17 стр.
29. Семенов В.А., Козлов Ж.А., Крэчун И., Матиеску Г., Морозов В.М., Опре А., Опре К., Падуреану И., Пучков А.В. Неупругое рассеяние медленных нейтронов ванадием при температурах 293-1773 К, 2007, Препринт ФЭИ-3098, Обнинск.
30. Титов А.Н., А.Н.Скоморохов, А.А.Титов, С.Г.Титова, В.А.Семенов, Влияние интеркалации на фононный спектр дихалькогенидов титана, Физика Твердого Тела 2007, Т. 49, №8, с.1460-1463.

CONFERENCES

1. Avdeev M.V., “Small angle neutron scattering” 4th Central European Training School on Neutron Scattering”, 23-27 April, Budapest, Hungary.
2. Avdeev M.V., Bica D., Vékás L., Marinica O., Aksenov V.L., Garamus V.M., Rosta L., Ivanov A.O., Mendelev V.S., “On the stable size of magnetite dispersed in organic non-polar carries with coating by non-saturated and saturated mono-carboxylic acids” 11th International Conference on Magnetic Fluids, 23-27 July, Kosice, Slovakia.
3. Avdeev M.V., Small-angle neutron scattering from nanosystems, The 2nd Joint Seminar JINR-Romania on Neutron Physics for Investigations of Nuclei , Condensed Matter and Life Sciences, September 11-16, 2007, Baia-Mare – Romania.
4. Baeva M., Beskrovnyy A.I. and Jadrowski E.L., Phase composition of the four-component nitrified steels at increasing manganese concentration, Proc. of six-th conference of Balcan physical union, 22-26 august 2006, Istambul, Turkey. New York, 2007, vol. 899, p. 583.

5. Baeva M., Beskrovnyy A.I., Boianova A. and Shelkova I., Investigation of renal stones by X-ray and neutron diffraction, Proc. of six-th conference of Balcan physical union, 22-26 august 2006, Istambul, Turkey. New York, 2007, vol. 899, p. 807.
6. Balagurov A.M. "Application of Reverse Time of Flight (RTOF) Neutron Diffraction for Residual Stress Investigations", IAEA Meeting "Development and applications of the technique of residual stress measurements in materials", Berlin, October 8 – 10, 2007.
7. Balagurov A.M., Kazimirov V.Yu., Khasanova N.R., Antipov E.V. "Crystal structure and lattice dynamics of stable and unstable Ni-hydroxides" European Conference of Neutron Scattering, Lund, June 25 – 29, 2007.
8. Balasoiu M., Kappel W., Cios M., Stancu N., Cios A., Kirilov A. S., Kutuzov S.A., Smirnov A.A., Gordeliy V.I., Erhan R., Ivan'kov A.E., Rogacev A.V., Kovalev Yu.S., Kuklin A.I.. New Magnetic System for Small Angle Neutron Scattering at Yumo Instrument. Book of abstracts 4-th European Conference on Neutron Scattering, 25-29 June 2007, Lund, Sweden. p484.
9. Balasoiu Maria, Anitas Eugen, Muresan Cristina, Kuklin Alexander, Kovalev Yurij, Bica Ion. Small Angle Neutron Scattering Investigations of Magnetic Elastomemers based on Ferrofluids. Book of abstracts 4-th European Conference on Neutron Scattering, 25-29 June 2007, Lund, Sweden, p.594.
10. Bodnarchuk V., "Neutron Spin Turners with Rotating Magnetic Field: First Experiments", 4th European Conference On Neutron Scattering, 25-29 June, Lund, Sweden.
11. Erhan R. V., Balasoiu M., Barna E., Morjan I., Kuklin A. I.. Carbon nanopowders studied by SANS. 4th Central European Training School on Neutron Scattering. 23-27 April 2007, Budapest, Hungary.
12. Erhan R. V., Balasoiu M., Barna E., Morjan I., Kuklin A. I.. Study of carbon nanostructures using small angle neutron scattering. Bucharest, Romania, Friday, June 01, 2007 - June 02, 2007, Bucharest University Physics Department 2007 Meeting.
13. Erhan Raul, Balasoiu Maria, Barna Emil, Kuklin Alexander, Morjan Ion. Structure Study of Carbon Nanopowders using SANS. Book of abstracts 4-th European Conference on Neutron Scattering, 25-29 June 2007, Lund, Sweden, p.598.
14. Feoktystov A.V., Avdeev M.V., Aksenov V.L., Bulavin L.A., Bica D., Vekas L., Garamus V.M., "SANS contrast variation on ferrofluid magnetite/myristic acid/benzene", 4th Central European Training School on Neutron Scattering", 23-27 April, Budapest, Hungary.
15. Feoktystov A.V., Avdeev M.V., Aksenov V.L., Bulavin L.A., Bica D., Vekas L., Garamus V.M., Almasan V., "Small-angle neutron scattering contrast variation on ferrofluid magnetite/myristic asid/benzene", 11th International Conference on Magnetic Fluids", 23-27 July, Kosice, Slovakia.
16. Feoktystov A.V., Avdeev M.V., Aksenov V.L., et al., "Small-angle neutron scattering contrast variation on ferrofluid magnetite/myristic asid/benzene", 4th European Conference On Neutron Scattering, 25-29 June, Lund, Sweden.
17. Gibhardt Holger, Haramagatti Chandrashekara, Islamov Akhmed, Kuklin Alexander, Eckold Goetz. Phase Transitions in Micellar solutions of Different Alkyl Trimethylammonium Bromide Surfactants with Various Chain Lengths. Book of abstracts 4-th European Conference on Neutron Scattering, 25-29 June 2007, Lund, Sweden.p.158.
18. Hall P., Hall E., Houtmann S., Salazar J., Natkanec I., Smirnov L.S., Ivanov A., Beskrovnyy A., Vasilovskiy S., Butorin P.. The study of diffraction and vibration spectra by means of neutron scattering from substances with nanocrystalline structures sorbed hydrogen. International Workshop "Dynamics of Molecules and Materials", 31 January-2 Februry 2007, Grenoble, France, p 56.
19. Ioffe A., Bodnarchuk V., Bussmann K., Müller R., "Larmor labeling by time-gradient magnetic fields" 4th Central European Training School on Neutron Scattering", 23-27 April, Budapest, Hungary.

20. Isaev-Ivanov Vladimir, Filatov Mikhail, Isalmov Akhmed, Kuklin Aleksandr, Lauter Hans, Lebedev Dmitry, Pantina Rimma, Toperverg Boris, Varfolomeeva Elena. Comparison of Nucleosome Arrangement in Native Nuclei of Different Cell Types by SANS. Book of abstracts 4-th European Conference on Neutron Scattering, 25-29 June 2007, Lund, Sweden.p.216.
21. Ivankina T.I. Application of neutron diffraction in geosciences. International Conference on Contemporary Physics (ICCP-IV). August 13-20, 2007, Ulaanbaatar, Mongolia.
22. Ivankina T.I., Kern H., Nikitin A.N. Neutron texture measurements and 3D velocity calculations on strongly foliated biotite gneisses from the Outokumpu Deep Drill Hole. Outokumpu Deep Drill Project, Second International Workshop, May 21-22, 2007, Espoo, Finland.
23. Ivankina T.I., Kern H.M., Lokajicek T, Nikitin A.N. and Pros Z.Textures and elastic anisotropies of biotite gneisses from the Outokumpu Deep Drill Hole. VIII международная конференция "Физико-химические и петрофизические исследования в науках о Земле", Октябрь 9-11, 2007, Москва.
24. Ivankina T.I., Nikitin A.N. Influence of temperature and long-time loading on texture and physical properties of marble. Деформирование и разрушение материалов с дефектами и динамические явления в горных породах и выработках. 17-23 Сентября, 2007, Украина, Алушта.
25. Jernenkov M., Klimko S., Lauter-Pasyuk V., Toperverg B.P., Lauter H.J., Aksenov V., "Larmor precession reflectometry for multilayer studies", European workshop on neutron optics NOP 2007, March 5-7, Villigen, Switzerland.
26. Karelov Denis, Lebedev Dmitry, Suslov Aleksandr, Shalguev Valeriy, Kuklin Aleksandr, Islamov Akhmed, Isaev-Ivanov Vladimir, Lanzov Vladislav. Large-scale Structure of RecA Protein from Deinococcus Radiodurance and its Complexes in Solution. Book of abstracts 4-th European Conference on Neutron Scattering, 25-29 June 2007, Lund, Sweden.p.217.
27. Kozlenko D.P., "Pressure tuning of magnetic states in $La_{1-x}Ca_xMnO_3$ manganites (x=0.25-0.85)", oral presentation on the 4th European Conference on Neutron Scattering, Lund, Sweden, 25-29 June 2007.
28. Kuklin A.I., Kutuzov S.A., Gabriel A., Eckold G., Utrobin P.K., Smirnov A.A., Islamov A.Kh., Kirilov A.S., Bogdzel A.A., Gordeliy V.I.The Parameters of Position Sensitive Detector with Central Hole and First Results in Small-angle and Backscattering Configurations. Book of abstracts 4-th European Conference on Neutron Scattering, 25-29 June 2007, Lund, Sweden, p.530.
29. Lashkarev G.V., Dmitriev A.I., Radchenko M.V., Butorin P.E., Sichkovskyi V.I., Kovalyuk Z.D., Beskrovny A.I. Neutron Diffraction Researches of Spintronic Layered Semiconductor InSe<Mn>. 6th International Conference on Nuclear and Particle Physics 17-21 Nov. 2007, Luxor, Egypt.
30. Lashkarev G.V., Slynko V.V., Sichkovskyi V.I., Radchenko M.V., Dmitriev A.I., Butorin P.E., Aleshkevych P., Szymczak R., Dobrowolski W., Minikaev R., Beskrovny A.I., Lytvyn P.M.Magnetic structure of sophisticated ferromagnetic semiconductor InSe<Mn> XXXV International School on the Physics of Semiconducting Compounds Jaszowiec 2007, Poland, P.42.
31. Lauter H., Lauter-Pasyuk V., "Nano-science with reflectometry", Conference on the use of scattering of synchrotron radiation, neutrons and electrons (RSNE-2007), November 12-17 2007, Moscow, Russia
32. Lauter H., Lauter-Pasyuk V., Avdeev M., Bodnarchuk V., Aksenov V., Ulyanov V., Project of Horizontal reflectometer on IBR-2 reactor. Complete reflectometry with Larmor precession, Workshop "ILL, 40 years", January 2007, Grenoble, France.

33. Lauter-Pasyuk V., "Nanoparticle-induced Morphological Transformation in Symmetric and Asymmetric Diblock Copolymer Films", 4th European Conference On Neutron Scattering, 25-29 June, Lund, Sweden.
34. Lauter-Pasyuk V., Ulyanov V., Lauter H.J., "Off-specular scattering from magnetic supermirrors during magnetization reversal", European workshop on neutron optics NOP 2007, March 5-7, Villigen, Switzerland.
35. Loginov N.I., N.M.Blagoveshchenskiy, V.A.Morozov, A.G.Novikov, M.A.Pashnev, V.V.Savostin and A.L.Shimkevich. Investigations of diffusion processes in liquid lithium and lithium–hydrogen melt by quasielastic neutron scattering. 13th Internaional Conference on Liquid and Amorphous Metals, 8-14 July 2007, Ekaterinburg, Russia. Poster DP9, Book of Abstracts, p. 100.
36. Mironova G.M., Balagurov A.M., Bobrikov I.A., "A new version of Time-Resolved Neutron Scattering and Transmission spectrometer at the IBR-2M high-flux pulsed reactor". International Symposium on Time-Resolved Processes in Condensed Matter, 27-28 September 2007, Georg-August University of Goettingen, Abstracts and Programme.
37. Moiseeva E.S., Reshetnyak A.B., Borshchevskiy V.I., Baeken C., Büldt G., and V.I. Gordeliy (2007) Comparative analysis of quality of membrain protein Bacteriorhodopsin crystals obtained in Octylglucoside and Octylthioglucoside. Book of abstracts the Sixth National Conference on Application of X-ray, Synchrotron Radiation, Neutrons and Electrons for Material Characterization November 12-17, 2007, Moscow, Russia, p. 329.
38. Nikitin A.N., Ivankina T.I. An investigation of thermal and deformation properties of quartzite at the temperature interval of polymorphic α-β transition by neutron diffraction and acoustic emission. Деформирование и разрушение материалов с дефектами и динамические явления в горных породах и выработках. Сентябрь 17-23, 2007, Украина, Алушта.
39. Novikov A.G., N.M.Blagoveshchenskiy, A.S.Kolokol, M.A.Pashnev, D.V.Savostin, V.V.Savostin and A.L.Shimkevich. Atomic dynamics of liquid lithium and lithium-hydrogen melt investigated by inelastic neutron scattering. 13th Internaional Conference on Liquid and Amorphous Metals, 8-14 July 2007, Ekaterinburg, Russia. Poster DP22, Book of Abstracts, p. 106.
40. Petrenko V.I., Avdeev M.V., Bulavin L.A., Aksenov V.L., Rosta L., «Behaviour of mono-carboxylic acids in non-polar organic solvent by small-angle neutron scattering», 4th Central European Training School on Neutron Scattering", 23-27 April, Budapest, Hungary.
41. Petrenko V.I., Avdeev M.V., Bulavin L.A., Aksenov V.L., Rosta L., «Interaction of mono-carboxylic acids in non-polar organic solvent by small-angle neutron scattering», 11th International Conference on Magnetic Fluids, 23-27 July, Kosice, Slovakia.
42. Rajewska A. SANS method study of aggregation in mixed micellar solutions nonionic and cationic classic surfactants. Book of Abstracts, 21st Conference of the European Colloid and Interface Society, September 10-14, (2007) Geneva (Switzerland).
43. Rajewska A. SANS study of the Gemini nonionic surfactant in micellar solutions. Book of Abstracts, V4 BENSC User`s Meeting , 23-25 May, 2007, Hahn-Meitner Institut, Berlin (Germany).
44. Rajewska A. Structure of water micellar solutions of nonionic classic surfactant heptaethylene glycol monoteradecylether.Book of Abstracts , International Conference on Neutron and X-Ray Scattering, Serpong, (Indonesia) 23- 28 July, 2007.
45. Rajewska A., Mędrzycka K., Hallmann E. "SANS method study of aggregation in mixed micellar solutions of nonionic and cationic classic surfactants". Book of Abstracts, page 394, T18 4th uropean Conference on Neutron Scattering, Lund (Sweden) 25 – 29 June, 2007.
46. Reshetnyak A., Borshchevskiy V., Klare J., Moiseeva E., Engelhard M., Buldt G., Gordeliy V.. Comparative analysis of structures of sensory rhodopsin II and sensory rhodopsin II in

complex with it's cognate transduser. International Symposium on Retinal Proteins: Experiments and theory. Bremen, Germany, September 23-26, 2007
47. Rogatchev Andrey, Cherny Alexander, Ozerin Alexander, Islamov Akhmed, Gordeliy Valentin, Kuklin Alexander. The Spherical Cone Model for Small Angle Neutron Scattering Dendrimers Curves Data Treatment. Book of abstracts 4-th European Conference on Neutron Scattering, 25-29 June 2007, Lund, Sweden.p.356.
48. Ryabova N.Yu., Kiselev M.A., Beskrovnyy A.I., Aksenov V.L. and Balagurov A.M., Kinetics of lipid membrane hydration: neutron diffraction study in real time. International Symposium on Time-Resolved Processes in Condensed Matter, 27-28 September 2007, Georg-August University of Goettingen, Abstracts and Programme, P. 29.
49. Scheffzuek Ch., Walther K., Frischbutter A., Pusenkov V.M., Manoshine S.A., Zhuravlov V.V., Churakov A.V., Bogdsel A.A., Kulikov S.A. & Schabalin E.P. "A proposal for a bent neutron guide at beam line 7A of the modernized fast pulsed reactor IBR-2M for the diffractometers EPSILON-MDS and SCAT" PAC of Condensed Matter Physics, Dubna (Russia), April 16-17, 2007.
50. Scheffzük Ch., Walther K., Frischbutter A. "Neutron time-of-flight diffraction for load and residual strain experiments on geological materials" MECA sens IV Conference on Stress evaluation, Vienna (Austria), September 24-26, 2007.
51. Sobolev O.V., N.M.Blagoveshchenskii, V.A.Morozov, A.G.Novikov, M.A.Pashnev, V.V.Savostin, A.L.Shimkevich, Quasielastic neutron scattering and diffusion in liquid lithium and lithium-hydrogen melt. 4th European conference on neutron scattering, 25-29 June 2007, Lund, Sweden.
52. Taran Yu.V. "About historical possibility of investigation of fatigue degradation and martensitic transformation of austenitic stainless steel in components of the primary cooling circuits of the IBR-2 and BR-10 fast nuclear reactors by neutron-physical methods" XV International Seminar on Interaction of Neutrons with Nuclei "Neutron Spectroscopy, Nuclear Structure, Related Topics", Dubna, Russia, 16-19 May 2007.
53. Taran Yu.V., Balagurov A.M., Schreiber J., Korsunsky A.M. "Investigation of an in-plane biaxially-fatigued stainless steel sample of cruciform geometry by neutron diffraction stress analysis" The 4th International Conference on Stress Evaluation using Neutrons and Synchrotron Radiation (MECA SENS IV), Vienna, Austria, 24-26 September 2007.
54. Taran Yu.V., Balagurov A.M., Schreiber J., Stuhr U. "Residual stresses in a shape welded steel tube by neutron diffraction" The 4th European Conference On Neutron Scattering, Lund, Sweden, 25-29 June 2007.
55. Taran Yu.V., Balagurov A.M., Sheverev S.G., Schreiber J., Korsunsky A.M., Vorster W.J.J., Bomas H., Stoeberl C. "Neutron diffraction investigation of in-plane biaxial fatigued stainless steel sample of cruciform geometry" The 4th European Conference On Neutron Scattering, Lund, Sweden, 25-29 June 2007.
56. Tropin T.V., Aksenov V.L., Kyzyma O.A., Bulavin L.A., Avdeev M.V., Korobov M.V., Rosta L., «Aggregation in C_{60}/NMP, C_{60}/NMP/water and C_{60}/NMP/toluene mixtures by UV-Vis spectroscopy and SANS», 4th Central European Training School on Neutron Scattering", 23-27 April, Budapest, Hungary.
57. Tropin T.V., Aksenov V.L., Kyzyma O.A., Bulavin L.A., Avdeev M.V., Korobov M.V., Rosta L., «Aggregation in C_{60}/NMP, C_{60}/NMP/water and C_{60}/NMP/toluene mixtures by UV-Vis spectroscopy and SANS», 8th Biennial International Workshop: Fullerenes and Atomic Clusters IWFAC 2007, 2-6 июля 2007, Санкт-Петербург, Россия.
58. Tropin T.V., Avdeev M.V., Aksenov V.L., "Small-angle neutron scattering study of C_{60}/CS_2 solutions" 8th Biennial International Workshop: Fullerenes and Atomic Clusters IWFAC 2007, 2-6 июля 2007, Санкт-Петербург, Россия.
59. Vasilovskiy S., Kononogov S., Kodess B., Sambueva S., Nechaev N. Standartization of procedure for performing the measurement of parameters. International Workshop

"Dynamics of Molecules and Materials", 31 January-2 February 2007, Grenoble, France, p 44.
60. Walther K., Scheffzük Ch., Frischbutter A., Pusenkov V.M., Bulkin A.P., Ulyanov V.A., Zhuravlev, V.V. "New neutron guides for the strain and texture diffractometers Epsilon and SKAT at the pulsed reactor IBR-2 in Dubna (Russia)" Workshop on Future Applications of Neutron Texture and Powder Diffraction in the Geosciences, Garching (Germany), November 15-16, 2007.
61. Walther, K., Scheffzük, Ch., Frischbutter, A., Pusenkov, V.M., Manoshine, S.A., Churakov, A.V., Bogdsel, A.A., Kulikov, S.A. & Schabalin, E.P. "A proposal for a bended neutron guide at beam line 7A of the modernized fast pulsed reactor IBR-2M, Dubna" 4th European Conference on Neutron Scattering, Lund (Sweden), June 25-29, 2007.
62. Zlokazov V.B "On the simulation of the anisotropic peak broadening in the diffractograms" Size-Strain V Conference (Diffraction Analysis of the Microstructure of Materials), Garmish-Partenkirchen, Germany, October 7-9, 2007.
63. Авдеев М.В. «Вариация контраста в малоугловом рассеянии на полидисперсных и суперпарамагнитных системах: подход базисных функций» VI Национальная конференция по применению рентгеновского, синхротронного излучений, нейтронов и электронов для исследования материалов, РСНЭ 2007, 12-17 ноября, Москва.
64. Авдеев М.В., Тропин Т.В., Аксенов В.Л., Рошта Л., Холмуродов М.Т. "К вопросу об образовании кластеров фуллерена в сероуглероде. Данные малоуглового рассеяния нейтронов и молекулярной динамики", VI Национальная конференция по применению рентгеновского, синхротронного излучений, нейтронов и электронов для исследования материалов, РСНЭ 2007, 12-17 ноября, Москва.
65. Базалеев Н.И., Воробьев И.Б., Иванкина Т.И., Клепиков В.Ф., Литвиненко В.В., Лонин Ю.Ф., Никитин А.Н. и др. Радиационные методы оценки рисков захоронения радиоактивных отходов в горных породах. Международная научно-практическая конференция «Проблемы экологической и ядерной безопасности объектов топливно-энергетического комплекса», Институт геохимии окружающей среды НАН и МЧС Украины, 27 – 29 ноября, 2007, Киев, Украина.
66. Балагуров А.М. "Мезоскопическая физика структурно-магнитного фазового расслоения в сложных оксидах переходных металлов" Конференция по физике конденсированного состояния, сверхпроводимости и материаловедению, Москва, 26 – 30 ноября, 2007.
67. Василовский С.Г., Бескровный А.И., Александров К.С., Флеров И.Н. Исследование структуры кристаллов Rb_2KAlF_6 и Rb_2KCrF_6. Актуальные проблемы физики твердого тела ФТТ-2007, 23-26 октября 2007 г., Минск, стр. 236-238.
68. Василовский С.Г., Комель И.Л. Разработка эталонных средств измерений для дифрактометрии монокристаллических веществ и материалов. Второй Международный конкурс "Лучший молодой метролог КООМЕТ", 19-20 июня 2007 г. Харьков, Украина, стр. 17-20.
69. Васин Р.Н., Никитин А.Н. Типизация кристаллографических текстур кварца в различных горных породах по данным нейтронной дифрактометрии. VIII международная конференция "Физико-химические и петрофизические исследования в науках о Земле", Октябрь 9-11, 2007, Москва.
70. Ермакова Е.В., Киселев М.А., Hauss Th., Dante S., Балагуров А.М., «Исследования наноструктуры лизоформы димиристоилфосфатидилхолина методом дифракции нейтронов», Сборник аннотаций докладов конференции по физике конденсированного состояния, сверхпроводимости и материаловедению, посвященной 50-летию исследовательского ядерного реактора ИРТ, 26-30 ноября 2007, Москва, РНЦ «Курчатовский институт», стр. 39.
71. Жерненков М., Аксенов В., Климко С., Топерверг Б.П., Миляев М., Рамашев Л., Устинов В., Лаутер-Пасюк В., Лаутер Х., «Рефлектометрия с Ларморовской

прецессией для исследования многослойных структур», VI Национальная конференция по применению рентгеновского, синхротронного излучений, нейтронов и электронов для исследования материалов, РСНЭ 2007, 12-17 ноября, Москва.

72. Калинин И.В., В.В.Лаутер-Пасюк, Х.Лаутер, А.В.Пучков «Нейтронография наноразмерных пленок жидкого гелия», Сборник аннотаций конференции по физике конденсированного состояния, сверхпроводимости и материаловедению, РНЦ КИ, 26-30 ноября 2007, Москва, с. 171.
73. Калинин И.В., Лаутер-Пасюк В.В., Лаутер Х., Пучков А.В. «Нейтронография наноразмерных пленок жидкого гелия» Конференция по физике конденсированного состояния, сверхпроводимости и материаловедению, РНЦ КИ, 26-30 ноября 2007, Москва.
74. Кизима Е.А., Авдеев М.В., Тропин Т.В., Снегирь С.В., Булавин Л.А., Аксенов В.Л., «Реорганизация кластеров фуллеренов в C_{60}/N-метил-2-пирролидон/вода системе», VI Национальная конференция по применению рентгеновского, синхротронного излучений, нейтронов и электронов для исследования материалов, РСНЭ 2007, 12-17 ноября, Москва.
75. Кичанов С.Е. VI Национальная конференция по применению рентгеновского, синхротронного излучений, нейтронов и электронов для исследования материалов (РСНЭ-2007), 12-17 ноября 2007 г, Москва, устный доклад «Порошковый дифрактометр для исследования микрообразцов на экспериментальной станции "Медиана" источника синхротронного излучения научного центра КИСИиНТ».
76. Кичанов С.Е. Ежегодная научная конференция по физике конденсированного состояния, сверхпроводимости и материаловедению, посвященная 50-летию первого исследовательского реактора ИРТ, 26-30 ноября 2007, Москва, стендовый доклад «Исследования легированного кремнием железа при высоких давлениях на порошковом дифрактометре экспериментальной станции «Медиана»».
77. Кичанов С.Е. Ежегодная научная конференция по физике конденсированного состояния, сверхпроводимости и материаловедению, посвященная 50-летию первого исследовательского реактора ИРТ, 26-30 ноября 2007, Москва, стендовый доклад «Исследования рениевокислого пиридина при высоких давлениях на порошковом дифрактометре экспериментальной станции «Медиана».
78. Кичанов С.Е. Международная научная конференция «Актуальные проблемы физики твердого тела ФТТ-2007», 23-26 октября 2007 г, г. Минск, Республика Беларусь, стендовый доклад «Исследования структуры и динамики солей пиридина $PyHNO_3$ и $PyHReO_4$ при высоком давлении».
79. Кичанов С.Е.. Ежегодная научная конференция по физике конденсированного состояния, сверхпроводимости и материаловедению, посвященная 50-летию первого исследовательского реактора ИРТ, 26-30 ноября 2007, Москва, устный доклад «Исследования на порошковом дифрактометре экспериментальной станции «Медиана» источника синхротронного излучения НТК КЦСИиНТ»,
80. Куклин А.И., Горшкова Ю.Е., Исламов А.Х., Ковалев Ю.С., Ефремов Р.Г., Мухамедзянов Р.И., Горделий В.И. “Результаты испытаний холодного метанового замедлителя на 4-м канале ИБР-2”. Тезисы докладов VI национальной конференции по применению рентгеновского, синхротронного излучений, нейтронов и электронов для исследования материалов. 12-17 ноября 2007, Москва, Россия. стр. 594.
81. Куклин А.И., Исламов А.Х., Корнышев А.А., Мергель Ю., Ярмилко А.В., Горделий В.И.. Исследование полиэлектролитных мембран методом малоуглового рассеяния нейтронов. Тезисы докладов VI национальной конференции по применению рентгеновского, синхротронного излучений, нейтронов и электронов для исследования материалов. 12-17 ноября 2007, Москва, Россия. стр. 203.
82. Куклин А.И., Кутузов С.А., Габриэль А., Экольд Г., Кирилов А.С., Утробин П.К., Богдзель А.А., Исламов А.Х., Ковалев Ю.С., Рогачев А.В., Иваньков А.И., Горделий

В.И. Результаты применения нового типа позиционно-чувствительного детектора в дифракционных и малоугловых экспериментах. Тезисы докладов VI национальной конференции по применению рентгеновского, синхротронного излучений, нейтронов и электронов для исследования материалов. 12-17 ноября 2007, Москва, Россия. стр. 593.

83. Лукин Е.В. Международная научная конференция «Актуальные проблемы физики твердого тела ФТТ-2007», 23-26 октября 2007 г, г. Минск, Республика Беларусь, стендовый доклад «Исследования кристаллической и магнитной структуры анион-дефицитного соединения $La_{0.7}Sr_{0.3}MnO_{3-d}$ при высоких давлениях».
84. Муругова Т.Н., Горделий В.И., Куклин А.И., Иваньков А.И., Солодовникова И.М., Юрков В.И., Ягужинский Л.С. “Исследование ультраструктуры митохондриальных мембран методом малоуглового рассеяния нейтронов”. Тезисы докладов VI национальной конференции по применению рентгеновского, синхротронного излучений, нейтронов и электронов для исследования материалов. 12-17 ноября 2007, Москва, Россия. стр. 143.
85. Муругова Т.Н., Горделий В.И., Куклин А.И., Солодовникова И.М., Ягужинский Л.С. "Изучение структуры митохондрий с помощью метода малоуглового рассеяния нейтронов", тезисы Первой Всероссийской Школы-семинара "Современные достижения бионаноскопии", 11-17 июня, 2007, Москва, С. 40-41.
86. Новиков А.Г., Н.М. Благовещенский, Н.И. Логинов, В.А. Морозов, В.В. Савостин, А.Л. Шимкевич. Диффузионные процессы в жидком литии и расплаве литий - водород. Материалы межведомственного семинара «Теплофизика – 2007».
87. Панков С.Е. Международная научная конференция «Актуальные проблемы физики твердого тела ФТТ-2007», 23-26 октября 2007 г, г. Минск, Республика Беларусь, устный доклад «Влияние высокого давления на кристаллическую и магнитную структуру манганита $Pr_{0.1}Sr_{0.9}MnO_3$».
88. Петренко В.И., Авдеев М.В., Аксенов В.Л., Булавин Л.А., Рошта Л., «Магнитные жидкости при избытке поверхностно-активных веществ по данным малоуглового рассеяния нейтронов», VI Национальная конференция по применению рентгеновского, синхротронного излучений, нейтронов и электронов для исследования материалов, РСНЭ 2007, 12-17 ноября, Москва.
89. Рогачев А.В., Черный А.Ю., Озерин А.Н., Музафаров А.М., Горделий В.И., Куклин А.И. Структура кремнийорганических дендримеров в растворе из данных МУРН: новые модели. Тезисы докладов VI национальной конференции по применению рентгеновского, синхротронного излучений, нейтронов и электронов для исследования материалов. 12-17 ноября 2007, Москва, Россия. стр. 329.
90. Сердюк И.Н., «New charachteristic for classification of the Living World: application to elongation factors EF1A», International Conference «Computational Phylogenetics and Molecular Systematics 2007"», Москва 16-19 Ноября
91. Уваров В.Т., Уваров В.В., Робук В.Н., Пономарев А.Г., Никитин А.Н., Лонин Ю.Ф., Литвиненко В.В., Иванкина Т.И. и др. Процессы массопереноса в образцах горных пород под действием импульсных сильноточных пучков электронов. XX Международный семинар по ускорителям заряженных частиц, Сентябрь 9-15. 2007, Алушта, Украина.
92. Феоктистов А.В., Авдеев М.В., Аксенов В.Л., Булавин Л.А., Бика Д., Векаш Л., Гарамус В.М., Виллумайт Р., «Вариация контраста в малоугловом рассеянии нейтронов на магнитной жидкости магнетит/миристиновая кислота/бензол», VI Национальная конференция по применению рентгеновского, синхротронного излучений, нейтронов и электронов для исследования материалов, РСНЭ 2007, 12-17 ноября, Москва.

NEUTRON NUCLEAR PHYSICS

Experimental investigations

1. Andrzejewski J., Gledenov Yu.M., Korejwo A., Sobczak K., Szalanski P.J.. Compensated ionization chamber for (n,α) reaction measurements at a spallation neutron source. Nucleonika. V.52(2), p. 51-57 (2007).
2. Atchison F., Blau B., Bodek K., van der Brandt D., Brys T., Daum M., Fierlinger P., Frei F., Geltenbort P., Hautle P., Henneck R., Heule S., Holley A., Kasprzak M., Kirch K., Konter P., Kuzniak M., Liu C.-Y., Morris C., Pichlmaier A., Plonka C., Pokotilovski Yu.N., Saunders A., Shin Y., Tortorella D., Wophlmuther H., Young A., Zsigmond G., "Cold neutron energy dependent production of ultracold neutrons in solid deuterium", Phys. Rev. Lett., 99 (2007) 262502.
3. Beda A.G., Skoi V.R., The Current State of Research on T Invariance in Neutron–Nuclear Reactions, Physics of Particles and Nuclei, 2007, Vol. 38, No. 6, 775.
4. Dutov A.G., Komar V.A., Shipilo N.V., Azarko I.I., Frontasyeva M.V., Pavlov S.S. Decrease of content of structural defects in crystalline diamonds under the influence of Al_2O_3 admixture and neutron irradiation. In the Book "Diamond and Related Materials. Editor Frank Columbus, Nova Science Publishers, Inc., USA, 2007.
5. Frei A., Sobolev Y., Altarev I., Eberhardt K., Gschrey A., Gutschmiedl E., Hackl R., Hampel G., Hartmann F.J., Heil W., Kratz J.V., Lauer Th., Lizon Aguilar A., Muller A.R., Paul S., Pokotilovski Yu., Schmid W., Tassini L., Tortorella D., Trautmann N., Trinks U., Whiel N., "First production of ultracold neutrons with a solid deuterium source at a pulse reactor TRIGA Mainz", Eur. Phys. Journ. A. 34 (2007) 119.
6. Granja C., Vykydal Z., Kopatch Y., Jakubek J., Pospisil S., Telezhnikov S.A., Position-sensitive spectroscopy of 252Cf fission fragments. Nucl.Instrum.Methods Phys.Res. A574, 472 (2007)
7. Honzatko J., Khitrov V. A., Panteleev C., Suchovoj A. M., Tomandl I. Intense two-step cascades and gamma-decay scheme of the 118Sn nucleus, Fizika B (Zagreb) 15 (2006) 189 - 206.
8. Kartashov D.G., Lychagin E.V., Muzychka A.Yu., Nekhaev G.V., Nesvizhevsky V. V. "An Investigation into the Origin of Small Energy Changes (~10^{-7} eV) of Ultracold Neutrons in Traps"// International Journal of Nanoscience, Vol. 6, No. 6 (2007)
9. Khuukhenkhuu G., Unenbat G., Odsuren M., Gledenov Yu.M., Sedysheva M.V., Bayarbadrakh B..The fast neutron induced (n,p) reaction cross sections. Compound Reaction Mechanism. JINR Communication E3-2007-25, Dubna, 2007.
10. Khuukhenkhuu G., Unenbat G., Odsuren M., Gledenov Yu.M., Sedysheva M.V., Bayarbadrakh B..The fast neutron induced (n,p) reaction cross sections. Pre-equilibrium Reaction Mechanism. JINR Communication E3-2007-26, Dubna, 2007.
11. Khuukhenkhuu G., Unenbat G., Odsuren M., Gledenov Yu.M., Sedysheva M.V., Bayarbadrakh B..The fast neutron induced (n,p) reaction cross sections. Direct Reaction Mechanism. JINR Communication E3-2007-27, Dubna, 2007.
12. Magli R., Mitsyna L.V., Nikolenko V.G., Parzhitski S.S., Popov A.B., Samosvat G.S.. On the possibility to estimate the n,e-scattering length from structure factors for liquid krypton. ISINN-14, E3-2007-23, p.183-189
13. Masuda Y., Scoy V., Ino T., Jeong S.C. and Watanabe Y., Observation of pulsed neutron Ramsey resonance, Physica B: Condensed Matter, Volume 397, Issues 1-2, 15 July 2007, Pages 147-149.

14. Masuda Y., Skoy V., Ino T., Jeong S.C. and Watanabe Y. Ramsey resonance for a pulsed beam, Physics Letters A, Volume 364, Issue 2, 23 April 2007, Pages 87-92.
15. Mezhov-Deglin L.P. , Efimov V.B. , Lokhov A.V. , Lychagin E.V. , Muzychko A.Y. , Nesvizhevskii V.V. , Strelkov A.V. “Scattering of Cold Neutrons on Gel Samples Formed by Impurity Clusters in Superfluid He-II” // J Low Temp Phys (2007) 148: 833–837
16. Mezhov-Deglin L.P., Efimov V.B., Lokhov A.V., Levchenko A.A., Kolmakov G.V., Abdurakhimov L.V. , Brazhnikov M.Y., Lebedeva E.V., May R., Nesvizhevsky V.V., Muzychka A.V. , Lychagin E.V., Strelkov A.V. “Neutron Studies of Impurity Gels of Heavy Waterand Deuterium in Superfluid He-II” // J Low Temp Phys (2007)
17. Muzhychka A.Yu., Furman W.I., Lychagin E.V., Krylov A.R., Nekhaev G.V., Sharapov E.I. , Shvetsov V.N., Strelkov A.V., Levakov B.G., Lyzhin A.E., Chernukhin Yu.I. , Kandiev Ya.Z., Mitchel G.E., Crawford B.E., Stephenson S.L. , Howell C.R., Tornow W. “Modeling and testing background for the neutron-neutron scattering experiment at the reactor YAGUAR”, Nuclear Physics A 789 (2007) 30–45
18. Nikolenko V.G., Popov A.B.. "What is the correct description of the slow neutron scattering in a gas?' // Eur. Phys. J. A 34,p.443-446 (2007)
19. Oprea C., Kobzev A. P., Codescu M., Szalansky P. I., Curuia M.. PIXE and RBS analysis of Fe - Cu nanoalloy. Vacuum 81 2007 1167-1170.
20. Oprea C., Kobzev A. P., Oprea I. A., Szalanski P. J., Buzguta V.. PIXE detection limits for dental enamel from some human teeth by excitation with protons and $^{4}He^{2+}$ ions from a 3 MeV Van der Graaff accelerator. Vacuum 81 2007 1164-1166.
21. Pokotilovski Yu.N., Natkaniec I., Holderna-Natkaniec K., “The experimental and calculated density of states and ultracold neutron loss coefficient of perfluorinated oils at low temperature”, Physica B.In press.
22. Samosvat G.S., Oprea C.C., Nikolenko V.G., Kozlov Zh.A., Oprea A.I., Popov A.B., Parzhitsky S.S., Semenov V.A., Puchkov A.V., Morozov V.M. “Proposal for the investigation of the neutron-electron scattering length in liquid Pb and Bi by TS-3000K thermostat at IBR-2 reactor” // ISINN-14, E3-2007-23, p.64.
23. Zhang Guohui, Cao Rongtai, Chen Jinxiang, Tang Guoyou, Gledenov Yu.M., Sedysheva M.V., Khuukhenkhuu G.. Differential cross section measurement for the $^{64}Zn(n,\alpha)^{61}Ni$ Reaction at 5.03 and 5.95 MeV. Nuclear Science and Engineering. Vol. 156, p. 115-119 (2007).
24. Андрианов В. Р., Вячин В.Н., Гундорин Н. А, Дружинин А. А., Жданова К. В., Лихачёв А. Н., Пикельнер Л. Б., Реброва Н. В., Саламатин И. М., Фурман В. И. «Измерение выхода запаздывающих нейтронов при делении ^{245}Cm тепловыми нейтронами», Сообщение ОИЯИ Р3-2007-123, Дубна, 2007.
25. Весна В.А., Гледенов Ю.М., Несвижевский В.В., Петухов А.К., Седышев П.В., Солднер Т., Циммер О., Шульгина Е.В.. Испытание нового метода регистрации токовых сигналов с увеличенной частотой переключения поляризации нейтронов при измерении Р-нечетных эффектов. Препринт ПИЯФ №2708, 2007, 9 с.
26. Гундорин Н.А., Жданова К.В., Жучко В.Е., Пикельнер Л.Б., Реброва Н.В., Саламатин И.М., Смирнов В.И., Фурман В.И. «Измерение выхода запаздывающих нейтронов при делении ^{237}Np тепловыми нейтронами», Ядерная Физика, 2007, том 70, №6, с.1-6.
27. Николенко В. Г., Окунев И. С., Паржицкий С. С., Попов Ю. П., Чувильский Ю. М.,«Оценка величин РТ-нарушающего эффекта и сохраняющих Т-инвариантность маскирующих спин-угловых корреляций в реакции $^{10}B(n,\alpha_1\gamma)^{7}Li$», Письма в ЭЧАЯ, 2007, т.4, № 1(137) с.42-53.
28. Суховой А.М., Хитров В.А.. Максимальное значение парциальных ширин первичных гамма-переходов в области 0.5 МэВ< Egamma <Bn и некоторые особенности

структуры возбужденных уровней ядер с массой 27<A<201. Вопросы атомной науки и техники, серия ядерные константы, 2006, вып. 1-2, с. 19-28.
29. Суховой А.М., Хитров В.А.Две области возможного резкого изменения структуры возбужденных состояний ядер любых типов. Вопросы атомной науки и техники, серия ядерные константы, 2006, вып. 1-2, с. 80-92.
30. Франк А.И., Гелтенборт П., Жентшель М., Кулин Г.В., Кустов Д.В., Носов В.Г., Стрепетов А.Н.. Новый гравитационный эксперимент с ультрахолодными нейтронами. Письма в ЖЭТФ, 86 (2007) 255-259.
31. Sukhovoj A.M., Khitrov V.A., Gamma decay of the compound state and change of structure of the 124Te excited levels, JINR communication E3-2007-22, Dubna, 2007.

Theoretical investigations

1. Игнатович В. К. и Шабалин Е.П.“Алгебраический метод расчета альбедо нейтронов”// Ядерная физика, Т.70, No.2, стр. 288-286 (2007)
2. Аксёнов В.Л., Игнатович В.К.и Никитенко Ю.В.“Отражение нейтронов от геликоидальой системы ” // Поверхность, No.9 стр. 40-48 (2007)
3. Ignatovich V.K., Neutrostriction in Neutron Stars, Concepts of Physics old and new, v.4, No.4, p. 575, 2007.
4. Gahler R., Ignatovich V.K., Neutron holography without reference beams, Physics letters A, Volume 362, issue numbers 5-6, the March 12, 2007 issue, on pages 393-400.
5. Lyuboshitz V.L., Lyuboshitz V.V.. “On the coherent inelastic processes in the interaction of hadrons and γ-quanta with nuclei at ultrarelativistic energies”. European Physical Journal A, v. 31 , No. 4, 2007, pp. 465-467 .
6. Lyuboshitz V.L., Lyuboshitz V.V.. “Strangeness conservation and pair correlations of neutral kaons with close momenta produced in inclusive multiparticle processes” . Письма в ЭЧАЯ, т. 4 , вып. 5 (141) , 2007, сс. 654-660 [Physics of Particles and Nuclei, Letters, v. 4, No. 5, 2007, pp. 388-392]
7. Lyuboshitz V.L., Lyuboshitz V.V.. “The coherent inelastic processes on nuclei at ultrarelativistic energies”. Ядерная физика, т. 70 (7), 2007, сс. 1224-1229 [Physics of Atomic Nuclei, v. 70 (7), 2007, pp. 1185-1190] (Материалы юбилейной сессии-конференции секции ядерной физики ОФН РАН, ИТЭФ, Москва, 5 – 9 декабря 2005 г.)
8. Lyuboshitz V.L., Lyuboshitz V.V.. “The process of Coulomb dissociation of weakly bound relativistic nuclei and hypernuclei within the two-cluster model”. Ядерная физика, т. 70 (9) , 2007 , сс. 1663-1667 [Physics of Atomic Nuclei, v. 70 (9), 2007, pp. 1317-1321] (Proceedings of the International Conference “Nuclear Structure and Related Topics” – NSRT-2006, Dubna, June 13 – 17, 2006)
9. Lyuboshitz V.L., Lyuboshitz V.V.. “On the process of Coulomb dissociation of weakly bound relativistic nuclei and hypernuclei”. Nuclear Physics A , v. 790, 2007,pp. 294c - 298c (Proceedings of the 18-th International IUPAP Conference on Few-Body Problems in Physics – FB18, Santos, Sao Paulo, Brazil, August 21 – 26, 2006)

Applied research

1. Anicic M., Frontasyeva M.V., M. Tomasevic, Popovic A.. Assessment of atmospheric deposition of heavy metals and other elements in Belgrade using the moss biomonitoring technique and neutron activation analysis. Environmental Monitoring and Assessment, DOI10.1007/s10661-00609354-y, 2007.

2. Barandovski L., Cekova M., Frontasyeva M.V., Pavlov S.S., Stafilov T., Steinnes E., Urumov V.. Atmospheric deposition of trace element pollutants in Macedonia studied by the moss biomonitoring technique. JINR Preprint, E18-2006-160, pp. 46.
3. Barandovski L., Cekova M., Frontasyeva M.V., Pavlov S.S., Stafilov T., Steinnes E., Urumov V.. Atmospheric deposition of trace element pollutants in Macedonia studied by the moss biomonitoring technique, 2007. Environmental Monitoring and Assessment, DOI10.1007/s10661-007-9747-6, 2007.
4. Budzynski P., Polanski K., Kobzev A.P.: Changes of Surface Layer of Nitrogen-Implanted AISI316L Stainless Steel. Preprint JINR E14 – 2007-101. Submitted to "Journal of Surface Investigation. X-Ray, Synchrotron and Neutron Techniques".
5. Florek M., Mankovska B., Oszlanyi J., Frontasyeva M.V., Ermakova E.V., Pavlov S.S.. The Slovak heavy metal survey by means the bryophyte technique. Ekologia (Bratislava), Vol. 26, No. 1, 2007, p. 99-114.
6. Gandbol G., Frontasyeva M.V., Ostrovnaya T.M., Pavlov S.S., Gerbish Sh., Baljinnyam N.. Assessment of hazardous impact of non-ferrous industry in the town of Erdenet, Mongolia, on the pasture animals. JINR Communication, E-18-2006-176, Dubna, 2007, pp. 15.
7. Korzekwa S., Pankratova Yu.S., Frontasyeva M.V.. Air pollution studies in Opole region, Poland, using the moss biomonitoring technique and neutron activation analysis. Ecological Chemistry and Engineering. Proceedings of ECOpole, Vol. 1 (1/2), 2007, p. 43-51.
8. Kulik M., Kobzev A.P., Jaworska D., Źuk J., Filiks J.: Investigation of indium diffusion process and optical effects in In^+ implanted GaAs. Vacuum 81 (2007) 1124-1128.
9. Latuszynski A., Pyszniak K., Drozdziel A., Turek M., Maczka D., Meldizon J., Effektivnost' termoemissionnogo ionnnogo istochnika on-lain PREPRINT ZIBJ P13-2007-9
10. Latuszynski A., Pyszniak K., Drozdziel A., Turek M., Maczka D., Meldizon J.: Atom ionization process in the thermoionization ion source, Vacuum 81(10), (2007), 1150.
11. Machajdík, D., Kobzev, A. P., Hušeková, K., Ťapajna, M., Fröhlich, K., and Schram, T.: Thermal stability of advanced gate stacks consisting of a Ru electrode and Hf-based gate dielectrics for CMOS technology. Vacuum 81 (2007) 1379-1384.
12. Merešová J., Florek M.,.Holý K, Sýkora I.,. Frontasyeva M.V, Pavlov S.S.. Concentration of elements in atmospheric aerosol in Bratislava, Acta Physica Universitatis Comenianae, Vol. XLVI-XLVII, 2007, p. 73-82,
13. Michalak L, Maczka D., Zuk J., Editorial, Vacuum, 81(10), 2007.
14. Mosulishvili L.M., Belokobylsky A.I., Kirkesali E.I., Frontasyeva M.V., Pavlov S.S., Aksenova N.G.. Neutron activation analysis for studying Cr uptake in the blue-green microalga Spirulina platensis. Journal of Neutron Research, Vol. 15, No. 1, 2007, p. 49-57.
15. Oprea C., Kobzev A.P., Codescu M., Shalanski P.J., and Curuia M.: PIXE and RBS analysis of Fe – Cu nanoalloy. Vacuum 81 (2007) 1164-1166.
16. Oprea C., Kobzev A.P., Oprea I.A., Shalanski P.J., and Burguta V.: PIXE detection limits for dental enamel from some human teeth by exitation with protons and $^4He^+$ ions from a 3 MeV Van de Graaff. Vacuum 81 (2007) 1167-1170.
17. Pyszniak K, Turek M., Drozdziel A., Sielanko J., Maczka D., Stanowisko do badania rozpylania jonowego wiazkami sredniej energii, Electronika 10, (2007), 51.
18. Pyszniak K., Drozdziel A., Turek M., Latuszynski A., Maczka D., Sielanko J., Vaganov Y.A., Yushkevich Y.V., Extractions of ions from a plasma source and formation of beams, Instruments and experimental techniques 50(4), 552-556, (2007)
19. Turek M., Pyszniak K., Drozdziel A., Sielanko J., Latuszynski A., Maczka D., Malinowski G., Vaganov Y.A., Yushkevich Y.V., Kompiuternoye modelirovaniye protsessa ekstraktsyi ionov iz plazmiennogo istochnika ionov , PREPRINT ZIBJ DUBNA P13-2007-113

20. Gorbunov A.V., Lyapunov S.M., Okina O.I., Frontasyeva M.V.. Experience in applying neutron activation analysis in Ecology: impact of phosphate ore processing plant on human organism. Engineering Physics, No. 5 (6), 2007, p. 113-124 (in Russian).
21. Гундорин Н.А., Дикусар Н.Д., Мазный Н.Г., Пикельнер Л.Б., Саламатин И.М., Цулаиа М.И.. "Экспресс-анализ спектров в прецизионных экспериментах", Препринт ОИЯИ, Р10-2007-94, Дубна, 2007.
22. Мазный Н.Г., Саламатин И.М., Саламатин К.М.. "Генерация программ автоматизации экспериментов из модулей в формате загрузки", Препринт ОИЯИ, Р13-2007-93, Дубна, 2007.

Reports at Schools and Conferences

1. Frank A. I., Geltenbort P., Jentschel M., Kulin G. V., Kustov D.V., Nosoм V. G., Plonka C., and Strepetov A.N.. First Observation and Investigation of the Acceleration Matter Effect in Neutron Optics. 4th European Conference on Neutron Scattering. 25-29June 2007. Lund, Sweden. Programme-Oral presentations. P.128.
2. Frank A. I., Geltenbort P., Jentschel M., Kulin G. V., Kustov D.V., Nosoм V. G., Plonka C., and Strepetov A.N.. Quantum optical experiment on measurement of gravity force acting on neutron. First Observation and Investigation of the Acceleration Matter Effect in Neutron Optics. 4th European Conference on Neutron Scattering. 25-29 June 2007. Lund, Sweden. Poster presentations. P.63
3. Горелова С.В., Гинс М.С., Кононков П.Ф., Фронтасьева М.В., Ермакова Е.В., Ляпунов С.М., Горбунов А.В., Окина О.И.. Биоаккумуляция химических элементов из почв овощными корнеплодными культурами. Роль физиолого-биохимических исследований в селекции овощных культур: Материалы Всероссийской научно-практической конференции, посвященной 75-летию со дня создания отдела физиологии и биохимии растений ВНИИССОК. Москва, РУДН, 2007, с. 143-159.
4. Aničić M., Tasić M., Frontasyeva M.V., Tomašević M., Rajšić S., Strelkova L.P. and Steinnes E.. Active moss biomonitoring of atmospheric trace element deposition in urban area using INAA and AAS analytical techniques. In "Nuclear Physics Methods and Accelerators in Biology and Medicine-2007", Editors: Granja C., Leroy C., Stekl I., AIP Conference Proceedings, Vol. 958, American Institute of Physics, New York, 2007, p. 222-225.
5. Goryaynova Z. I., Frontasyeva M.V., Pavlov D.F., and Pankratova Yu. S.. Chemical composition study of the Rybinsk Reservoir ecosystem using NAA. In "Nuclear Physics Methods and Accelerators in Biology and Medicine-2007", Editors: Granja C., Leroy C., Stekl I., AIP Conference Proceedings, Vol. 958, American Institute of Physics, New York, 2007, p. 226-227.
6. Korzekwa S., Pankratova Yu. S. and Frontasyeva M.V.. Air pollution studies in Opole Region, Poland, using the moss biomonitoring and INAA. In "Nuclear Physics Methods and Accelerators in Biology and Medicine-2007", Editors: Granja C., Leroy C., Stekl I., AIP Conference Proceedings, Vol. 958, American Institute of Physics, New York, 2007, p. 230-231.
7. Pankratova Yu.S., Frontasyeva M.V., Berdnikov A.A., and Pavlov S.S.. Air pollution studies in the Republic of Udmurtia, Russian Federation, using moss biomonitoring and INAA. In "Nuclear Physics Methods and Accelerators in Biology and Medicine-2007", Editors: Granja C., Leroy C., Stekl I., AIP Conference Proceedings, Vol. 958, American Institute of Physics, New York, 2007, p. 236-237.

8. Vergel' K.N., Frontasyeva M.V., Pavlov S.S., and Povtoreyko E.A.. Air pollution studies in Tver Region of Russia using moss-biomonitoring with nuclear analytical methods. In "Nuclear Physics Methods and Accelerators in Biology and Medicine-2007", Editors: Granja C., Leroy C., Stekl I., AIP Conference Proceedings, Vol. 958, American Institute of Physics, New York, 2007, p. 240-241.
9. Florek M., Maňkovská B., Oszlanyi J., Holý K., Frontasyeva M.V., Ermakova E.V., Pavlov S.S.. Atmospheric deposition of trace elements in selected regions of Slovakia studied by the moss technique using NAA and AAS. Proc. of ISINN´14, JINR, Dubna, ISBN 5-9530-0139-8, 2007, p. 330-338.
10. Andrianov V.R., Druzhinin A. A., Furman V. I., Gundorin N. A., Lihachev A. N., Pikelner L. B., Rebrova N. V., Salamatin I. M., Vyachin V. N., Zhdanova K. V. «Measurement of delayed neutron yields from thermal neutron induced fission of ^{245}Cm», Proc. of ISINN-15 (2007).
11. Lyuboshitz V.L., Lyuboshitz V.V.. "Role of spin effects in the "forward" nucleon charge-exchange reaction n + p $\rightarrow$ p + n ". Proc. of ISINN-14 (Dubna, May 24 – 27, 2006), JINR E3-2007-23 , Dubna, 2007 , pp. 64-74 .
12. Lyuboshitz V.L., Lyuboshitz V.V.. "Strangeness conservation and pair correlations of neutral kaons with close momenta produced in inclusive multiparticle processes". Proceedings of the VI International Workshop on Very High Multiplicity Physics – VHMP'05 (Dubna, April 16 – 17, 2005), JINR Д 1,2-2007-67, Dubna, 2007, pp. 507-513
13. Lyuboshitz V.L., Lyuboshitz V.V.. "On the coherent inelastic processes in the interaction of hadrons and γ-quanta with nuclei at ultrarelativistic energies". Proceedings of the IV International Conference on Quarks and Nuclear Physics – QNP06 (Madrid, Spain, June 5 – 10, 2006), Springer, Berlin – Heidelberg, 2007, pp. 87-89
14. Lyuboshitz V.L., Lyuboshitz V.V.. "Strangeness conservation and pair correlations of neutral kaons with low relative momenta produced in inclusive multiparticle processes". Proceedings of the IV International Conference on Quarks and Nuclear Physics – QNP06 (Madrid, Spain, June 5 – 10, 2006), Springer, Berlin – Heidelberg , 2007, pp. 109-112
15. Lyuboshitz V.L., Lyuboshitz V.V.. "The process of Coulomb dissociation of weakly bound relativistic nuclei and hypernuclei within the two-cluster model". Proceedings of the XI International Seminar on Electromagnetic Interactions of Nuclei – EMIN-2006 (Moscow, September 21 – 24, 2006), Moscow, 2007, pp. 96 - 103 .

    The paper is also published in the online version of Proceedings on the EMIN-2006 website http://www.inr.ac.ru/~pnlab/emin2006/trudy2006/11_lyuboshitz.pdf
16. Lyuboshitz V.L., Lyuboshitz V.V.. "Role of spin effects in the nucleon charge-exchange process n + p $\rightarrow$ p + n at zero angle". Proceedings of the XI International Seminar on Electromagnetic Interactions of Nuclei – EMIN-2006 (Moscow, September 21 – 24, 2006), Moscow, 2007, pp. 187-191 .

    The paper is also published in the online version of Proceedings on the EMIN-2006 website: http://www.inr.ac.ru/~pnlab/emin2006/trudy2006/22_lyuboshitz2.pdf)
17. Lyuboshitz V.L., Lyuboshitz V.V.. " Spin structure of the charge-exchange process n + p $\rightarrow$ p + n at zero angle". Proceedings of the 17-th International Spin Physics Symposium – SPIN2006 (Kyoto, Japan, October 2 – 7, 2006), Melville, New York, 2007 (AIP Conference Proceedings, v. 915), pp. 789-794
18. Lyuboshitz V.L., Lyuboshitz V.V.. "On the correlations of polarizations in the system of two photons". Proceedings of the 17-th International Spin Physics Symposium – SPIN2006 (Kyoto, Japan, October 2 – 7, 2006), Melville, New York, 2007 (AIP Conference Proceedings, v. 915), pp. 268-271

19. Lyuboshitz V.L., Lyuboshitz V.V.. “The coherent inelastic processes on nuclei at ultrarelativistic energies” . Proceedings of the XVIII International Baldin Seminar on High Energy Physics Problems – ISHEPP-18 (Dubna, September 25 – 30, 2006), Dubna, 2007 (в печати)
20. Prokhorova E., Gonnenwein F., Kopatch Yu., Mutterer M., Hanappe F., Kinnard V., Stuttgé L., Dorvaux O., Wollersheim H.-J., Triple Neutron-Neutron-Fragment Correlations in Spontaneous Fission of ^{252}Cf , in Proc. Int. Conf. “Neutron Spectroscopy, Nuclear Structure, Related Topics: (ISINN-14), Dubna, May 24-27, 2006, 13/ 6/2007. - p.128-133
21. Prokhorova E., Gonnenwein F., Kopatch Yu., Mutterer M., Hanappe F., Kinnard V., Stuttgé L., Dorvaux O., Wollersheim H.-J.,Angular Correlations Between Fragment Spin and Prompt Neutron Evaporation in Spontaneous Fission of ^{252}Cf: CORA-Demon Experiment, in Proc. Int. Conf. “International Symposium on Exotic Nuclei” (EXON-2006), Khanty-Mansiysk, Russia, 17-22 July 2006, 13/ 8/2007. - p.179-184
22. Petrov G.A., Gagarski A.M., Guseva I.S., Kopatch Yu.N., Goennenwein F., Mutterer M., About Further Investigations of T-odd Asymmetry Effects of Light Particle Emission in Ternary Fission Induced by Polarised Neutrons. NUCLEUS-2007. LVII Internatrional Conference on Nuclear Physics. June 25 -29, 2007. Voronezh, Russia. Book of Abstracts. Saint-Petersburg, p.37.
23. Frontasyeva M.V. and Lyapunov S.M.. Workplace monitoring and occupational health studies at the centre for production of phosphorus mineral fertilizers in Voskresensk (Moscow Region, Russia), using nuclear and related analytical techniques. CHEMRAWN XII Conference – The role of chemistry in sustainable agriculture and human well-being in Africa (2-5 December, 2007, Stellenbosch, South Africa). Book of Abstracts, Saneri, 2007, p. 61.
24. Florek M., Holy K., Meresova J., Sykora I., Burda C., Melicherova T., Frontasyeva M.V., Pavlov S.S.. The results of environmental research in Slovakia employing nuclear and related analytical techniques. IXth Banská Štiavnica Days, (September, 2007, Slovakia).
25. Spiric Z., Frontasyeva M.V., Stafilov T., Enimiteva V., Bukovec D., Mesic Z.. Environmental and health consequences of mercury air pollution. Int. Cond Trace Elements in Diet, Nutrition & Health. Essentiality and Toxicity (October 21-26, 2007, Crete, Greece). The International Society for trace element research in humans. Book of Abstracts, p. 97-98.
26. Spiric Z., Frontasyeva M.V., Stafilov T., Barandovski L., Gundorina S.F., Ostrovnaya T.M., Bukovec D., Mesic Z.: Moss as bioindicator of Air Pollution. 5th Croatian conference «Air protection 2007», Zadar 9-13 October 2007, Sega, Kresimir (ed.). Book of Abstracts, Zagreb, 2007, p. 251-256.
27. Aničić M., Tasić M., Frontasyeva M.V., Tomašević M., Rajšić S., Nešić M.. Atmospheric bulk deposition and active biomonitoring of trace elements in Belgrade urban area. In the Book of Abstracts of the 8th European Meeting o Environmental Chemistry (5-8 December 2007, Inverness, Scotland).
28. Frontasyeva M.V., Stafilov T., Spiric Z., Culicov O., Krmar M., Coscun M.. Trace element atmospheric pollution in the Balkans studied by the moss technique, ENAA and AAS. In the Book of Abstracts of the III Congress of Ecologists of the Republic of Macedonia (October 6-9, 2007, Struga, Macedonia), Macedonian Ecological Society, p. 216.
29. Стафилов Т., Панчевски З., Фронтасјева М., Стрелкова Л., Шајн Р.. Дистрибуција на тешки метали во почвите од Велес и неговата околина. (in Macedonian). In the Book of Abstracts of the III Congress of Ecologists of the Republic of Macedonia (October 6-9, 2007, Struga, Macedonia), Macedonian Ecological Society, p. 127.
30. Stafilov T., Panchevski Z., Frontasyeva M., Strelkova L., Sajn R.. Distribution of some elements due to industrial pollution in surface soils in the Veles Region in Macedonia. In the

Book of Abstracts of the III Congress of Ecologists of the Republic of Macedonia (October 6-9, 2007, Struga, Macedonia), Macedonian Ecological Society, p. 128.

31. Frontasyeva M.V.. JINR contribution to trace elements atmospheric deposition study in some selected countries of Europe and Asia based on moss analysis. Book of Abstracts 20th Task Force Meeting of the ICP Vegetation (Dubna, March, 5-9, 2007), JINR E-18-2007-24, p. 21.
32. Pankratova Yu.S., Frontasyeva M.V., Zelnitchenko N.I., Pavlov S.S.. Atmospheric deposition of heavy metals and other elements in the Republic of Udmurtia, Russian Federation, studied by the moss biomonitoring, NAA and GIS technology. In the Book of Abstracts 20th Task Force Meeting of the ICP Vegetation (Dubna, March, 5-9, 2007), JINR E-18-2007-24, p. 32.
33. Vergel' K.N., Ermakova E.V., Frontasyeva M.V., Pavlov S.S.. Air pollution studies in Central part of Russia using the moss-biomonitoring technique: moss-surveys 2000 and 2005. Book of Abstracts 20th Task Force Meeting of the ICP Vegetation (Dubna, March, 5-9, 2007), JINR E-18-2007-24, p. 41.
34. Aleksiayenak Yu., Frontasyeva M.V., Ostrovnaya T.M.. Trace element atmospheric deposition in the Republic of Belarus: Minsk and Grodno case study. Book of Abstracts 20th Task Force Meeting of the ICP Vegetation (Dubna, March, 5-9, 2007), JINR E-18-2007-24, p. 46.
35. Barandovski L., Cekova M., Frontasyeva M.V., Pavlov S.S., Urumov V.. Air pollution in the Republic of Macedonia: moss biomonitoring stuidy–2005. Book of Abstracts 20th Task Force Meeting of the ICP Vegetation (Dubna, March, 5-9, 2007), JINR E-18-2007-24, p. 49.
36. Krmar M., Radnovic D., Frontasyeva M.V., Pavlov S.S., Pankratova Yu.S.. Comparison of moss surveys 2000 and 2005 in Northern Serbia. Book of Abstracts 20th Task Force Meeting of the ICP Vegetation (Dubna, March, 5-9, 2007), JINR E-18-2007-24, p. 60.
37. Spiric Z., Kusan V., Mesic Z., Frontasyeva M.V., Gundorina S.F., Ostrovnaya T.M.. The moss survey 2006 in the Republic of Croatia. Book of Abstracts 20th Task Force Meeting of the ICP Vegetation (Dubna, March, 5-9, 2007), JINR E-18-2007-24, p. 68.
38. My Trinh T.T., Frontasyeva M.V., Nguyen Hong Nhung. Leaves of Tamarindus Indica used to monitor metal contamination in Hochiminh City, Vietnam. Book of Abstracts 20th Task Force Meeting of the ICP Vegetation (Dubna, March, 5-9, 2007), JINR E-18-2007-24, p. 72.
39. Oszlanyi J., Mankovska B., Frontasyeva M., Ermakova E.. Use of mosses as biomonitors of heavy metal deposition in the Carpathian mountains (Slovak part). Book of Abstracts, 20th Task Force Meeting of the ICP Vegetation (Dubna, March, 5-9, 2007), E-18-2007-24, p. 63.
40. Frontasyeva M.V.. Nuclear and Related analytical techniques for trace element atmospheric deposition study in the Balkans. 12th International Conference on Modern Trends in Activation Analysis (MTAA-12), (Tokyo, Japan, 16-21 September, 2007).
41. Tsibakhashvili N., Murusidze I., Kerkenjia S., Kalabegishvili T., Mosulishvili L., Kirkesali E., Holman H.-Y., Frontasyeva M.V., Gundorina S.F.. Biotechnology of Cr(VI) transformation into Cr(III) complexes. 12th International Conference on Modern Trends in Activation Analysis (MTAA-12), (Tokyo, Japan, 16-21 September, 2007).
42. Судницын И.И., Крупенина И.И., Фронтасьева М.В., Павлов С.С., Гундорина С.Ф.. Химический состав почв Москвы и Дубны, Тезисы докладов XVIII Менделеевского съезда по общей и прикладной химии (под эгидой Международного союза по теоретической и прикладной химии (IUPAC), 23-28 сентября, 2007, Москва) (в 5-и томах), т. 1., Москва, Граница, с. 447.
43. Cristache C., Culicov O., Toma M., Frontasyeva M., Duliu O.G., Oaie G.. Application of nuclear techniques in geological samples. ISCBPU-5, The Fifth International Student Conference of the Balkan Physical (21-24 August, 2007, Bodrum, Turkey).

44. Cristache C., Culicov O., Toma M., Frontasyeva M., Duliu O.G., Oaie G.. Determination of elemental content in geological samples, The 7th International Balkan Workshop on Applied Physics (5-7 July 2007, Constanta, Romania).
45. Cristache C., Culicov O., Gmeling K., Toma M., Frontasyeva M., Duliu O.G., Oaie G.. PGAA-ENAA comparative study of the Black See sediment profiles. 2nd Joint Seminar-School JINR-ROMANIA on Neutron Physics (8-16 September, 2007, Baia Mare, Romania).
46. Мазный Н.Г., Саламатин И.М., Саламатин К.М. «Генерация программ автоматизации экспериментов из модулей в формате загрузки», доклад на 57 Международной конференции «Ядро 2007», Воронеж, 25-29 июня 2007.
47. Гундорин Н.А., Дикусар Н.Д., Мазный Н.Г., Пикельнер Л.Б., Саламатин И.М., Цулаиа М.И. «Экспресс-анализ спектров в прецизионных экспериментах», доклад на 57 Международной конференции «Ядро 2007», Воронеж, 25-29 июня 2007.
48. Погребняк А.Д., Кобзев А.П., Левитант Н., Ердыбаева Н.К., Братушка С.Н., Маликов Л.В., Кульментьева О.П., Гриценко Б.П. Двойная имплантация ионов газов и металлов в NiT. 7-я международная конференция «Взаимодействие излучения с твёрдым телом», Минск, 26-28 сентября 2007г.
49. Pyszniak K., Drozdziel A., Sielanko J., Maczka D. Simulation of Beam Extraction from Hollow Cathode Ion Sources, 5-th International Conference NEET 2007, Zakopane, Poland, Abstract book p.158.
50. Bystritsky V.M., … , Parzhitski S.S. et al., Proceedings of the International Conference on Muon Catalyzed Fusion and Relative Topics, MCF-07, Dubna, Russia, 18-21 June, 2007.
51. Oprea C., Oprea A.I., Samosvat G.S., Nikolenko V.G.. Savostin V.V., Morozov V.M. “Experiment for the measurement of the neutron-electron scattering length in liquid Pb at the TS-3000K thermostat from IBR-2 reactor.” // ISINN-15, Abstracts, E3-2007-49, p.63.
52. Mitsyna L.V., Nikolenko V.G., Popov A.B., Samosvat G.S. On neutron electromagnetic constants derived from neutron scattering by 208Pb. ISINN-15, Abstracts, E3-2007-49, p.38.
53. Popov A.B., Tretyakova T.Yu.. "Comments to the problem of experimental determination of the neutron-electron scattering length and its theoretical interpritation" ISINN-15, Abstracts, E3-2007-49, p.42.
54. Ignatovich V. “Temperature Dependence of Neutron Scattering in He-4 Gas” // ISINN-14, E3-2007-23, p.41
55. Oprea A. I., Oprea C., Gledenov Yu. M., Sedyshev P. V.. Recent Result in the Study of Asymmetries in Neutron p-Resonances of ^{14}N at Neutron Energies up to 1 MeV. In: Proc. of ISINN-14, Dubna, 2007, p. 170-176.
56. Gledenov Yu.M., Sedysheva M.V., Zhang Guohui, Cao Rongtai, Chen Jinxiang, Tang Guoyou, Khuukhenkhuu G.. Measurement of Differential and Angle-integrated Cross-Section of the ^{64}Zn(n,α)^{61}Ni Reaction at 5.0 and 6.0 MeV. In: Proc. of ISINN-14, Dubna, 2007, p. 223-227.
57. Khuukhenkhuu G., Gledenov Yu.M., Bayarbadrakh B., Odsuren M., Sedysheva M.V.. Statistical Model Analysis for Isotopic Effect in (n,p) Cross Sections. In: Proc. of ISINN-14, Dubna, 2007, p. 228-234.
58. Vesna V. A., Gledenov Yu. M., Nesvizhevsky V. V., Petukhov A. K., Sedyshev P. V., Soldner T., Shul’gina E. V., Zimmer O.. Observation of the P-odd asymmetry of triton emission in the ^{6}Li(n,α)^{3}H reaction with cold polarized neutrons. ISINN-14. Neutron Spectroscopy, Nuclear Structure, Related Topics. (Dubna: JINR, 2007) E3-2007-23, p. 243-248.
59. Chedea Veronica, Oprea Cristiana. Minimizing pollution risk targeting the agri-environmental policy 50/07 ISSN 1454-7376 Horticulture series, 5p

60. Madalina Nedelcu, Oprea Cristiana. The radiochemical studies of moss plants and soil using INAA and AAS 50/07 ISSN 1454-7376 Horticulture series, 5p
61. Alexandru Mihul, Oprea Cristiana. PCA statistical analysis in the geochemical studies in Danube Delta. 50/07 ISSN 1454-7376 Horticulture series, 6p
62. Gledenov Yu. M. Sedysheva M.V., Khuukhenkhuu G., Zhang Jiaguo, Cao Rongtai, Guo Li-an, Chen Jinxiang, Wang Jianyong, Zhang Guohui. Differential and Angle-Integrated Cross-Section Measurement for the $^{64}Zn(n,\alpha)^{61}Ni$ Reaction at 2.5, 4.0 and 5.5 MeV. In: "Neutron Spectroscopy, Nuclear Structure, Related Topics". XV International Seminar on Interaction of Neutrons with Nuclei, 2007, Dubna, p.20.
63. Khuukhenkhuu G., Bayarbadrakh B., Odsuren M., Gledenov Yu.M., Sedysheva M.V.. Statistical Model Analysis for (n, α) Reaction Cross Sections. In: "Neutron Spectroscopy, Nuclear Structure, Related Topics". XV International Seminar on Interaction of Neutrons with Nuclei, 2007, Dubna, p.26.
64. Oprea A. I., Oprea C., Gledenov Yu. M., Sedyshev P. V.. Multilevel Approach in the Evaluation of the Asymmetry Effects on (n,p) Reaction for ^{35}Cl and ^{14}N Nuclei. In: "Neutron Spectroscopy, Nuclear Structure, Related Topics". XV International Seminar on Interaction of Neutrons with Nuclei, 2007, Dubna, p.40.
65. Vesna V.A., Gledenov Yu. M., Nesvizhevsky V.V., Petukhov A.K., Sedyshev P.V., Soldner T., Shulgina E.V., Zimmer O.. “Zero” Experiment and Final Result of the Measurements of the P-odd Asymmetry in the $^{6}Li(n,\alpha)^{3}H$ Reaction. In: "Neutron Spectroscopy, Nuclear Structure, Related Topics". XV International Seminar on Interaction of Neutrons with Nuclei, 2007, Dubna, p.64.
66. Oprea C., Mihul A. Oil pollution in relation with land use. Book of Abstracts, 37 Congress ESNA, Sept. 10-14, Dubna, 2007, 16
67. Oprea C., Login. V., Oprea I. A., Gorghiu G., Nicolescu C. Neural network application in agricultural studies. Book of Abstracts, 37 Congress ESNA, Sept. 10-14, Dubna, 2007, 17
68. Podina C., Oprea C. and Nedelcu M. Passive biomonitoring of airborne chemistry. Book of Abstracts, 37 Congress ESNA, Sept. 10-14, Dubna, 2007, 19
69. Radoviciu E., Oprea C., Cupsa D., Tomulescu I., Oprea I. A., Teusdea A., Burca I. The investigation of food quality in crops by AAS and NAA. Book of Abstracts, 37 Congress ESNA, Sept. 10-14, Dubna, 2007, 26
70. Nedelcu M., Oprea C., Podina C., Cupsa D., Oprea I. A., Teusdea A., Burca I. Impact of hazardous substances in/on soil. Book of Abstracts, 37 Congress ESNA, Sept. 10-14, Dubna, 2007, 85
71. Podina C., Nedelcu M., Oprea C., Cupsa D., Oprea I. A., Teusdea A., Burca I. X-ray fluorescence analysis of trace elements in pine needels for pollution monitoring. Book of Abstracts, 37 Congress ESNA, Sept. 10-14, Dubna, 2007, 73
72. Chedea S. V., Oprea C. An assessment of the impacts of agri-environmental issues. Book of Abstracts, 37 Congress ESNA, Sept. 10-14, Dubna, 2007, 76
73. Oprea C., Grigoras M. A., Chedea V., Oprea I. A., Holeab C. Environmental pressures and sustainable use of natural resources Book of Abstracts, 37 Congress ESNA, Sept. 10-14, Dubna, 2007, 88
74. Oprea C., Chedea S. V. Detection of trace elements in chernozem using different analytical methods. Book of Abstracts, 37 Congress ESNA, Sept. 10-14, Dubna, 2007, 88
75. Panteleev Ts., Oprea C., Oprea A.I. New experimental method to determine the averaged squared radius of the nuclei in the process of the direct and isomer fission. Book of Abstracts, ISINN-15, May 15-19, Dubna, 2007, 41

76. Oprea C., Oprea A.I. Factor analysis of neutron data Book of Abstracts, ISINN-15, May 15-19, Dubna, 2007, 60
77. Oprea C., Oprea A.I. Development of a PIXE program for the EG-5 experimental installation Book of Abstracts, ISINN-15, May 15-19, Dubna, 2007, 61
78. Oprea C., Oprea A.I. Calculation of the double differential neutron production cross-section in reactions induced by high-energy ions Book of Abstracts, ISINN-15, May 15-19, Dubna, 2007, 62
79. Oprea C., Oprea A.I., G.S. Samosvat, V.G. Nikolenko, V.V. Savostin, V.M.Morozov. Experiment for the measurement of the neutron-electron scattering length in liquid Pb at the TS-3000K thermostat from IBR-2 reactor. Book of Abstracts, ISINN-15, May 15-19, Dubna, 2007, 63
80. Oprea C., Oprea A.I., Nedelcu M. Indicators of pollution soil impact. Book of Abstracts, ISINN-15, May 15-19, Dubna, 2007, 12
81. Oprea C., Oprea A.I., Chedea V. An assumption on atmospheric transport and deposition modeling. Book of Abstracts, ISINN-15, May 15-19, Dubna, 2007, 12
82. Lyuboshitz V.L., Lyuboshitz V.V.. "Sign of the singlet length of neutron scattering on the proton, neutron radiative capture by the proton and problem of the virtual level of the (np) system". ISINN-15 (Dubna, May 16 – 19, 2007). Abstracts. JINR E3-2007-49, Dubna, 2007, p. 34
83. Lyuboshitz V.L., Lyuboshitz V.V.. "Spin structure of the "forward" charge-exchange process $n + p \to p + n$ and deuteron charge-exchange breakup $n + d \to p + (nn)$". LVII International Conference on Nuclear Physics "NUCLEUS 2007" (57-th International Meeting on Nuclear Spectroscopy and Nuclear Structure, Voronezh, Russia, June 25 – 29, 2007) . Book of Abstracts. Saint-Petersburg, 2007, p. 220
84. Lyuboshitz V.L., Lyuboshitz V.V.. "Spin structure of the "forward" charge-ex-change reaction $n + p \to p + n$ and the deuteron charge-exchange breakup $d + p \to (pp) + n$ ". XII Advanced Research Workshop on High Energy Spin Physics – DUBNA-SPIN-07 (Dubna, September 3 – 7, 2007) . Abstracts. JINR E1,2-2007-99, Dubna, 2007, pp. 20 –21
85. Lyuboshitz V.L., Lyuboshitz V.V.. "Spin structure of the "forward" charge-exchange reaction $n + p \to p + n$ and deuteron charge-exchange breakup $d + p \to (pp) + n$ ". 20-th European Conference on Few-Body Problems in Physics – EFB20 (Pisa, Italy, September 10 – 14, 2007). Book of Abstracts. Pisa, 2007, p. 60
86. Lyuboshitz V.L., Lyuboshitz V.V.. "Spectrum of relative momenta of the neutron and proton at deuteron peripheral breakup in the limit of very low momentum transfer". 20-th European Conference on Few-Body Problems in Physics – EFB20 (Pisa, Italy, September 10 – 14, 2007) . Book of Abstracts. Pisa, 2007, p. 134
87. Lyuboshitz V.L., Lyuboshitz V.V.. "Correlations of polarizations and entangled states in the two-photon system" . The 4-th International Workshop "Quantum Physics and Communication" – QPC-2007 (Dubna, October 15 – 19, 2007) . Book of Abstracts. JINR Д18-2007-137 , Dubna, 2007, p. 33
88. Sukhovoj A.M., Khitrov V.A., Pham Dinh Khang, Vuong Huu Tan, Nguyen Xuan Hai. On the Correctness of Various Approaches in the Extraction of the Nucleus Parameters on Example of Analysis of the Two-Step gamma-Cascades in 163Dy Compound Nucleus In: XIV International Seminar on Interaction of Neutrons with Nuclei, Dubna, May 2006, E3-2007-23, Dubna, 2007, pp. 257-265.
89. Khitrov V.A., Sukhovoj A.M., Pham Dinh Khang, Vuong Huu Tan, Nguyen Xuan Hai, Possibilities to Verify the Level Density and Radiative Strength Functions, Extracted from the Two-Step gamma-Cascade Intensities In: XIV International Seminar on Interaction of Neutrons with Nuclei, Dubna, May 2006, E3-2007-23, Dubna, 2007, pp. 266-273.

90. Nguyen Xuan Hai, Pham Dinh Khang, Vuong Huu Tan, Sukhovoj A.M., Khitrov V.A. The Initial Results of Research on Two-Step Cascades in the Dalat Research Reactor, In: XIV International Seminar on Interaction of Neutrons with Nuclei, Dubna, May 2006, E3-2007-23, Dubna, 2007, pp. 274-278.
91. Pham Dinh Khang, Vuong Huu Tan, Nguyen Xuan Hai, Nguyen Duc Tuan, Ho Huu Thang, Khitrov V.A., Sukhovoj A.M. New Facility for the (n,2gamma) Reaction Investigation at the Dalat Reactor, In: XIV International Seminar on Interaction of Neutrons with Nuclei, Dubna, May 2006, E3-2007-23, Dubna, 2007, pp. 279-283.
92. Sukhovoj A.M., Khitrov V.A., About Nucleus "Superfluid-Normal" State Transition Dynamics In: XIV International Seminar on Interaction of Neutrons with Nuclei, Dubna, May 2006, E3-2007-23, Dubna, 2007, pp. 284-295.

DEVELOPMENT AND CONSTRUCTION OF ELEMENTS OF NEUTRON SPECTROMETERS FOR CONDENSED MATTER INVESTIGATIONS

1. Belushkin A., et al. 1D Position-sensitive detector for thermal neutrons. PTE, 2007, v.50, N6, pp.23-29.
2. Belushkin A., et al. Two-dimensional monitor position-sensitive detector of thermal neutrons. JTPh, 2008, v 78, N.1. pp.121-125.
3. Belushkin A., et al. 2D Position-sensitive detector for thermal neutrons. Report to “XXI International Symposium on Nuclear Electronics & Computing”, NEC’2007. Book of Abstracts, JINR E10,11-2007-119, Dubna, 2007, p.22.
4. Murashkevich S., et al. Remote instrument supervision and control for the IBR-2M reactor. Ibid, p.42.
5. Balasoiu M., Kappel W., Cios M., Stancu N., Cios A., Kirilov A. S., Kutuzov S.A., Smirnov A. A., Gordeliy V. I., Erha1 R., Ivan’kov A. I., Rogacev A.V., Kovalev Yu. S., Kuklin A. I. New Magnetic System for Small Angle Neutron Scattering at YuMO Instrument. Book of abstracts 4-th European Conference on Neutron Scattering, June 2007, Lund, Sweden. p.484.
6. Kuklin A.I., Kutuzov S.A., Gabriel A., Eckold G., Kirilov A.S., Utrobin P.K., Bogdzel A.A., Islamov A.Kh., Kovalev Yu.S., Rogachev A.V., Ivan’kov A.I., Gordeliy V.I. The results of application of new type PSD in diffraction and small angle experiments. Book of abstracts the VI National Conference on Application of X-ray, Synchrotron Radiation, Neutrons and Electrons for Material Characterization. November 12-17, 2007, Moscow, Russia p.593.
7. Levchanovsky F.V., Litvinenko E.I., Nikiforov A.S., Gebauer B., Schulz Ch., Wilpert Th. Software modules of DAQ PCI board (DeLiDAQ) for position-sensitive MWPC detectors with delay line readout, NIM A 569 (2006) 900-904, See also NIM A 572 (2007) 1004.
8. Zsigmond G., Manoshin S., Lieutenant K., Seeger P., Christiansen P., Willendrup P., Lefmann K. Monte Carlo simulations for the development of polarized neutron instrumentation: An overview Physica B: Condensed Matter, v 397, Issues 1-2, 15 July 2007, pp. 115-119.
9. Manoshin S., Ioffe A. New modules for the VITESS software package: time-gradient magnetic fields and neutron refractive lenses. Accepted in NIM B, 2007, in press.
10. Журавлев В.В., Кириллов А.С., Петухова Т.Б.и Сиротин А.П. «Система управления исполнительными механизмами спектрометра на реакторе ИБР-2 как современная локальная сеть контроллеров – CAN», ОИЯИ, Р13-2007-170, Дубна, 2007.
11. Trofimov V.N., Chernikov A.N., Zaitsev-Zotov S.V., Dyuzhikov I.N., Shevlyuga V.M., Eltsov K.N. «An ultrahigh-vacuum nitrogen-free helium cryostat with small heat losses. Instruments and Experimental Techniques» (2007), v.50, 6, p 838-841.

6. PRIZES

JINR Prizes:

Scientific and Methodical Investigations:

First Prize:

V.L.Aksenov, V.I.Bodnarchuk, Ye.B.Dokukin, V.K.Ignatovich, S.V.Kozhevnikov, D.A.Korneev, V.V.Lauter, K.N.Zhernenkov, Yu.V.Nikitenko, A.V.Petrenko. «Reflectometry of polarized neutrons at the IBR-2 pulsed reactor».

Applied Physics Research:

Second Prize:

R.N.Vasin, E.V.Ermakova, T.I.Ivankina, H.Kern, D.M.Levin, A.L.Kulakovskii, A.N.Nikitin. «Neutron, X-ray and ultrasonic investigations of geological materials and industrial wastes for solution of ecological problems».

7. SEMINARS

Date	Authors	Title
19.04.07	E.P.Shabalin (FLNP JINR)	Experimental investigation of irradiated solid methane swelling
4.07.07	Yu.V.Nukitenko (FLNP JINR)	Neutron standing waves in layered systems
19.09.07	A.V.Shikanov (MEPhI)	50 years of pulsed neutron logging (Flerov G.N. 1956-1958)
27.09.07		Seminar dedicated to V.K.Ignatovich's and A.V.Strelkov's jubilees.
	D.N.Bondarenko (RRC KI)	Neutron activation analysis using UCN and VCN as a method for determining elemental composition of surfaces and their contamination and for measuring neutron inelastic scattering cross-sections in the ultralow energy region.
	V.I.Morozov (RRC KI)	Project for precise neutron lifetime measurements by the method of storage of ultracold neutrons with registration of inelastic scattering neutrons
	Yu.V.Nikitenko (FLNP JINR)	Reflectometry with polarized thermal neutrons.

8. ORGANIZATION AND USER INTERACTION

8.1. STRUCTURE OF LABORATORY AND SCIENTIFIC DEPARTMENTS

Directorate:
Director:
A.V.Belushkin
Deputy Director:
V.N.Shvetsov
Scientific Secretary:
O.A.Culicov

Reactor and Technical Departments
Chief engineer: A.V.Vinogradov
IBR-2 reactor
Chief engineer: A.V.Dolgikh
Department of IREN
Head: V.G.Pyataev
Mechanical maintenance division
Head: A.A.Belyakov
Electrical engineering department
Head: V.A.Trepalin
Design bureau
Head: A.A.Kustov
Experimental workshops
Head: A.N.Kuznetsov

Scientific Departments and Sectors
Condensed matter department
Head: D.P.Kozlenko
Nuclear physics department
Head: Yu.N.Kopatch
Department of IBR-2 spectrometers complex
Head: S.A.Kulikov

Administrative Services
Deputy Director: S.V.Kozenkov
Secretariat
Finances
Personnel

Scientific Secretary Group
Translation
Graphics
Photography
Artwork

NEUTRON SCATTERING STUDIES OF CONDENSED MATTER

Sub-Division	Title	Head
Sector 1: Neutron Diffraction. Head: A.M.Balagurov		
Group No.1	HRFD	V.Yu.Pomjakushin
Group No.2	DN-2	A.I.Beskrovnyi
Group No.3	DN-12	B.N.Savenko
Group No.4	Geomaterials	A.N.Nikitin
Group No.5	SCAT	Ch.Scheffzük
Sector 2: Neutron Optics. Head: V.L.Aksenov		
Group No.1	Surfaces	Yu.V.Nikitenko
Group No.2	Nanostructures	M.V.Avdeev
Small angle scattering group. Head: V.I.Gordeliy		
Inelastic scattering group. Head: I.Natkaniec		

NUCLEAR PHYSICS DEPARTMENT

Sub-Division	Title	Head
Sector 1. Correlation γ-spectroscopy and development of experimental installations.		**Head: N.A.Gundorin**
Sector 2. Polarized neutrons and nuclei.		**Head: V.R.Skoy**
Group No.1	Polarized nuclear targets	V.R.Skoy
Group No.2	Thermal polarized neutrons	M.I.Tsulaya
Sector 3. Neutron activation analysis.		**Head: M.V.Frontasyeva**
Group No.1	Analytical	M.V.Frontasyeva
Group No.2	Experimental	S.S.Pavlov
Group No.2	**Neutron spectroscopy**	**Yu.N.Kopatch**
Group No.5	**Proton and α-decay**	**Yu.M.Gledenov**
Group No.6	**Properties of γ-quanta**	**A.M.Sukhovoy**
Group No.7	**Neutron structure**	**V.G.Nikolenko**
Group No.8	**Ultra-cold neutrons**	**E.V.Lychagin**
Group No.9	**Neutron optics**	**A.I.Frank**
Group No.11	**Theory**	**V.K.Ignatovich**
Group No.12	**Electrostatic generator-5**	**A.P.Kobzev**

DEPARTMENT OF IBR-2 SPECTROMETERS COMPLEX

Sub-Division	Title	Head
Group No.1	Scintillation detectors	E.S.Kuzmin
Group No.2	Gaseous detectors	Ts.Panteleev
Sector No.1	**Electronics**	**V.I.Prikhodko**
Group No.1	Analog electronics	A.A.Bogdzel
Group No.2	Digital electronics	V.F.Levchanovsky
Group No.3	Software	A.S.Kirilov
Group No.4	Local network	G.A.Sukhomlinov
Sector No.2	**Spectrometers**	**A.P.Sirotin**
Group No.1	Development of spectrometer elements	A.P.Sirotin
Group No.2	Sample environment	A.N.Chernikov

8.2. MEETINGS AND CONFERENCES

In 2007, FLNP organized the following meetings:

1. *20th Task Force Meeting of the UNECE ICP Vegetation, Dubna, March 5-9.*
2. *XV International Seminar on Interaction of Neutrons with Nuclei ISINN-15, Dubna, May 16-19.*
3. *Meeting of the Forum on Cooperation of Regulatory Bodies and Updating Nuclear and Radiation Safety at Research Nuclear Facilities, Dubna, July 3-5.*
4. *Workshop of European Society for New Methods in Agricultural Research (ESNA), Dubna, September 10-14.*
5. *2nd Joint Seminar-School JINR-Romania on Neutron Physics for Investigations of Nuclei, Condensed Matter and Life Sciences, Baia Mare, Romania, September 11-16.*
6. *IAEA TC 1st Workhop "Harmonization of QA/QC Systems According to ISO and International Standards in Nuclear Analytical Laboratories of the Russian Federation", Dubna, December 10-14.*

In the year 2008, FLNP will organize the following meetings:

1. *International Seminar-School "Pulsed Advanced Neutron Sources" PANS-III dedicated to the centenary of the birth of D.I.Blokhinzev, Dubna, January 29 – February 4.*
2. *XVI International Seminar on Interaction of Neutrons with Nuclei ISINN-16, Dubna, May 28-31.*
3. *International Seminar Dedicated to the centenary of the birth of I.M. Frank, Dubna, October 23-24.*

8.3. COOPERATION

List of Visitors from Non-Member States of JINR in 2007

Name	Organization	Country	Dates
V.NESVIZHEVSKY	ILL, Grenoble	France	31.01-01.02
M.TOMASEVIC	VINCA INS, Belgrade	Serbia	03.03-07.03
V.URUMOV	Univ. Saints Cyril &Methodius, Skopje	Macedonia	03.03-11.03
M.ANICIC	VINCA INS, Belgrade	Serbia	04.03-11.03 03.04-30.06
Z.SPIRIC	Inst. Of Applied Ecology, Zagreb	Croatia	04.03-11.03
K.ULLEMEYER	Univ. Freiburg	Germany	25.03-05.04
J.WUMMEL	Potsdam Geol. Res. Center	Germany	11.04-20.04
A.FRISCHBUTTER	Potsdam Geol. Res. Center	Germany	11.04-20.04
H.THILE	Potsdam Geol. Res. Center	Germany	11.04-20.04
V.LAUTER	ILL, Grenoble	France	15.04-26.04
H.-J.LAUTER	ILL, Grenoble	France	15.04-26.04
K.WALTHER	Potsdam Geol. Res. Center	Germany	17.04-27.04
S.C.OLSEN	NECSA, Pretoria	South Africa Rep.	14.05-14.06
Guohui ZHANG	Inst. of Heavy Ion Physics, Beijing	China	15.05-02.06
Jianyong WANG	Inst. of Heavy Ion Physics,	China	15.05-02.06

	Beijing		
A.FAANHOF	NECSA, Pretoria	South Africa Rep.	03.06-15.06
J.ZEEVART	NECSA, Pretoria	South Africa Rep.	03.06-09.06
D.KOTZE	NECSA, Pretoria	South Africa Rep.	03.06-08.06
D.BONDOUX	ILL, Grenoble	France	05.06-27.06
V.NESVIZHEVSKY	ILL, Grenoble	France	05.06-27.06
N.ZWETNOW		Norway	06.06-08.06
F.THOMAS	ILL, Grenoble	France	07.06-27.06
J.-P.GONZALES	ILL, Grenoble	France	07.06-27.06
H.J.LAUTER	ILL, Grenoble	France	19.06-22.06
V.LAUTER	ILL, Grenoble	France	19.06-22.06
A.SCHAEFFER	On-line Res./Writers, Palmer	USA	20.06-07.07
Gui Nyun KIM	Kyungpook Nat.Univ., Daegu	Korea Rep.	25.07-29.07
Man Woo LEE	Kyungpook Nat.Univ., Daegu	Korea Rep.	25.07-08.08 25.08-09.09 30.09-20.10
A.VENTER	NECSA, Pretoria	South Africa Rep.	18.09-23.09
E.STEINNES	Univ. of Sci.&Technol., Trondheim	Norway	22.10-29.10
H.-J.LAUTER	ILL, Grenoble	France	06.11-17.11
Man Woo LEE	Kyungpuk Nat.Univ.e, Daegu	Korea Rep.	11.11-25.11
N.KOCH	NECSA, Pretoria	South Africa Rep.	18.11-18.12
L.PILANE	NECSA, Pretoria	South Africa Rep.	03.12-16.12
A.NTSHABELE	NECSA, Pretoria	South Africa Rep.	03.12-21.12
J.TOPKIN	NECSA, Pretoria	South Africa Rep.	03.12-21.07
D.JANSEN	NECSA, Pretoria	South Africa Rep.	03.12-22.12
A.FAANHOF	NECSA, Pretoria	South Africa Rep.	03.12-22.12

8.4. EDUCATION

The objective of the FLNP educational program is the training of specialists in the field of neutron methods for condensed matter and nuclear physics research. The students of the Neutron Diffraction Department of MSU, of the Interfaculty Center «Structure of Matter and New Materials» and of the Electronics and Automatics Department of MIREA (Moscow State Institute of Radioengineering, Electronics and Automatics) perform their term and diploma works in FLNP. At the University Centre of JINR the students from Tula State University, Belgorod State University, Tver State University and other universities of Russia and JINR Member States write their term papers and do summer and winter practical works in FLNP.

On February – May 2007 the practical work for the students of the University Centre of JINR, the Neutron Diffraction Department of MSU and the Interfaculty Center «Structure of Matter and New Materials» was held.

On 25.06.07 – 06.07.07 the practical work for the students of the University Centre of JINR was organized.

On 10.07.07 – 22.07.07 the practical work for the students of the University Centre of JINR and the students from Tula State University was organized.

8.5. PERSONNEL

Distribution of the Personnel per Department as of 01.01.2007

Theme	Departments	Main staff
-1036-	Nuclear Physics Department	49
-1031-	Condensed Matter Physics Department	39
-1052-	IBR-2 Spectrometers Complex Department	37
-0993-	IREN Department	10
-0851-	IBR-2 Department	41
	Mechanical and Technical Department	43
	Electric and Technical Department	27
	Central Experimental Workshops	39
	Nuclear Safety Group	3
	Cold Moderator Group	7.5
	Design Bureau	5
	FLNP infrastructure:	
	Directorate	8.5
	Services and Management Department	21
	Scientific Secretary Group	4.5
	Supplies Group	3.5
Total		**338**

Personnel of the Directorate as of 01.01.2008

Country	People
Armenia	1
Bulgaria	2
Vietnam	1
Germany	2
Georgia	2
KPDR	5
Kazakstan	1
Mongolia	3
Poland	3
Romania	5
Russia	26
Ukraine	9
TOTAL	**60**

8.6. FINANCE

Financing of the FLNP Scientific Research Plan in 2007 (th. USD)

No.	Theme	Financing plan, $ th.	Expenditures For 12 months, $ th.	In % of FLNP Budget
I	**Condensed matter physics**	5258,0	5885,1	111,9
	-1031-	1544,5	1686,0	109,2
	-0851-	2976,0	3519,6	118,3
	-1052-	737,5	679,5	92,1
II	**Neutron nuclear physics**	1430,5	1561,6	109,2
	-1036-	1015,0	1103,6	108,7
	-0993-	415,5	458,0	110,2
III	**Elementary particle physics**	5,3	6,0	113,2
	-1007-			
	TOTAL:	**6693,8**	**7452,7**	**111,4**